# DESIGN OF MACROCYCLIC COMPOUNDS FOR BIOMEDICAL APPLICATIONS

EDITED BY: Pavel Padnya, Xin Wu, Andrea Erxleben and Susana Santos Braga
PUBLISHED IN: Frontiers in Chemistry

frontiers Research Topics

ISSN 1664-8714
ISBN 978-2-88971-286-1
DOI 10.3389/978-2-88971-286-1

## About Frontiers

Frontiers is more than just an open-access publisher of scholarly articles: it is a pioneering approach to the world of academia, radically improving the way scholarly research is managed. The grand vision of Frontiers is a world where all people have an equal opportunity to seek, share and generate knowledge. Frontiers provides immediate and permanent online open access to all its publications, but this alone is not enough to realize our grand goals.

## Frontiers Journal Series

The Frontiers Journal Series is a multi-tier and interdisciplinary set of open-access, online journals, promising a paradigm shift from the current review, selection and dissemination processes in academic publishing. All Frontiers journals are driven by researchers for researchers; therefore, they constitute a service to the scholarly community. At the same time, the Frontiers Journal Series operates on a revolutionary invention, the tiered publishing system, initially addressing specific communities of scholars, and gradually climbing up to broader public understanding, thus serving the interests of the lay society, too.

## Dedication to Quality

Each Frontiers article is a landmark of the highest quality, thanks to genuinely collaborative interactions between authors and review editors, who include some of the world's best academicians. Research must be certified by peers before entering a stream of knowledge that may eventually reach the public - and shape society; therefore, Frontiers only applies the most rigorous and unbiased reviews.
Frontiers revolutionizes research publishing by freely delivering the most outstanding research, evaluated with no bias from both the academic and social point of view. By applying the most advanced information technologies, Frontiers is catapulting scholarly publishing into a new generation.

## What are Frontiers Research Topics?

Frontiers Research Topics are very popular trademarks of the Frontiers Journals Series: they are collections of at least ten articles, all centered on a particular subject. With their unique mix of varied contributions from Original Research to Review Articles, Frontiers Research Topics unify the most influential researchers, the latest key findings and historical advances in a hot research area! Find out more on how to host your own Frontiers Research Topic or contribute to one as an author by contacting the Frontiers Editorial Office: frontiersin.org/about/contact

# DESIGN OF MACROCYCLIC COMPOUNDS FOR BIOMEDICAL APPLICATIONS

Topic Editors:
**Pavel Padnya,** Kazan Federal University, Russia
**Xin Wu,** The University of Sydney, Australia
**Andrea Erxleben,** National University of Ireland Galway, Ireland
**Susana Santos Braga,** University of Aveiro, Portugal

**Citation:** Padnya, P., Wu, X., Erxleben, A., Braga S. S., eds. (2021). Design of Macrocyclic Compounds for Biomedical Applications. Lausanne: Frontiers Media SA. doi: 10.3389/978-2-88971-286-1

# Table of Contents

frontiers in Chemistry

EDITORIAL
published: 08 July 2021
doi: 10.3389/fchem.2021.730111

# Editorial: Design of Macrocyclic Compounds for Biomedical Applications

*Pavel L. Padnya[1]*, Xin Wu[2]*, Andrea Erxleben[3]* and Susana S. Braga[4]**

[1]A.M. Butlerov' Chemistry Institute, Kazan Federal University, Kazan, Russia, [2]School of Chemistry, The University of Sydney, Sydney, NSW, Australia, [3]School of Chemistry, National University of Ireland Galway, Galway, Ireland, [4]LAQV/REQUIMTE – Associated Laboratory for Green Chemistry, Department of Chemistry, University of Aveiro, Aveiro, Portugal

**Keywords: macrocycles, self-assembly, molecular recognition, drug delivery, biosensors**

## Editorial on the Research Topic

## Design of Macrocyclic Compounds for Biomedical Applications

The search for new biologically active compounds to tackle global health challenges is an important goal in organic synthesis, biochemistry, and medicine. The biological activity of macrocyclic structures is an actively developing area of science. Macrocyclic compounds have unique physicochemical properties, such as spatial preorganization, presence of a size-defined cavity, propensity of undergoing self-assembly, low pharmacologically active concentrations, low toxicity, antiallergenicity, etc. Macrocyclic compounds such as crown ethers, cyclodextrins, cucurbiturils, calixarenes, porphyrins, pillararenes and cyclic peptides have been used in various biomedical applications. In this Research Topic, we present a collection of original research and review articles that show the significant recent advances made in the synthesis of new macrocycles and their biomedical applications.

One of the ways to overcome the antimicrobial resistance of microorganisms is the use of macrocycle-antibiotic hybrids, as reviewed by Surur et al.. This review article describes the synthesis and properties of the most well-known hybrids of macrocyclic compounds with antibiotics such as rifamycins, vancomycin, etc. It is known that the major limitation of the use of antibiotic hybrids is the increase in molecular weight. However, progresses and advances in this area show the possibility of improving the oral bioavailability of bulky molecules for systemic clinical use.

Ibrahim et al. have developed novel Tröger's base derivatives and studied their anticancer properties. The synthesized Tröger's base phenhomazines derivatives were screened for anticancer activity, and 1,4,7,10-tetraoxa[10](2,8) trögerophane has shown a promising selectivity on a colon cell line with $IC_{50}$ = 92.7 μg/ml. The obtained results open up prospects for the development of new promising anticancer agents.

It is known that macrocyclic compounds can be used in targeted delivery systems as containers for drugs. It has been shown by Chandra et al. that cucurbit[7]uril is able to form a host-guest complex with the neurotransmitter serotonin. In this case, the binding affinity is pH-dependent. The results demonstrate promising biological applications in the delivery and pH-controlled release of serotonin. Saleh et al. described the use of cucurbit[7]uril as a liver protective agent and an adjuvant in toxicological pharmacology. The protective effects of cucurbit[7]uril were evaluated in the biochemical study of the extracted livers of mice following cyanobacterial crude extract treatment with or without cucurbit[7]uril. The addition of cucurbit[7]uril has been shown to significantly reduce the toxicity of cyanotoxin-induced hepatotoxicity ($P < 0.05$) *in vivo*.

Supramolecular chemistry is useful in the controlled and/or local delivery of immunomodulatory drugs, as reviewed by Soni et al.. In their review, macrocycles such as cyclodextrins are highlighted for

OPEN ACCESS

***Edited and reviewed by:***
*Tony D. James,*
*University of Bath, United Kingdom*

****Correspondence:***
*Pavel L. Padnya*
*padnya.ksu@gmail.com*
*Xin Wu*
*xin.wu@sydney.edu.au*
*Andrea Erxleben*
*andrea.erxleben@nuigalway.ie*
*Susana S. Braga*
*sbraga@ua.pt*

***Received:*** *24 June 2021*
***Accepted:*** *28 June 2021*
***Published:*** *08 July 2021*

***Citation:***
*Padnya PL, Wu X, Erxleben A and Braga SS (2021) Editorial: Design of Macrocyclic Compounds for Biomedical Applications. Front. Chem. 9:730111. doi: 10.3389/fchem.2021.730111*

their drug solubilizing and stabilizing actions and the utility of polymer-based hydrogels and nanomaterials in local drug delivery is also described. Besides drug delivery, cyclodextrin-based supramolecular systems have found applications in other biomedically relevant areas such as the separation of biomolecules, enzymatic catalysis, sensing, diagnosis and therapy, as summarized by Luo et al.

The chirality of cyclodextrins makes them suitable for the separation of biomolecules. According to the molecular mechanics simulation conducted by Alvira, even a very simple and affordable native cyclodextrin such as β-cyclodextrin is able to discriminate the enantiomeric forms of the amino acids alanine, valine, leucine, and isoleucine.

The development of macrocyclic chemistry has contributed to the design of new materials with effective and selective catalytic properties. In a mini-review, Shang et al. have described recent advances in the use of macrocyclic compounds as building blocks for the design of bioinspired catalysts. The described materials, from single-molecule to metal-organic framework materials, have unique catalytic properties and binding affinity for biologically significant substrates. The authors agree that the materials obtained have a lower catalytic activity in comparison with natural enzymes at this stage of research. However, the trend in the development of synthetic catalysts may lead to future application.

Facilitation of ion transport across lipid bilayers is an important supramolecular function with potential applications in biophysics research and the treatment of ion channel diseases. Macrocyclic ionophores are of particular interest for achieving high membrane transport selectivity as exemplified by the almost perfect $K^+$ over $Na^+$ selectivity exhibited by the natural product valinomycin. Zhao et al. have developed a cyclic azapeptide anionophore with a small binding cavity that facilitates selective transmembrane transport of fluoride ions. Remarkably, this anionophore shows negligible transport for larger anions including chloride and acetate.

Overall, this article collection includes several excellent studies in the design and investigation of macrocyclic structures and covers various fields of chemistry, biology and medicine. As guest editors of this article collection, we thank all authors and reviewers for their valuable contributions. We hope that the publications presented in this collection will attract even greater interest in the chemistry of macrocyclic compounds and supramolecular chemistry.

## AUTHOR CONTRIBUTIONS

All authors listed have made a substantial, direct, and intellectual contribution to the work, and approved it for publication.

## FUNDING

PP acknowledges of the grant of the President of the Russian Federation for state support of young scientists and leading scientific schools of the Russian Federation (MK-12.2020.3, NSh-2499.2020.3) for financial support. SB acknowledges Fundação para a Ciência e a Tecnologia/Ministério da Ciência, Tecnologia e Ensino Superior (FCT/MCTES) for financial support to the associated laboratory LAQV-REQUIMTE (project reference UIDB/50006/2020).

**Conflict of Interest:** The authors declare that the research was conducted in the absence of any commercial or financial relationships that could be construed as a potential conflict of interest.

frontiers in Chemistry

ORIGINAL RESEARCH
published: 08 September 2020
doi: 10.3389/fchem.2020.00823

# Molecular Simulation of the Separation of Some Amino Acid Enantiomers by β-Cyclodextrin in Gas-Phase

*Elena Alvira**

*Departamento de Física, Universidad de La Laguna, San Cristóbal de La Laguna, Spain*

The complexes formed by β-cyclodextrin and some amino acids (alanine, valine, leucine, and isoleucine) in vacuo are studied by molecular mechanics and dynamics simulations. These methods have been improved with respect to our previous studies with amino acids, regarding the determination of molecular structures or initial enantiomer dispositions in the molecular dynamics trajectories. The greatest contribution to the interaction energy is from the van der Waals term, although the discrimination between enantiomers is due mainly to the electrostatic contribution. The lowest energy structures of the complexes obtained from molecular mechanics are inclusion complexes in which the carboxylic end of amino acids is pointing toward the narrow (D-) or wide rim (L-) of β-cyclodextrin. The position probability density provided by molecular dynamics also confirms inclusion complex formation, because the guests spend most time inside the cavity of β-cyclodextrin along its axis, with the carboxylic end pointing toward the narrow rim. The L-amino acids are the first eluted enantiomers in all cases and chiral discrimination increases with the size of guests, except leucine, which has the lowest capacity to discriminate. During the simulation, Ala and Val remain in weakly enantioselective regions, while Leu and Ile stay in zones with great chiral selectivity.

**Keywords: cyclodextrins, amino acids, enantiomers, molecular mechanics, molecular dynamics, inclusion complex, elution order**

OPEN ACCESS

***Edited by:***
*Susana Santos Braga,*
*University of Aveiro, Portugal*

***Reviewed by:***
*Khaleel Assaf,*
*Jacobs University Bremen, Germany*
*Narayanan Selvapalam,*
*Kalasalingam University, India*

***Correspondence:**
*Elena Alvira*
*malvira@ull.edu.es*

***Specialty section:***
*This article was submitted to Supramolecular Chemistry, a section of the journal Frontiers in Chemistry*

***Received:*** *23 June 2020*
***Accepted:*** *04 August 2020*
***Published:*** *08 September 2020*

***Citation:***
*Alvira E (2020) Molecular Simulation of the Separation of Some Amino Acid Enantiomers by β-Cyclodextrin in Gas-Phase. Front. Chem. 8:823. doi: 10.3389/fchem.2020.00823*

## INTRODUCTION

Cyclodextrins (CDs) are macrocyclic molecules composed of glucose units (6 for α-CD, 7 for β-CD, 8 for γ-CD, etc.) forming truncated cone shaped compounds. These have cavities with different internal diameters capable of including molecules with different structure, size and composition (Szejtli and Osa, 1996; Lipkowitz, 1998, 2001). CDs are extensively used in catalysis and separation of enantiomers, which are very useful techniques in the pharmaceutical, cosmetic, chemistry and food industries (Maier et al., 2001). Amino acids are biologically important organic compounds, which in the form of proteins comprise the largest component (other than water) of human cells, muscles and other tissues. The enantiodiscrimination and inclusion complex formation of amino acids and amino-acid derivatives by CDs have been experimentally studied with different techniques such as electrospray mass spectrometry, capillary electrophoresis and gas chromatography (Ramanathan and Prokai, 1995; Boniglia et al., 2002).

Experimental results also reveal the influence of organic modifiers and pH conditions on the enantiomer separation of amino acids and inclusion complex formation with CDs (Zia et al., 2001; Sebestyén et al., 2012; Stepniak et al., 2017). In particular, the chiral separation and inclusion complexes formed by valine, leucine, and isoleucine (among other amino acids, but not alanine) with partially methylated β-CD in gas-phase, have been analyzed both experimentally and theoretically (Ramirez et al., 2000). It has been established that the enantiomers can locate almost totally inside the cavity in the complexes of minimum energy, and the L-amino acid is the first eluted enantiomer. The study of chiral differentiation of alanine enantiomers by permethylated β-CD, using infrared multiple photon dissociation (IRMPD) spectroscopy combined with mass spectrometry, also showed the inclusion complex formation (Lee et al., 2017). However, the density functional theory calculations provided by Lee et al. (2017) for the lowest energy structures, were not consistent with those experimental results. The inclusion complexes formed by L-Ile zwitterions with both α- and β-CD showing 1:1 stoichiometry are confirmed by NMR (nuclear magnetic resonance techniques), surface tension and conductivity measurements (Roy et al., 2016).

Previously, we studied the inclusion complex formation and chiral discrimination of several amino acids with β-CD, by means of molecular mechanics (MM) and dynamics (MD) simulations (Alvira, 2013, 2015, 2017a, 2019). We have studied alanine (Ala), valine (Val), leucine (Leu), and isoleucine (Ile) in vacuo and with solvents like water, considering two configurations for the amino acids: non-polar and zwitterion. Furthermore, some improvements were made in the simulation method applied to each amino acid, concerning the calculation of molecular structures, parameters of interaction energies, or the number of trajectories in MD, among other factors. We showed that Ala, Val, Leu, and Ile were able to form inclusion complexes with β-CD in water and other solvents, but only Ile was included in vacuo. This diverged from the results proposed by Ramirez et al. (2000) and Lee et al. (2017). The most useful modification in the molecular simulation applied to Ile (Alvira, 2019) was the *ab initio* method used to determine the amino acid configurations, instead of the force field proposed by Weiner et al. for the molecular mechanics simulation of nucleic acids and proteins (Weiner et al., 1984, 1986), used in our earlier studies (Alvira, 2013, 2015, 2017a). The aim of the present work was to apply the model proposed for Ile to theoretically examine the interaction between Ala, Val, and Leu with β-CD in vacuo. To achieve this, the configuration of complexes formed by these molecules is determined by MM, as well as the differences in interaction energies between the enantiomers that cause the discrimination. Elution order, residence time, and capacity for inclusion complex formation are deduced from MD. The most important result and main difference with respect to our previous results is the capacity of Ala, Val, Leu, and Ile to form inclusion complexes with β-CD in vacuo. This is in agreement with the conclusions obtained by Ramirez et al. (2000), not only those related to inclusion complex formation, but also the lowest energy structure of the complexes and the elution order in the separation of these amino acid enantiomers.

# MATERIALS AND METHODS

## Molecular Mechanics Simulation

The minimum energy complex structure is determined by MM simulation, and it is considered an inclusion complex if the guest (amino acid) is totally or partially inside the host (β-CD). The molecular configuration of β-CD and atomic charges are taken from the literature (Kinglert and Rihs, 1991), but the atomic coordinates of amino acids are calculated by the Hartree-Fock method, as previously for Ile (Alvira, 2019). The 6-31G** basis set implemented in the MOLPRO package (Werner et al., 2012a,b, MOLPRO) is used to determine the amino acid structures, instead of the force field model proposed by Weiner et al. (1984, 1986) for nucleic acids and proteins. This is one of the improvements in the simulation method with respect to our previous studies (Alvira, 2013, 2015, 2017a, 2019). We considered an all-atom model for the molecules, as the H atoms can participate in H-bonds that can be important in structuring the complex. The interaction energy between the enantiomers and β-CD is calculated by locating the guest center of mass on a grid, and with different orientations (about 23,000) with respect to the host. The distance between two consecutive grid points is 0.1 Å, from −5 to 5 Å on each axis. The space-fixed reference system is located over the principal axis of β-CD, with the origin at the center of mass of the cavity and the XY plane perpendicular to the cavity axis. The guest orientation is defined by the Euler angles formed between the principal axis of the amino acids and the absolute reference system. The host-guest complex with the lowest energy is normally the complex configuration. The interaction energy $E$ between β-CD and the amino acids (Ala, Val, Leu, and Ile) is determined as the sum of intermolecular $E_{\text{inter}}$ and intramolecular $E_{\text{intra}}$ terms, as in the AMBER force file proposed by Weiner et al. for molecular mechanics simulation of nucleic acids and proteins (Weiner et al., 1984, 1986). The van der Waals, electrostatic and H-bond energies contribute to $E_{\text{inter}}$.

Amino acids are neutral molecules, but under some pH conditions or with polar solvents the amino acid appears as a zwitterion. The difference between the amino acid configurations (non-polar and zwitterion) are due to the presence of the $NH_3^+$ and $COO^-$ groups instead of $NH_2$ and $COOH$, which affects both the molecular structure and charge distribution. In our previous studies with amino acids, we analyzed the influence of various solvents (such as water) on the separation of enantiomers. To represent the solvent polarity, different values of $\varepsilon$ were selected, as well as two atomic charge distributions and molecular structures for the amino acids. The presence of water in the separation process was simulated by $\varepsilon = 80$ and a zwitterion configuration for the enantiomers in those studies. The electrostatic contribution to the interaction energy between the amino acids and β-CD in the presence of water was about −0.4 kcal/mol, the discrimination between the enantiomers being due to the van der Waals contribution in this case. Residence times with water are generally shorter than in vacuo, although they depend on the amino acid enantiomer and initial conditions in the trajectories of MD (Alvira, 2013, 2015, 2017a, 2019). Ramirez et al. assumed a non-polar structure for the guest molecule and a dielectric constant of 1, in the molecular

dynamics calculations of the inclusion complexes formed by some amino acids and β-CD in gas-phase (Ramirez et al., 2000). This was despite the fact that the authors started the experiment with a solution that was electrosprayed into the Fourier transform mass spectrometer (Ramirez et al., 2000). In the present study, we use the same conditions as Ramirez et al. to simulate the separation of some amino acid enantiomers by β-CD in vacuo (a non-polar structure and $\varepsilon = 1$). The H-bond term only contributes to $E_{\text{inter}}$ when the complex configuration fits the distances and angles required to form this type of bond (O-H, N-H) (Weiner et al., 1984, 1986). $E_{\text{intra}}$ represents the conformational adaptation of host and guest; it is the result of adding the torsional energy, bond stretching and bending functions.

The optimized parameters (ff99SB-ILDN) for the torsion potential of the AMBER ff99SB protein force field are used for Leu (N-$C^{\alpha} - C^{\beta} - C^{\gamma}$) and Ile (N-$C^{\alpha} - C^{\beta} - C^{\gamma 2}$) (Lindorff-Larsen et al., 2010). This is another variation included in the present molecular modeling process, although its influence on the results and conclusions is not as important as the method used to calculate molecular structures, since $E_{\text{intra}}$ is not very different for the enantiomers and its magnitude is usually smaller than $E_{\text{inter}}$.

However, the enantioseparation is a dynamic process in which the amino acid is continually moving, and the complex does not always adopt the lowest energy configuration. Therefore, the different interaction energies between the enantiomers and β-CD (chiral discrimination) do not depend only on their minimum value. MM provides the minimum energies in the guest dispositions on the grid inside and outside the cavity (the potential energy surface, PES). The results of MM are also shown in the penetration potential W, which represents the minimum energy in each plane parallel to XY, against the cavity axis. The shape of W allows us to predict if the guest can be included more or less easily in β-CD or can even be repelled from the cavity, depending on whether W resembles a well or a barrier potential. Since the guest is not able to adopt the most energetically favorable disposition in each grid position, we also determined the PES in a different way. This involved calculating the average Boltzmann energy for the different orientations of the enantiomer instead of the minimum value. We are really interested in the capacity of β-CD to separate the amino acid enantiomers, therefore the difference in the PES is useful to identify the regions with greater chiral discrimination (greater differences in energy).

## Molecular Dynamics Simulation

The relative motion between host and guest is determined in MD by solving the classical equations of motion due to their mutual interaction. The solution cannot be obtained analytically but numerically, since there are many particles in the system, each with many constraints. To integrate the equations, we used an in-house computer program written in Fortran with the MD simulation performed at constant temperature (293 K). For this, a variant of the leap-frog scheme proposed by Brown and Clarke (1984) was used, in which the kinetic energies of rotational and translational motions are separately constrained (Fincham et al., 1986). Moreover, both types of movement are posed and solved in different equations, since the translation of the guest center of mass is due to the total force acting on the particle, and the rotation about this center of mass is a consequence of the total torque. The rotational equations of motion for the guest are posed as a function of four quaternions instead of angular variables, to avoid the problems of divergence. Therefore, these equations include quaternions, their first derivatives, and angular velocities and their time derivatives (Allen and Tildesley, 1987; Rapaport, 1995; Frenkel and Smit, 2002). In this way, MD reveals the evolution of the molecules, i.e., the variation in atomic positions and velocities through time (trajectory). However, the solution of the equations of motion, and therefore the resultant trajectory, depends on the initial conditions considered for the velocities (rotational and translational) and molecular dispositions. Therefore, some trajectories are determined in the simulation to reflect different situations the system can reach in the separation process. The magnitude of initial velocities is calculated consistently with the temperature at which the process occurs (293 K). Their direction is randomly computed; it is the same for all the amino acids, to avoid the simulation being influenced by factors other than the interaction with β-CD. However, the initial disposition of enantiomers in the trajectories cannot be the same because they are mirror images and, although there is no single method to select them, it is a question insufficiently dealt with in MD simulations. In our previous studies with amino acids, we tested different models to calculate the initial dispositions of enantiomers based on energetic, numerical or geometrical criteria (Alvira, 2017b). The method applied in the present study minimizes the differences in the van der Waals energy and average atomic distances between the enantiomers, as we already adopted in our more recent research with Ile (Alvira, 2019). The smallest differences in both energy and atomic positions are those of Val (average values $3.8 \times 10^{-6}$ kcal/mol, 0.11 Å), very similar to Ile ($1.6 \times 10^{-5}$ kcal/mol, 0.14 Å), then Leu ($2.8 \times 10^{-5}$ kcal/mol, 0.40 Å). The smallest amino acid (Ala) has the greatest differences ($3.7 \times 10^{-4}$ kcal/mol, 0.96 Å). Twenty trajectories are calculated in the simulation, with initial enantiomer dispositions outside the cavity facing the rims of β-CD, since when the guest starts from positions near the cavity walls it does not enter the cavity but moves away. We consider different guest orientations parallel to the rims and pointing toward the wide or narrow rim of β-CD (Alvira, 2019), doing the same for all the amino acids to make the results comparable. The simulation time for each trajectory is 5 ns with a step of 1 fs, and the energies and guest dispositions were registered every 100 steps. However, the interaction between the amino acid and β-CD is weaker outside than inside the cavity, moreover it decreases as the distance between them increases, to such an extent that at some guest positions their interaction is not attractive enough to include the amino acid in β-CD. The molecule usually enters the cavity where it stays for some period of time, moving continually and then leaving the CD. However, there are some trajectories in which the amino acid cannot be included totally or partially in the cavity (external trajectories). The number of external trajectories for each amino acid is different despite the initial conditions being the same for all of

them, and it does not depend on the initial dispositions of the enantiomers. We integrate the equations of motion during the period of time the guest remains near the cavity, both inside the cavity (residence time) or outside for the external trajectories. To locate the most probable position of the enantiomers under the influence of β-CD, we determine the position probability density as the number densities of guest positions in a volume element, divided by the total number of guest positions in the simulation (Lipkowitz et al., 1997a,b). The number density is obtained from a grid in which the distance between two consecutive points is 0.5 Å. The position probability density reflects the external trajectories and indicates the capacity to form inclusion complexes, since it represents the most probable positions of the guest center of mass. The enantiomers are moving continually, but they also have preferential orientations when they are in the preferred locations, these dispositions being the most probable configurations of the complexes deduced from MD. Whereas, the position probability density indicates the capacity to form inclusion complexes, the enantioselectivity is provided by the difference in the binding free energy $F$ of the enantiomers. $F$ indicates if the complex is more energetically favorable than the reactants and is calculated in each trajectory (Rapaport, 1995). The energy in $F$ is calculated as the sum of intermolecular and intramolecular terms, this way the effect of the conformational adaptation of host and guest is also included in the results: binding free energies, elution order, residence times, position probability densities and the most probable configuration of complexes. The elution order is determined by the difference in $F_{mean}$ between the enantiomers $\Delta F_{mean}$, where $F_{mean}$ is the average binding free energy in the simulation. If $\Delta F_{mean} > 0$, the D-enantiomer of amino acids is more tightly bound and the L-enantiomer is eluted first. The MD model used in the present research was previously applied in our study with Ile, but it includes some improvements on the simulations carried out with Ala, Val and Leu, regarding the number of trajectories (6 for Ala and Val, 12 for Leu), simulation time (3 ns) and the most influential initial enantiomer dispositions.

# RESULTS AND DISCUSSION

## Molecular Mechanics Simulation

The configuration of complexes formed by the amino acids and β-CD is obtained in MM by the guest orientation and position with respect to the cavity, for which the interaction energy is the lowest $E_{\min}$. To determine this absolute minimum, the energy $E$ must first be calculated in each guest position inside and outside the CD for different orientations of amino acids. The minimum result of $E$ is assigned at each grid point. The potential energy surface (PES) represents these minima for the different dispositions of amino acids with respect to β-CD, the energy $E$ being determined by the sum of inter- and intramolecular terms. The intermolecular energy $E_{\text{inter}}$ is calculated by adding the Lennard-Jones (LJ), electrostatic (ELE) and H-bonds contributions, and the penetration potential W represents the consecutive minima of $E_{\text{inter}}$ in each plane perpendicular to the cavity axis. This W allows us to visualize if the guest can enter or is repelled by the CD, depending on whether it resembles a well or barrier potential. The main contribution to W is due to the Lennard-Jones term ($W_{LJ}$), which appears as a well potential for the enantiomers (**Figures 1A,B**) and therefore contributes to the inclusion of amino acids into the cavity. The larger amino acid is the deeper $W_{LJ}$, and its sharpened shape is due to the difficulty for the guest to orientate freely inside the cavity. The difference in $W_{LJ}$ between the enantiomers of an amino acid (**Figures 1A,B**) also increases with the molecular size, and corresponds to inner more than outer guest positions. For the isomers Leu and Ile, $W_{LJ}$ differs more for D- than L-enantiomers and occurs when the molecule is near the narrow rim of β-CD. The H-bond energy only contributes to $E_{\text{inter}}$ in those guest dispositions that fit the conditions needed to form H bonds, between the O and H atoms of amino acids and CD (Weiner et al., 1984, 1986). The maximum value of this term is −0.5 kcal/mol, similar for all the amino acids, although its influence in $E_{\text{inter}}$ is different due to the percentage it amounts to for each one. Whereas, $W_{LJ}$ appears as a well potential, the electrostatic contribution to W ($W_{ELE}$) for the amino acids seems a barrier potential because its minimum is located outside the CD, and it increases inside the cavity (**Figures 1C,D**). $W_{ELE}$ is very similar for the L-enantiomers, both the extreme values (minimum and maximum) and the location of the greatest value near the cavity center (**Figure 1C**). However, the ELE energy is very different for the D-enantiomers in shape and magnitude. The maximum value of $W_{ELE}$ inside the cavity corresponds to D-Ile and is located near the narrow rim of β-CD, while the greatest ELE energy for D-Ala and D-Leu occurs near the wide rim (**Figure 1D**). This term can reach 30 % of W, and the differences in $W_{ELE}$ between the amino acid enantiomers inside the cavity increases with the molecular size, from 1.40% (for Ala) to 78.09% (for Ile). In fact, their discrimination is due mainly to this term, as deduced by comparing the curves $W_{LJ}$ (**Figures 1A,B**) and W (**Figures 1E,F**). The ELE is also directly related to a barrier potential in W for some amino acids, between the narrow rim and the center of the cavity. It is also related to the guest orientation with respect to the cavity axis. The height of this barrier is similar for L-Ala, L-Val, L-Ile, and D-Ile, but the width decreases as the size of the guest increases. Isoleucine is the most stable amino acid and its enantiomers present the lowest differences in W, both in shape (potential barrier) and magnitude. To represent the PES, the interaction energy $E$ in each grid point is determined as the average Boltzmann energy corresponding to different guest orientations, instead of the minimum value. This is because the molecule is not always able to adopt the most stable configuration in the separation process. **Figure 2A** shows the projections of $E_L - E_D$ in the XY and XZ planes, $E_L$ and $E_D$ being the energies for each enantiomer of Ala, Val and Ile. A schematic representation of the projections of β-CD in those planes is included. The positions at which $E_L - E_D < 0$ are represented by red circles and blue crosses denote the most stable positions for the D enantiomer. The more intense the symbol, the greater difference in energy it represents. The potentially most discriminating regions for all of the amino acids are located near the cavity walls, where the interaction energy changes from negative to positive values. However, the stability of enantiomers and the zones where the differences in energy are greater depend

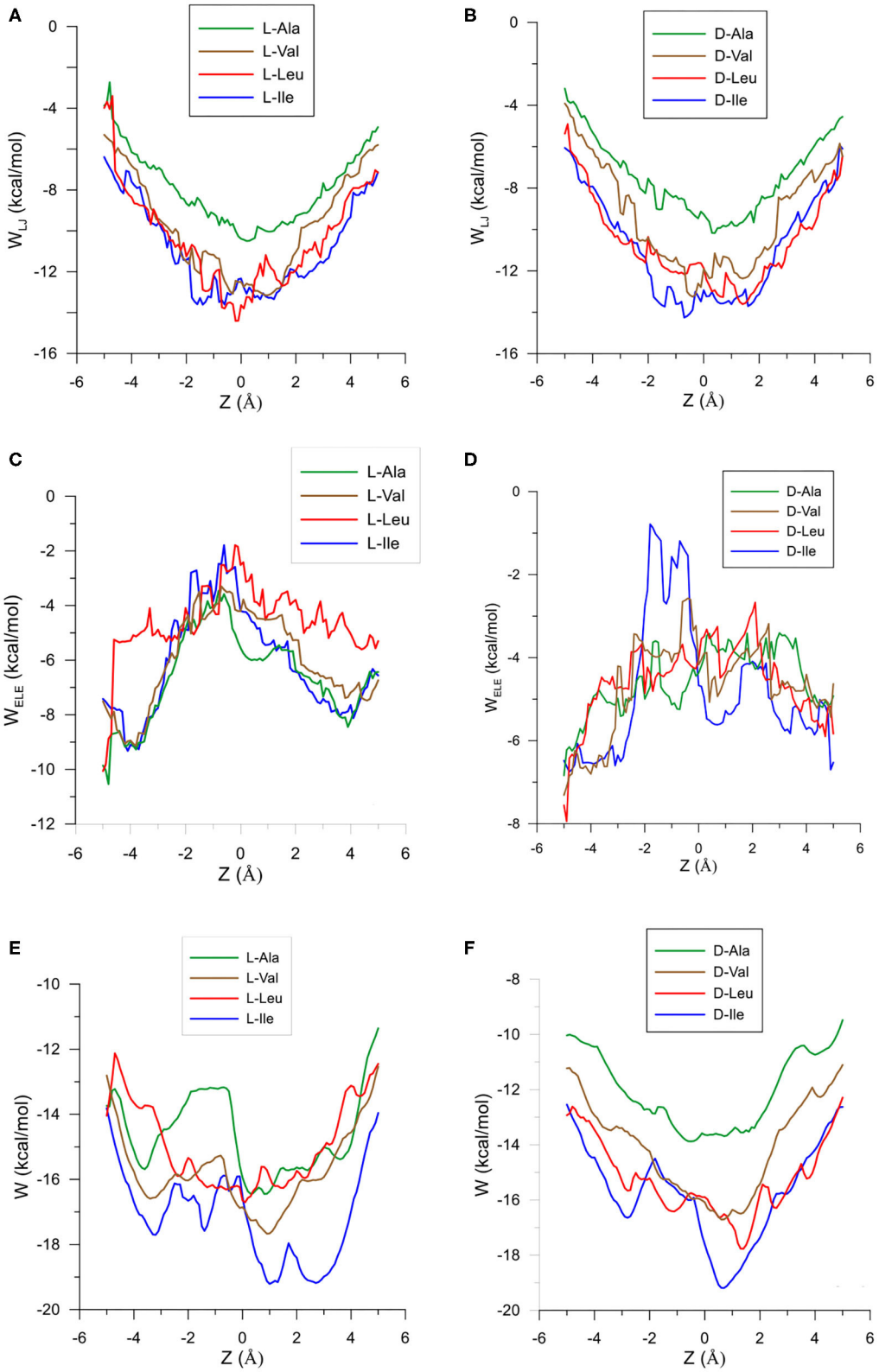


**FIGURE 1 |** The Lennard-Jones contribution to the penetration potential $W_{LJ}$ (kcal/mol) for the interaction between β-CD and **(A)** L-enantiomers of the amino acids, **(B)** D-enantiomers of the amino acids. The ELE contribution to the penetration potential $W_{ELE}$ (kcal/mol) for the interaction between β-CD and **(C)** L-enantiomers of the amino acids, **(D)** D-enantiomers of the amino acids. The penetration potential W for the interaction between β-CD and **(E)** L-enantiomers of the amino acids, **(F)** D-enantiomers of the amino acids.

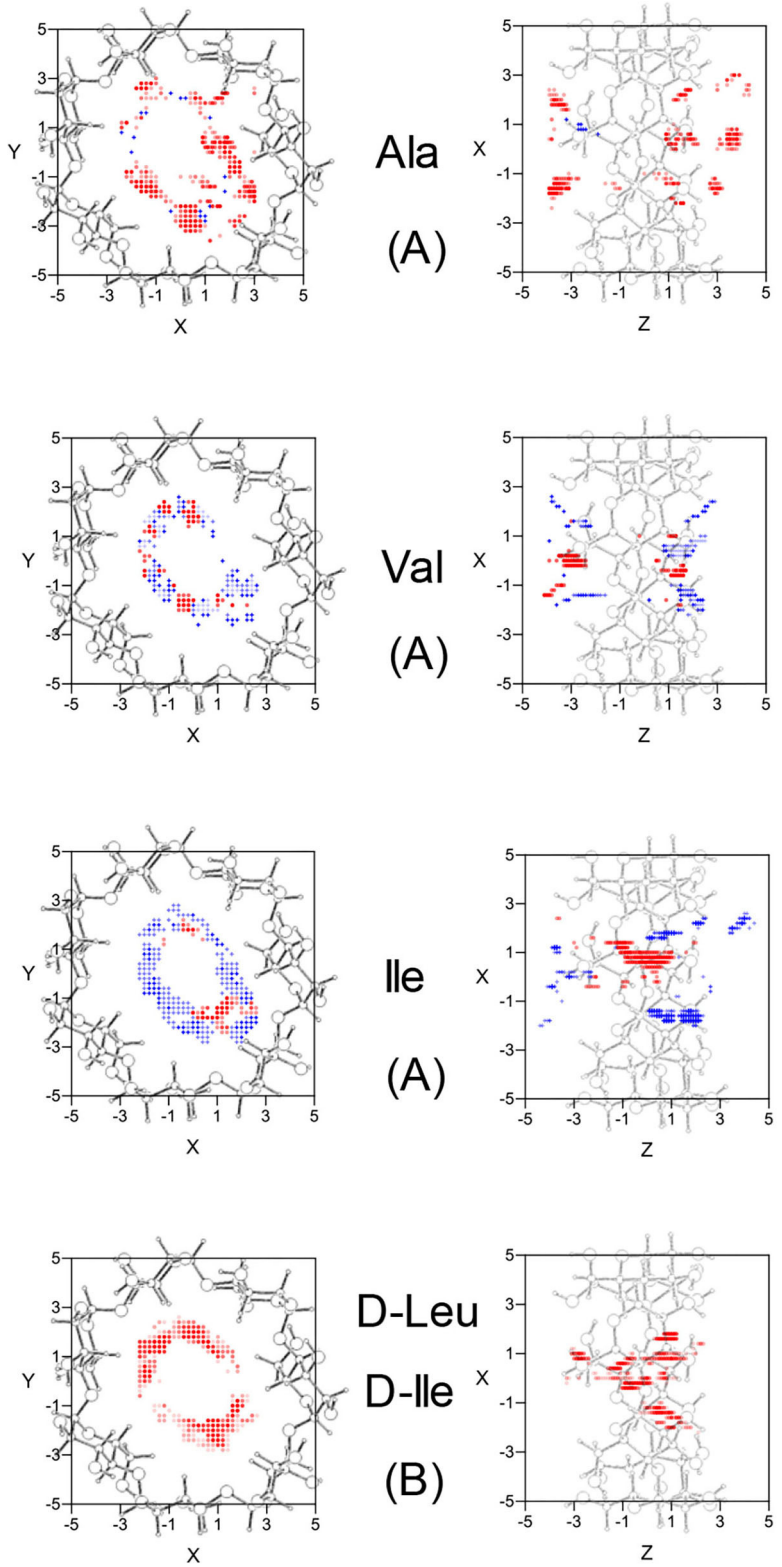


**FIGURE 2 | (A)** The projections in the XY and XZ planes of the potentially most discriminating regions for the amino acid enantiomers of Ala, Val, and Ile. The zones where the L-enantiomers are more stable are represented by red circles, those for D-enantiomers by blue crosses, and the more intense the symbol the greater difference in energy it represents. **(B)** The projections in the XY and XZ planes of the potentially most discriminating regions for the isomers D-Leu and D-Ile. The zones where D-Ile is more stable are represented by red circles, those for D-Leu by blue crosses, and the more intense the symbol the greater difference in energy it represents. A schematic representation is included of the projections of β-CD in those planes.

**TABLE 1 |** The minimum interaction energy $E_{min}$ obtained with the AMBER force field for each enantiomer and the different contributions: Lennard-Jones $E_{LJ}$, electrostatic $E_{ele}$, hydrogen bonding $E_{H\text{-}bond}$, bond stretching $E_{bond}$, angle bending $E_{angle}$, and torsion energy $E_{torsion}$.

| Amino acid | $E_{min}$ (kcal/mol) | | $E_{LJ}$ (kcal/mol) | | $E_{ele}$ (kcal/mol) | | $E_{H\text{-}bond}$ (kcal/mol) | | $E_{bond}$ (kcal/mol) | | $E_{angle}$ (kcal/mol) | | $E_{torsion}$ (kcal/mol) | |
|---|---|---|---|---|---|---|---|---|---|---|---|---|---|---|
| | L | D | L | D | L | D | L | D | L | D | L | D | L | D |
| Ala | −11.51 | −9.04 | −10.83 | −8.95 | −5.85 | −4.98 | 0.00 | 0.00 | 1.59 | 1.80 | 3.42 | 3.03 | 0.16 | 0.06 |
| Val | −11.08 | −11.66 | −13.14 | −11.65 | −4.55 | −4.73 | 0.00 | −0.44 | 1.54 | 1.42 | 4.32 | 3.04 | 0.75 | 0.70 |
| Leu | −7.94 | −8.19 | −13.79 | −13.59 | −2.56 | −3.79 | −0.49 | −0.46 | 1.42 | 1.43 | 4.71 | 4.97 | 2.77 | 3.25 |
| Ile | −10.91 | −10.82 | −11.89 | −13.60 | −7.38 | −5.67 | 0.00 | 0.00 | 1.45 | 1.52 | 4.76 | 4.81 | 2.15 | 2.12 |

on the size of the amino acids. Whereas, L-Ala is the most stable enantiomer in broader zones of PES, D-Ile frequently has lower energies. Moreover, the regions with greater chiral discrimination are located in inner positions as the size of the amino acids increases, so L-Ala is more stable outside the CD cavity while L-Ile is more stable inside. Isoleucine is also more stable than Leu at every point of the potential surface; the greatest differences are found at the inner positions (**Figure 2B**).

The absolute minimum interaction energy $E_{min}$, the values for the enantiomers and their different contributions are included in **Table 1**. The complexes formed by β-CD with Val are the most stable while Leu is the least. The Lennard-Jones term makes the greatest contribution to $E_{min}$ for the amino acids, and the energy due to the angle bending $E_{angle}$ contributes most to the intramolecular energy $E_{intra}$. The bond lengths, bond angles and torsional angles of amino acids that contribute most to $E_{intra}$ is different for the enantiomers, they are related to the atoms of guests located nearer the cavity walls in the complexes formed with β-CD. However, the average variations in angles and bond lengths due to the conformational adaptation of host and guest, is the order of $10^{-4}$ (degrees) and $10^{-5}$ Å, independently of the size of amino acids. The difference between enantiomers increases in order Ile < Leu < Val < Ala, being due mainly to the van der Waals energy except for Leu, in which it is caused by the electrostatic energy.

**Figure 3** shows the configurations of the complexes with $E_{min}$ formed in vacuo by β-CD with the amino acids (Kokalj, 2003). The guest molecule has been superimposed in **Figure 3** for clarity, but they are inclusion complexes because the guest is totally or partially inside the cavity. D-Ala, D-Val and L-Leu are located near the cavity center in the complexes formed with β-CD, while L-Ala, L-Val and the enantiomers of Ile are near the cavity walls (**Table 2**). In these complexes, the amino acids are oriented in such a manner as to include the greatest part of the molecule, and therefore to achieve the maximum interaction with the CD. D-Leu and L-Ile are nearly parallel to the wide rim of the cavity, and this is due to the location of their center of mass. The guest orientation is different for the enantiomers: whereas the carboxylic end of L-amino acids is nearer the wide rim of CD, being oriented toward the narrow rim for D-amino acids. If we consider the unit vector defined by the chiral center of amino acids and the most distant C atom of the chain, the angles in spherical coordinates $(\theta, \varphi)$ formed by the enantiomers with respect to the absolute reference system are shown in **Table 2**. The configurations of L-Val, D-Ile and L- and D-Leu agree with the results of Ramirez et al. (2000) regarding inclusion complex formation, and the lowest energy structure of complexes in gas-phase.

## Molecular Dynamics Simulation

To determine the elution order, retention time and capacity for inclusion complex formation in MD, some trajectories (20) are calculated, starting from different initial conditions. In each trajectory, the molecule usually moves toward the β-CD and only in a few cases does not enter the cavity and remain a short time near β-CD (external trajectories). In most cases, the guest enters the CD, where it remains totally or partially during some period of time (residence time) and then moves away. The external trajectories have been excluded from the calculations in the simulation, because the utility of CDs for catalysis and separation processes is based on their capacity to form inclusion complexes. The initial disposition of enantiomers influences the evolution of guests in the trajectories and then the binding free energy and elution order. Therefore, the starting positions and orientations of enantiomers must be selected in such a way that the differences in their simulation were mainly due to their mirror image structures, instead of the calculation method. In the present study, the starting dispositions are determined by minimizing the difference in atomic positions and interaction energies. Furthermore, to compare the results of different amino acids, the same initial conditions (configurations and velocities) are considered. The evolution of enantiomers in each trajectory is due both to the initial disposition and molecular characteristics. In fact, only L-Ala and D-Val have not external trajectories, in spite of the same initial conditions for the amino acids. The probability of remaining outside the cavity is greater when the guest starts from dispositions near the narrow rim, with the carboxylic end pointing toward the cavity.

The elution order is determined from the average binding free energy, which is obtained for each trajectory $F$ in the simulation. The results are shown in **Figure 4** except for external trajectories (**Table 3**). The values of $F$ are substantially lower for inner than outer trajectories, where $F$ can even become positive. These results confirm that the ability of CDs to perform catalysis and separation processes is due to their inner cavity. The same initial conditions produce different energies $F$ for each molecule because $F$ is related to the guest evolution in the trajectories, which is due in turn to the molecular structure and composition. The binding free energy for each amino acid in the simulation

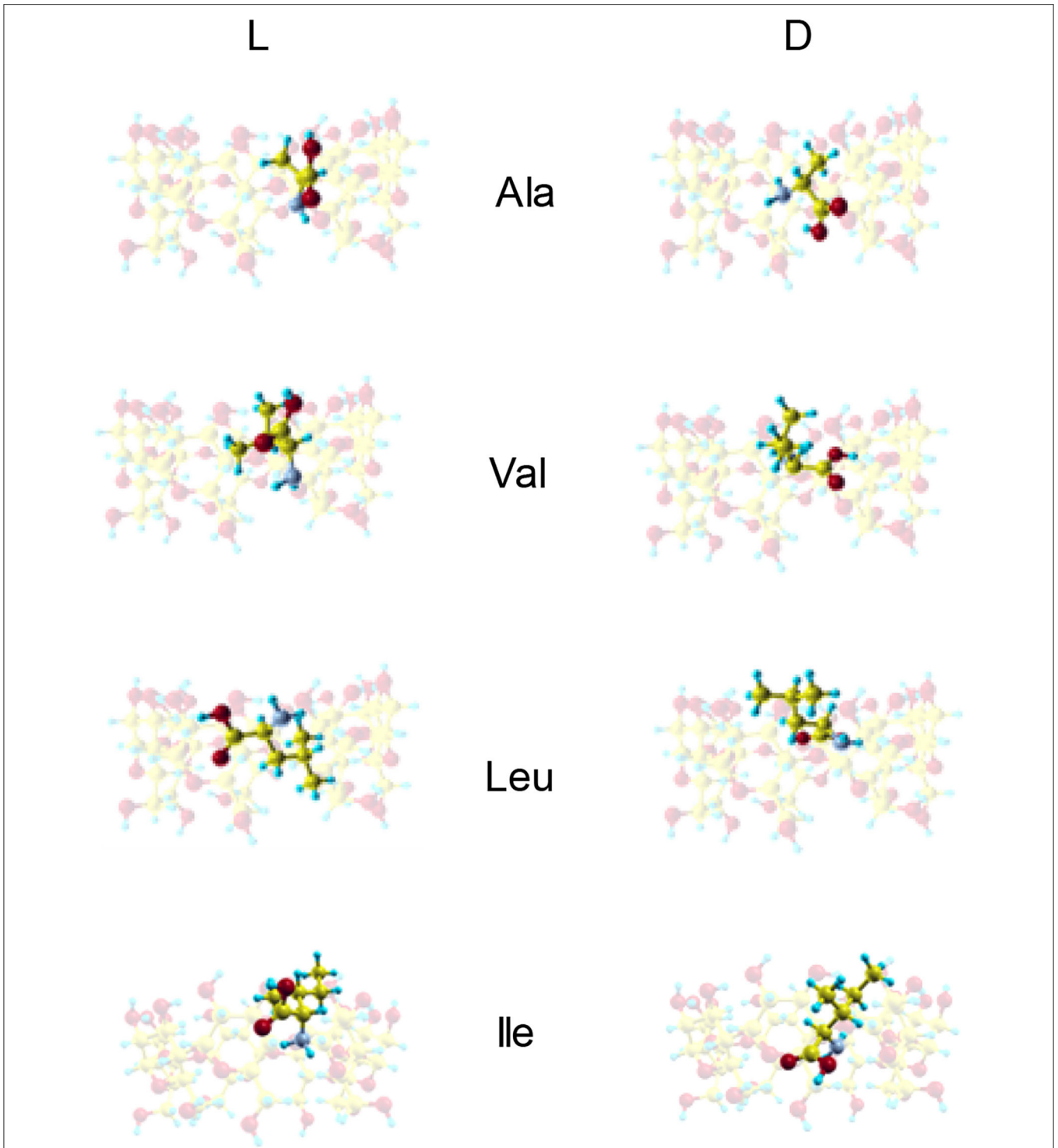


**FIGURE 3 |** The configurations of the complexes with minimum interaction energy formed by β-CD and the amino acids in vacuo obtained from molecular mechanics. The guest molecule has been superimposed for clarity, but it is always located inside the cavity.

$F_{mean}$ is determined as the average value of $F$, considered only the inner trajectories (**Table 3**). D-Valine is the amino acid with the lowest energy $F_{mean}$, while L-Leu has the greatest value, moreover $F$ is lower for D- than L-enantiomer of Val and Ile in every trajectory. The difference in $F_{mean}$ for the enantiomers $\Delta F_{mean}$ of each amino acid increases in the order Leu < Ala <

**TABLE 2 |** The guest center of mass positions and angles in the configurations of the complexes with $E_{min}$ formed in vacuo by β-CD with the amino acids.

| Amino acids | Center of mass (x, y, z) | | Angles ($\theta, \varphi$) | |
|---|---|---|---|---|
| | L | D | L | D |
| Ala | (0.6, −1.5, 0.3) | (0.7, −0.7, −0.6) | (51.80°, 63.63°) | (49.16°, 315.90°) |
| Val | (0.1, −1.2, 0.9) | (0.0, −0.5, 0.7) | (38.96°, 125.95°) | (46.72°, 20.18°) |
| Leu | (−0.6, −0.2, 0.1) | (−0.4, −0.1, 1.4) | (94.21°, 321.21°) | (61.80°, 168.17°) |
| Ile | (1.7, −0.4, 2.7) | (1.1, −0.9, 0.7) | (69.68°, 130.50°) | (43.29°, 270.93°) |

Val < Ile, so if the capacity of β-CD to discriminate is related to this magnitude, Ile exerts the clearest enantiodiscrimination. The elution order is obtained from $\Delta F_{mean}$, the molecule least bound to β-CD (greater $F_{mean}$) spends less time inside the cavity. The first eluted enantiomer in vacuo for each guest is the L-amino acid, in agreement with the experimental findings and molecular simulation provided by Ramirez et al. (2000). The present study is also in accordance with theirs in that the chiral discrimination increases with the size of amino acids, except in the case of Leu, for which they obtained the same selectivity as Ile. The average residence time $t_{\mathrm{mean}}$ for each amino acid in the simulation (**Table 3**) is not directly related to $F_{mean}$, as can be deduced from the fact that Leu has greater residence times but lesser free energy. This question can be justified because $F_{mean}$ depends on the interaction energy with β-CD and then on the guest dispositions during the trajectories. However, the amino acids are not always able to adopt the orientation with minimum energy in each location. Therefore, the guest can stay totally or partially inside the cavity but with configurations other than the minima. The greatest difference in $t_{\mathrm{mean}}$ between enantiomers is that for Ile, in accordance with $\Delta F_{mean}$, then Leu, Ala and finally Val. However, the new feature introduced by the present study is that the first eluted enantiomers also spend shorter times inside the cavity. The agreement between the elution order and $t_{\mathrm{mean}}$ was not achieved in our previous studies of amino acids, and this issue also confirms the improvement of the simulation method applied in the present research.

Both $F_{mean}$ and $t_{mean}$ indicate that the complexes formed by β-CD and the amino acids are inclusion complexes, as predicted by other authors (Ramirez et al., 2000; Lee et al., 2017), and the most probable configurations in MD are deduced from the position probability density (Lipkowitz et al., 1997a,b). The location where the guest center of mass spends most time in the simulation is the center of the cavity for Ala and Val, but Leu and Ile remain near the wide rim (L-Leu, D-Ile) or the narrow rim (D-Ile, L-Ile) of β-CD (**Figure 5**). The capacity of guest molecules to move freely within the CD is related to their size and structure, among other factors. Ala and Val can move through the cavity and then the preferred center of mass position does not depend on the initial disposition of amino acids. The most probable zones for the guest in the inclusion complexes formed by Ala and Val are stable positions with lower interaction energies and also slightly enantioselective regions. The molecule is rotating continually along the trajectories, but the most frequent guest orientation for Ala and Val locates the carboxylic end pointing toward the narrow rim of β-CD (**Figure 5**) (Kokalj, 2003). The guest molecule has been superimposed in **Figure 5** for clarity, but it is always located inside the cavity. The configurations of D-enantiomers are similar to the absolute minima energies, and only L-Val is in accordance with that proposed by Ramirez et al. (2000). There are two regions where Leu and Ile remain more time in the simulation, near each rim of β-CD. This can be explained by the existence of a barrier potential in the energy W, related to the molecular orientation with respect to the cavity axis. Alanine and Val remain in zones that are not so enantioselective, whereas Leu and Ile frequent regions with great chiral discrimination. Since Leu and Ile are unable to rotate freely inside the cavity, their evolution through the simulation depends on their initial orientation and which rim of CD they approach from Alvira (2019). The greater residence times for Leu and Ile correspond to trajectories with initial dispositions of the amino acid near the wide rim and with the amino end pointing to β-CD. However, in the preferred locations of these amino acids, the carboxylic end is near the narrow rim of the cavity (**Figure 5**) (Kokalj, 2003). The most probable configuration of the complexes formed by Ile and β-CD can explain their clearest enantiodiscrimination, since this amino acid possesses two chiral centers, whose interactions with β-CD contribute more significantly to the energy. Therefore, whereas only one chiral center of L-Ile is near the cavity, the two chiral centers of D-Ile are located inside, increasing the difference in energy with L-Ile. The host-guest complexes formed by D-Leu and D-Ile are consistent with those proposed by Ramirez et al. (2000), and the configuration of D-Ile is also similar to that of minimum energy obtained by MM.

## CONCLUSIONS

The inclusion complexes formed by β-cyclodextrin and some amino acids in vacuo, as well as the chiral separation of these enantiomers, are simulated in this study by molecular mechanics and dynamics. The greatest contribution to the interaction energy obtained from MM is the van der Waals term, although the discrimination between the enantiomers is due mainly to the electrostatic energy. The configurations of absolute minimum energy for the amino acids correspond to inclusion complexes, in which the carboxylic end is near the wide rim of β-CD for L-enantiomers and pointing toward the narrow rim for D-enantiomers. The differences in the potential energy surfaces indicate the more enantioselective regions, which are located near the cavity walls in every case. However, the zones where each enantiomer is more stable depend on the size of amino acids: while L-Ala is more stable in wider zones outside the CD, L-Ile has lower energies inside the cavity.

The elution order, capacity to form inclusion complexes, and residence times are determined in MD by the calculation of some trajectories with different initial conditions. The elution order obtained from the average binding free energy indicates

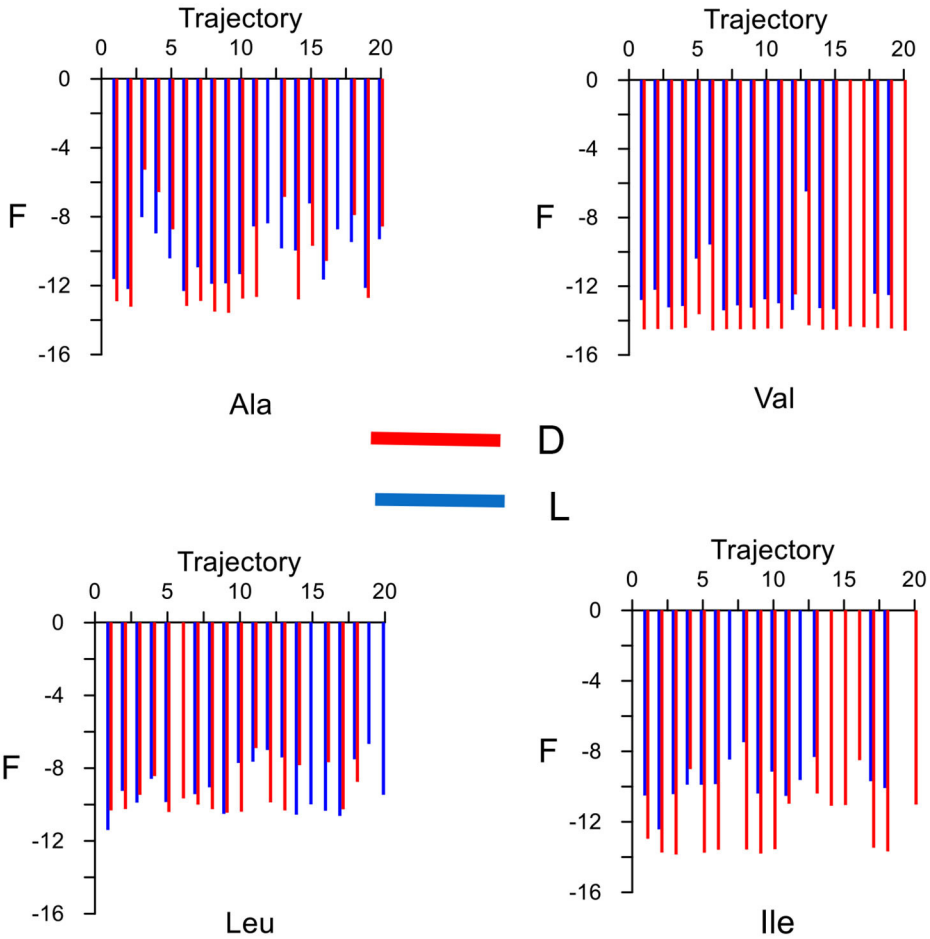


**FIGURE 4 |** The average binding free energy for each amino acid derived from the trajectories in the molecular dynamics simulation. The external trajectories are excluded.

**TABLE 3 |** The average binding free energy $F_{mean}$, elution order and average residence time $t_{mean}$ obtained for each enantiomer in the molecular dynamics simulation.

| Amino acids | Number of trajectories | | $F_{mean}$(kcal/mol) | | Elution order | $t_{mean}$ (ps) | |
|---|---|---|---|---|---|---|---|
| | L | D | L | D | | L | D |
| Ala | 20 | 18 | −10.23 ± 1.56 | −10.78 ± 2.72 | L | 476.27 | 1683.71 |
| Val | 17 | 20 | −12.24 ± 1.77 | −14.32 ± 0.47 | L | 3400.55 | 4484.07 |
| Leu | 19 | 17 | −9.09 ± 1.37 | −9.47 ± 1.13 | L | 1682.58 | 3165.90 |
| Ile | 15 | 17 | −9.77 ± 1.11 | −12.22 ± 1.76 | L | 751.13 | 4582.92 |

that L- is the first eluted enantiomer of amino acids, and the chiral discrimination increases in the order Leu < Ala < Val < Ile. The position probability density indicates the formation of inclusion complexes whose configurations are similar for the amino acids, inside and along the cavity axis, with the carboxylic end pointing toward the narrow rim of β-CD. During the simulation, Ala and Val remain in zones that are not so enantioselective, whereas Leu and Ile occupy regions with great chiral discrimination. Some of the results from the present research are in agreement with those proposed by Ramirez et al.: the lowest energy structure of complexes obtained from MM for L-Val, D-Ile, and L- and D-Leu; the elution order, inclusion complex formation, and the dependence of selectivity on the size of amino acids (except Leu) from MD. The improvement in the simulation method can be confirmed by the results obtained for Ala, Val, Leu, and Ile in vacuo, completely different from

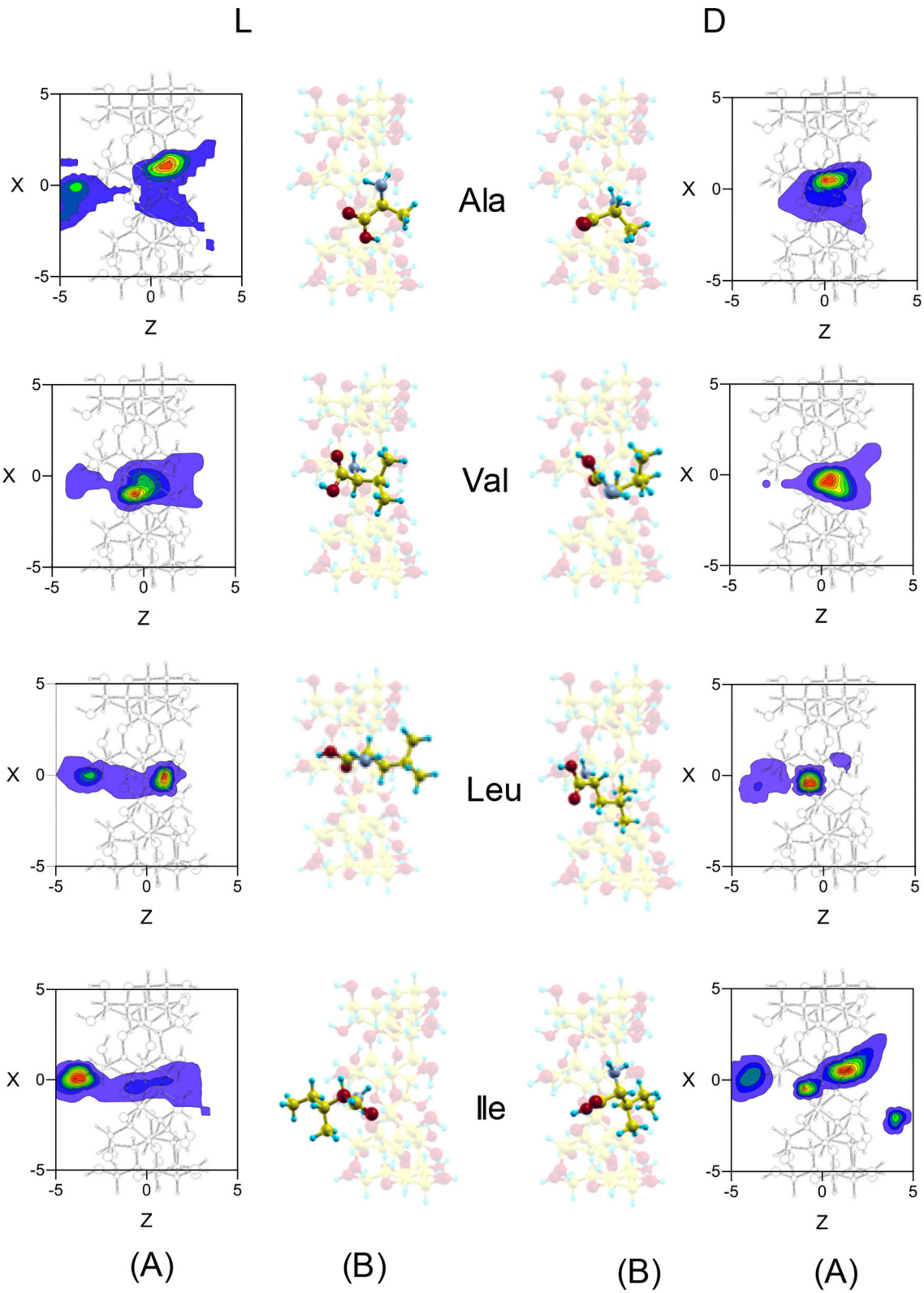


**FIGURE 5 | (A)** The projections in the XZ plane of the position probability densities for the enantiomers of amino acids obtained from the molecular dynamics simulation. A schematic representation is included of the projection of β-CD in that plane. **(B)** The most probable configurations of the complexes formed by β-CD and the amino acids in vacuo, obtained from the molecular dynamics simulation. The guest molecule has been superimposed for clarity, but it is always located inside the cavity.

our previous results. However, the model proposed must be tested by new studies with more amino acids and other types of molecules.

## DATA AVAILABILITY STATEMENT

All datasets generated for this study are included in the article/supplementary material.

## AUTHOR CONTRIBUTIONS

The author confirms being the sole contributor of this work and has approved it for publication.

## FUNDING

This research was funded by the Ministerio de Economía y Competitividad (FIS2016-79596-P, AEI/FEDER, UE).

## REFERENCES

Allen, M. P., and Tildesley, D. J. (1987). *Computer Simulation of Liquids*. Oxford: Clarendon Press.

Alvira, E. (2013). Molecular dynamics study of the influence of solvents on the chiral discrimination of alanine enantiomers by β-cyclodextrin. *Tetrahedron Asymm.* 24, 1198–1206. doi: 10.1016/j.tetasy.2013.08.006

Alvira, E. (2015). Theoretical study of the separation of valine enantiomers by β-cyclodextrin with different solvents: a molecular mechanics and dynamics simulation. *Tetrahedron Asymm.* 26, 1198–1206. doi: 10.1016/j.tetasy.2015.06.013

Alvira, E. (2017a). Influence of solvent polarity on the separation of leucine enantiomers by β-cyclodextrin: a molecular mechanics and dynamics simulation. *Tetrahedron Asymm.* 28, 1414–1422. doi: 10.1016/j.tetasy.2017.09.020

Alvira, E. (2017b). Influence of valine enantiomer configuration on the molecular dynamics simulation of their separation by β-cyclodextrin. *Chem. Phys. Lett.* 679, 31–37. doi: 10.1016/j.cplett.2017.04.062

Alvira, E. (2019). Molecular simulation of the separation of isoleucine enantiomers by β-cyclodextrin. *Molecules* 24, 1021–1034. doi: 10.3390/molecules24061021

Boniglia, C., Carratù, B., and Sanzini, E. (2002). Enantiomer separation of D-L branched amino acids by capillary electrophoresis in sport nutritional supplements. *J. Food Sci.* 67, 1352–1355. doi: 10.1111/j.1365-2621.2002.tb10287.x

Brown, D., and Clarke, J. H. R. (1984). A comparison of constant energy, constant temperature and constant pressure ensembles in molecular dynamics simulations of atomic liquids. *Mol. Phys.* 51, 1243–1248. doi: 10.1080/00268978400100801

Fincham, D., Quirke, N., and Tildesley, D. J. (1986). Computer simulation of molecular liquid mixtures. I. A diatomic Lennard-Jones model mixture for $CO_2/C_2H_6$. *J. Chem. Phys.* 84, 4535–4541. doi: 10.1063/1.450824

Frenkel, D., and Smit, B. (2002). *Understanding Molecular Simulation*. San Diego: Academic Press.

Kinglert, B., and Rihs, G. J. (1991). Molecular encapsulation of transition metal complexes in cyclodextrins. Part 3. Structural consequences of varying the guest geometry in channel-type inclusion compounds. *J. Chem. Soc. Dalton Trans.* 10, 2749–2760. doi: 10.1039/dt9910002749

Kokalj, A. (2003). Computer graphics and graphical user interfaces as tools in simulations of matter at the atomic scale. *Comp. Mater. Sci.* 28, 155–168. doi: 10.1016/S0927-0256(03)00104-6

Lee, S.-S., Park, S., Hong, Y., Lee, J.-U., Kim, J.-H., Yoon, D., et al. (2017). Chiral differentiation of D- and L-alanine by permethylated β-cyclodextrin: IRMPD spectroscopy and DFT methods. *Phys. Chem. Chem. Phys.* 19, 14729–14737. doi: 10.1039/C7CP01085K

Lindorff-Larsen, K., Piana, S., Palmo, K., Maragakis, P., Klepeis, J. L., Dror, R. O., et al. (2010). Improved side-chain torsion potentials for the AMBER ff99SB protein force field. *Proteins* 78, 1950–1958. doi: 10.1002/prot.22711

Lipkowitz, K. B. (1998). Applications of computational chemistry to the study of cyclodextrins. *Chem. Rev.* 98, 1829–1873. doi: 10.1021/cr9700179

Lipkowitz, K. B. (2001). Atomistic modeling of enantioselection in chromatography. *J. Chromatogr. A* 906, 417–442. doi: 10.1016/S0021-9673(00)00946-8

Lipkowitz, K. B., Coner, B., and Peterson, M. A. (1997b). Locating regions of maximum chiral discrimination: a computational study of enantioselection on a popular chiral stationary phase used in chromatography. *J. Am. Chem. Soc.* 119, 11269–11276. doi: 10.1021/ja972327e

Lipkowitz, K. B., Pearl, G., Coner, B., and Peterson, M. A. (1997a). Explanation of where and how enantioselective binding takes place on permethylated β-cyclodextrin, a chiral stationary phase used in gas chromatography. *J. Am. Chem. Soc.* 119, 600–610. doi: 10.1021/ja963076x

Maier, N. M., Franco, P., and Lindner, W. (2001). Separation of enantiomers: needs, challenges, perspectives. *J. Chromatogr. A* 906, 3–33. doi: 10.1016/S0021-9673(00)00532-X

Ramanathan, R., and Prokai, L. (1995). Electrospray ionization mass spectrometric study of encapsulation of amino acids by cyclodextrins. *J. Am. Soc. Mass Spectrom.* 6, 866–871. doi: 10.1016/1044-0305(95)00482-S

Ramirez, J., Ahn, S., Grigorean, G., and Lebrilla, C. B. (2000). Evidence for the formation of gas-phase inclusion complexes with cyclodextrins and amino acids. *J. Am. Chem. Soc.* 122, 6884–6890. doi: 10.1021/ja000717m

Rapaport, D. C. (1995). *The Art of Molecular Dynamics Simulation*. Cambridge: Cambridge University Press.

Roy, M. N., Roy, A., and Saha, S. (2016). Probing inclusion complexes of cyclodextrins with amino acids by physicochemical approach. *Carbohydr. Polym.* 151, 458–466. doi: 10.1016/j.carbpol.2016.05.100

Sebestyén, Z., Buvári-Bareza, A., and Rohonczy, J. (2012). pH-Dependent complex formation of amino acids with β-cyclodextrin and quaternary ammonium β-cyclodextrin. *J. Incl. Phenom. Macrocycl. Chem.* 73, 199–210. doi: 10.1007/s10847-011-0043-2

Stepniak, P., Lainer, B., Chmurski, K., and Jurczak, J. (2017). pH-Controlled recognition of amino acids by urea derivatives of β-cyclodextrin. *RSC Adv.* 7, 15742–15746. doi: 10.1039/C7RA02127E

Szejtli, J., and Osa, T. (1996). *Comprehensive Supramolecular Chemistry*. Oxford: Pergamon/Elsevier.

Weiner, S. J., Kollman, P. A., Case, D. A., Singh, U. C., Ghio, C., Alagona, G., et al. (1984). A new force field for molecular mechanical simulation of nucleic acids and proteins. *J. Am. Chem. Soc.* 106, 765–784. doi: 10.1021/ja00315a051

Weiner, S. J., Kollman, P. A., Nguyen, D. T., and Case, D. A. (1986). An all atom force field for simulations of proteins and nucleic acids. *J. Comp. Chem.* 7, 230–252. doi: 10.1002/jcc.540070216

Werner, H.-J., Knowles, P. J., Knizia, G., Manby, F. R., and Schütz, M. (2012a). Molpro: a general-purpose quantum chemistry program package. *WIREs Comput. Mol. Sci.* 2, 242–253. doi: 10.1002/wcms.82

Werner, H.-J., Knowles, P. J., Knizia, G., Manby, F. R., and Schütz, M. (2012b). *MOLPRO, version.1, a Package of Ab initio Programs*.

Zia, V., Rajewski, R. A., and Stella, V. J. (2001). Effect of cyclodextrin charge on complexation of neutral and charged substrates: comparison of $(SBE)_{7M}$-β-CD to HP-β-CD. *Pharm. Res.* 18, 667–673. doi: 10.1023/A:1011041628797

**Conflict of Interest:** The author declares that the research was conducted in the absence of any commercial or financial relationships that could be construed as a potential conflict of interest.

frontiers in Chemistry

ORIGINAL RESEARCH
published: 23 October 2020
doi: 10.3389/fchem.2020.582757

# Supramolecular Encapsulation of a Neurotransmitter Serotonin by Cucurbit[7]uril

*Falguni Chandra*†, *Tanoy Dutta*† *and Apurba L. Koner**

*Bionanotechnology Laboratory, Department of Chemistry, Indian Institute of Science Education and Research Bhopal, Bhopal, India*

pH-dependent host-guest complexation of a monoamine neurotransmitter, Serotonin, with cucurbit[7]uril has been thoroughly investigated. The binding phenomena were explored using steady-state and time-resolved fluorescence spectroscopy at different pH values. At lower pH, i.e., protonated Serotonin, the binding affinity with cucurbit[7]uril was significantly higher compared to higher pH. Furthermore, detailed NMR titration experiments depicted the solution structure of the host-guest complex through the complexation induced chemical shift values. A competitive binding assay with cesium ions at pD 2.8 was subsequently performed for the further manifestation of the binding. Finally, the molecular docking studies provided well-documented proof of the 1:1 inclusion complex and the geometry of the complex. We believe that understanding from such studies can be important for pH-controlled delivery of serotonin for biological applications.

**Keywords: supramolecular encapsulation, cucurbit[7]uril, neurotransmitter, serotonin, complexation induced NMR shift, competitive assay, drug delivery**

OPEN ACCESS

***Edited by:***
*Pavel Padnya,*
*Kazan Federal University, Russia*

***Reviewed by:***
*Jyotirmayee Mohanty,*
*Bhabha Atomic Research Centre (BARC), India*
*Debapartim Das,*
*Indian Institute of Technology Guwahati, India*
*Ruibing Wang,*
*University of Macau, China*
*Xin Xiao,*
*Guizhou University, China*

***Correspondence:**
*Apurba L. Koner*
*akoner@iiserb.ac.in*

†*These authors have contributed equally to this work*

***Specialty section:***
*This article was submitted to Supramolecular Chemistry, a section of the journal Frontiers in Chemistry*

***Received:*** *13 July 2020*
***Accepted:*** *16 September 2020*
***Published:*** *23 October 2020*

***Citation:***
*Chandra F, Dutta T and Koner AL (2020) Supramolecular Encapsulation of a Neurotransmitter Serotonin by Cucurbit[7]uril. Front. Chem. 8:582757. doi: 10.3389/fchem.2020.582757*

## INTRODUCTION

Serotonin (5-hydroxytryptamine, SRT, for structure see **Figure 1A**) is a naturally occurring tryptamine derivative and biogenic amine acts as a neurotransmitter for both central as well as the peripheral nervous system. It was discovered by an Italian pharmacologist Vittorio Erspamer in 1952, identifying enteramine as 5-hydroxytryptamine (Erspamer and Asero, 1952). Later, SRT was synthesized by a second tryptophan hydroxylase isoform (Walther et al., 2003). It is exclusively found in all types of mammals including the human gastrointestinal tract, blood platelets, and nervous system. Approximately 80–90% of the total SRT is located in the enterochromaffin cells in the gut of humans and the remaining 10–20% is synthesized in serotonergic neurons in the Central Nervous System (CNS) and blood platelets (Mawe and Hoffman, 2013; Lv and Liu, 2017). SRT is widely distributed in the brain (Carhart-Harris and Nutt, 2017) and controls a variety of physiological and behavioral processes e.g., sleep, addiction, sexual activity, aggression, locomotion, anxiety, cognition, and food intake (Veenstra-Vanderweele et al., 2000; Berger et al., 2009). Especially, the food intake takes a significant dip due to activated serotonergic activity causing short-term food deprivation (Johnston and Glanville, 1992; Ruibal et al., 2002). The unwanted disruption of SRT balance in body systems may cause mental disorders such as Alzheimer's disease, infantile autism, schizophrenia, and depression (Dubovsky and Thomas, 1995; Voet and Voet, 2006). SRT is intrinsically fluorescent in the living

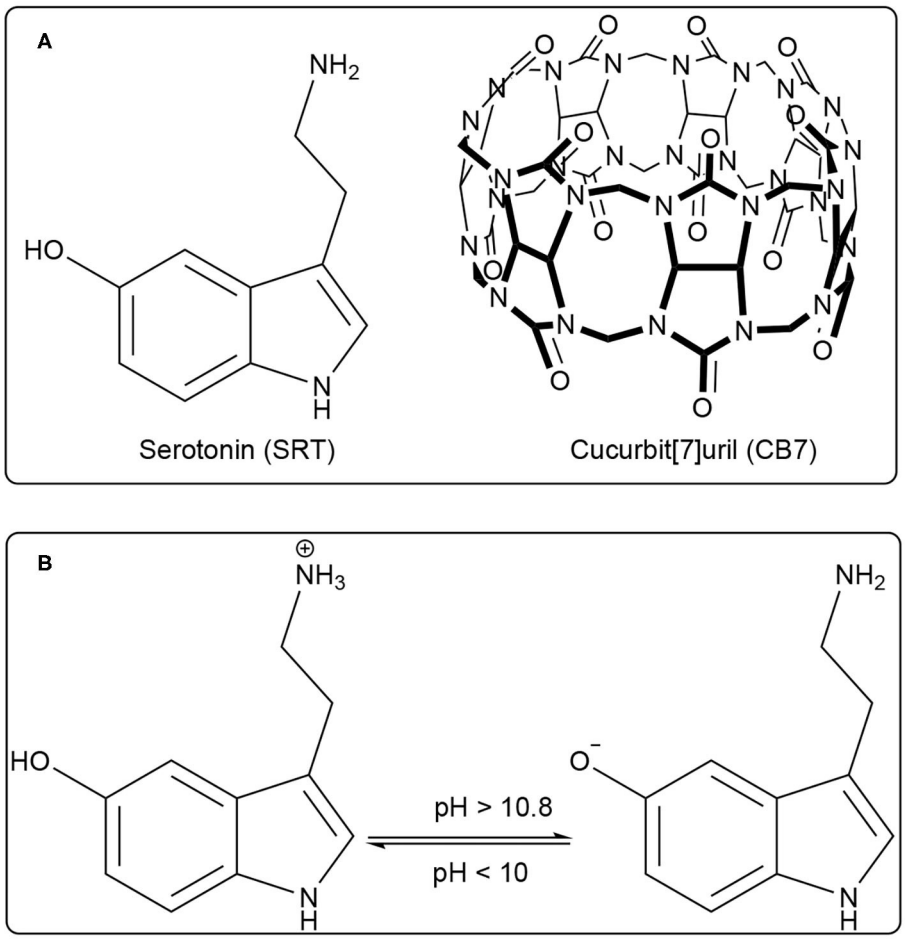


**FIGURE 1 | (A)** Chemical structure of Serotonin (SRT, guest) and Cucurbit[7]uril (CB7, host), **(B)** Prototropic equilibrium of SRT with different pH.

system and it emits around 335 nm (Hernandez-Mendoza et al., 2020). Kishi and co-workers reported that the SRT shows different fluorescence properties at various pH values (Kishi et al., 1977). Chattopadhyay and co-workers reported a detailed characterization of its photophysical properties upon modulation by ionization and polarity of the medium (Chattopadhyay et al., 1996). Various literature reported that the SRT has two acid dissociation constant ($pK_a$) value, i.e., one is 9.97 for an aliphatic amino group and 10.73 (see **Figure 1B**) for an aromatic hydroxyl moiety (Chattopadhyay et al., 1996; Pratuangdejkul et al., 2006). Ouyang and Vogel studied the interaction of SRT with metal-binding protein calmodulin using UV-Vis., fluorescence, and NMR spectroscopic techniques (Hui and Vogel, 1998). Considering the biological importance of SRT, its delivery using a supramolecular approach will be highly desirable for the therapies associated with SRT syndrome.

Water-soluble macrocyclic host molecules are very important for encapsulating polar and non-polar guest molecules with an offering of a hydrophobic cavity. Macrocycle molecules can have a quite rigid and well-defined cavity which can strongly encapsulate hydrophobic drug molecules with reasonable binding constant. The macrocyclic host molecules build a supramolecular host-guest system which provides an opportunity to study the nature of intermolecular interactions (Dsouza et al., 2011). Interestingly, the host-guest complexation is untangling of the dynamic nature of the formation of simple supramolecular assembly. The interaction of small organic molecules with a macrocyclic water-soluble host molecule is the prototype example of supramolecular interaction. Calixarenes, cyclodextrins, charged-cyclophane, and crown ethers, the popular drug-delivery carriers, are water-soluble macrocyclic host molecules and they have variable cavity size which is of nano-dimension with changing the monomer unit (Ghosh and Nau, 2012; Zhang et al., 2020). In comparison, a new class of water-soluble macrocyclic host molecule, cucurbit[n]urils (CBn, $n = 5$–10) are composed with "$n$" glycoluril units bridged by methylene groups (Nau et al., 2011). CBn has two symmetrical portals made of "$n$" carbonyl groups. CB7 has seven carbonyl groups presented in both the portals (**Figure 1A**). Both the portals of CBn are capable of binding positively charged molecules or ions. The cationic guest molecules comprising of a hydrophobic part are encapsulated in the hydrophobic

nano-cavity of CBn driven by ion-dipole interaction, hydrogen bonding with carbonyl portals (Mondal et al., 2015; Ahmed et al., 2016; Yin and Wang, 2018). Such encapsulation causes a significant shift in the acid-dissociation constant and can effectively cause enhanced solubility of the guest, controlled release for drug delivery applications, and sensing using electronic spectroscopy for optically active molecules (Saleh et al., 2008, 2011, 2016; Wang et al., 2009; Koner et al., 2011; Ghosh and Nau, 2012; Lazar et al., 2016; Mallick et al., 2016; Kuok et al., 2017; Yin et al., 2017; Das et al., 2019; Wu et al., 2019) The formation of ternary complex with guest molecues and CBn is frequently obtained and formation of such the complexes have produced multifaceted applications (Bhasikuttan et al., 2007; Choudhury et al., 2010; Barooah et al., 2017). In last decade, new derivatives of CB are getting significant popularity and showed immense potential for various applications (Dsouza et al., 2011; Cong et al., 2016; Gao et al., 2017; Liu et al., 2019a,b).

Of late, our group reported the detailed photophysical properties of anti-malarial drug Quinine and $\beta$-carboline-based drug Norharmane upon binding with CB7 (Mallick et al., 2016; Chandra et al., 2018). The encapsulation resulted in greater solubility and excited state p$K_a$ shift in both the cases which impacts reduced phototoxicity, improved bioavailability of the drug molecules. In view of further advancement in this field, we took interest in serotonin (SRT) which has manifold roles in our physiological system. We have studied the complexation of SRT by CB7 using UV-Vis. and fluorescence spectroscopy, time-resolved anisotropy, NMR spectroscopy, and molecular docking studies. A significant difference in pH-dependent binding affinity of SRT was observed upon CB7 encapsulation. As the complexation-induced chemical shifts helped to understand the orientation of SRT inside the CB7 cavity, the docking studies provided with the complex geometry along with the stoichiometry.

## MATERIALS AND PHYSICAL METHODS

Serotonin (5-hydroxytryptamine) was purchased from Alfa Aesar (USA). HCl and NaOH were purchased from SDFCL, India) and Rankem, India, respectively. The pH of the solutions was adjusted using dilute HCl and NaOH solution. $D_2O$, DCl, and NaOD were purchased from Sigma Aldrich, USA. All chemicals were used as received without any further purification. CB7 was synthesized and purified according to the previous report (Marquez et al., 2004) and characterized by $^1$H NMR spectroscopy and mass spectrometry. The experiments in water were carried out using Milli-Q grade water using Milli-Q water purification set up from Merck (USA) with resistivity 18.2 MΩ·cm at 298 K.

### Steady-State Absorption and Fluorescence Spectroscopy Experiments

All steady-state absorption and fluorescence measurements were carried out using Cary 5000 UV-Vis. spectrophotometer (Agilent Technologies) and HORIBA Jobin Yvon Fluorolog 3 instrument, respectively. Fluorescence spectra were recorded from 290 to 450 nm by exciting at 280 nm. All measurements were performed with a 1 cm path length quartz cuvette keeping both excitation and emission slit width 2 nm. All the experiments were carried out using a 10 μM SRT at room temperature (298 K). A concentrated stock solution of 1 mM SRT was prepared in Milli-Q water and diluted accordingly using Milli-Q water for absorption and fluorescence spectroscopic measurements. A dilute solution of the dye was taken for all the measurements to keep the absorption value low to avoid the inner filter effect. pH titrations by UV-Vis and fluorescence were performed in Milli-Q water and the pH/pD of the solution was adjusted by adding a minimal amount of concentrated HCl/DCl and NaOH/NaOD solution in water to avoid any dilution effect. The pH/pD was also measured at the end of the titration to test the pH/pD stability during titration.

### Time-Resolved Experiments

Time-resolved fluorescence and anisotropy decay measurement were performed using a Hamamatsu MCP photomultiplier (R-3809U-50). The time-correlated single-photon counting (TCSPC) setup consists of an Ortec 9327 pico-timing amplifier and using a pulsed Diode laser ($\lambda_{ex} = 280$ nm) with fwhm ∼143 ps with a setup target 10,000 counts. The instrument response function (IRF) was collected using a dilute suspension of Ludox (colloidal silica, purchased from Sigma Aldrich). The emission and excitation polarizer was set at a magic angle (54.75°) to each other. The mono and bi-exponential fitting functions were employed by iterative deconvolution method using software DAS v6.2. The quality of the fitted data was judged from the reduced chi-squared value ($\chi^2$), calculated using the IBH software provided with the instrument. Following is the type of fitting function used.

$$\frac{\mathbf{I(t)}}{\mathbf{I(0)}} = \sum \mathbf{a_i} \mathbf{ex}\,\mathrm{p}\left(\frac{-\mathbf{t}}{\tau_\mathbf{i}}\right)$$

### NMR Titration

$^1$H NMR spectra were recorded using Bruker Avance III 400 MHz NMR spectrometer. Chemical shifts (δ) values are reported in ppm. All NMR titrations were performed in $D_2O$ at 298 K and the pD value of the solution was adjusted using NaOD and DCl. Dilute solutions of NaOD and DCl were prepared by diluting their concentrated stock in $D_2O$. For NMR titration, the concentration of SRT was kept fixed to 0.5 mM in $D_2O$ and a concentrated stock solution of CB7 with same pD value was added accordingly to get the desired concentration. All NMR spectra from a binding titration were obtained on the same day and the data was collected immediately after making the respective solution.

### Molecular Docking

Molecular docking studies of SRT•CB7 inclusion complex was performed using the PatchDock server (Duhovny et al., 2002; Schneidman-Duhovny et al., 2005). The input files were optimized initially and uploaded to the server in PDB format. PatchDock uses different sets of parameters for the complex type field settings to automatically determine complementarity

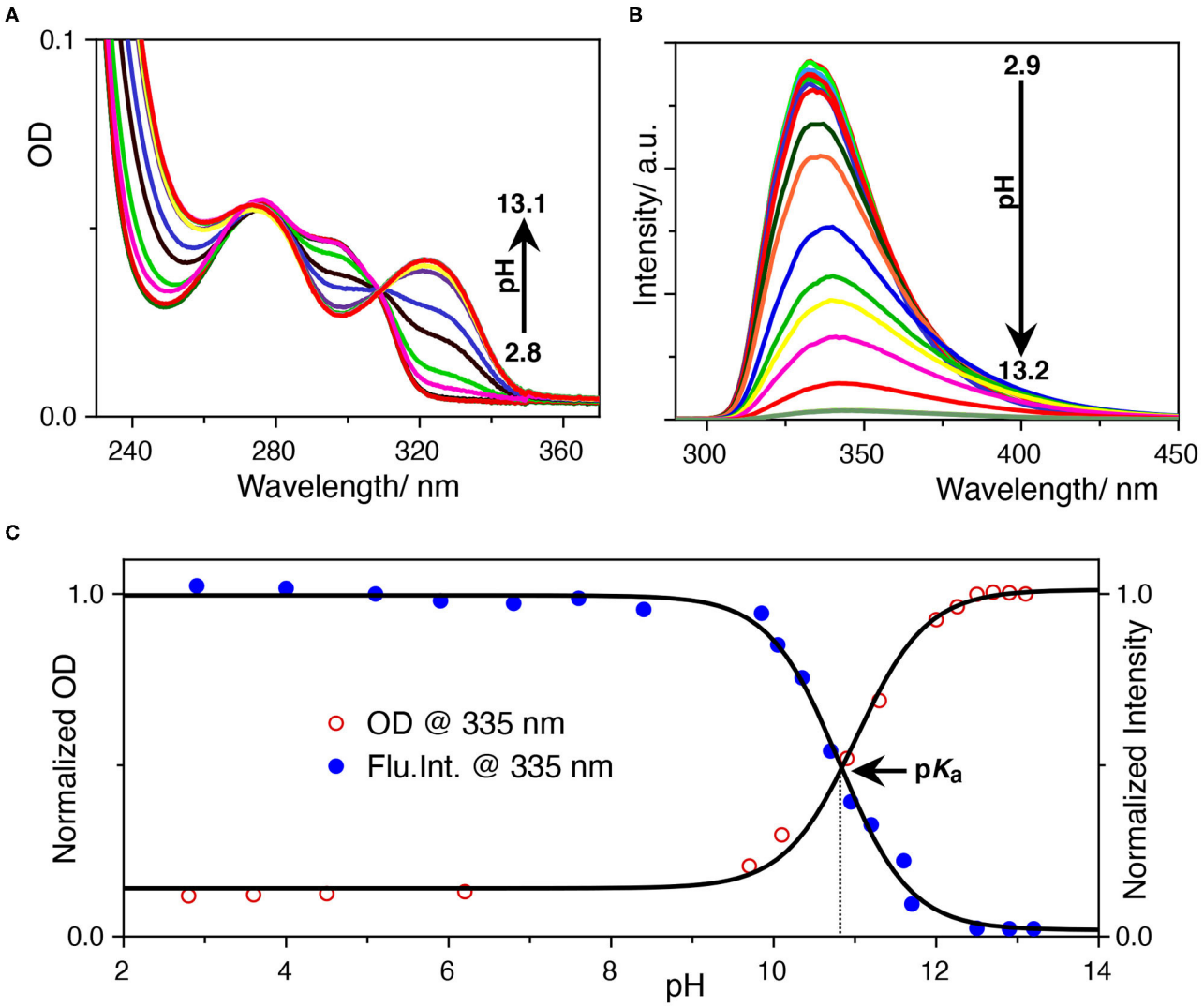


**FIGURE 2 | (A)** UV-Vis.-based pH titration, the 333 nm absorption peak increases with pH, **(B)** fluorescence-based pH titration, the fluorescence peak at 335 nm decreases with pH, **(C)** determination of the p$K_a$ value from UV-Vis. and fluorescence titration. The normalized optical density at 333 nm and the fluorescence intensity at 335 nm was plotted against the pH of the solution. The data points were fitted with a sigmoidal fitting function using Origin pro software to obtained the p$K_a$ value.

determining regions (CDR) of the host/receptor molecule. In the final stage of clustering, RMSD (root mean square deviation) clustering is performed to discard the superfluous modeled structures. The output is based on the geometric score, interface area size, and atomic contact energies of the docked structures.

## RESULTS AND DISCUSSIONS

### pH-Dependent UV-Vis. and Fluorescence Measurements

The photophysics of SRT is sensitive to the pH of the solution. In acidic pH, it exhibits two absorption maxima at 277 and 297 nm while increasing the pH, 297 nm band diminishes and gives rise to another one with a maxima at 325 nm (**Figure 2A**). The isosbestic point at 309 nm signifies the conversion between neutral and protonated species. The origin of the red-shifted band at 325 nm indicates an increase in the conjugation of the chromophore unit. This could only be because of the deprotonation of the hydroxyl group present at the 5-position of the indole ring. After deprotonation of the phenolic -OH group, the negative charge of the phenolate ion has participated in the ring resonance and increased the conjugation length of the indole ring. Thereafter, we have performed a sigmoidal fitting of the optical density data measured at 335 nm obtained from UV-Vis. titration. We have obtained a p$K_a$ value of 10.8 for the phenolic -OH group (**Figure 2C**). To understand the effect of pH on the emission properties of SRT, the pH-dependent fluorescence spectra were recorded upon excitation

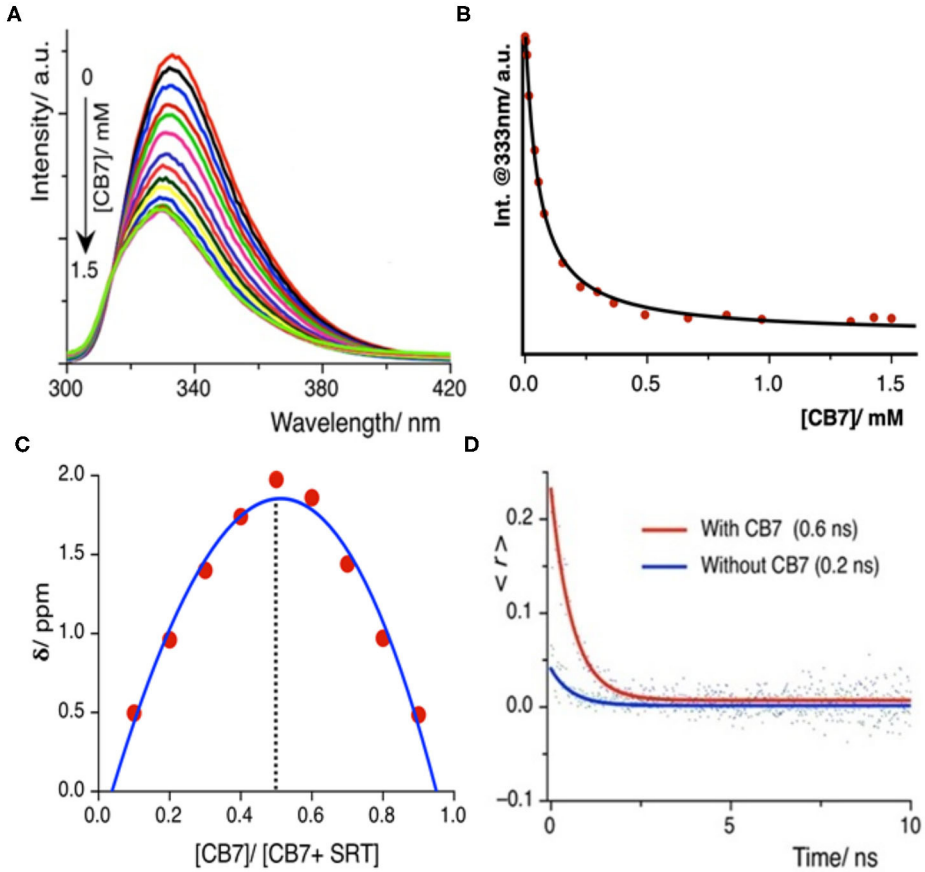


**FIGURE 3 | (A)** Fluorescence titration of SRT with CB7 at pH 3.0; intensity gradually decreases upon encapsulation, **(B)** the fitted plot using a 1:1 binding equation yields a binding constant value (23,000 ± 500) $M^{-1}$ **(C)** Job's plot using the change in chemical shift against the relative concentration of CB7 shows 1:1 binding stoichiometry, **(D)** time-resolved anisotropy decay plot of SRT in presence and absence of CB7 at pH 3.

at 280 nm at different pH. It was observed that the intensity became negligible with the increasing pH. This phenomenon can be attributed to the lower absorbance value of the ionized SRT at the excitation wavelength, which leads to the gradual decrease in the intensity above physiological pH. Similar to the absorption, we have also obtained a p$K_a$ value of 10.8 from the fluorescence titration (**Figures 2B,C**). It is reported that the p$K_a$ value of the primary amine of SRT is 9.9 (Chattopadhyay et al., 1996; Pratuangdejkul et al., 2006). So, below this pH value, the primary amine group is also protonated and bears a positive charge. The p$K_a$ value obtained from the pH titration using absorption and emission spectroscopy are identical. This indicates that there is no change in the p$K_a$ value upon electronic excitation.

## Binding Studies and Time-Resolved Anisotropic Behavior of the Complex From Fluorescence

Once we explored the pH-sensitivity in the ground and excited-state photophysical properties of SRT, the complexation with CB7 was to be well-understood. At first, we have performed a UV-Vis. titration of 5 μM SRT at pH 3.0 with an increasing concentration of CB7. This titration leads to an isosbestic point at 280 nm indicating the formation of a well-defined complex between SRT and CB7 upon encapsulation (**Supplementary Figure 1**). However, we did not observe a significant change in the absorption spectra to obtain an accurate binding constant. Thus, we have performed a fluorescence-based titration, which is known to be more sensitive toward complexation, with 10 μM SRT with an increasing concentration of CB7 at pH 3. The fluorescence intensity gradually decreased with increasing concentration of CB7 and saturation could only be achieved after the addition of 1.5 mM CB7 (**Figure 3A**). Such a decrease of fluorescence intensity indicated the formation of host-guest complex and the supramolecular environment is responsible for the attenuation of the fluorescence intensity. From this titration, we have plotted the fluorescence intensity at 333 nm against the concentration of the CB7, and the data points were fitted using a 1:1 binding equation (see **Supplementary Materials**). The fitted model provided a binding constant of 23,000 ± 500

$M^{-1}$ (**Figure 3B**). The binding stoichiometry of the complex was also confirmed experimentally by the Job's plot obtained from NMR titrations (**Figure 3C**).

The time-resolved anisotropy is also a useful tool to determine the restriction offered by the macrocyclic environment to the encapsulated guest molecule upon binding (Scholtbach et al., 2015; Chandra et al., 2016). If the host-guest complex is formed then the guest would exhibit a non-zero limiting anisotropy decay. Thus, we have measured the anisotropy of free SRT and in the presence of CB7 at pH 3. The anisotropy decay results show that at lower pH (pH∼ 3.0) the anisotropy of SRT increases from 0.2 to 0.6 ns upon treatment with CB7 (**Figure 3D**). The greater anisotropy of SRT in the presence of CB7 at lower pH indicates the hindrance of free rotation caused by the encapsulation of SRT into the hydrophobic cavity. The fluorescence lifetime of SRT did not change upon CB7 encapsulation (**Supplementary Figure 2**). To understand the binding of deprotonated SRT, we have also performed the binding titration of deprotonated SRT with CB7 at pH 12.0 using fluorescence spectroscopy (**Supplementary Figure 3**). We have avoided higher pH to reduce the interference from sodium ions from the base. A minute change in the fluorescence intensity indicated the feeble binding with CB7 which is also confirmed by NMR titration (*vide infra*). This goes along the same well-established fact that CB7 binds very weakly with negatively-charged species. Therefore, at higher pH, due to weak complexation, the anisotropy remained unchanged for SRT. The binding titration of SRT with CB7 was also performed in $D_2O$ at a lower pD. Similar to pH 3.0, we observed a quenching in SRT fluorescence upon complexation with CB7. However, the extent of quenching is lower compared to the same measured in $H_2O$ (**Supplementary Figure 4**). The binding constant obtained from these titrations is weakened by a factor of two on moving from $H_2O$ to $D_2O$ and this is in accordance with the previous report by Biedermann et al. (2013). Such a reduction in binding strength confirms a strong contribution originated from the host-guest binding enthalpy. Additionally, to understand the SRT and CB7 binding in physiological pH, we have performed fluorescence-based titration (**Supplementary Figure 5**). Not surprisingly, the binding constant values obtained in $H_2O$ and $D_2O$ are similar (**Supplementary Figures 5A–C**) to that of in lower pH as there is no structural change of the encapsulation SRT molecule.

## NMR-Based Study of SRT•CB7 Complex Formation

After investigating the binding strength of SRT with CB7 using steady-state and time-resolved fluorescence spectroscopy, we were interested to investigate the mode of binding and the structure of the complex in solution. To understand the structure of any host-guest complex in solution and the interaction between them, NMR spectroscopy is one of the best methods.

The Complexation Induced Shift (CIS) in the NMR chemical shift due to the re-location of the guest molecule in the macrocyclic host cavity can allow us to understand the nature of the interaction and geometry of the complex (Hunter and Packer, 1999; Gomila et al., 2002). The CIS of the guest signal is monitored to quantify the binding strength of complexation for a host-guest system. The $^1H$ NMR signal showing an up-field CIS value indicates an encapsulation of the guest molecules in the hydrophobic environment while downfield signals indicate the positioning of the hydrogen just in the interface of the host cavity. We have performed an NMR titration of 0.5 mM SRT with an increasing concentration of CB7 up to 4.0 mM at two different pH. Each proton present in the SRT was assigned before analyzing the titration data (**Figure 4A**). At lower pH, *ca.* pD 3.0, a strong up-field CIS was observed in $H_b$, $H_c$, and $H_f$ which indicate that those hydrogen atoms of SRT are present in the core of the CB7 cavity (**Figure 4C**). On the other hand, a small up field CIS $H_a$, $H_d$, and $H_e$ suggested encapsulation of these protons are present relatively nearer to the portal of the CB7. The full-length NMR spectra are shown in **Supplementary Figure 6**. To evaluate the binding strength between SRT and CB7, we plotted the change in the chemical shift of six different protons present in SRT against the concentration of CB7 added during the NMR titration (**Figure 4B**). The data points were fitted by 1:1 binding equation and get the average binding constant (9,200 ± 1,200) $M^{-1}$ which is very similar to the value obtained from fluorescence binding titration in $D_2O$. Further, we have also performed an NMR titration at pD 7.4 with 0.2 mM SRT and an increasing concentration of CB7 up to 3.2 mM. The average binding constant value obtained using the 1:1 equation from fitting all the NMR peaks at pD 7.4 is (11,500± 1,800) $M^{-1}$ (see **Supplementary Figures 7**, **8**). This is similar to the value measured at pD 7.4 using fluorescence spectroscopy. Such a binding geometry could eventually cause a significant shift in the p$K_a$ value. Unfortunately, we could not monitor the p$K_a$ value of SRT in SRT•CB7 complex as the p$K_a$ value was out of range in experimental pH conditions. Nonetheless, it is interesting to note that at pH 13 there is no change in CIS for host-guest complexation (**Supplementary Figure 9**). Hence, it is evident that no complex formation occurs in basic pH and the shift in the p$K_a$ is less than two logarithmic units owing to the competition provided by the sodium ions present in the basic pH range.

## Understanding the Role of $Cs^+$ as a Competitor on the Stability of SRT•CB7

To understand the stability, stoichiometry, and the depth of inclusion of the SRT•CB7 complex, we have performed a competition titration experiment with the help of a bulky mono-cationic alkali metal. The selection of cesium ion was based on mainly two reasons. Firstly, it can act as the lid on the top/bottom of the CB7 portal due to the ion-dipole interaction. As the previous studies show that $Cs^+$ has a strong affinity to form a 1:1 complex with CB7 (Whang et al., 1998; Pichierri, 2013). Secondly, it is an NMR innocent alkali metal ion. Hence, we carried out the NMR-based competition assay at pD 2.8 of the pre-formed SRT•CB7 complex with an increasing concentration of CsCl up to 10 mM (**Figure 5A**, **Supplementary Figure 10**).

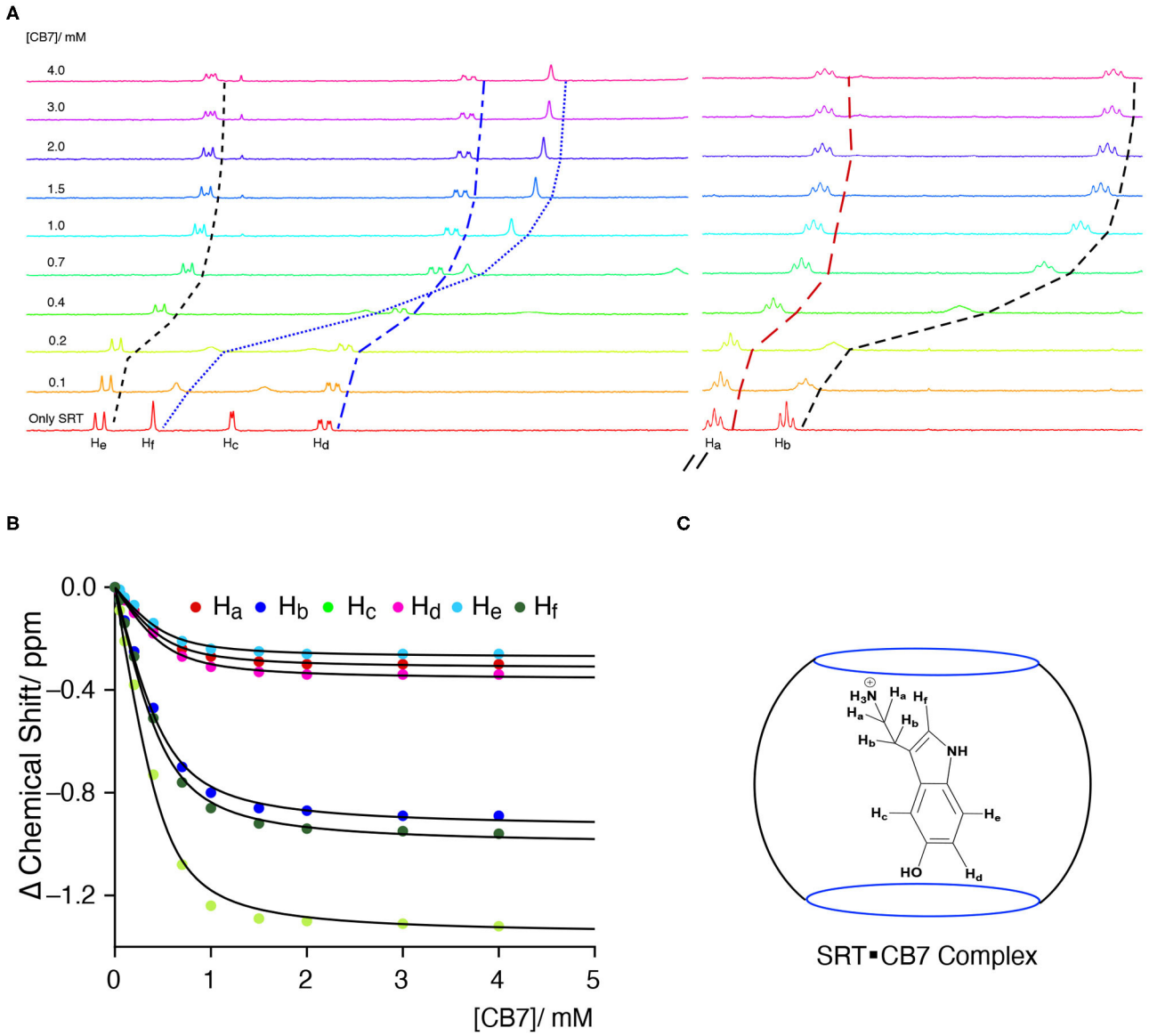


**FIGURE 4 | (A)** NMR-based titration of 0.5 mM SRT with increasing concentration of CB7 up to 4.0 mM at pD 2.8; left part showing the aromatic region and right part the aliphatic region of NMR titration, **(B)** fitted plot of the change in Complexation Induced Shift (CIS) vs. concentration of CB7, **(C)** schematic representation of plausible $SRTH^+$•CB7 complex.

In this experiment, we anticipated the displacement of bound SRT by $Cs^+$. With the increasing concentration of CsCl, the $^1H$ NMR signal showed a small downfield shift in the peak positions. To our surprise, the extent of the downfield shift strongly indicated no displacement of SRT from the CB7 cavity (**Figure 5B**). The $Cs^+$ ion binds to the portal of the CB7, and with increasing the concentration it re-orientates SRT inside the CB7 cavity. This was further validated with a fluorescence titration by adding CsCl in a pre-formed SRT•CB7 complex (see **Supplementary Figure 11**). In fact, the initially up-field shifted peaks due to SRT•CB7 complexation were partially shifted to down-field. Hence, we did not observe a full recovery of the peak position. This confirms that there is a formation of a ternary complex formation (SRT•CB7•$Cs^+$, **Figure 5C**) where $Cs^+$ ion acts as a lid possibly from the one side of the portal.

## Molecular Docking Studies

Based on the NMR titration experiments, it is evident that SRT resides inside the cavity of CB7 while the amine group protrudes along with the portal. Even as complete inclusion of the main framework was suggested by the

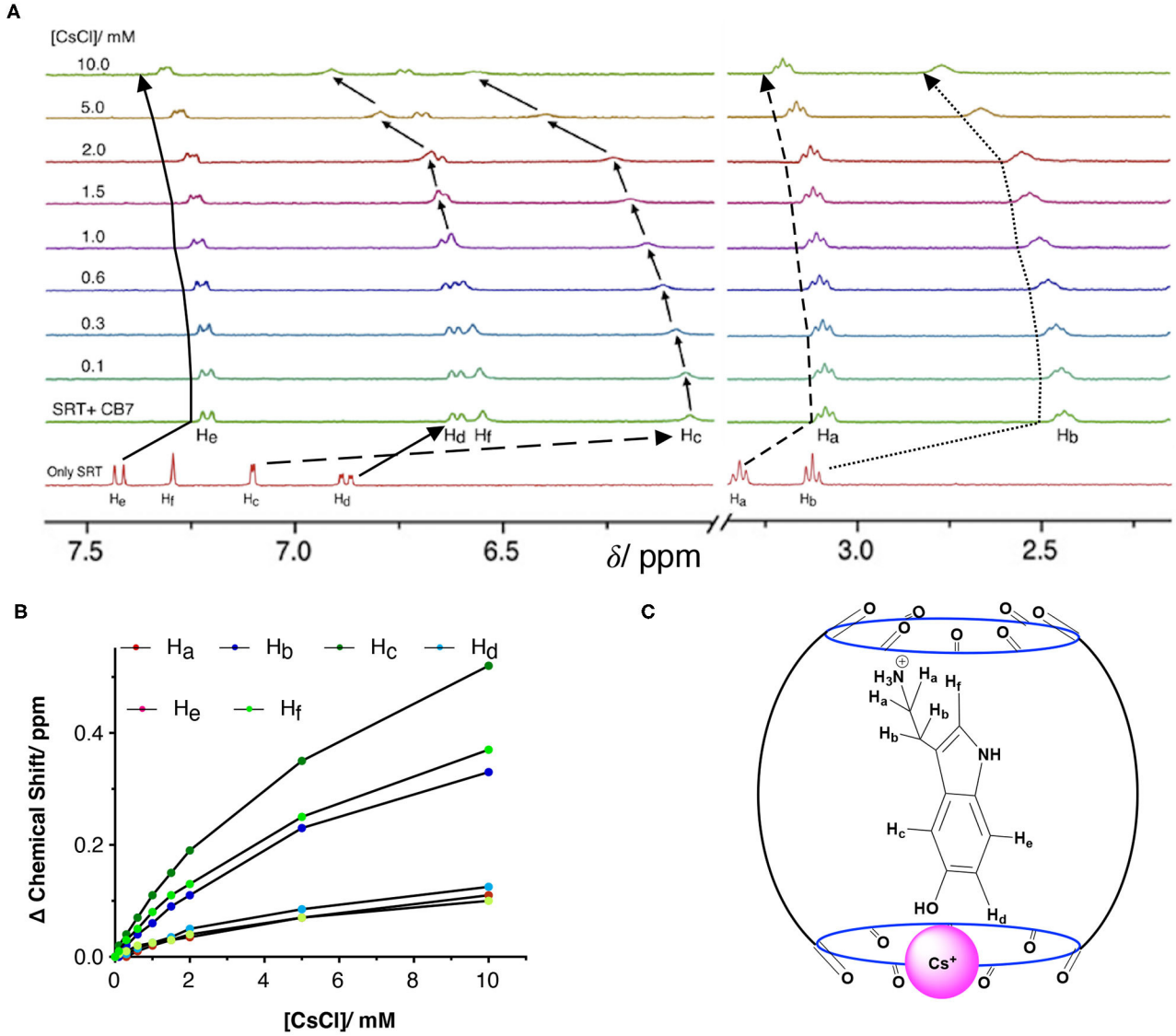


**FIGURE 5 | (A)** NMR-based titration of the SRT•CB7 (0.5 mM SRT and complex with increasing concentration of CsCl up to 10 mM at pD 2.5; part showing the aromatic region and right part the aliphatic region of NMR spectra. **(B)** A fitted plot of the difference in chemical shift (in ppm) against the concentration of CsCl. **(C)** Schematic representation of SRT•CB7•$Cs^+$ complex.

proton chemical shifts, the actual orientation could not be understood. Hence, we performed molecular docking using the PatchDock server (Duhovny et al., 2002; Schneidman-Duhovny et al., 2005). The 3D structure of CB7 was obtained from the PDBe database and optimized by the PM3 method using Gaussian 09W. The protonated structure of SRT was optimized using the B3LYP method at 6-31G* level. Several probable structures were received from the PatchDock server program based on the geometric shape complementarity score, approximate interface area of the complex and, atomic contact energy (ACE). The structure of the individual molecules and inclusion complex, shown in **Figures 6A–D**, has the highest geometric shape complementarity score 3,056, an approximate interface area of 319.90 $Å^2$, and ACE is −349.13 kcal/mol (**Supplementary Table 1**). The orientation of SRT inside CB7 well corroborates with the proton chemical shifts obtained from the NMR titration.

## CONCLUSIONS

In summary, we have extensively explored the encapsulation of a well-known neurotransmitter molecule serotonin with a rigid water-soluble macrocyclic host CB7 using different spectroscopic

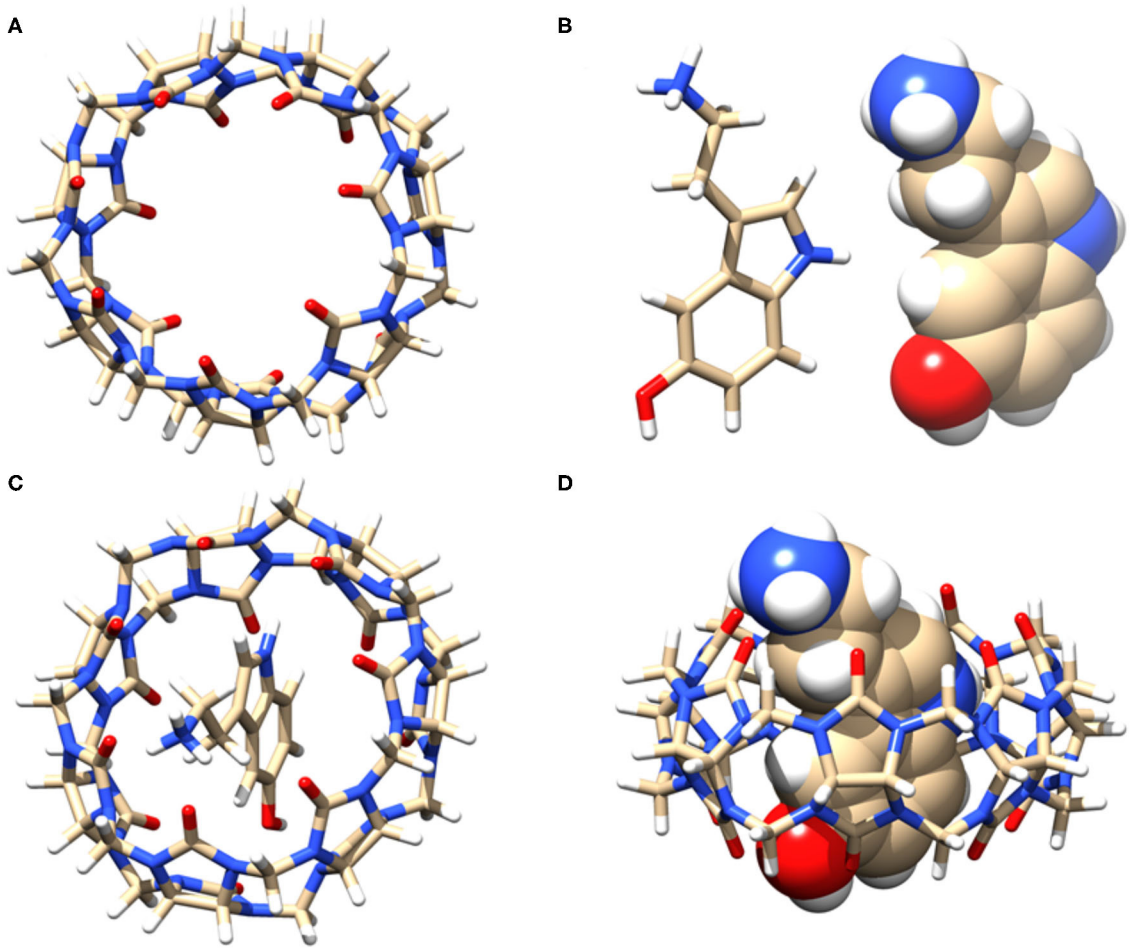


**FIGURE 6 | (A)** Stick model of the guest CB7 (top view), **(B)** stick and sphere model of SRT in acidic pH, **(C)** top view, and **(D)** side view of the of 1:1 inclusion complex of SRT•CB7 and **(D)**. The carbon, hydrogen, nitrogen, and oxygen atoms are shown in gray, white, blue, and red, respectively.

techniques and molecular docking. Primarily, the pH-dependent photophysical properties of serotonin were investigated. The host-guest complexation between CB7 and serotonin in different pH revealed an efficient binding of the amine-protonated species of serotonin, whereas, in basic pH, no complex was formed. The 1:1 stoichiometry of the complex was assessed using Job's plot. Interestingly, we observed a binding constant difference of two times in favor of $H_2O$ compared to $D_2O$ due to strong enthalpic contribution in the complexation between serotonin and CB7. Further confirmation of the complexation was obtained from fluorescence anisotropy and NMR. From NMR titration, the complexation induced chemical shift values were evaluated to understand the solution structure of the complex. Subsequently, $Cs^+$ driven competition of bound serotonin indicated the formation of the ternary complex originated from the pre-formed 1:1 complex where $Cs^+$ acts as the lid. Finally, the molecular docking studies were performed to validate the geometrical orientation and stoichiometry of the complex. We believe this study will be useful for serotonergic drug delivery and treatment of serotonin syndrome, considering the numerous roles of serotonin in physiological and pathophysiological processes and being one of the most important neurotransmitters.

## DATA AVAILABILITY STATEMENT

All datasets generated for this study are included in the article/**Supplementary Material**.

## AUTHOR CONTRIBUTIONS

AK designed the project. FC and TD performed all the experiments and calculations. They have plotted and analyzed the data with the help of AK. All authors contributed to manuscript writing.

## FUNDING

This work was supported by Science and Engineering Research Board (SERB) under the Department of Science and Technology (DST), India (Project no: SERB/CS-253/2013).

## ACKNOWLEDGMENTS

We would like to thank the Department of Chemistry at the Indian Institute of Science Education and Research Bhopal (IISERB) for the instrumentation and infrastructural facility and Science and Engineering Research Board (SERB) for funding. The NMR facility at Central Instrumentation Facility (CIF) at IISERB is highly appreciated for its constant support.

## SUPPLEMENTARY MATERIAL

The Supplementary Material for this article can be found online at: https://www.frontiersin.org/articles/10.3389/fchem.2020.582757/full#supplementary-material

## REFERENCES

Ahmed, S., Singha, N., Pramanik, B., Mondal, J. H., and Das, D. (2016). Redox controlled reversible transformation of a supramolecular alternating copolymer to a radical cation containing homo-polymer. *Polymer Chem*. 7, 4393–4401. doi: 10.1039/C6PY00809G

Barooah, N., Kunwar, A., Khurana, R., Bhasikuttan, A. C., and Mohanty, J. (2017). Stimuli-responsive cucurbit[7]uril-mediated BSA nanoassembly for uptake and release of doxorubicin. *Chem. Asian J*. 12, 122–129. doi: 10.1002/asia.201601411

Berger, M., Gray, J. A., and Roth, B. L. (2009). The expanded biology of serotonin. *Annu. Rev. Med*. 60, 355–366. doi: 10.1146/annurev.med.60.042307.110802

Bhasikuttan, A. C., Mohanty, J., Nau, W. M., and Pal, H. (2007). Efficient fluorescence enhancement and cooperative binding of an organic dye in a supra-biomolecular host–protein assembly. *Angew. Chem. Int. Ed*. 46, 4120–4122. doi: 10.1002/anie.200604757

Biedermann, F., Vendruscolo, M., Scherman, O. A., De Simone, A., and Nau, W. M. (2013). Cucurbit[8]uril and blue-box: high-energy water release overwhelms electrostatic interactions. *J. Am. Chem. Soc*. 135, 14879–14888. doi: 10.1021/ja407951x

Carhart-Harris, R. L., and Nutt, D. J. (2017). Serotonin and brain function: a tale of two receptors. *J. Psychopharmacol*. 31, 1091–1120. doi: 10.1177/0269881117725915

Chandra, F., Kumar, P., and Koner, A. L. (2018). Encapsulation and modulation of protolytic equilibrium of beta-carboline-based norharmane drug by cucurbit[7]uril and micellar environments for enhanced cellular uptake. *Colloids Surf. B* 171, 530–537. doi: 10.1016/j.colsurfb.2018.07.061

Chandra, F., Pal, K., Lathwal, S., and Koner, A. L. (2016). Supramolecular guest relay using host-protein nanocavities: an application of host-induced guest protonation. *Mol. Biosys*. 12, 2859–2866. doi: 10.1039/C6MB00423G

Chattopadhyay, A., Rukmini, R., and Mukherjee, S. (1996). Photophysics of a neurotransmitter: Ionization and spectroscopic properties of serotonin. *Biophys. J*. 71, 1952–1960. doi: 10.1016/S0006-3495(96)79393-1

Choudhury, S. D., Mohanty, J., Pal, H., and Bhasikuttan, A. C. (2010). Cooperative metal ion binding to a cucurbit[7]uril–thioflavin T complex: demonstration of a stimulus-responsive fluorescent supramolecular capsule. *J. Am. Chem. Soc*. 132, 1395–1401. doi: 10.1021/ja908795y

Cong, H., Ni, X. L., Xiao, X., Huang, Y., Zhu, Q.-J., Xue, S.-F., et al. (2016). Synthesis and separation of cucurbit[n]urils and their derivatives. *Org. Biomol. Chem*. 14, 4335–4364. doi: 10.1039/C6OB00268D

Das, D., Assaf, K. I., and Nau, W. M. (2019). Applications of cucurbiturils in medicinal chemistry and chemical biology. *Front. Chem*. 7:619. doi: 10.3389/fchem.2019.00619

Dsouza, R. N., Pischel, U., and Nau, W. M. (2011). Fluorescent dyes and their supramolecular host/guest complexes with macrocycles in aqueous solution. *Chem. Rev*. 111, 7941–7980. doi: 10.1021/cr200213s

Dubovsky, S. L., and Thomas, M. (1995). Beyond specificity - effects of serotonin and serotonergic treatments on psychobiological dysfunction. *J. Psychosom. Res*. 39, 429–444. doi: 10.1016/0022-3999(94)00043-5

Duhovny, D., Nussinov, R., and Wolfson, H. J. (2002). Efficient unbound docking of rigid molecules. *Algorith. Bioinformatics Proceed.* 2452, 185–200. doi: 10.1007/3-540-45784-4_14

Erspamer, V., and Asero, B. (1952). Identification of enteramine, the specific hormone of the enterochromaffin cell system, as 5-hydroxytryptamine. *Nature* 169, 800–801. doi: 10.1038/169800b0

Gao, R. H., Chen, L. X., Chen, K., Tao, Z., and Xiao, X. (2017). Development of hydroxylated cucurbit[n]urils, their derivatives and potential applications. *Coord. Chem. Rev*. 348, 1–24. doi: 10.1016/j.ccr.2017.07.017

Ghosh, I., and Nau, W. M. (2012). The strategic use of supramolecular pK(a) shifts to enhance the bioavailability of drugs. *Adv. Drug Deliv. Rev*. 64, 764–783. doi: 10.1016/j.addr.2012.01.015

Gomila, R. M., Quiñonero, D., Rotger, C., Garau, C., Frontera, A., Ballester, P., et al. (2002). Predicting experimental complexation-induced changes in 1H NMR chemical shift for complexes between zinc-porphyrins and amines Using the ab Initio/GIAO-HF methodology. *Org. Lett*. 4, 399–401. doi: 10.1021/ol0170962

Hernandez-Mendoza, G. A., Aguirre-Olivas, D., Gonzalez-Gutierrez, M., Leal, H. J., Qureshi, N., Trevino-Palacios, C. G., et al. (2020). Fluorescence of serotonin in the visible spectrum upon multiphotonic photoconversion. *Biomed. Opt. Express* 11, 1432–1448. doi: 10.1364/BOE.380412

Hui, O. Y., and Vogel, H. J. (1998). Melatonin and serotonin interactions with calmodulin: NMR, spectroscopic and biochemical studies. *Biochim. Biophys. Acta Protein Struct. Mol. Enzymol*. 1383, 37–47. doi: 10.1016/S0167-4838(97)00157-X

Hunter, C. A., and Packer, M. J. (1999). Complexation-induced changes in H-1 NMR chemical shift for supramolecular structure determination. *Chem. Eur. J*. 5, 1891–1897. doi: 10.1002/(SICI)1521-3765(19990604)5:6<1891::AID-CHEM1891>3.0.CO;2-G

Johnston, W. L., and Glanville, N. T. (1992). Effect of feeding and fasting on plasma tryptophan and tryptophan to large neutral amino acid ratio, and on brain serotonin turnover in rainbow trout, *Oncorhynchus mykiss*. *Fish Physiol. Biochem*. 10, 11–22. doi: 10.1007/BF00004650

Kishi, T., Tanaka, M., and Tanaka, J. (1977). Electronic absorption and fluorescence-spectra of 5-hydroxytryptamine (Serotonin) - protonation in excited-state. *Bull. Chem. Soc. JPN*. 50, 1267–1271. doi: 10.1246/bcsj.50.1267

Koner, A. L., Ghosh, I., Saleh, N. I., and Nau, W. M. (2011). Supramolecular encapsulation of benzimidazole-derived drugs by cucurbit[7]uril. *Can. J. Chem*. 89, 139–147. doi: 10.1139/V10-079

Kuok, K. I., Li, S., Wyman, I. W., and Wang, R. (2017). Cucurbit[7]uril: an emerging candidate for pharmaceutical excipients. *Ann. N.Y. Acad. Sci*. 1398, 108–119. doi: 10.1111/nyas.13376

Lazar, A. I., Biedermann, F., Mustafina, K. R., Assaf, K. I., Hennig, A., and Nau, W. M. (2016). Nanomolar binding of steroids to cucurbit[n]urils: selectivity and applications. *J. Am. Chem. Soc*. 138, 13022–13029. doi: 10.1021/jacs.6b07655

Liu, M., Kan, J., Yao, Y., Zhang, Y., Bian, B., Tao, Z., et al. (2019a). Facile preparation and application of luminescent cucurbit[10]uril-based porous supramolecular frameworks. *Sens. Actuators B Chem*. 283, 290–297. doi: 10.1016/j.snb.2018.12.024

Liu, M., Yang, M., Yao, Y., Zhang, Y., Zhang, Y., Tao, Z., et al. (2019b). Specific recognition of formaldehyde by a cucurbit[10]uril-based porous supramolecular assembly incorporating adsorbed 1,8-diaminonaphthalene. *J. Mater. Chem. C* 7, 1597–1603. doi: 10.1039/C8TC06339G

Lv, J. H., and Liu, F. (2017). The role of serotonin beyond the central nervous system during embryogenesis. *Front. Cellular Neurosci*. 11:74. doi: 10.3389/fncel.2017.00074

Mallick, S., Pal, K., Chandra, F., and Koner, A. L. (2016). Investigation of the effect of cucurbit[7]uril complexation on the photophysical and acid-base properties of the antimalarial drug quinine. *Phys. Chem. Chem. Phys*. 18, 30520–30529. doi: 10.1039/C6CP04931A

Marquez, C., Huang, F., and Nau, W. M. (2004). Cucurbiturils: molecular nanocapsules for time-resolved fluorescence-based assays. *IEEE Trans. Nanobiosci*. 3, 39–45. doi: 10.1109/TNB.2004.824269

Mawe, G. M., and Hoffman, J. M. (2013). Serotonin signalling in the gut–functions, dysfunctions and therapeutic targets. *Nat. Rev. Gastroenterol Hepatol.* 10, 473–486. doi: 10.1038/nrgastro.2013.105

Mondal, J. H., Ahmed, S., Ghosh, T., and Das, D. (2015). Reversible deformation–formation of a multistimuli responsive vesicle by a supramolecular peptide amphiphile. *Soft Matter* 11, 4912–4920. doi: 10.1039/C5SM00491H

Nau, W. M., Florea, M., and Assaf, K. I. (2011). deep inside cucurbiturils: physical properties and volumes of their inner cavity determine the hydrophobic driving force for host-guest complexation. *ISR J.Chem*. 51, 559–577. doi: 10.1002/ijch.201100044

Pichierri, F. (2013). DFT study of caesium ion complexation by cucurbit[n]urils (n=5-7). *Dalton Trans*. 42, 6083–6091. doi: 10.1039/C2DT32180G

Pratuangdejkul, J., Nosoongnoen, W., Guerin, G. A., Loric, S., Conti, M., Launay, J. M., et al. (2006). Conformational dependence of serotonin theoretical pK(a) prediction. *Chem. Phys. Lett*. 420, 538–544. doi: 10.1016/j.cplett.2006.01.035

Ruibal, C., Soengas, J., and Aldegunde, M. (2002). Brain serotonin and the control of food intake in rainbow trout (*Oncorhynchus mykiss*): effects of changes in plasma glucose levels. *J. Comp. Physiol. A* 188, 479–484. doi: 10.1007/s00359-002-0320-z

Saleh, N. I., Al-Handawi, M. B., Bufaroosha, M. S., Assaf, K. I., and Nau, W. M. (2016). Tuning protonation states of tripelennamine antihistamines by cucurbit[7]uril. *J. Phys. Org. Chem*. 29, 101–106. doi: 10.1002/poc.3504

Saleh, N. I., Koner, A. L., and Nau, W. M. (2008). Activation and stabilization of drugs by supramolecular pKa shifts: drug-delivery applications tailored for cucurbiturils. *Angew. Chem. Int. Ed*. 47, 5398–5401. doi: 10.1002/anie.200801054

Saleh, N. I., Meetani, M. A., Al-Kaabi, L., Ghosh, I., and Nau, W. M. (2011). Effect of cucurbit[n]urils on tropicamide and potential application in ocular drug delivery. *Supramol. Chem*. 23, 650–656. doi: 10.1080/10610278.2011.593631

Schneidman-Duhovny, D., Inbar, Y., Nussinov, R., and Wolfson, H. J. (2005). PatchDock and symmdock: servers for rigid and symmetric docking. *Nucl. Acids Res*. 33, W363–W367. doi: 10.1093/nar/gki481

Scholtbach, K., Venegas, I., Bohne, C., and Fuentealba, D. (2015). Time-resolved fluorescence anisotropy as a tool to study guest-cucurbit[n]uril-protein ternary supramolecular interactions. *Photochem. Photobiol. Sci*. 14, 842–852. doi: 10.1039/C4PP00479E

Veenstra-Vanderweele, J., Anderson, G. M., and Cook, E. H. (2000). Pharmacogenetics and the serotonin system: initial studies and future directions. *Eur. J. Pharmacol*. 410, 165–181. doi: 10.1016/S0014-2999(00)00814-1

Voet, D., and Voet, J. G. (2006). *Biochemistry*. New Jersey, NJ: John Wiley & Sons, Inc.

Walther, D. J., Peter, J. U., Bashammakh, S., Hortnagl, H., Voits, M., Fink, H., et al. (2003). Synthesis of serotonin by a second tryptophan hydroxylase isoform. *Science* 299:76. doi: 10.1126/science.1078197

Wang, R. B., Bardelang, D., Waite, M., Udachin, K. A., Leek, D. M., Yu, K., et al. (2009). Inclusion complexes of coumarin in cucurbiturils. *Org. Biomol. Chem*. 7, 2435–2439. doi: 10.1039/b903057c

Whang, D., Heo, J., Park, J. H., and Kim, K. (1998). A molecular bowl with metal ion as bottom: reversible inclusion of organic molecules in cesium ion complexed cucurbituril. *Angew. Chem. Int. Ed*. 37, 78–80. doi: 10.1002/(SICI)1521-3773(19980202)37:1/2<78::AID-ANIE78>3.0.CO;2-9

Wu, X., Chen, Y., Yu, Q., Li, F.-Q., and Liu, Y. (2019). A cucurbituril/polysaccharide/carbazole ternary supramolecular assembly for targeted cell imaging. *Chem. Commun*. 55, 4343–4346. doi: 10.1039/C9CC01601E

Yin, H., Chen, L., Yang, B., Bardelang, D., Wang, C., Lee, S. M. Y., et al. (2017). Fluorescence enhancement and pKa shift of a rho kinase inhibitor by a synthetic receptor. *Org. Biomol. Chem*. 15, 4336–4343. doi: 10.1039/C7OB00547D

Yin, H., and Wang, R. (2018). Applications of cucurbit[n]urils (n=7 or 8) in pharmaceutical sciences and complexation of biomolecules. *ISR J. Chem*. 58, 188–198. doi: 10.1002/ijch.201700092

Zhang, Y. M., Liu, Y. H., and Liu, Y. (2020). Cyclodextrin-based multistimuli-responsive supramolecular assemblies and their biological functions. *Adv. Mater*. 32:e1806158. doi: 10.1002/adma.201806158

**Conflict of Interest:** The authors declare that the research was conducted in the absence of any commercial or financial relationships that could be construed as a potential conflict of interest.

frontiers in Chemistry

ORIGINAL RESEARCH
published: 12 January 2021
doi: 10.3389/fchem.2020.621323

# Transmembrane Fluoride Transport by a Cyclic Azapeptide With Two β-Turns

*Zhixing Zhao, Miaomiao Zhang, Bailing Tang, Peimin Weng, Yueyang Zhang, Xiaosheng Yan*, Zhao Li and Yun-Bao Jiang**

*The MOE Key Laboratory of Spectrochemical Analysis and Instrumentation, Department of Chemistry, College of Chemistry and Chemical Engineering, Collaborative Innovation Center of Chemistry for Energy Materials (iChEM), Xiamen University, Xiamen, China*

OPEN ACCESS

**Edited by:**
*Andrea Erxleben, National University of Ireland Galway, Ireland*

**Reviewed by:**
*Huaqiang Zeng, A*STAR, Singapore*
*Hennie Valkenier, Free University of Brussels, Belgium*

***Correspondence:**
*Xiaosheng Yan*
*xshyan@xmu.edu.cn*
*Yun-Bao Jiang*
*ybjiang@xmu.edu.cn*

**Specialty section:**
*This article was submitted to Supramolecular Chemistry, a section of the journal Frontiers in Chemistry*

**Received:** *26 October 2020*
**Accepted:** *26 November 2020*
**Published:** *12 January 2021*

**Citation:**
*Zhao Z, Zhang M, Tang B, Weng P, Zhang Y, Yan X, Li Z and Jiang Y-B (2021) Transmembrane Fluoride Transport by a Cyclic Azapeptide With Two β-Turns. Front. Chem. 8:621323. doi: 10.3389/fchem.2020.621323*

Diverse classes of anion transporters have been developed, most of which focus on the transmembrane chloride transport due to its significance in living systems. Fluoride transport has, to some extent, been overlooked despite the importance of fluoride channels in bacterial survival. Here, we report the design and synthesis of a cyclic azapeptide (a peptide-based *N*-amidothiourea, **1**), as a transporter for fluoride transportation through a confined cavity that encapsulates fluoride, together with acyclic control compounds, the analogs **2** and **3**. Cyclic receptor **1** exhibits more stable β-turn structures than the control compounds **2** and **3** and affords a confined cavity containing multiple inner –NH protons that serve as hydrogen bond donors to bind anions. It is noteworthy that the cyclic receptor **1** shows the capacity to selectively transport fluoride across a lipid bilayer on the basis of the osmotic and fluoride ion-selective electrode (ISE) assays, during which an electrogenic anion transport mechanism is found operative, whereas no transmembrane transport activity was found with **2** and **3**, despite the fact that **2** and **3** are also able to bind fluoride via the thiourea moieties. These results demonstrate that the encapsulation of an anionic guest within a cyclic host compound is key to enhancing the anion transport activity and selectivity.

**Keywords: cyclic azapeptide, β-turn, fluoride, ion recognition, transmembrane transport**

## INTRODUCTION

In the past decade, artificial transmembrane anion transport has attracted much attention, and a variety of synthetic carriers (Wu et al., 2018, 2019) or channels (Ren et al., 2018a,b) have been developed to facilitate the transport of anions, e.g., chloride (Valkenier et al., 2019), bicarbonate (Gale et al., 2010), and sulfate (Busschaert et al., 2014), across the cell membranes or artificial lipid bilayers, showcasing potential application in treating diseases caused by faulty anion channels, such as cystic fibrosis (also known as channelopathies; Sheppard et al., 1993), Bartter syndrome (Simon et al., 1996), and Dent's disease (Dutzler et al., 2002).

Fluoride is the smallest halide anion, which is closely related to the life and health of humans and other living organisms. For example, fluoride is an indispensable additive in toothpastes to prevent dental caries of children and adolescents (Marinho et al., 2003). However, long-term exposure to environments containing high-level fluoride will cause fluorosis (Zhang et al., 2017). Therefore, the concentration of fluoride in drinking water should be carefully monitored: a $F^-$ concentration lower than 0.5 mg/L may lead to dental decay (Yuan et al., 2020); a high $F^-$ concentration is linked with dental fluorosis (1.5–4.0 mg/L; Rwenyonyi et al., 1999) and skeletal fluorosis (>4 mg/L; He et al., 2020). Fluoride is toxic to microorganisms because it inhibits their phosphoryl-transfer enzymes (Breaker, 2012). With an acidic extracellular environment, unicellular organisms would take up the membrane permeable hydrofluoric acid (HF) and accumulate $F^-$ in the cytoplasm (known as the weak acid accumulation effect) leading to $F^-$-induced toxicity. Many microorganisms have developed fluoride resistance through the action of fluoride-exporting proteins to counter the weak acid accumulation effect. Recently, fluoride channels, $CLC^F$ $F^-/H^+$ antiporters (Baker et al., 2012; Stockbridge et al., 2012; Brammer et al., 2014) and "Fluc" proteins (Ji et al., 2014; Stockbridge et al., 2014, 2015), have been found. These membrane proteins contain small pores to achieve the selectivity for fluoride, which is essential to the survival of unicellular organisms and eukaryotes under fluoride-containing environments.

However, the design of a fluoride selective transporter is still challenging, owing to the intrinsic nature of fluoride, in terms of small size and basic and high hydration energy. In fact, only a few examples of fluoride carriers are reported, including heavy pnictogenium cations (Park et al., 2019), phosphonium boranes (Park and Gabbai, 2020), and strapped calix[4]pyrroles (Clarke et al., 2016), but they are also active for chloride transport. In view of the small size of fluoride and the small pore in Fluc proteins that facilitates $F^-$ selectivity, it is anticipated that creating a cyclic molecule with a small cavity could be a design strategy for fluoride selective transport. Meanwhile, secondary structures play a vital role in maintaining the shape and function of ion channel proteins (Ketchem et al., 1993). We therefore decided to introduce a small secondary structure, i.e., β-turn, into cyclic molecule to improve the lipophilic property of the transporter.

Herein, by employing alanine-based *N*-amidothiourea motif, a structural scaffold featuring β-turn structure (Yan et al., 2013, 2018, 2019; Cao et al., 2017), we design and synthesize a cyclic azapeptide **1** and two acyclic analogs **2** and **3** (**Figure 1**) for fluoride transmembrane transport. The facile synthesis of cyclic receptor **1** is facilitated by the *meta*-position of the two benzene linkers and the 2-folded β-turns, which offer a small confined cavity for fluoride binding, leading to good selectivity in fluoride transmembrane transport across lipid bilayers according to an electrogenic anion uniport mechanism. Acyclic control compounds **2** and **3** are able to bind fluoride via the thiourea moieties but show no fluoride transmembrane transport activity. From these results, it is believed that a cyclic host of small cavity with a conformation mimicking the secondary structure of proteins could be a key to designing effective and selective fluoride transporters.

# RESULTS AND DISCUSSIONS

## Synthesis and Characterization

Equal molar bilateral alanine-based hydrazides **4** (0.67 g, 2 mmol) and 1,3-phenylene diisothiocyanate **5** (0.38 g, 2 mmol) were dissolved in 50 mL $CH_3CN$ and stirred at 80°C for 12 h (**Figure 1A**). Removing the solvent through evaporation in vacuum, the crude product showed a set of well-resolved $^1H$ NMR signals (**Supplementary Figure 1**), indicating the formation of a main product with well-defined structure and of high purity and high yield. This product was suggested to be the cyclic azapeptide **1** according to the MALDI-TOF mass spectrum that shows a sharp peak of 528.03 (**Supplementary Figure 2**, calcd for $[\mathbf{1}+H]^+$ $[C_{22}H_{24}N_9O_4S_2]^+$: 529.14). After recrystallizing in $CH_3CN$, pure product **1** of high isolated yield (72%) was obtained. Generally, the two-point reaction could result in diverse oligomers, polymers, and cyclic compounds, which have not been found during the synthesis of **1**. The *meta*-position of the two benzene linkers and the folded β-turn structures are expected to contribute to the accessible synthesis of **1**. Acyclic analogs **2** and **3** (**Figure 1B**) were synthesized according to the procedures described in Scheme S1 in **Supplementary Material**.

## β-Turn Structures

β-Turn structure has been well-identified in alanine-based *N*-amidothiourea in our previous works. The calculated structure of cyclic azapeptide **1** features two β-turns as shown in **Figure 2A**. $^1H$ NMR spectra of **1** were recorded in 90:10 (v/v) $CD_3CN$–DMSO-$d_6$ mixtures at variable temperatures (**Supplementary Figure 3**), from which the temperature coefficients of the chemical shift of –NH protons were obtained (**Figure 2B**). Different from $-NH_a$ (−7.66 ppb/°C), $-NH_b$ (−7.21 ppb/°C), and $-NH_c$ (−10.91 ppb/°C), which have very negative values, a much more positive temperature coefficient of thioureido $-NH_d$ (−1.94 ppb/°C) was observed, suggesting the protection of $-NH_d$ by intramolecular interaction, ascribed to the intramolecular 10-membered ring hydrogen bonds that maintain the two β-turns in **1** (**Figure 2A**) (Cao et al., 2017; Yan et al., 2019; Zhang et al., 2020). The obvious NOE signals of $H_e$-$H_f$ and $H_d$-$H_f$ again support the folded β-turn structures in cyclic azapeptide **1** (**Supplementary Figure 4** and **Figure 2C**).

Folded β-turn structures also exist in acyclic control compounds **2** and **3**, suggested by the DFT calculated structures (**Supplementary Figure 5**), as well as the temperature coefficients of the chemical shift of the –NH protons (**Supplementary Figures 6–9**). Given the more positive temperature coefficient of the $-NH_d$ in **1** (-1.94 ppb/°C) than those in **2** and **3** (−2.65 and −2.64 ppb/°C, respectively, **Table 1**), it is believed that the intramolecular hydrogen bonds in **1** are more stable than those in **2** and **3**, owing to the rigid cyclic conformation that stabilizes the β-turn structures. Meanwhile, CD spectra in $CH_3CN$ show an obvious CD signal at 270 nm of **1** and weak signals for **2** and **3**, suggesting the more efficient intramolecular chirality transfer from chiral alanine residues to achiral phenylthiourea

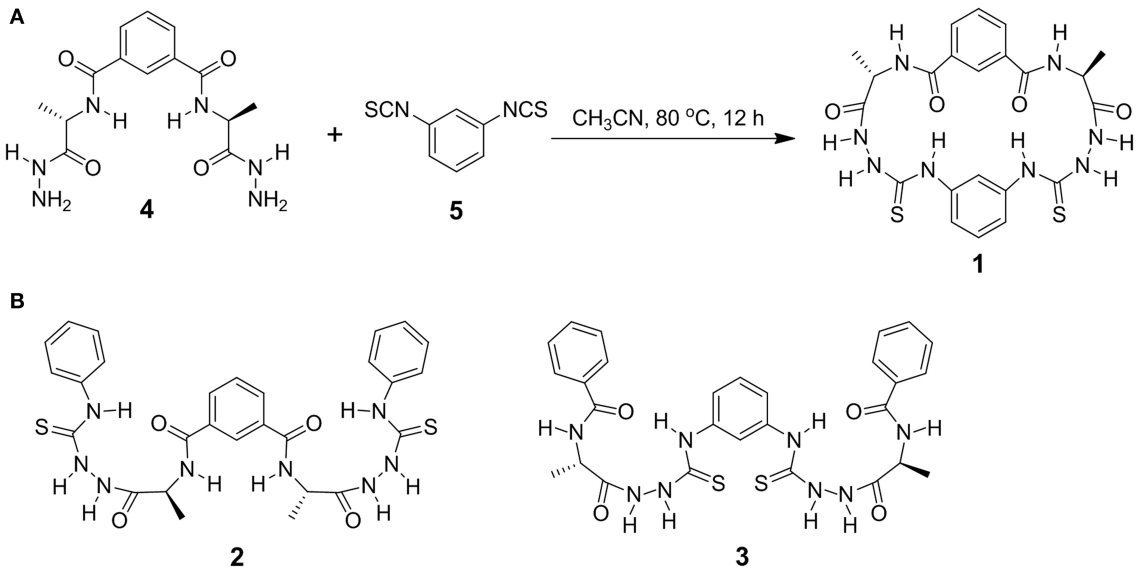


**FIGURE 1 |** Synthesis of cyclic azapeptide **1 (A)** and molecule structures of acyclic counterparts **2** and **3 (B)**. All alanine residues are of L-configuration.

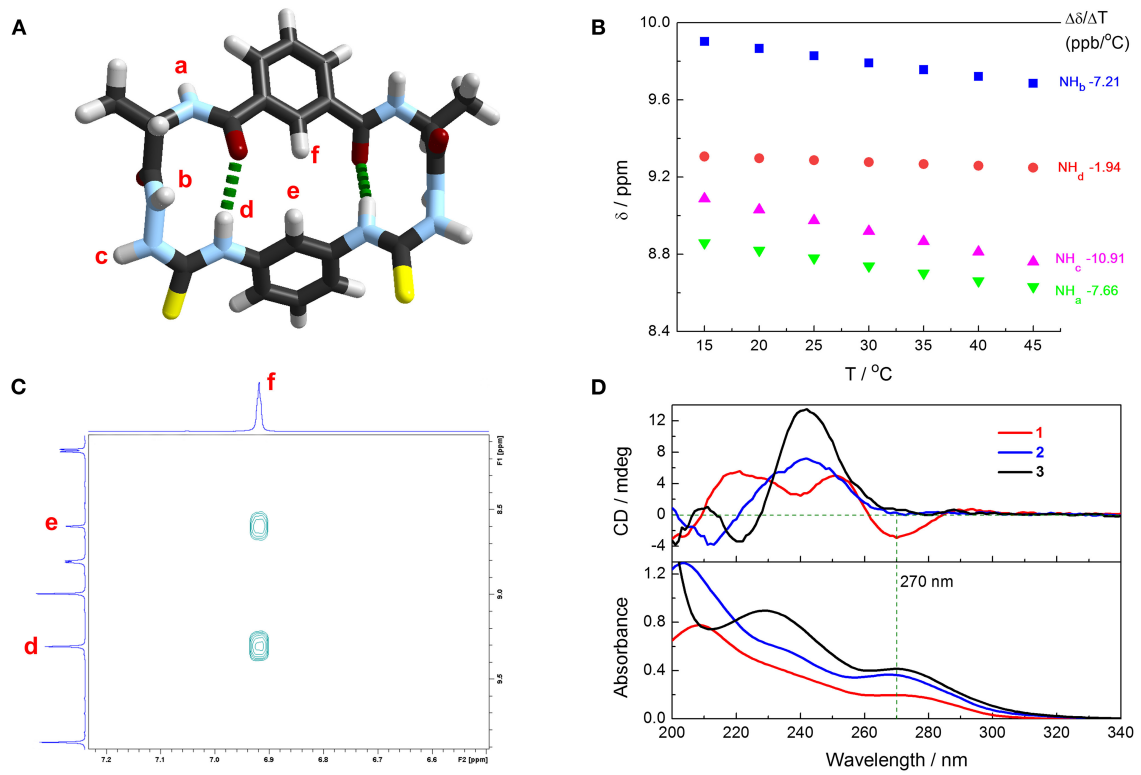


**FIGURE 2 | (A)** Calculated structure of cyclic azapeptide **1** with two β-turns. Dashed green lines highlight the intramolecular hydrogen bonds of β-turn structures. Method for calculation: B3LYP DFT with the 6-311G** basis set. **(B)** Influence on –NH protons resonances of **1** in 90:10 (v/v) $CD_3CN$/DMSO-$d_6$ mixtures by temperatures (600 MHz) and the fitted temperature coefficients. [**1**] = 1 mM. **(C)** Partial 2D NOESY spectrum of **1** in 90:10 (v/v) $CD_3CN$/DMSO-$d_6$ mixtures. [**1**] = 1 mM. **(D)** Absorption and CD spectra of **1** (red line), **2** (blue line), and **3** (black line) in $CH_3CN$. [**1**] = [**2**] = [**3**] = 20 μM.

chromophore in **1**, deduced from the absorption spectra (**Figure 2D**). Meanwhile, the cyclic conformation also leads to higher lipophilicity of **1**, supported by their retention times in reverse-phase HPLC (**Supplementary Table 1**). This could be a potential advantage of **1** for anion transmembrane transport (Valkenier et al., 2014).

**TABLE 1 |** Temperature coefficients of –NH protons' chemical shifts of **1**, **2**, and **3** in 90:10 (v/v) $CD_3CN$/DMSO-$d_6$ mixtures.

| Compound | 1 | 2 | 3 |
|---|---|---|---|
| Temperature coefficient (ppb/°C) -$NH_a$ | −7.66 | −8.97 | −9.63 |
| -$NH_b$ | −7.21 | −8.24 | −8.41 |
| -$NH_c$ | −10.91 | −8.52 | −8.84 |
| -$NH_d$ | −1.94 | −2.65 | −2.64 |

## Anion Binding

The binding capacity of **1** toward halide anions in $CH_3CN$ was next examined. Despite no perceivable binding to $Cl^-$, $Br^-$, and $I^-$ (**Supplementary Figures 10–12**), a substantial change in absorption and CD spectra of **1** was observed in the presence of $F^-$ (**Figure 3** and **Supplementary Figure 13**), undergoing multiple processes since the two binding groups, thiourea moieties, in **1** are in close proximity. Upon the addition of $F^-$ from 0.0 to 1.0 eq, the absorbance at 272 nm that from the thiourea chromophore is increased, along with the development of a new band at 315 nm, which is assigned to the charge transfer band of the anion–thiourea complex (**Figure 3A**). Significantly, a new CD band develops at 315 nm, suggesting the occurrence of intermolecular chirality transfer. With increasing $F^-$ concentration from 1.0 to 2.0 eq, the absorption at 272 nm blue shifts to 263 nm, while that at 315 nm shifts to 295 nm. While the CD signals at 272 and 315 nm become more negative, the positive signals at 238 and 215 nm are also enhanced, leading to bisignate and coupled Cotton effects at 272 and 238 nm (**Figure 3B**). From 2.0 to 5.0 eq $F^-$, both absorption and CD spectra are changed slightly (**Figure 3C**). Thus, a final 1:2 binding complex is suggested for **1** in the presence of $F^-$. The optimized structure of **1**·2$F^-$ complex shows that one $F^-$ interacts with **1** through three N–H···$F^-$ hydrogen bonds in the cavity of each side, breaking the β-turn structures. Therefore, one **1** molecule binds two $F^-$ ions through six hydrogen bonds (**Supplementary Figure 14** and **Supplementary Table 2**), resulting in a high binding energy up to−158.12 kcal $mol^{-1}$ or−79.06 kcal $mol^{-1}$ per $F^-$ ion. Moreover, the calculated CD spectrum performed by TD-DFT is similar to the experimental spectrum of **1** in the presence of 2.0 eq $F^-$ (**Supplementary Figure 15**), indicating the reliability of the calculated binding model.

Acyclic compounds **2** and **3** can also bind with fluoride in $CH_3CN$ by employing two thiourea groups. In **2**, the two thiourea moieties are distant, so only one equal binding process is shown in the titration spectra, in which the absorbance at 292 nm can be assigned to the $F^-$ binding complex of charge transfer transition (**Supplementary Figure 16**). Thereby, intermolecular chirality transfer is indicated by the emerged Cotton effects at 292 nm. Differently, the two thiourea groups in **3** are in close proximity, and the resultant binding complexes exhibit enhanced absorption and CD peaks at 266 nm, while the CD signals at 242 nm from the alanine residues are decreased (**Supplementary Figure 17**). The binding constants of acyclic **2** ($K = 2.2 \times 10^5$ $M^{-1}$, **Supplementary Figure 16**) and **3** ($K_{11} = 5.9 \times 10^5$ $M^{-1}$, $K_{12} = 8.5 \times 10^3$ $M^{-1}$, **Supplementary Figure 17**) with $F^-$ are fitted to be much lower than those of cyclic **1** with $F^-$ ($K_{21} = 1.7 \times 10^5$ $M^{-1}$, $K_{11} = 1.9 \times 10^8$ $M^{-1}$, $K_{12} = 8.6 \times 10^5$ $M^{-1}$, **Supplementary Figure 13**). No binding events are observed for **2** and **3** in the presence of $Cl^-$, $Br^-$, and $I^-$ (**Supplementary Figures 18–23**).

## Osmotic Assay

The selective binding of **1–3** to fluoride implies that they might be candidates for selective transport of fluoride. We thus studied the fluoride transport activities of **1–3** according to osmotic assay as shown in **Figure 4A** (Clarke et al., 2016). Large unilamellar vesicles (LUVs, 400 nm), composed of 1-palmitoyl-2-oleoyl-*sn*-glycero-3-phosphocholine (POPC), were loaded with a buffered KF solution (300 mM) and suspended in a buffered $K^+$ gluconate solution (300 mM). Transporters were added in the presence and absence of valinomycin (Vln, 0.5 μM, 0.1 mol%) to initiate the transport process (**Figure 4A**). The large hydrophilic anion gluconate was used as the extravesicular anion, which rules out an anion exchange mechanism. Without Vln, a fluoride transporter will create a membrane potential under the concentration gradient of fluoride, preventing fluoride efflux. Then Vln, a natural potassium carrier, can dissipate the membrane potential by transporting potassium leading to observable fluoride efflux. The overall KF cotransport will give rise to an osmotic gradient and drive the efflux of water from vesicles, leading to vesicle shrinkage. This process can be monitored by a fluorometer as an increase of 90° light scattering that results from the vesicle shrinkage. In the absence of Vln, the compounds **1–3** show no response from osmotic assay (**Supplementary Figure 24**), suggesting that the transporters cannot facilitate $K^+/F^-$ symport or $F^-$/gluconate antiport. Then Vln was added before the measurement began, and compound **1** leads to a significant increase in light scattering intensity, which was not observed for **2** and **3** (**Figure 4B** and **Supplementary Figure 25**), implying that transporter **1** is capable of transporting fluoride via an electrogenic anion uniport mechanism. The transport activity was quantified by employing transporter **1** at different concentrations (**Figure 4C**). Fitting the data with Hill equation, $EC_{50}$ (the effective concentration to reach 50% of maximum transport at 300 s) and n (Hill coefficient) are obtained and shown in **Figure 4D**. The concentration of lipids in osmotic assay is 500 μM; the $EC_{50}$ value (53.12 μM) corresponds to a transporter/lipid ratio of 10.62 mol%. The corresponding Hill coefficient n (2.24) is attributed to $F^-$ being transported as a 2:1 (transporter:anion) complex, which presumably leads to more effective shielding of the negative charge of $F^-$ compared with 1:1 and 1:2 complexes. Although acyclic counterparts **2** and **3** can bind fluoride as shown by absorption and CD titrations, they show no fluoride transport activity from the osmotic assay, even in the presence of Vln (**Supplementary Figure 25**), ascribed to their much lower lipophilicity (**Supplementary Table 1**), as well as lower $F^-$ affinity.

## ISE Assay

Ion-selective electrode (ISE) assay was next applied to directly measure the fluoride transport and confirm the transport

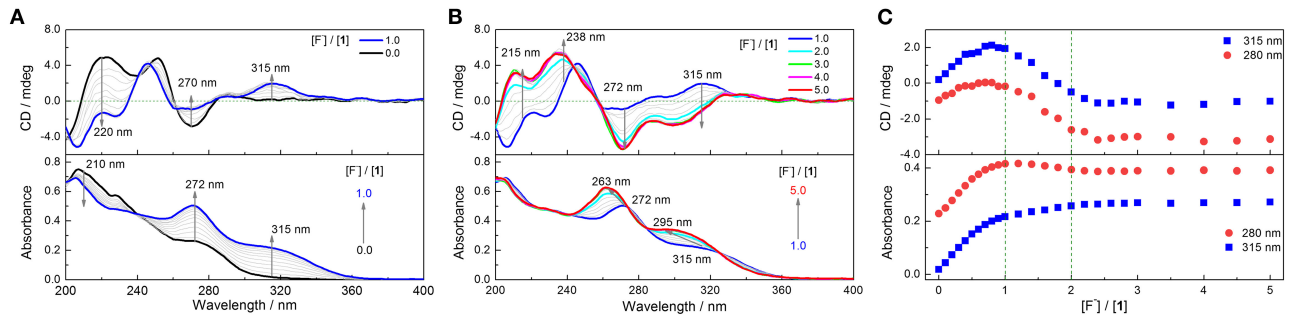


**FIGURE 3 |** Absorption and CD spectra of **1** in $CH_3CN$ in the presence of $F^-$ from 0 to 1.0 eq **(A)** and from 1.0 to 5.0 eq **(B)**. **(C)** Plots of absorbance and CD intensity at 280 and 315 nm vs. concentration of $F^-$. [**1**] = 20 μM. $F^-$ exists as the $(n\text{-Bu})_4N^+$ salt.

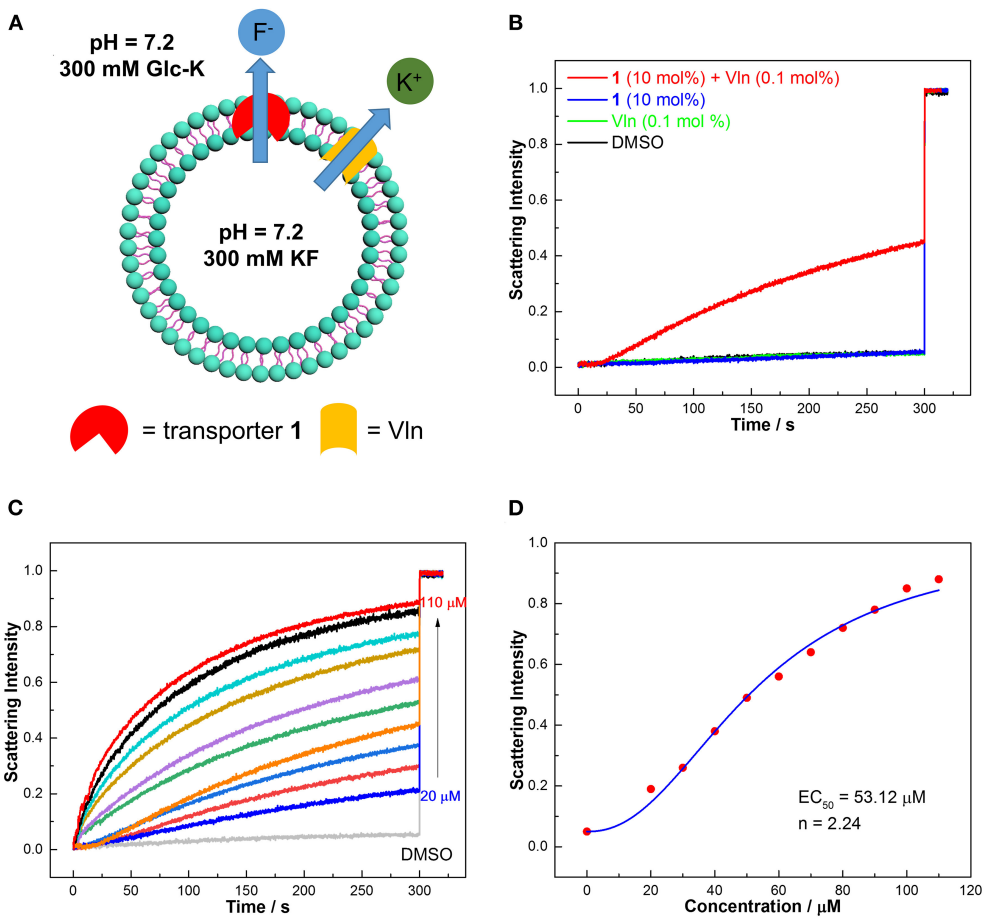


**FIGURE 4 | (A)** Schematic representation of osmotic assay for fluoride transport by exerting a concentration gradient of fluoride. Inside LUVs: 100 mM KF, 10 mM HEPES, pH 7.2. Outside LUVs: 100 mM Glc-K, 10 mM HEPES, pH 7.2. **(B)** Normalized fluoride efflux obtained by the addition of compound **1** (50 μM, 10 mol%) in the presence and absence of Vln (0.5 μM, 0.1 mol%). At 300 s, FCCP (25 μM, 5 mol%) and Vln (0.5 μM, 0.1 mol%) (if not added previously) were added to obtain a light scattering intensity corresponding to 100% transport for calibration. **(C,D)** Hill plot analysis of fluoride efflux when **1** is coupled with Vln (0.5 μM, 0.1 mol%).

mechanism (Wu et al., 2016). POPC LUVs (mean diameter 200 nm) were prepared and used in this section. In the absence of Vln, negligible efflux of fluoride was detected, even when the concentration of transporter **1** is high up to 40 mol%. In the presence of Vln, the KF efflux could reach 47% in the presence of 40 mol% **1** and was increased to be 85% when the concentration of transporter **1** was up to 80 mol% (**Figure 5**). The transport activity of **1** depends on the presence or absence of Vln,

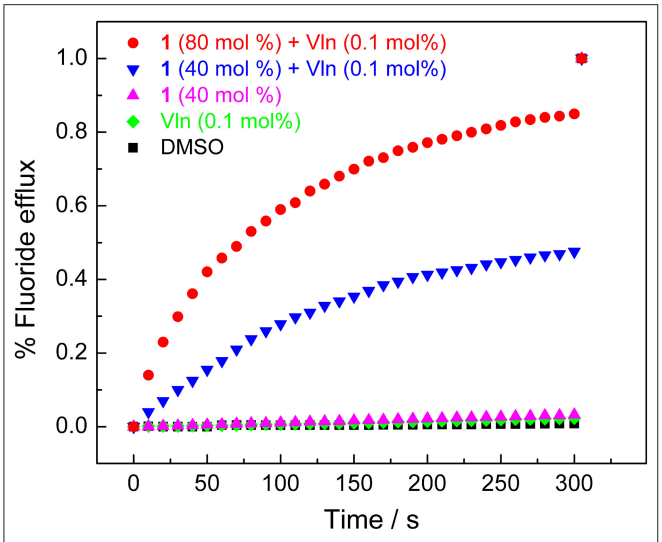


**FIGURE 5 |** ISE assay for fluoride efflux obtained by addition of compound **1** (40 and 80 mol%) in the presence and absence of Vln (0.1 mol%).

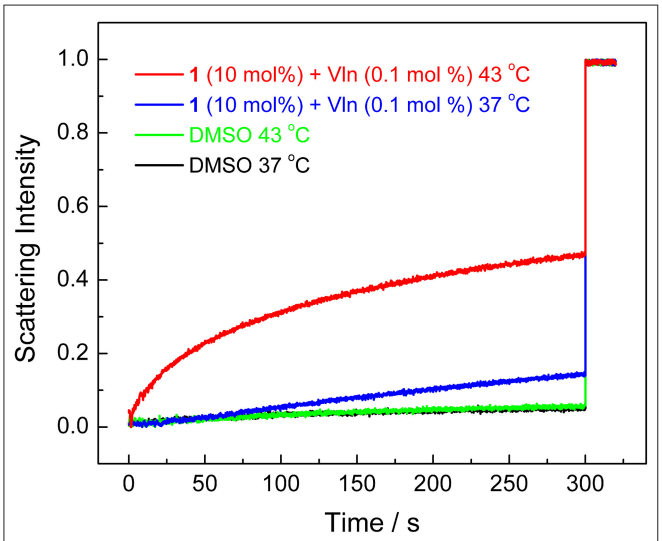


**FIGURE 6 |** Normalized KF efflux quantified by lipids composed of DPPC under 37 and 43°C in the osmotic assay.

confirming the electrogenic anion transport mechanism. Again, acyclic compounds **2–3** show negative response in the ISE assay (**Supplementary Figure 26**).

## Transport Mechanism Studies

The transport mechanism (carrier or channel) was next investigated by employing lipids composed of dipalmitoylphosphatidylcholine (DPPC), which feature a phase transition at 41°C (Wu et al., 2015). The decreased fluidity of lipids below 41°C could suppress the transport activity of ion carriers but not ion channels. The amount of $F^-$ transport of **1** at 300 s decreased from 47% at 43°C to 15% at 37°C in the osmotic assay (**Figure 6**), supporting the carrier transport mechanism.

It is noteworthy that HF is membrane permeable, and this could lead to an artifact in $F^-$ transport studies when the transporter facilitates $H^+$ ($OH^-$) transport (Clarke et al., 2016). In the $F^-$ transport artifact, the pH gradient generated by the HF efflux is dissipated by the $H^+$ influx (or $OH^-$ efflux) facilitated by the test transporter coupled to the $K^+$ efflux facilitated by Vln, leading to the net KF efflux. Therefore, a $H^+$ or $OH^-$ transporter (e.g., FCCP) can generate a positive response in a $F^-$ transport assay even if the transporter does not facilitate "true" $F^-$ transport by reversibly binding $F^-$ ions. KOAc-loaded vesicles were thus utilized to rule out $H^+$ and $OH^-$ transport, under which condition membrane-permeable acetic acid forms and would lead to the KOAc efflux in the presence of Vln and a $H^+$ ($OH^-$) transporter. Alternatively, acetate ion transport facilitated by a transporter would also lead to a response in the presence of Vln. If a transporter does not facilitate $H^+$ ($OH^-$) transport or acetate transport, acetate will stay inside the LUVs in the form of membrane-impermeable acetate ion. In our experiment, no detectable efflux of acetate was found (**Supplementary Figure 27**), confirming that transporter **1** is unable to transport $H^+$ ($OH^-$) or acetate. Thus, the KOAc-loaded osmotic assay, together with the KF-loaded osmotic assay, provides unambiguous evidence that cyclic compound **1** is capable of transporting fluoride via an electrogenic anion uniport mechanism. The integrity of the lipid bilayer can be evidenced by the calcein leakage assay (Wu et al., 2015). Calcein was encapsulated inside POPC LUVs; its fluorescence intensity was monitored to study whether pores are formed in lipids. Only negligible leakage of calcein occurred during the measurement (**Supplementary Figure 28**), confirming that cyclic compound **1** is functioning as a carrier rather than destroying the vesicle structure or forming large pores.

## Transport Selectivity of Fluoride Over Chloride

In view of the fact that the reported fluoride transporters are also active for chloride transport (Clarke et al., 2016; Park et al., 2019; Park and Gabbai, 2020), it is necessary to investigate the selectivity of fluoride over chloride. Hence, LUVs loaded with KCl (300 mM) were prepared to evaluate the transport activity toward chloride (**Supplementary Figure 29A**). Gratifyingly, no positive response could be observed in the Vln-coupled KCl efflux (**Supplementary Figure 29B**), suggesting the inactivity of **1–3** toward chloride transport, and thereby a transport selectivity of **1** toward fluoride over chloride. This highlights the importance of a small cyclic structure for selective ion transport.

# CONCLUSIONS

In summary, we developed a novel cyclic azapeptide, a peptide-based *N*-amidothiourea **1**, which can selectively bind and transport fluoride across lipid bilayers. NMR studies and DFT calculations verified the existence of β-turn structures in cyclic **1** and acyclic control compounds **2** and **3**, with the cyclic

structure affording the strongest hydrogen bonding in β-turn structures. Osmotic and ISE assays were employed to explore the transport activities toward fluoride and chloride. We found that cyclic azapeptide **1** can act as a carrier to transport fluoride, operating via an electrogenic anion uniport mechanism. The cyclic structure with a confined cavity facilitates the encapsulation of fluoride, which is the key to the selectivity in anion binding and transport. These results illustrate the significance of encapsulation and offer instructions for design halide-selective anion receptors and transporters.

# MATERIALS AND METHODS

## Materials

Isophthalic acid, benzoic acid, L-alanine, 1,3-phenylene diisothiocyanate, phenyl isothiocyanate, acetonitrile for reaction, and acetonitrile for spectroscopy were purchased from Sigma Aldrich Co. and used directly without purification. Acetonitrile-$D_3$ and dimethyl sulfoxide-$D_6$ were purchased from Cambridge Isotope Laboratories Inc. All other starting materials were obtained from Sinopharm Chemical Reagent Ltd.

## Instrumentation

$^1$H and $^{13}$C NMR spectra were recorded on a Bruker AV600MHz or AV850MHz spectrometer. High-resolution mass spectra (HRMS) were acquired on a Bruker micro TOF-Q-II mass spectrometer. Circular dichroism (CD) spectra were recorded on Jasco J-1500. Absorption spectra were recorded on a Shimadzu UV-2700 UV-Vis spectrophotometer. Fluorescence spectra were obtained on a Horiba Fluorolog-3 spectrometer or a Hitachi F-7000 spectrometer. ISE assay was conducted by an Orion Dual Star.

## Synthetic Procedures for 1–3

Cyclic compound **1** and reference linear compound **2–3** were synthesized according to reported literatures with little modification (Yan et al., 2019). Isophthaloyl dichloride was synthesized by refluxing isophthalic acid (10.0 mmol) with $SOCl_2$ (15.0 mmol) in $CH_2Cl_2$ (50.0 mL) overnight, evaporating solvent and unreacted $SOCl_2$ on a rotary evaporator to obtain white solid without further purification. Isophthaloyl dichloride was mixed with **AOEt·HCl** (2.0 g, 13.0 mmol) and $Et_3N$ (3.0 mL) in $CHCl_3$ (50.0 mL) and stirred overnight. The mixture was washed successively with $\mathbf{NH_3 \cdot H_2O}$ (1%, 50.0 mL), HCl (1%, 50.0 mL), and saturated NaCl solutions (50.0 mL). Then pure product **6** (80% yield averagely) was obtained by drying the solution over anhydrous $Na_2SO_4$ and concentrating *in vacuo*. To synthesize product **4**, excess aqueous hydrazine (85%, 6.0 mL) was added to **6** in EtOH (50.0 mL) and refluxed the mixture for 24 h. The solvent was removed by evaporation to obtain a crude product and washed with $CH_3CN$ several times to afford pure white product **6** (65% yield averagely).

Linear compound **2** was synthesized by refluxing **4** (1.0 mmol) with an excess amount of **Ph(NCS)** (2.2 mmol) in $CH_3CN$ for 24 h. Pure product **2** (90% yield averagely) precipitated from the solution and could be used directly without further purification.

**8** was synthesized and purified under the similar way as **4**, then **3** can be acquired by refluxing excess **8** (2.2 mmol) with **5** (1.0 mmol) in CH3CN for 24 h. After filtrating, pure solid product **3** was obtained (90% yield averagely).

**1**: $^1$H NMR (600 MHz, DMSO-$d_6$): $\delta$ (ppm) 10.44 (s, 2H), 9.81 (s, 2H), 9.28 (d, $J$ = 5.3 Hz, 2H), 9.23 (s, 2H), 8.61 (s, 1H), 8.19 (dd, $J$ = 7.8, 1.7 Hz, 2H), 7.86 (dd, $J$ = 8.1, 1.9 Hz, 2H), 7.65 (t, $J$ = 7.7 Hz, 1H), 7.36 (t, $J$ = 8.1 Hz, 1H), 6.91 (t, $J$ = 1.9 Hz, 1H), 4.32–4.25 (m, 2H), 1.38 (d, $J$ = 7.1 Hz, 6H); $^{13}$C NMR (214 MHz, DMSO): $\delta$ (ppm) 180.98, 171.88, 167.21, 139.44, 133.88, 130.71, 128.77, 128.55, 127.48, 123.84, 120.30, 49.69, 16.75; HRMS (ESI): calcd for $[C_{22}H_{24}N_8O_4S_2Na]^+$: 551.1254, found: 551.1245.

**2**: $^1$H NMR (600 MHz, DMSO-$d_6$): $\delta$ (ppm) 10.43 (s, 2H), 9.75 (s, 2H), 9.30 (s, 2H), 9.04 (s, 2H), 8.43 (s, 1H), 8.06 (d, $J$ = 7.4 Hz, 2H), 7.65 (d, $J$ = 25.5 Hz, 4H), 7.61 (t, $J$ = 7.6 Hz, 1H), 7.33 (t, $J$ = 7.3 Hz, 4H), 7.14 (t, $J$ = 6.9 Hz, 2H), 4.40 (s, 2H), 1.43 (d, $J$ = 6.3 Hz, 6H); $^{13}$C NMR (151 MHz, DMSO): $\delta$ (ppm) 180.74, 172.28, 167.48, 139.48, 134.19, 131.04, 128.74, 128.62, 127.69, 125.26, 124.62, 49.52, 17.19.; HRMS (ESI): calcd for $[C_{28}H_{30}N_8O_4S_2Na]^+$: 629.1724, found: 629.1726.

**3**: $^1$H NMR (600 MHz, DMSO-$d_6$): $\delta$ (ppm); 10.43 (s, 2H), 9.76 (s, 2H), 9.38 (s, 2H), 8.92 (s, 2H), 8.07 (s, 1H), 7.93 (d, $J$ = 7.3 Hz, 4H), 7.54 (t, $J$ = 7.3 Hz, 2H), 7.49 (t, $J$ = 7.4 Hz, 4H), 7.41 (d, $J$ = 7.7 Hz, 2H), 7.32 (t, $J$ = 8.0 Hz, 1H), 4.34 (s, 2H), 1.41 (d, $J$ = 6.7 Hz, 6H); $^{13}$C NMR (214 MHz, DMSO): $\delta$ (ppm) 180.71, 172.37, 167.97, 139.38, 133.66, 132.09, 128.75, 128.21, 127.94, 121.84, 121.68, 49.58, 17.06; HRMS (ESI): calcd for $[C_{28}H_{30}N_8O_4S_2Na]^+$: 629.1724, found: 551. 629.1713.

## Osmotic Response Assay

The large unilamellar vesicles (LUVs, mean diameter 400 nm) of POPC were prepared by freeze/thaw cycles; 30.4 mg POPC dissolved in $CHCl_3$ (50 mL) was slowly evaporated using a rotary evaporator and dried under high vacuum at room temperature for 4 h. The obtained lipid film was rehydrated by mixing with 4 mL saline solution (300 mM KF, 10 mM HEPES, pH 7.2) and vortexing for 2 min. Then the mixture was subjected to 10 freeze–thaw cycles and extruded through a 0.45-μm polycarbonate membrane for at least five times. Then the suspension (10 mM LUVs) can be used without further treatment.

In each run, 100 μL lipids stock (300 mM KF, 10 mM HEPES, pH 7.2, 10 mM LUVs) was added to 1.99 mL external solution (300 mM Glc-K, 10 mM HEPES, pH 7.2, 10 mM LUVs). DMSO (40 μL) solutions of transporters or DMSO (40 μL) was added at time 0. The light scattering intensity at 600 nm was monitored by a fluorimeter ($\lambda_{ex}$ = 600 nm, $\lambda_{em}$ = 600 nm). In this section, none of the three compounds show any response in osmotic assay, so valinomycin (Vln, 0.5 μM, 0.1 mol%) was added to accelerate the outflow of $K^+$. If the outflow of $F^-$ accompanied the outflow of $K^+$, an osmotic gradient will be formed, causing vesicle shrinkage and increasing the amount of 90° light scattering. At 300 s, FCCP (25 μM, 5 mol%) and Vln (0.5 μM, 0.1 mol%) (if not added previously) were added to accelerate the transport process to the end for calibration. The fractional light scattering intensity ($I_f$) was calculated based on

the following equation:

$$I_f = \frac{R_t - R_0}{R_f - R_0} \times 100\%$$

In the equation, $R_t$ is the light scattering intensity at time t, $R_f$ is the final light scattering intensity obtained by the addition of FCCP and Vln, and $R_0$ is the light scattering intensity at time 0. Different concentrations of the transporter molecule were added to obtain a series of fractional light scattering intensity ($I_f$). Fitting $I_f$ vs. molecule concentration was performed using the following equation:

$$y = y_0 + (y_{\max} - y_0)\frac{x^n}{K + x^n}$$

In the equation, $y$ is the value of $I_f$ corresponding to the carrier molecule loaded at concentration $x$, $y_0$ is the $I_f$ value measured at no compound added, $y_{max}$ is the maximum $I_f$ value, $n$ is the Hill coefficient, and $K$ is the $EC_{50}$ value.

## ISE Assay

The large unilamellar vesicles (LUVs, mean diameter 200 nm) of POPC were prepared by freeze/thaw cycles; 50 mg POPC dissolved in $CHCl_3$ (50 mL) was slowly evaporated using a rotary evaporator and dried under high vacuum at room temperature for 4 h. The obtained lipid film was rehydrated by mixing with a 5 mL saline solution (300 mM KF, 10 mM HEPES, pH 7.2) and vortexing for 2 min. Then the mixture was subjected to 10 freeze–thaw cycles and extruded through a 0.22-μm polycarbonate membrane for at least five times. The obtained lipid suspension (3.8 mL, 0.05 mmol) was transferred to size exclusion chromatography (stationary phase Sephadex G-50; mobile phase 300 mM Glc-K, 10 mM HEPES, pH 7.2) and diluted with the mobile phase to acquire 10 mL of 5 mM lipids stock solution.

In the $F^-$ transport study, 1 mL of the lipid stock solution was added to 4 mL Glc-K (300 mM buffered to pH 7.2 using 10 mM HEPES) to generate a solution with a concentration gradient. As the former osmotic assay demonstrates that the transporter may work in an electrogenic way, Vln was added before the measurement. Then DMSO (40 μL) solutions of transporters or DMSO (40 μL) was added at time 0. The fluoride efflux was monitored by a fluoride selective electrode. At 300 s, Triton X-100 [100 μL, 20% (v/v)] was added as a detergent to lysate the LUVs for calibration.

## Ion Transport Mechanism Study by DPPC Experiments

DPPC LUVs (mean diameter 400 nm) were prepared as follows. A chloroform solution (30.4 mg DPPC) was evaporated slowly by a rotary evaporator and dried under high vacuum at room temperature for 4 h. After drying, the lipid film was rehydrated by vortexing with a 4 mL saline solution (300 mM KF, 10 mM HEPES, pH 7.2) and vortexing for 2 min at 55°C. The mixture was subjected to 10 freeze–thaw cycles (water bath was maintained at 55°C) and extruded through a 0.45-μm polycarbonate membrane for at least five times at 55°C. Then the suspension (10 mM LUVs) can be used without further treatment.

The transport of $F^-$ was performed by the same way as above-mentioned. The lipid solution was stirred and thermostated in a polystyrene cuvette at 37 or 43°C.

## Ion Transport Mechanism by Calcein Leakage Assay

POPC LUVs (mean diameter 200 nm) were prepared as follows. A chloroform solution (10 mg POPC) was evaporated slowly by a rotary evaporator and dried under high vacuum at room temperature for 4 h. After drying, the lipid film was rehydrated by vortexing with a 1 mL calcein solution (100 mM NaCl, 10 mM HEPES, 100 mM calcein, pH 7.0) and vortexing for 2 min. The mixture was subjected to 10 freeze–thaw cycles and extruded through a 0.22-μm polycarbonate membrane for at least five times. The unentrapped calcein was separated by size exclusion chromatography (stationary phase Sephadex G-50; mobile phase 100 mM NaCl, 10 mM HEPES, pH 7.0) and diluted with the mobile phase to acquire 5 mL of 2 mM lipid stock solution.

For each run, 0.1 mL of the lipid stock solution was added to a 1.88 mL buffer solution to a final lipid concentration of 100 μM. DMSO (20 μL) solutions of transporters or DMSO (20 μL) was added at time 0. The fluorescence emission at time t ($\lambda_{ex}$ = 495 nm, $\lambda_{em}$ = 515 nm) was recorded over 30 min. At 30 min, Triton X-100 [10 μL, 20% (v/v)] was added as a detergent to lysate the LUVs for calibration. The fractional fluorescence intensity ($I_f$) was calculated based on the following equation:

$$I_f = \frac{R_t - R_0}{R_f - R_0} \times 100\%$$

In the equation, $R_t$ is the fluorescence intensity at time t, $R_f$ is the final fluorescence intensity obtained by the addition of detergent, and $R_0$ is the fluorescence intensity at time 0.

## DATA AVAILABILITY STATEMENT

The original contributions presented in the study are included in the article/**Supplementary Materials**, further inquiries can be directed to the corresponding author/s.

## AUTHOR CONTRIBUTIONS

XY and Y-BJ contributed to the conception and design of the study. ZZ and MZ finished the synthesis and transmembrane experiments. Absorption and CD spectra were collected by BT. PW and YZ carried out DFT calculations involved in this work. ZL contributed to the molecular design. All authors contributed to the article and approved the submitted version.

## FUNDING

We greatly appreciate the support of this work by the NSF of China (Grant Numbers 21435003, 21521004,

21820102006, and 91856118), and the MOE of China through Program for Changjiang Scholars and Innovative Research Team in University (Grant Number IRT13036), and the scientific and technological plan project in Xiamen (Grant Number 3502Z20203025).

## SUPPLEMENTARY MATERIAL

The Supplementary Material for this article can be found online at: https://www.frontiersin.org/articles/10.3389/fchem.2020.621323/full#supplementary-material

## REFERENCES


Baker, J. L., Sudarsan, N., Weinberg, Z., Roth, A., Stockbridge, R. B., and Breaker, R. R. (2012). Widespread genetic switches and toxicity resistance proteins for fluoride. *Science* 335, 233–235. doi: 10.1126/science.1215063

Brammer, A. E., Stockbridge, R. B., and Miller, C. (2014). $F^-/Cl^-$ selectivity in CLCF-type $F^-/H^+$ antiporters. *J. Gen. Physiol.* 144, 129–136. doi: 10.1085/jgp.201411225

Breaker, R. R. (2012). New insight on the response of bacteria to fluoride. *Caries Res.* 46, 78–81. doi: 10.1159/000336397

Busschaert, N., Karagiannidis, L. E., Wenzel, M., Haynes, C. J. E., Wells, N. J., Young, P. G., et al. (2014). Synthetic transporters for sulfate: a new method for the direct detection of lipid bilayer sulfate transport. *Chem. Sci.* 5:1118. doi: 10.1039/c3sc52006d

Cao, J., Yan, X., He, W., Li, X., Li, Z., Mo, Y., et al. (2017). C-I...π halogen bonding driven supramolecular helix of bilateral *N*-amidothioureas bearing beta-turns. *J. Am. Chem. Soc.* 139, 6605–6610. doi: 10.1021/jacs.6b13171

Clarke, H. J., Howe, E. N., Wu, X., Sommer, F., Yano, M., Light, M. E., et al. (2016). Transmembrane fluoride transport: direct measurement and selectivity studies. *J. Am. Chem. Soc.* 138, 16515–16522. doi: 10.1021/jacs.6b10694

Dutzler, R., Campbell, E. B., Cadene, M., Chait, B. T., and MacKinnon, R. (2002). X-ray structure of a ClC chloride channel at 3.0 A reveals the molecular basis of anion selectivity. *Nature* 415, 287–294. doi: 10.1038/415287a

Gale, P. A., Tong, C. C., Haynes, C. J., Adeosun, O., Gross, D. E., Karnas, E., et al. (2010). Octafluorocalix[4]pyrrole: a chloride/bicarbonate antiport agent. *J. Am. Chem. Soc.* 132, 3240–3241. doi: 10.1021/ja9092693

He, X., Li, P., Ji, Y., Wang, Y., Su, Z., and Elumalai, V. (2020). Groundwater arsenic and fluoride and associated arsenicosis and fluorosis in China: occurrence, distribution and management. *Expos. Health.* 12, 355–368. doi: 10.1007/s12403-020-00347-8

Ji, C., Stockbridge, R. B., and Miller, C. (2014). Bacterial fluoride resistance, Fluc channels, and the weak acid accumulation effect. *J. Gen. Physiol.* 144, 257–261. doi: 10.1085/jgp.201411243

Ketchem, R., Hu, W., and Cross, T. (1993). High-resolution conformation of gramicidin A in a lipid bilayer by solid-state NMR. *Science* 261, 1457–1460. doi: 10.1126/science.7690158

Marinho, V. C., Higgins, J. P., Sheiham, A., and Logan, S. (2003). Fluoride toothpastes for preventing dental caries in children and adolescents. *Cochrane Database Syst. Rev.* 7:CD002284. doi: 10.1002/14651858.CD002284

Park, G., Brock, D. J., Pellois, J. P., and Gabbai, F. P. (2019). Heavy pnictogenium cations as transmembrane anion transporters in vesicles and erythrocytes. *Chem* 5, 2215–2227. doi: 10.1016/j.chempr.2019.06.013

Park, G., and Gabbai, F. P. (2020). Phosphonium boranes for the selective transport of fluoride anions across artificial phospholipid membranes. *Angew. Chem. Int. Ed.* 59, 5298–5302. doi: 10.1002/anie.201914958

Ren, C., Ding, X., Roy, A., Shen, J., Zhou, S., Chen, F., et al. (2018a). A halogen bond-mediated highly active artificial chloride channel with high anticancer activity. *Chem. Sci.* 9, 4044–4051. doi: 10.1039/C8SC00602D

Ren, C., Zeng, F., Shen, J., Chen, F., Roy, A., Zhou, S., et al. (2018b). Pore-forming monopeptides as exceptionally active anion channels. *J. Am. Chem. Soc.* 140, 8817–8826. doi: 10.1021/jacs.8b04657

Rwenyonyi, C., Bjorvatn, K., Birkeland, J., and Haugejorden, O. (1999). Altitude as a risk indicator of dental fluorosis in children residing in areas with 0.5 and 2.5 mg fluoride per litre in drinking water. *Caries Res.* 33, 267–274. doi: 10.1159/000016528

Sheppard, D. N., Rich, D. P., Ostedgaard, L. S., Gregory, R. J., Smith, A. E., and Welsh, M. J. (1993). Mutations in CFTR associated with mild-disease-form $Cl^-$ channels with altered pore properties. *Nature* 362, 160–164. doi: 10.1038/362160a0

Simon, D. B., Karet, F. E., Hamdan, J. M., DiPietro, A., Sanjad, S. A., and Lifton, R. P. (1996). Bartter's syndrome, hypokalaemic alkalosis with hypercalciuria, is caused by mutations in the Na-K-2Cl cotransporter NKCC2. *Nat. Genet.* 13, 183–188. doi: 10.1038/ng0696-183

Stockbridge, R. B., Koide, A., Miller, C., and Koide, S. (2014). Proof of dual-topology architecture of Fluc $F^-$ channels with monobody blockers. *Nat. Commun.* 5:5120. doi: 10.1038/ncomms6120

Stockbridge, R. B., Kolmakova-Partensky, L., Shane, T., Koide, A., Koide, S., Miller, C., et al. (2015). Crystal structures of a double-barrelled fluoride ion channel. *Nature* 525, 548–551. doi: 10.1038/nature14981

Stockbridge, R. B., Lim, H. H., Otten, R., Williams, C., Shane, T., Weinberg, Z., et al. (2012). Fluoride resistance and transport by riboswitch-controlled CLC antiporters. *Proc. Natl. Acad. Sci. U.S.A.* 109, 15289–15294. doi: 10.1073/pnas.1210896109

Valkenier, H., Akrawi, O., Jurček, P., Sleziaková, K., Lízal, T., Bartik, K., et al. (2019). Fluorinated bambusurils as highly effective and selective transmembrane $Cl^-/HCO3^-$ antiporters. *Chem* 5, 429–444. doi: 10.1016/j.chempr.2018.11.008

Valkenier, H., Haynes, C. J. E., Herniman, J., Gale, P. A., and Davis, A. P. (2014). Lipophilic balance – a new design principle for transmembrane anion carriers. *Chem. Sci.* 5, 1128–1134. doi: 10.1039/c3sc52962b

Wu, X., Busschaert, N., Wells, N. J., Jiang, Y. B., and Gale, P. A. (2015). Dynamic covalent transport of amino acids across lipid bilayers. *J. Am. Chem. Soc.* 137, 1476–1484. doi: 10.1021/ja510063n

Wu, X., Howe, E. N. W., and Gale, P. A. (2018). Supramolecular transmembrane anion transport: new assays and insights. *Acc. Chem. Res.* 51, 1870–1879. doi: 10.1021/acs.accounts.8b00264

Wu, X., Judd, L. W., Howe, E. N. W., Withecombe, A. M., Soto-Cerrato, V., Li, H., et al. (2016). Nonprotonophoric electrogenic $Cl^-$ transport mediated by valinomycin-like carriers. *Chem* 1, 127–146. doi: 10.1016/j.chempr.2016.04.002

Wu, X., Small, J. R., Cataldo, A., Withecombe, A. M., Turner, P., and Gale, P. A. (2019). Voltage-switchable HCl transport enabled by lipid headgroup-transporter interactions. *Angew. Chem. Int. Ed.* 58, 15142–15147. doi: 10.1002/anie.201907466

Yan, X., Zou, K., Cao, J., Li, X., Zhao, Z., Li, Z., et al. (2019). Single-handed supramolecular double helix of homochiral bis(*N*-amidothiourea) supported by double crossed C-I...S halogen bonds. *Nat. Commun.* 10:3610. doi: 10.1038/s41467-019-11539-5

Yan, X. S., Luo, H., Zou, K. S., Cao, J. L., Li, Z., and Jiang, Y. B. (2018). Short azapeptides of folded structures in aqueous solutions. *ACS Omega* 3, 4786–4790. doi: 10.1021/acsomega.8b00041

Yan, X. S., Wu, K., Yuan, Y., Zhan, Y., Wang, J. H., Li, Z., et al. (2013). Beta-turn structure in glycinylphenylalanine dipeptide based *N*-amidothioureas. *Chem. Commun.* 49, 8943–8945. doi: 10.1039/c3cc44336a

Yuan, L., Fei, W., Jia, F., Jun-Ping, L., Qi, L., Fang-Ru, N., et al. (2020). Health risk in children to fluoride exposure in a typical endemic fluorosis area on

Loess Plateau, north China, in the last decade. *Chemosphere* 243:125451. doi: 10.1016/j.chemosphere.2019.125451

Zhang, L. E., Huang, D., Yang, J., Wei, X., Qin, J., Ou, S., et al. (2017). Probabilistic risk assessment of Chinese residents' exposure to fluoride in improved drinking water in endemic fluorosis areas. *Environ. Pollut.* 222, 118–125. doi: 10.1016/j.envpol.2016.12.074

Zhang, Y., Yan, X., Cao, J., Weng, P., Miao, D., Li, Z., et al. (2020). Turn conformation of beta-amino acid-based short peptides promoted by an amidothiourea moiety at C-terminus. *J. Org. Chem.* 85, 9844–9849. doi: 10.1021/acs.joc.0c01139

**Conflict of Interest:** The authors declare that the research was conducted in the absence of any commercial or financial relationships that could be construed as a potential conflict of interest.

frontiers in Chemistry

ORIGINAL RESEARCH
published: 28 January 2021
doi: 10.3389/fchem.2020.633065

# Synthesis and Characterization of Macrocyclic Chiral Tröger's Base Phenhomazine Candidates as Anticancer Agent

*Alhussein A. Ibrahim[1], Korany A. Ali[1], Naglaa A. Abdel Hafez[1], Mohamed A. Elsayed[1], Khalid M. H. Mohamed[2], Hanaa M. Hosni[3], Abd El-Galil E. Amr[4,5]* and Elsayed A. Elsayed[6,7]*

[1]Applied Organic Chemistry Department, National Research Centre, Giza, Egypt, [2]Pharmacognosy Department, National Research Centre, Giza, Egypt, [3]Pesticide Chemistry Department, National Research Center, Cairo, Egypt, [4]Pharmaceutical Chemistry Department, Drug Exploration and Development Chair (DEDC), College of Pharmacy, King Saud University, Riyadh, Saudi Arabia, [5]Organic Chemistry Department, Chemical Industries Research Division, National Research Centre, Cairo, Egypt, [6]Bioproducts Research Chair, Zoology Department, Faculty of Science, King Saud University, Riyadh, Saudi Arabia, [7]Chemistry of Natural and Microbial Products Department, National Research Centre, Cairo, Egypt

OPEN ACCESS

**Edited by:**
*Pavel Padnya, Kazan Federal University, Russia*

**Reviewed by:**
*Peter Cragg, University of Brighton, United Kingdom*
*Carmine Gaeta, Department of Chemistry and Biology Adolfo Zambelli, University of Salerno, Italy*

***Correspondence:**
*Abd El-Galil E. Amr*
*aamr@ksu.edu.sa*

**Specialty section:**
*This article was submitted to Supramolecular Chemistry, a section of the journal Frontiers in Chemistry*

**Received:** *24 November 2020*
**Accepted:** *23 December 2020*
**Published:** *28 January 2021*

**Citation:**
*Ibrahim AA, Ali KA, Hafez NAA, Elsayed MA, Mohamed KMH, Hosni HM, Amr AE-GE and Elsayed EA (2021) Synthesis and Characterization of Macrocyclic Chiral Tröger's Base Phenhomazine Candidates as Anticancer Agent. Front. Chem. 8:633065. doi: 10.3389/fchem.2020.633065*

1,4,7,10-Tetraoxa[10](2,8)trögerophane **5** was synthesized from its corresponding precursors. Heating of **2** with p-nitrophenoxide afforded bis(p-nitrophenyl)ether **3**, which was treated with hydrazine hydrate to give bis(p-aminophenyl)ether **4**. Treatment of **4** with paraformaldehyde and triflouroacetic anhydride gave trögerophane **5**. Reaction of **5** with trifluroacetic anhydride afforded phenhomazine derivative **6**, which was treated with potassium carbonate to afford tetrahydrophenhomazine **7**. Finally, reaction of **7** with phenacylchloride, bromoacetic acid, or ethyl bromoacetate in the presence of triethyl amine under reflux, afforded the corresponding macrocyclic compounds **8, 9** and **10**, respectively. The synthesized trögerophane,precursors and its newly synthesized phenhomazines derivatives were screened for anticancer activity. Results revealed that 1,4,7,10-tetraoxa[10](2,8)trögerophane had a promising selectivity towards colon cancer cell line with an $IC_{50}$ of 92.7 µg/ml.

**Keywords: chiral macrocyclic, tröger's base, trögerophane, phenhomazines, anticancer activity**

## INTRODUCTION

Tröger's base, "5,11-methano-2,8-dimethyl-5,6,11,12-tetrahydrodibenzo[b,f][1,5]diazocine" (**Figure 1**), was first prepared by Julius Tröger in 1887 by condensing dimethoxymethane with p-toluidine in the presence of hydrochloric acid (Tröger, 1887). In 1998, Alhussein et al. have reported a series of macrocyclic Tröger bases and their optical and complexing properties and named them for the first time as Trögerophanes (Ibrahim, et al., 1998; Miyahara, et al., 1999).

Tröger base and some of its macrocyclic analogues have been reported as anticancer agents (Johnson, et al., 1993; Gaslonde, et al., 2011; Paul, et al., 2012), antibacterial, antifungal and antifeedant (Thirunarayanan, 2017) and cytostatic activities (Kaplánek, et al., 2015). Although Tröger base and its analogues have attracted interest of many researcher groups due to their fascinating structures and properties (Yuan, et al., 2011), however, attention has been inadequately focused on these compounds from the biological point of view (Bailly, et al., 2000; Baldeyrou, et al., 2002; Manda, et al., 2014; Yang, et al., 2015). In addition, some of macrocyclic hetero-nitrogen derivatives have been synthesized (Abu-Ghalia, et al., 2012; Amr, et al., 2019; Naglah, et al., 2020) and have shown promising biological activity, i.e. analgesic and anticonvulsant (Amr, 2005),

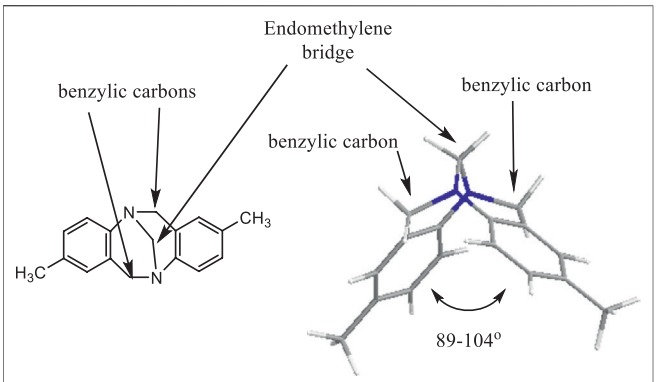


**FIGURE 1 |** Tröger's base structure.

antimicrobial (Amr, et al., 2006; Azab, et al., 2016), anti-proliferative, 5α-reductase inhibiting (Alanazi, et al., 2020), pharmacological (Al Thagfan, et al., 2018), anticancer (Amr et al., 2018), as well as biological activities (Khayyat and Amr, 2014). In view of these observations and in continuation of our previous work in macrocyclic chemistry, we synthesized some new Trögerophane derivatives and tested their anticancer activities.

# MATERIALS AND METHODS

## Materials

Triethylene glycol bis(p-aminophenyl) ether 4 was synthesized according to previously reported procedure (Ibrahim, et al., 1998). Paraformaldehyde, methanol, trifluroacetate, hydrazine hydrate, triethyl amine, phenacyl chloride, bromoacetic acid, and ethyl bromoacetate were all purchased from Sigma-Aldrich (Switzerland). All melting points were measured on a Gallenkamp melting point apparatus (Weiss Gallenkamp, London, UK). The infrared spectra were recorded in potassium bromide disks on a Pye Unicam SP 3300 and Shimadzu FT IR 8101 PC infrared spectrophotometers (Pye Unicam Ltd. Cambridge, England and Shimadzu, Tokyo, Japan, respectively). The NMR spectra were recorded on a Varian Mercury VX-300 NMR spectrometer (Varian, Palo Alto, CA, United States). 1H NMR spectra were run at 300 MHz and 13C NMR spectra were run at 75.46 MHz in deuterated chloroform (CDCl3) or dimethyl sulfoxide (DMSO-d6). Chemical shifts are given in parts per million and were related to that of the TMS as internal reference. Mass spectra were recorded on a Shimadzu GCMS-QP 1000 EX mass spectrometer (Shimadzu) at 70 eV. Elemental analyses were carried out at the Microanalytical Centre of Cairo University, Giza, Egypt and recorded on Elementar-Vario EL (Germany) automatic analyzer. TLC was performed on silica gel aluminum sheets, 60 F254 (E. Merck). Compounds 2-4 were prepared according to the reported literature (Ibrahim, et al., 1998).

## Synthesis of 1,4,7,10-tetraoxa[10](2,8) trögerophane (5)

To a mixture of triethylene glycol bis(p-aminophenyl) ether 4 (0.62 g, 0.0019 mol), conc. HCl (114 ml), and TFA (50 ml) in ethanol (240 ml) was stirred with cooling in an ice-bath to −10°C, paraformaldehyde (0.5 g) was added portion-wise while stirring. The reaction mixture was allowed to cool to room temperature and left for stirring at 60–70°C for further 18 h. Then, the mixture was concentrated under vacuum, basified with 28% ammonia solution, and extracted with methylene chloride (100 ml x 3). The methylene chloride phases were combined, dried (magnesium sulfate), and evaporated under vacuum to give a crude product which was purified by column chromatography (20 cm × 4 cm, silica gel 60, chloroform) to give **5** as colorless cubic crystals after recrystallization from ethanol/methylene chloride. Yield 43%, m.p. 233–235 °C (Lit. mp: 234–235 °C [2]). IR (film): ν = 3030, 3000 (C-H aromatic), 2930, 2900 (C-H aliphatic), 1605 (C-C stretching) cm−1. 1H NMR (300 MHz, $CDCl_3$): δ = 2.53–2.70 (m, 4H, O-$CH_2$-CH2), 3.50–3.63 (m, 4H, O-$CH_2$-$CH_2$), 3.98 (d, 2H, J = 16.17 Hz, -$CH_2$-Ar), 4.09–4.22 (m, 4H, O-$CH_2$-$CH_2$), 4.46 (s, 2H, -N-$CH_2$-N-), 4.57 (d, 2H, J = 16.17 Hz, -$CH_2$-Ar), 6.49 (d, 2H, J = 2.97 Hz. Ar-H), 6.83 (dd, 2H, $J_1$ = 5.94 Hz, $J_2$ = 2.64 Hz, Ar-H), 7.01 (d, 2H, J = 8.58 Hz, Ar-H). 13C NMR (75 MHz, $CDCl_3$): δ = 155.41, 141.58, 128.66, 125.07, 118.24, 116.86, 72.78, 69.88, 69.51, 68.40, 60.63 (21 C). MS (EI, 70 eV): m/z (%) = 368 (32) $[M]^+$. $C_{21}H_{24}N_2O_4$ (368.43). Calcd: C 68.46; H 6.57; N 7.60; found: C 68.29; H 6.57; N 7.45.

## Synthesis of N-Trifluroacetamide Phenhomazine Trifluroacetate (6)

The trögerophane **5** (0.239 g, 0.0065 mol) in trifluroacetic anhydride (10 ml) was refluxed for 65 h, after which the unreacted anhydride was recovered using a Dean-Stark trap. To the remaining residue, ethanol (20 ml) was added and the mixture was boiled under atmospheric pressure to get rid of the least traces of the anhydride. The remaining ethanol was removed under vacuum. The resulting colorless viscous liquid was treated with diethyl ether to afford colorless needles of the desired salt **6**. Yield 92%, m.p. 150–151°C (Dec.). IR (film): ν = 1697 (C=O) $cm^{-1}$. 1H NMR (300 MHz, $CDCl_3$): δ = 7.27 (d, 1H, J = 8.91 Hz, Ar-H), 7.23–7.86 (brs, 2H, N-H, exchangeable with $D_2O$), 6.94 (d, 1H, J = 8.58 Hz, Ar-H), 6.87–6.80 (m, 2H, Ar-H), 6.54 (d, 1H, J = 2.64 Hz, Ar-H), 6.44 (d, 1H, J = 2.97 Hz, Ar-H), 5.48 (d, 1H, J = 14.5 Hz, Ar-$CH_2$-N), 4.84 (d, 1H, J = 13.5 Hz, Ar-$CH_2$-N), 4.35–3.99 (m, 4H, O-$CH_2$-$CH_2$), 4.23 (d, 1H, J = 14.9 Hz, Ar-$CH_2$-N), 4.22 (d, 1H, J = 13.5 Hz, Ar-$CH_2$-N), 3.68–3.51 (m, 4H, O-$CH_2$-$CH_2$), 3.41–3.18 (m, 4H, O-$CH_2$-$CH_2$). MS (EI, 70 eV): m/z (%) = 566 (42) $[M]^+$. $C_{24}H_{24}N_2O_7F_6$ (566.45). Calcd: C 50.89; H 4.27; N 4.95; found: C 51.03; H 4.40; N 4.94.

## Synthesis of 1,4,7,10-Tetraoxa [10](2,8)-5,6,11,12-tetrahydrophenhomazine (7)

A mixture of trifluroacetate salt **6** (0.368 g, 0.0065 mol) and potassium carbonate (1.01 g) in methanol (15 ml) was stirred at 50 °C for 3 h. The solvent was evaporated under reduced pressure and the residue was treated with chloroform. The undissolved matter was filtered off, and the filtrate was evaporated under vacuum to give the free base as a white

powder which could be recrystallized from ethyl acetate to afford 7 as colorless crystals. Yield 79%, m.p. 172–173 °C. IR (film): ν = 3397 (N-H) $cm^{-1}$. 1H NMR (300 MHz, $CDCl_3$): δ = 6.68 (d, 1H, J = 2,51 Hz, Ar-H), 6.66 (d, 1H, J = 2,51 Hz, Ar-H), 6.50 (d, 2H, J = 2,51 Hz, Ar-H), 6.49 (d, 1H, J = 2,51 Hz, Ar-H), 6.47 (s, 1H, Ar-H), 4.79 (d, 2H, J = 13,55 Hz, Ar-$CH_2$-N), 4.29–4.20 (m, 2H, O-$CH_2$-$CH_2$), 4.08–3.96 (m, 2H, O-$CH_2$-$CH_2$), 3.97 (d, 2H, J = 14.05 Hz, Ar-$CH_2$-N), 3.96–3.72 (br.s, 2H, N-H, exchangeable with $D_2O$), 3.69–3.59 (m, 2H, O-$CH_2$-$CH_2$), 3.48–3.38 (m, 2H, O-$CH_2$-$CH_2$), 3.11–3.01 (m, 2H, O-$CH_2$-$CH_2$), 2.88–2.79 (m, 2H, O-$CH_2$-$CH_2$). 13C NMR (75 MHz, $CDCl_3$): δ = 152.99, 143.18, 128.81, 120.59, 119.62, 117.14, 71.03, 69.60, 68.86, 51.84 (20 C). MS (EI, 70 eV): m/z (%) = 356 (25) $[M]^+$. $C_{20}H_{24}N_2O_4$ (356.42). Calcd: C 67.40; H 6.79; N 7.86; found: C 67.34; H 6.85; N 7.77.

## Synthesis of N,N`-Diphenacyl Phenhomazine (8)

To a mixture of the tetrahydrophenhomazine **7** (0.356 g, 0.001 mol), and phenacyl chloride (0.308 g, 0.002 mol) in ethanol (100 ml), triethyl amine (1.0 ml) was added dropwisely. The reaction mixture was refluxed for 2 h. The reaction was followed up by TLC. At the end, the reaction mixture was evaporated under vacuum. The solid formed was collected and recrystallized from ethanol to give **8**. Yield 64.4%, m.p. 190–192°C. IR (film): ν = 3044, 3020, 2982, 2966, 1698, 1694 $cm^{-1}$. 1H NMR (300 MHz, $CDCl_3$): δ = 7.61–7.58 (m, 4H, Ar-H), 7.45–7.39 (m, 6H, Ar-H, 6.70 (d, 2H, J = 8,56 Hz, Ar-H), 6.60 (dd, 2H, $J_1$ = 2,62 Hz, $J_2$ = 8.56 Hz, Ar-H), 6.43 (d, 2H, J = 8,56 Hz, Ar-H), 5.55 (d, 2H, J = 13,90 Hz, Ar-$CH_2$-N), 4.50 (s, 4H, N-$CH_2$-CO-), 4.45 (d, 2H, J = 13,90 Hz, Ar-$CH_2$-N), 4.28–4.20 (m, 2H, O-$CH_2$-$CH_2$), 4.03–3.95 (m, 2H, O-$CH_2$-$CH_2$), 3.62–3.44 (m, 4H, O-$CH_2$-$CH_2$), 3.37–3.16 (m, 2H, O-$CH_2$-$CH_2$), 2.99–2.82 (m, 2H, O-$CH_2$-$CH_2$). 13C NMR (75 MHz, $CDCl_3$): δ = 189.3, 145.2, 140.2, 135.1, 133.2, 129.1, 128.9, 127.4, 113.5, 111.1, 109.5, 67.3, 66.9, 65.3, 62.5, 59.6 (36 C). MS (EI, 70 eV): m/z (%) = 592 (16) [M]+. $C_{36}H_{36}N_2O_6$ (592.69). Calcd: C 72.95; H 6.12; N 4.73; found: C 72.84; H 6.07; N 4.60.

## Synthesis of N,N`-Dicarboxymethyl Phenhomazine (9)

Triethylamine (1.0 ml) was added dropwisely to a refluxing mixture of tetrahydrophenhomazine **7** (0.356 g, 0.001 mol), and bromoacetic acid (0.278 g, 0.002 mol) in ethanol (100 ml). The mixture was refluxed for 2 h. At the end of the reaction as indicated by TLC, the reaction mixture was evaporated under vacuum. The solid formed was collected and recrystallized from ethanol to give **9**. Yield 70.3%, m.p. 210–212 °C. IR (film): ν = 3400–2800, 1710, 1706, 1210, 1195 $cm^{-1}$. 1H NMR (300 MHz, $CDCl_3$): δ = 12.5 (s, 2H, COOH), 6.64 (d, 2H, J = 8.58 Hz, Ar-H), 6.56 (dd, 2H, $J_1$ = 2.62 Hz, $J_2$ = 8.58 Hz, Ar-H), 6.39 (d, 2H, J = 2,62 Hz, Ar-H), 4.54 (d, 2H, J = 13.8 Hz, Ar-$CH_2$-N), 4.36 (d, 2H, J = 13.8Hz, Ar-$CH_2$-N), 4.20 (s, 4H, N-$CH_2$-CO-), 4.28-4.20 (m, 2H, O-$CH_2$-$CH_2$), 4.03-3.95 (m, 2H, O-$CH_2$-$CH_2$), 3.62–3.44 (m, 4H, O-$CH_2$-$CH_2$), 3.37–3.16 (m, 2H, O-$CH_2$-$CH_2$), 2.99–2.82 (m, 2H, O-$CH_2$-$CH_2$). 13C NMR (75 MHz, $CDCl_3$): δ = 175.3, 147.2, 145.3, 140.9, 125.5, 113.6, 109.9, 107.5, 68.3, 67.8, 67.1, 62.9 (24 C). MS (EI, 70 eV): m/z (%) = 472 (24) $[M]^+$. $C_{24}H_{28}N_2O_8$ (472.18). Calcd: C 61.01; H 5.97; N 5.93; found: C 60.90; H 5.85; N 5.81.

## Synthesis of N,N`-Diethoxycarbonylmethyl Phenhomazine (10)

To a refluxing mixture of tetrahydrophenhomazine **7** (0.356 g, 0.001 mol), and ethyl bromoacetate (0.334 g, 0.002 mol) in ethanol (100 ml), triethylamine (1.0 ml) was added dropwisely. The reflux was continued for 2 h. The reaction was followed up by TLC. At the end, the reaction mixture was evaporated under vacuum. The solid obtained was collected and recrystallized from ethanol to give **10**. Yield 77.6%, m.p. 199–201°C. IR (film): ν = 1732, 1729, 1245, 1187 $cm^{-1}$. 1H NMR (300 MHz, $CDCl_3$): δ = 6.65 (d, 2H, J = 8.58 Hz, Ar-H), 6.58 (dd, 2H, $J_1$ = 2.64 Hz, $J_2$ = 8.58 Hz, Ar-H), 6.40 (d, 2H, J = 2,64 Hz, Ar-H), 5.54 (d, 2H, J = 14 Hz, Ar-$CH_2$-N), 4.25 (s, 4H, N-$CH_2$-CO-), 4.36 (d, 2H, J = 14 Hz, Ar-$CH_2$-N), 4.28-4.20 (m, 2H, O-$CH_2$-$CH_2$), 4.10 (q, 4H, J = 8 Hz, $CH_3$-$CH_2$-CO-), 4.03-3.95 (m, 2H, O-$CH_2$-$CH_2$), 3.62–3.44 (m, 4H, O-$CH_2$-$CH_2$), 3.37-3.16 (m, 2H, O-$CH_2$-$CH_2$), 2.99-2.82 (m, 2H, O-CH2-CH2), 1.11 (t, 6H, J = 8 Hz, CH3-CH2-CO-). 13C NMR (75 MHz, $CDCl_3$): δ = 170.1, 147.2, 142.1, 125.5, 112.3, 109.3, 107.7, 68.3, 67.8, 67.3, 61.0, 60.6, 58.5, 14.2 (28 C). MS (EI, 70 eV): m/z (%) = 528 (22) $[M]^+$. $C_{28}H_{36}N_2O_8$ (528.25). Calcd: C 63.62; H 6.86; N 5.30; found: C 63.31; H 6.18; N 4.93.

## Anti-Cancer Screening

The newly synthesized derivatives were assessed against three cancer cell lines; namely hepatocellular carcinoma (HepG-2), breast adenocarcinoma (MCF-7) and Colon Carcinoma (HCT-116) using standard MTT assay (El-Faham, et al., 2014; Elsayed, et al., 2016; Amr, et al., 2018). The assay depends on the mitochondrial reduction of yellow MTT (3-(4,5-dimethylthiazol-2-yl)-2,5-diphenyltetrazolium bromide) to purple formazan. Briefly, cells were propagated in RPMI-1640 medium supplemented with 1% antibiotic–antimycotic mixture and 1% L-glutamine at 37°C and 5% CO2. Upon investigation, cells were plated at a concentration of 104 cells/well in 96-well microtiter plates and incubated for 24 h. Accordingly, exhausted medium was aspirated and fresh medium was added. Then cells were treated with different concentrations of the prepared compounds (0.78–100.00 μg/ml), and inmcubation proceeded for another 48 h. Afterwards, medium was aspirated and 40 μl MTT (2.5 mg/ml/well) was added and the plates were futher incubated for 4 h. The reaction as terminated by the addition of 200 μl/well of 10% sodium dodecyl sulfate, and the plates were incubated overnight to dissolve the developed formazan dey. Doxorubicin was used as positive control. DMSO is the vehicle used for dissolution of compounds, and its final concentration on the cells was less than 0.2%. Absorbance was read using a microplate multi-well reader at 595/620 nm. Results were statistically evalued using an independent *t* test and SPSS 11

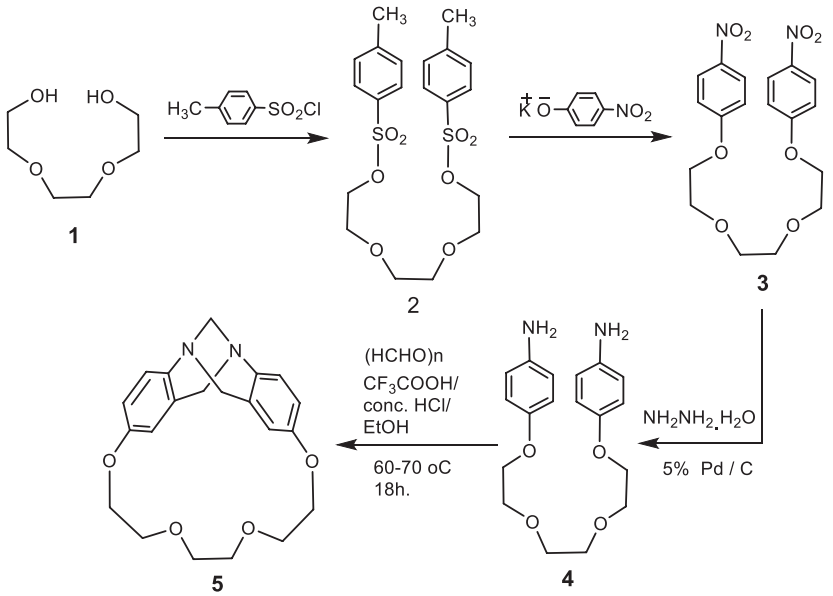


**SCHEME 1 |** Synthetic rout for trögerophane 5.

program. The percentage inhibition in cell viability was calculated:

(Absorbanceextract/AbsorbanceDMSO)−1 × 100%

A probit analysis was carried for IC50 and IC90 determination using the SPSS 11 program.

## RESULTS AND DISCUSSION

### Synthesis

In the present study, we synthesized some newly phenhomazine derivatives, **6–10**, using 1,4,7,10-tetraoxa[10](2,8)trögerophane, **5** as a starting material. The rigidity, V-shape, and the presence of a C2 axis of symmetry, have imparted unique structural features on the molecule. Including crown ether oxygens was thought to provide the macrocycle with many important and interesting characteristics. Accordingly, oxygen atoms can increase the solubility in organic solvents by taking advantage of the flexibility of the ether linkage. Also, crown ether linkage can provide the macrocyle with complexing capabilities. In addition, it can keep the chirality of the molecule unchanged when the endomethylene bridge is removed. Therefore, increasing the energy barrier against inversion of the dibenzodiazocine moiety will produce in one fixed conformation for this macrocycle. Earlier, we have reported the synthesis of this trögerophane 5 (Ibrahim, et al., 1998; Miyahara, et al., 1999). In this work we aimed at improving the method used to synthesize this compound, in addition to introduce an unprecedented study about the biological activities of **5** with some of its precursors and its newly synthesized phenhomazine derivatives. The requisite precursors for the cyclization were synthesized via simple processes. Heating triethylene glycol bis(p-toluenesulfonate) **2** with p-nitrophenoxide afforded the corresponding bis(p-nitrophenyl)ether 3, which was treated with hydrazine hydrate in the presence of 5% Pd/C as catalyst to give bis(p-aminophenyl)ether **4** (Ibrahim, et al., 1998; Miyahara, et al., 1999). In the reported method, the intramolecular condensation cyclization of 4 to form 5 in 45% yield, was carried out by reaction with 37% formalin in the presence of concentrated hydrochloric acid under moderately dilute conditions in ethanol at room temperature for 13 days. In order to reduce longer reaction time (13 days) as well as higher solvent consumption, a wide variety of reaction conditions were searched by analyzing the products via HPLC. From the modified method, it can be concluded that raising the reaction temperature to 60–70 °C and using TFA with conc. HCl, and replacing formalin with p-formaldehyde, shortens the reaction time to 18 h, as well as decreasing the amount of consumed ethanol without significantly affecting the yields of trögerophane **5** (43%) (**Scheme 1**).

Treatment of trögerophane **5** with refluxing trifluroacetic anhydride afforded the N-trifluroacetamide phenhomazine trifluroacetate **6**, which was stirred with potassium carbonate in methanol for 3 h to afford a good yield of 1,4,7,10-tetraoxa [10](2,8)-5,6,11,12-tetrahydrophenhomazine **7** (Scheme 2). The structures of both **6** and **7** were confirmed on the basis of their elemental and spectral data. The IR spectrum of **7** reveals only one absorption band for the N-H stretching at ν 3398 $cm^{-1}$ indicating the symmetry of the molecule and the absence of intramolecular hydrogen bonding between the secondary amine protons and the transanular nitrogen. 1H-NMR spectrum showing two N-H protons appearing as broad singlet at δ 3.96–3.72 ppm is consistent with the assumed. Reaction of tetrahydrophenhomazine **7** with active electrophiles, namely phenacyl chloride, bromoacetic acid, and ethyl bromoacetate, in the presence of triethyl amine under reflux, afforded the

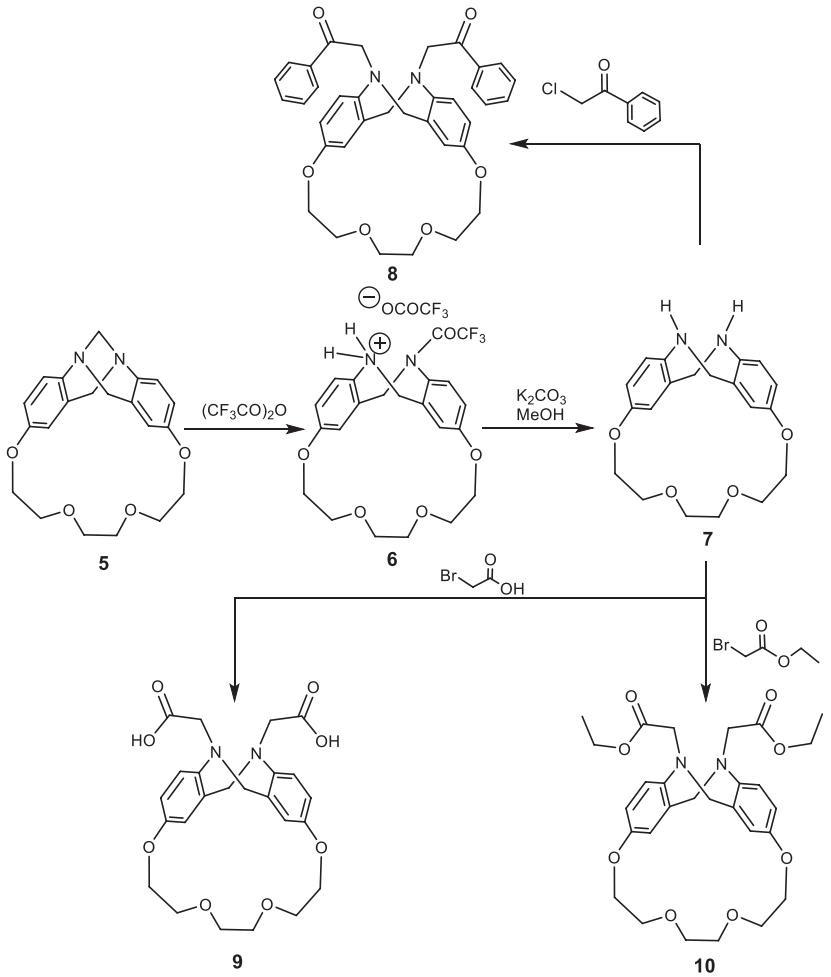


**SCHEME 2 |** Synthetic routs for phenhomazine derivatives 6–10.

corresponding N,N`-disubstituted phenhomazines **8, 9** and **10**, respectively (**Scheme 2**).

The IR spectrum of N, N`-diphenacyl phenhomazine **8** revealed two bands at ν 1698, 1694 $cm^{-1}$ indicating the phenacyl C=O bonds. In case of the N,N`-dicarboxymethyl phenhomazine **9**, a broad band at ν 3400–2800 $cm^{-1}$ was clearly indicating that hydrogen bonded carboxylic O-H, and others at ν 1710, 1706 $cm^{-1}$ were due to the C=O of the carboxylic group. Furthermore, N,N`-diethoxycarbonylmethyl phenhomazine **10**, gave bands at ν 1732, 1729 $cm^{-1}$ which can be related to the ester C=O bonds. In addition to these IR data, the absence of the stretching vibration band of the N-H of the tetrahydrophenhomazine, proved that the electrophylic substitution reaction has occurred as expected. In addition to their 13C-NMR, which were consistent with the proposed structures of **8, 9,** and **10**, their 1H NMR spectra revealed highly indicative peaks which supported the claimed structures. For example, the singlet at δ 4.5 ppm indicated 4 protons of the two methylene groups of the phenacyl moiety. The singlet at δ 12.5 ppm in the 1H NMR spectrum of **9** is quiet enough to confirm the presence of the carboxylic protons. Finally, the presence of a quartet at δ 4.10 ppm, and a triplet at δ 1.11 ppm with the same coupling constant (J = 8 Hz), proved the presence of the ethyl group protons in the structure of **10**.

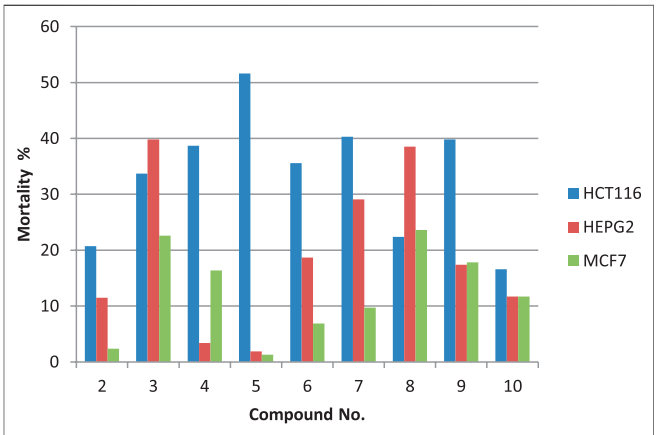


**FIGURE 2 |** Percent mortality values for the prepared compounds against different cancer cell lines tested at 100 μg/ml.

## Anticancer Activity

The cytotoxic potentials of the prepared compounds **2–10** against the investigated human tumor cell lines HCT-116, HepG-2 and MCF-7) were investigated using standard MTT assay with doxorubicin as the reference drug. DMSO was used as the negative control. Cells were exposed to different concentrations of the prepared compounds (0.78–100.00 μg/ml). Results presented in **Figure 2** show that only trögerophane **5** had promising cytotoxic effects against HCT-116 carcinoma cell, where the obtained with $IC_{50}$ recorded 92.7 μg/ml. Other tested compounds showed some sort of weak cytotoxicity, however, the investigated concentration range was not appropriate to obtain $IC_{50}$ values for these compounds. Results also revealed that the obtained $IC_{50}$ value for the most potent compound, **5**, against HCT-116, was almost similar to that obtained by the tested positive drug, doxorubicin (85.3 μg/ml).

Results showed that different synthesized derivative reacted differently towards various cell lines. This is expected, since different cell types react differently towards affecting compounds due to their inherent differences in membrane structures and functions (Kaplánek et al., 2015; Elsayed, et al., 2016; Amr, et al., 2018). Furthermore, our results revealed that the prepared trögerophane **5** had showed the most promising cytotoxic effect against colon cancer cell line. This is in good agreement with those results published earlier, where Gaslonde et al. (2011) reported the cytotoxic potentials of their prepared trögerophanes against L1210 leukemia and KB-3-1 solid tumor cell lines. They also found that the prepared trögerophane were more potent than their corresponding parent molecules. Furthermore, Kaplánek et al. (2015) synthesized and evaluated the anticancer potentials of different hydrazone derivatives prepared based on tröger's base structure. They also reported promising cytotoxic potentials against various cancer cell lines ranging from 0.05 to >100 μM. However, it is difficult to compare our obtained $IC_{50}$ values with those previously reported in the literature against the same cell line due to different descriptors of activities, i.e $IC_{50}$, $EC_{50}$, $GI_{50}$, etc.), different structures, as well as different experimental conditions.

## DATA AVAILABILITY STATEMENT

The original contributions presented in the study are included in the article/Supplementary Material, further inquiries can be directed to the corresponding author.

## AUTHOR CONTRIBUTIONS

The listed authors contributed to this work as described in the following: AI, KA, NH, and ME gave the concepts of the work, interpretation of the results, the experimental part and prepared the manuscript, HH, and AA cooperated in the preparation of the manuscript and performed the revision before submission. KM and EE contributed to the anticancer activity. All authors have read and agreed to the published version of the manuscript.

## FUNDING

The authors are grateful to the Deanship of Scientific Research, king Saud University for funding through Vice Deanship of Scientific Research Chairs.

## REFERENCES

Abu-Ghalia, M. H., Abd El-Hamid, M., Zweel, M. A., Amr, A. E., and Moafi, S. A. (2012). Synthesis and reactions of new chiral linear and macrocyclic tetra- and penta-peptide candidates. *Z. Naturforsch*. 67b, 806–818. doi:10.5560/ZNB.2012-0116

Al Thagfan, S. S., Fayed, A. A., Bahshwan, S. A., Amr, A. E., Aljuhani, N., Al-Omar, M. A., et al. (2018). Pharmacological activities of some synthesized chiral macrocyclic pentapeptide Schiff base candidates. *Biomedical Research* 29, 3605–3609. doi:10.4066/biomedicalresearch.29-18-1058

Alanazi, M. M., Amr, A. E., Naglah, A. M., Abdel-Mageid, R. E., and Elsayed, E. A. (2020). Anti-proliferate activity and 5α-reductase inhibitors of chiral macrocyclic (nα-di-nicotinoyl)[l-phenylalaninyl-l-leucinyl]pentapeptide candidates against lncap and pc-3 prostate cancer cell lines. *J. Sci. Ind. Res.* 79, 60–65. Available at: http://nopr.niscair.res.in/handle/123456789/53460

Amr, A. E., Abo-Ghalia, M. H., and Abdalla, M. M. (2006). Synthesis of novel macrocyclic peptido-calix[4]arenes and peptidopyridines as precursors for potential molecular metallacages, chemosensors and biologically active candidates. *Z. Naturforsch*. 61b, 1335–1345. doi:10.1515/znb-2006-1104

Amr, A. E., Abo-Ghalia, M. H., Moustafa, G. O., Al-Omar, M. A., Nossir, E., and Elsayed, E. A. (2018). Design, synthesis and docking studies of novel macrocyclic pentapeptides as anticancer multi-targeted kinase inhibitor. *Molecules* 23, 2416. doi:10.3390/molecules23102416

Amr, A. E., El-Naggar, M., Al-Omar, M. A., Elsayed, E. A., and Abdalla, M. M. (2018). *In Vitro* and in Vivo anti-breast cancer activities of some synthesized pyrazolinyl-estran-17-one candidates. *Molecules* 23, 1572. doi:10.3390/molecules23071572

Amr, A. E., Naglah, A. M., Sabry, N. M., Ibrahim, A. A., Elsayed, E. A., and Attar, A. (2019). Synthesis and investigation of 3,5-bis-linear and macrocyclic tripeptidopyridine candidates by using l-valine, N,N′-(3,5-pyridinediyldicarbonyl)bis-dimethyl ester as synthon. *Z. Naturforsch. B Chem. Sci.* 74b, 473–478. doi:10.1515/znb-2019-0006

Amr, A. E. (2005). Synthesis of some new linear and chiral macrocyclic pyridine carbazides as analgesic and anticonvulsant agents. *Z. Naturforsch*. 60b, 990–998. doi:10.1515/znb-2005-0914

Azab, M. E., Flefel, E. M., Sabry, N. M., and Amr, A. E. (2016). Synthesis and antimicrobial activity of some linear dipeptide pyridine and macrocyclic pentaazapyridine candidates. *Z. Naturforsch*. 71, 803–810. doi:10.1515/znb-2016-0018

Bailly, C., Laine, W., Demeunynck, M., and Lhomme, J. (2000). Enantiospecific recognition of DNA sequences by a proflavine Tröger base. *Biochem. Biophys. Res. Commun.* 273, 681–685. doi:10.1006/bbrc.2000.2997

Baldeyrou, B., Tardy, C., Bailly, C., Colson, P., Houssier, C., Charmantray, F., et al. (2002). Synthesis and DNA interaction of a mixed proflavine-phenanthroline Tröger base. *Eur. J. Med. Chem.* 37, 315–322. doi:10.1016/S0223-5234(02)01356-9

El-Faham, A., Elzatahry, A., Al-Othman, Z., and Elsayed, E. A. (2014). Facile method for the synthesis of silver nanoparticles using 3-hydrazino-isatin derivatives in aqueous methanol and their antibacterial activity. *Int. J. Nanomed.* 9, 1167–1174. doi:10.2147/ijn.s58571

Elsayed, E. A., Sharaf-Eldin, M. A., El-Enshasy, H. A., and Wadaan, M. (2016). *In vitro* assessment of anticancer properties of moringa peregrina essential seed oil on different cell lines. *Pakistan J. Zool.* 48, 853–859. doi:0030-9923/2016/0003-0853

Gaslonde, T., Leonce, S., Pierre, A., Pfeiffer, B., and Michel, S. (2011). Tröger's bases in the acronycine, benzo[a]acronycine, and benzo[b]acronycine series. *Tetrahedron Lett* 52, 4426–4429. doi:10.1016/j.tetlet.2011.06.064

Ibrahim, A. A., Matsumoto, M., Miyahara, Y., Izumi, K., Suenaga, M., Shimizu, N., et al. (1998). Synthesis and properties of a new series of trögerophanes. *J. Heterocycl. Chem.* 35, 209–215. doi:10.1002/jhet.5570350139

Johnson, R. A., Gorman, R. R., Wnuk, R. J., Crittenden, N. J., and Aiken, J. W. (1993). Tröger's base. An alternate synthesis and a structural analog with thromboxane A2 synthetase inhibitory activity. *J. Med. Chem.* 36, 3202–3206. doi:10.1021/jm00073a023

Kaplánek, R., Havlík, M., Dolenský, B., Rak, J., Džubák, P., Konečný, P., et al. (2015). Synthesis and biological activity evaluation of hydrazone derivatives based on a Tröger's base skeleton. *Bioorg. Med. Chem.* 23, 1651–1659. doi:10.1016/j.bmc.2015.01.029

Khayyat, S., and Amr, Ael-G. (2014). Synthesis and biological activities of some new (Nα-dinicotinoyl)-bis-L-leucyl linear and macrocyclic peptides. *Molecules* 19, 10698–10716. doi:10.3390/molecules190810698

Manda, B. R., Alla, M., Ganji, R. J., and Addlagatta, A. (2014). Discovery of Tröger's base analogues as selective inhibitors against human breast cancer cell line: design, synthesis and cytotoxic evaluation. *Eur. J. Med. Chem.* 86, 39–47. doi:10.1016/j.ejmech.2014.08.044

Miyahara, Y., Izumi, K., Ibrahim, A. A., and Inazu, T. (1999). Novel C2 chiral diamine ligands derived from cyclic Tröger bases. *Tetrahedron Letters* 40, 1705–1708. doi:10.1016/S0040-4039(99)00032-5

Naglah, A. M., Amr, A. E., Abdel-Mageid, R. E., Al-Omar, M. A., and Abd El-Salam, O. I. (2020). Synthesis of chiral 3,5-bis(l-phenylalaninyl-l-leucinyl)pyridine Schiff base and their macrocyclic carboxaimide derivatives using 3,5-bis(l-phenylalaninyl)-pyridine methyl ester. *Z. Naturforsch. B Chem. Sci.* 75b, 251–258. doi:10.1515/znb-2019-0146

Paul, A., Maji, B., Misra, S. K., Jain, A. K., Muniyappa, K., and Bhattacharya, S. (2012). Stabilization and structural alteration of the G-quadruplex DNA made from the human telomeric repeat mediated by Tröger's base based novel benzimidazole derivatives. *J. Med. Chem.* 55, 7460–7471. doi:10.1021/jm300442r

Thirunarayanan, G. (2017). Antimicrobial and insect antifeedant activities of some Tröger's bases. *Arab. J. Chem.* 10, S636–S643. doi:10.1016/j.arabjc.2012.10.025

Tröger, J. (1887). Ueber einige mittelst nascirenden Formaldehydes entstehende Basen. *J. Prakt. Chem.* 36, 225–245. doi:10.1002/prac.18870360123

Yang, Z., Zhang, H., Yu, B., Zhao, Y., Ma, Z., Ji, G., et al. 2015). Azo-functionalized microporous organic polymers: synthesis and applications in CO2 capture and conversion. *Chem Commun (Camb)* 51, 11576–11579. doi:10.1039/c5cc03151f

Yuan, C., Xin, Q., Liu, H., Wang, L., Jiang, M., and Tao, X. (2011). Λ-shaped optoelectronic materials based on Tröger's base. *Sci. China Chem.* 54, 587–595. doi:10.1007/s11426-011-4224-z

**Conflict of Interest:** The authors declare that the research was conducted in the absence of any commercial or financial relationships that could be construed as a potential conflict of interest.

frontiers in Chemistry

MINI REVIEW
published: 17 February 2021
doi: 10.3389/fchem.2021.635507

# Design of Cyclodextrin-Based Functional Systems for Biomedical Applications

*Wanjia Xu[1], Xiumei Li[1], Liang Wang[1], Siyuan Li[1], Shengnan Chu[1], Jiachun Wang[2], Yijia Li[1], Jinxing Hou[1], Quan Luo[1,2,3]* and Junqiu Liu[1]*

[1]State Key Laboratory of Supramolecular Structure and Materials, College of Chemistry, Jilin University, Changchun, China, [2]Key Laboratory of Emergency and Trauma, Ministry of Education, College of Emergency and Trauma, Hainan Medical University, Haikou, China, [3]Key Laboratory for Molecular Enzymology and Engineering of Ministry of Education, School of Life Sciences, Jilin University, Changchun, China

Cyclodextrins (CDs) are a family of α-1,4-linked cyclic oligosaccharides that possess a hydrophobic cavity and a hydrophilic outer surface with abundant hydroxyl groups. This unique structural characteristic allows CDs to form inclusion complexes with various guest molecules and to functionalize with different substituents for the construction of novel sophisticated systems, ranging from derivatives to polymers, metal-organic frameworks, hydrogels, and other supramolecular assemblies. The excellent biocompatibility, selective recognition ability, and unique bioactive properties also make these CD-based functional systems especially attractive for biomedical applications. In this review, we highlight the characteristics and advantages of CDs as a starting point to design different functional materials and summarize the recent advances in the use of these materials for bioseparation, enzymatic catalysis, biochemical sensing, biomedical diagnosis and therapy.

**Keywords: cyclodextrin, selective recognition, inclusion complexes, functional materials, biomedical applications**

OPEN ACCESS

***Edited by:***
*Tony D. James,*
*University of Bath, United Kingdom*

***Reviewed by:***
*Bang-Jing Li,*
*Chinese Academy of Sciences, China*
*Eric Monflier,*
*Artois University, France*

****Correspondence:***
*Quan Luo*
*luoquan@jlu.edu.cn*

***Specialty section:***
*This article was submitted to Supramolecular Chemistry, a section of the journal Frontiers in Chemistry*

***Received:*** *30 November 2020*
***Accepted:*** *07 January 2021*
***Published:*** *17 February 2021*

***Citation:***
*Xu W, Li X, Wang L, Li S, Chu S, Wang J, Li Y, Hou J, Luo Q and Liu J (2021) Design of Cyclodextrin-Based Functional Systems for Biomedical Applications. Front. Chem. 9:635507. doi: 10.3389/fchem.2021.635507*

## INTRODUCTION

CDs are well-known macrocyclic compounds that contain five or more α-D-glucopyranoside units linked by α-1,4-glycosidic bonds in the shape of a hollow truncated cone. In nature, α-, β-, and γ-CDs are three main types of members with six, seven, and eight units of glucose, respectively (Saenger, 1980) (see **Figure 1**). These molecules have a distinctive feature in their stereochemical structures, a relatively hydrophobic inner cavity with the diameter increased with the number of glucose units and a hydrophilic outer surface covered with abundant hydroxyl groups (Chen and Jiang, 2011). Thus, CDs can provide a favorable microenvironment to form inclusion complexes with various organic and bioactive molecules in different stoichiometry ratios (1:1, 1:2, 2:1 or 2:2) (Szejtli, 1998; Pinho et al., 2014). The selectivity of host-guest recognition arises from a size/shape-matching mechanism that requires the guest molecules to be trapped entirely or partially into the apolar CD cavities (Liu and Chen, 2006). The hydroxyl groups of CDs are also involved in the binding processes via electrostatic forces, Van der Waals, and hydrogen bonding interactions (Liu and Guo, 2002). The binding strength relies on the synergistic effect of these weak and reversible noncovalent interactions. This encapsulation ability will change the physiochemical properties of the included guest molecules, which has been widely explored for practical applications in biomedical fields by developing CD-based functional systems (Uekama et al., 1998; Davis and Brewster, 2004).

Natural CDs are hydrophilic, but exhibit a relatively low aqueous solubility due to the formation of aggregates via strong intermolecular hydrogen bonding (Coleman et al., 1992),

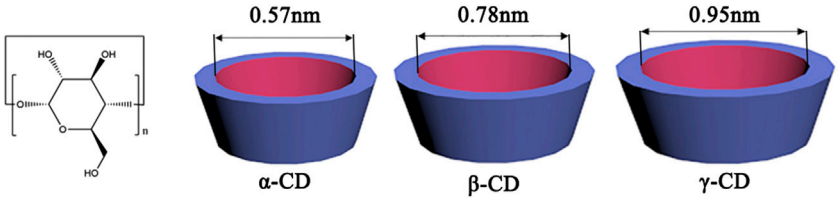


**FIGURE 1 |** The structures of α-CD (n = 6), β-CD (n = 7), and γ-CD (n = 8).

which limits the range of their applicability. This shortcoming may cause nephrotoxicity when there is an accumulation of insoluble cyclodextrin crystals or cyclodextrin-cholesterol complexes in kidneys (Frijlink et al., 1991). Over the past few decades, a great effort has been devoted to improving the performances of CDs with the desired properties through various chemical modifications (Bellia et al., 2009; Řezanka, 2019). CDs have three types of hydroxyl groups, including the easily modified 6-OH groups on the upper rim and the most acidic 2-OH and the least accessible 3-OH groups on the lower rim. The different reactivity of these hydroxyl groups offers the possibility of regioselective substitution to yield more than 11,000 cyclodextrin derivatives by grafting with a large amount of functional groups (e.g., amines, amino acids, peptides, and aromatic groups) for improving their solubility and complexation capacity. In addition, the structural complexity can also be widened by the formation of inclusive complex between the bridged/branched CDs and guest molecules to construct more sophisticated supramolecular systems such as polymers, metal-organic frameworks, hydrogels, and other supramolecular assemblies (Nakahata et al., 2017; He et al., 2019; Zhang et al., 2020). These high-level superstructures allow for the functionalization with the bioactive moieties through supramolecular interactions or physical entrapment to achieve diverse functions by designing molecular receptors, delivery vectors, enzyme mimics, and fluorescence indicators.

In this review, the recent advance in the development of CD-based functional systems was summarized. The design strategies, physicochemical properties, and functional diversity of different CD derivatives and their high-level assemblies were discussed in detail. We also highlighted the unique advantages of these materials to achieve excellent performances, which show great potential in the field of bioseparation, enzymatic catalysis, biochemical sensing, biomedical diagnosis, and therapy for biomedical applications.

## CHIRAL RECOGNITION FOR BIOSEPARATION

Chiral discrimination is a hot topic in the field of biomedicines. This interest is driven by the different bioactivities and biotoxicities of chiral molecules when they participate in the biochemical processes through specific interactions with the biomolecules. Since the possibility of chiral separation was first demonstrated by using chiral stationary phases for chromatography in 1980 (Berthod, 2010), a wide variety of powerful techniques based on chromatography and electrophoresis have been developed (Sánchez-López et al., 2015). Chiral selectors act as a key factor to achieve enantioselective resolution by the formation of diastereomeric complexes with chiral analytes via intermolecular interactions, such as ion interactions, π-π interactions, van der Waals interactions, and hydrogen bonds. CDs are widely used chiral selectors, which have the following advantages (Rezanka et al., 2014): 1) The OH groups can be modified to design diverse derivatives for enantioseparation in different environments, including aqueous, polar organic, and nonpolar organic and 2) CDs can provide a chiral lipophilic cavity for selective recognition of nonpolar analytes without strict structural restriction.

### Drug Enantioseparation

Chiral drugs account for more than 40% of the market share, which involves the treatment of a variety of diseases (Calcaterra and D'Acquarica, 2018). The use of pure drug stereoisomers will elicit more exact therapeutic effects to guarantee the safety. Since the United States Food and Drug Administration (FDA) and the European Committee for Proprietary Medicinal Products (CPMP) have claimed that the property of each enantiomer must be studied before it is marketed as one of the enantiomers or racemic drugs in 1992 (FDA, 1992), the demand for chiral drugs is met by developing the methods of chiral drug detection and separation. Native CDs exhibit enantiorecognition to differentiate enantiomeric species through the formation of diastereomeric complexes, which extend the applicability of current methods by adding to the stationary phase or the background electrolyte. Moreover, a large number of derivatives (e.g., neutral, cationic, and anionic CDs) were also created by introducing neutral or charged functional groups (Fillet et al., 2000; Zhou et al., 2015). These charged CDs have the obvious advantages of good solubility, increased cavity depth, and strong complexation ability with chiral drugs, which further improve the efficiency, time, and consumption of enantioseparation processes. For example, Yu and coworkers (Sun et al., 2019) simplified the preparation process by bonding a per-4-chlorophenylcarbamate-β-CD to chiral stationary phase. The resolution and selectivity of voriconazole reached 16.80 and 15.41. Chromatographic studies showed that 4-chlorophenylcarbamate group enhance the interactions of analyte–chiral substrate including hydrogen bonding, π–π and dipole–dipole interactions.

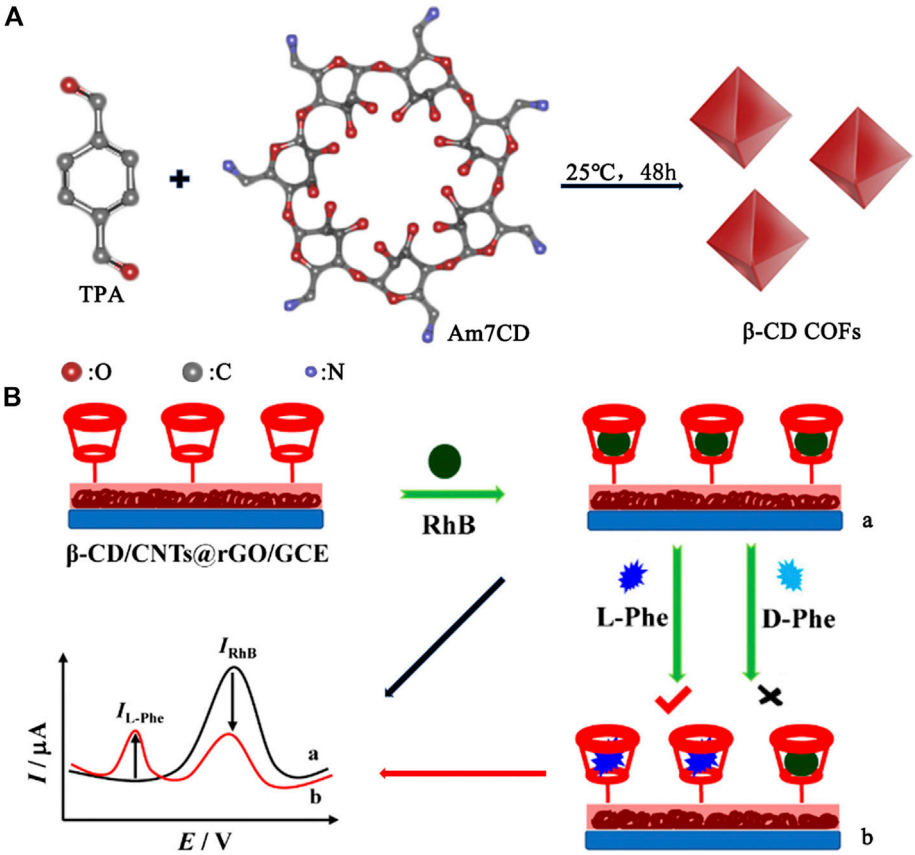


**FIGURE 2 | (A)** The preparation of the chiral stationary phase: β-CD COFs. **(B)** The electrochemical sensor platform for recognition chiral phenylalanine enantiomers.

In **Figure 2A**, Ji et al. used the condensation reaction of Heptakis (6-amino-6-deoxy)-β-CD (Am7CD) and terephthalaldehyde (TPA) to fabricate β-CD covalent organic frameworks (β-CD COFs) (Wang et al., 2019), a new chiral stationary phase that can achieve baseline separation of six chiral drugs (including (±)-sotalol, (±)-terbutaline, (±)-propranolol, (±)-metoprolol, (±)-salbutamol, and (±)-esmolol). The hydroxyl and amino groups in Am7CD provided additional driving forces to form inclusion complexes in addition to hydrogen bonds and van der Waals forces. And the porous material COF made CD units integrate, providing more interaction sites.

## Amino Acid Enantioseparation

Amino acids possess Levorotatory (L-)/dextrorotatory (D-) enantiomer pairs due to their asymmetric carbon center bonding to four different groups. These amino acid enantiomers have dissimilar biochemical function and properties: L-amino acids are the structural units of proteins found abundantly in organisms; however, D-amino acids seldom exist in higher animals and are often associated with various diseases such as Alzheimer (Sievers et al., 2011), schizophrenia (Chumakov et al., 2002), and amyotrophic lateral sclerosis (Paul and de Belleroche, 2012). Quantitative chiral separations and identification of some important D-amino acids like D-serine and D-aspartate are beneficial for studying the pathological changes (Szökő et al., 2016). Many experimental results revealed that cyclodextrins show a selectivity for L-amino acids, while the complexes of cyclodextrin and transition metal cations have specific interactions with D-amino acids to create sufficient mobility differences for effective separation (Chiu, 2013). In **Figure 2B**, a highly selective and sensitive electrochemical sensor for recognition chiral phenylalanine enantiomers (D-and L -Phe) was constructed based on CNTs@rGO (carbon nanotubes wrapped with reduced graphene oxide) allied with β-CD (Yi et al., 2019). In this model system, rhodamine B (RhB) was introduced as a probe and recognized by β-CD through host-guest interactions exhibiting remarkable oxidation peak current. In the presence of L-Phe, the peak current of RhB decreased and the peak current of L-Phe appeared due to the stronger interaction between L-Phe and β-CD. However, there was only a weaker interaction between β-CD and D-Phe. Nagy et al. used CDs in conjunction with a cationic group for high-resolution separation of D- and L-Ser, Asp and Thr in short times (Nagy et al., 2018). Using less ion manipulations and serpentine ultralong path with extended routing ion mobility (IM) platform, analyte ions are separated in extremely short times according to their mobilities and mass-to-charge ratio.

### Psychoactive Substance Enantioseparation

Psychoactive substances can act on the central nervous system to change the mood, consciousness, and behavior temporarily. Common psychoactive substances include derivatives, dissociative substances, opioids, and novel neuroactive substances. Many psychoactive substances possess a stereogenic center or contain positional isomers with the side chains on different substituent positions of a phenyl ring (e.g., ortho-, meta, or para-substitution). These enantiomers differ in their pharmacological effects, potency, or toxicity. Therefore, it is necessary to select appropriate chiral selectors for enantioseparation of psychoactive substances (Schmid and Hagele, 2020). CDs are one of the ideal candidates due to their multivalent weak interactions with psychoactive substances. The enantioseparation efficiency relies on the chiral recognition mechanism of CDs (Gübitz and Schmid, 2008), involving the inclusion of bulky hydrophobic groups into the chiral CD cavity and the second interactions between the hydroxyl groups at C2/C3 positions of CDs and the hydrophilic groups of psychoactive substances. Schmid and coworkers (Hägele et al., 2019) presented a chiral capillary zone electrophoresis method using four different β-CDs, namely, native β-CD, acetyl-β-CD, 2-hydroxypropyl-β-CD, and carboxymethyl-β-CD, as chiral selectors for the enantioseparation of 61 cathinone derivatives. Different modifications on their external surfaces had a huge impact on the formation and stability of inclusion compounds, so the separation of cathinone derivatives by the four β-CD derivatives was different. Under the optimized conditions, 58 of 61 tested cathinone derivatives were partially or baseline separated with at least one of the different CD-electrolytes within 40 min.

## DELIVERY VECTORS FOR BIOMEDICAL THERAPY

The development of drug delivery system is an effective strategy to improve the curative efficacy and safety of therapeutic molecules. Among them, CDs and their derivatives show the ability to increase the solubility, stability, dissolution rate, and bioavailability of poorly soluble drugs through the formation of inclusion complexes and thereby are widely used for pharmaceutical applications. In addition, the advantages of CDs as a carrier also include (1) chemical derivatization by site-specific substitution; (2) the tunable cavity sizes; and (3) low toxicity and immunogenicity (Kurkov and Loftsson, 2013; Syukri et al., 2015). The drug molecules can be partially or entirely inserted into the hydrophobic CD cavity under the driving forces of hydrophobic, electrostatic, van der Waals, charge-transfer interactions, etc. New targeting strategies that introduce receptor groups to CDs' surface further enhance the site-selective delivery capability of CDs (Guo et al., 2020; Peng et al., 2020). For instance, the receptor peptides and lipophilic groups are typically modified to CDs for penetrating the blood-brain barrier to improve drug treatment. Besides these designed derivatives, CDs may also self-aggregate into supramolecular polymers or networks through hydrogen bonds and host-guest interactions or may be linked to form larger structures via covalent bonds to construct optimal architectures with both high delivery efficiency and low cytotoxicity (Hu et al., 2014). These CD-based drug delivery vectors can be dosed by oral, nasal, ocular, rectal, and dermal delivery and have proven to enhance the drug absorption, mask odors, drug release, and drug permeability through the biological barrier (Brewster and Loftsson, 2007; Carrier et al., 2007).

### Antimicrobial Drug Delivery

The resistance of bacteria to antibiotics is a serious global problem in the field of medicine. Although new antimicrobial agents such as metal nanoparticles (NPs), quaternized ammonium compounds, carbon nanomaterials, triclosan, herbal extracts, and antimicrobial biopolymers are being developed (Moellering, 2011; Dong et al., 2020), it still hard to neutralize the bacterial defense mechanisms due to the rapid evolution of bacteria. Another effective strategy to overcome antibiotic resistance is to encapsulate antimicrobial agents into a delivery system for the reduced dosages or the targeting characteristics. CDs are the most representative host complexation agents in delivery systems, which can act as reservoirs to improve the undesirable properties of antimicrobial agents. In addition, chemically modified CDs like hydroxypropyl-, methylated-, and sulfobutylether cyclodextrin not only exhibit stronger complexation ability, but also disrupt the crystalline structure of CDs for more efficient drug solubilization. Moreover, some exceptional features (e.g., specific surface area, high charge density, and controlled release ability) can also be obtained by covalently attachment or physically assembly of CDs to a variety of organic/inorganic materials, leading to bacterial cell membrane damage and bacterial death (Cutrone et al., 2017; Liu et al., 2019). As shown in **Figure 3A**, Wang et al. reported that α-CD, β-CD, and $\gamma$-CD formed complexes with a star-shaped cationic trimeric surfactant (DTAD), respectively, which improved the mildness of the DTAD, enhanced interaction with cell membrane, and maintained good antibacterial activity to Gram-negative *E. coli* (minimal inhibitory concentration values are 2.22–2.48 μM) (Zhou et al., 2016a). Maria and coworkers chose β-CD as a stabilizer and glucose as a reducing agent to synthesize silver nanoparticles for antimicrobial (Andrade et al., 2014). In particular, the β-CD stabilizing layer around the silver nanoparticles, which is very related to the nanoparticle stability and biocompatibility, was characterized in detail. The β-CD-coated silver nanoparticles showed a promising bactericidal activity against the microorganism *Escherichia coli* (a minimum inhibitory concentration was 20 $\mu g \cdot ml^{-1}$).

### Antioxidant Drug Delivery

Reactive oxygen species (ROS), a byproduct of aerobic metabolism, can cause many diseases under excessive conditions in the body (Sies, 1986; Wirth, 2015). The synthesis of artificial antioxidant enzymes (Jiang et al., 2019) and the delivery of natural antioxidant drugs such as flavonoids (Nagula and Wairkar, 2019), usnic acid (Chemico-Biological

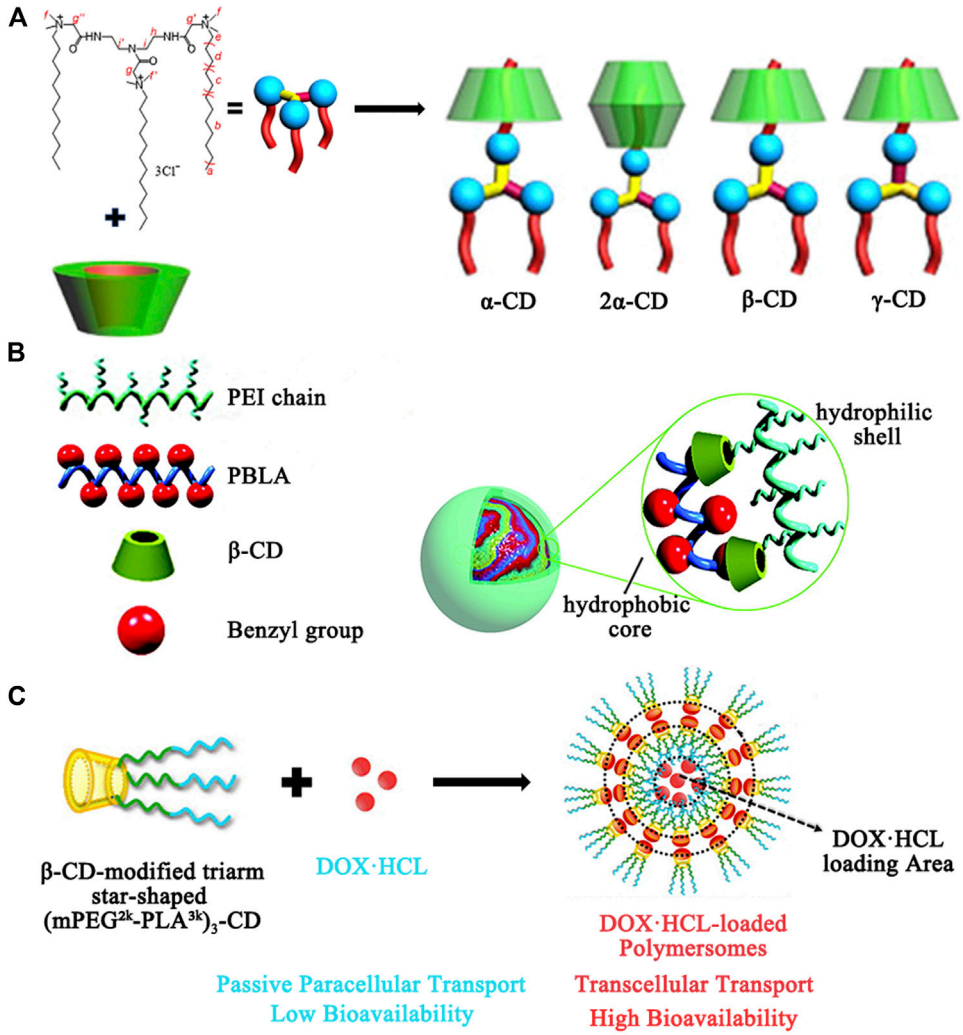


**FIGURE 3 | (A)** Illustration of structure of the complexes of CDs and DTAD. **(B)** Illustration of structure of the core-shell nanoassemblies based on PEI-CD/PBLA by a host-guest interaction for dexamethasone delivery. **(C)** Illustration of the structure and the property of the polymersome for carrying DOX·HCl.

Interactions 2020, 332, 109297), celastrol (Journal of Molecular Liquids 2020, 318, 113936), and quercetin (Xu et al., 2019) are the two main directions of scavenging excess ROS. In most cases, chemical modification of CDs is still an important method to construct multifunctional antioxidant systems. Site-specific modification of β-CD at 6-OH position with functional substituents like cinnamic acid derivatives leads to significantly enhanced solubility (>600 mg/ml) and new antioxidant function in scavenging DPPH radicals (Colloids and Surfaces A, 2020, 606, 125382). To avoid the drawbacks of these synthetic antioxidative compounds (e.g., nonspecific distribution, rapid metabolism, and low delivery efficiency), a new generation of nanotherapy based on the functionalization of β-CD with an oxidation-labile compound PBAP to form nanoparticles exhibits a broad spectrum of antioxidative properties and is capable of targeting the inflamed gastrointestinal tissues for selective drug release (Biomater. Sci., 2020, 8, 7117). Moreover, CD carriers are excellent delivery systems for encapsulation of antioxidant drugs in order to 1) stabilize these active compounds, 2) prevent the enzymatic/chemical degradation, and 3) improve their solubility, permeability, and pharmacological activity. Liang and coworkers prepared a simple coevaporation method to synthesize the inclusion complex of hydroxypropyl-β-cyclodextrin (HP-β-CD) and phloretin (Wei et al., 2017). The formation of the complex led to a 5808-fold increase in the solubility of phloretin compared with that in pure water at 25°C and still maintained the ability of scavenging DPPH similar to that of free phloretin *in vitro*.

## Anti-inflammatory Drug Delivery

Inflammation is a defensive response of the body to tissue injury. Clinically, the use of anti-inflammatory drugs (e.g., indomethacin, dexamethasone, and ibuprofen) is one of the major routes for the treatment of inflammatory disorders, which may cause some inevitable side effects such as gastric irritation, ulceration, hepatic

failure, and skin rashes (Rainsford, 2007). The CDs have the cavities compatible with the polarity, size, and shape of drug structures and are suitable for their encapsulation to extend the physicochemical properties of drug formulations. Furthermore, a combination of CDs and other materials [e.g., polymers, metal-organic framework (Rajkumar et al., 2019), and hydrogels (Arslan et al., 2020)] provides more versatility in nanocarriers engineering, which allows precise and controlled administration of the anti-inflammatory drugs by surface modification of CD nanocarriers for favorable interactions with the inflammatory microenvironment. As shown in **Figure 3B**, Ma et al. constructed core-shell nanocarriers for delivery of dexamethasone (DMS) and plasmid DNA, simultaneously (Zhang et al., 2010). Polyethyleneimine (PEI) modified with β-CD by a nucleophilic substitution reaction was used as a hydrophilic shell, while poly (β-benzyl *L*-aspartate) (PBLA) with benzyl groups forms a hydrophobic core by inclusion interaction between the benzyl group and the CD unit. The hydrophobic core serves as a nanocontainer for DMS, and 5.8% DMS was loaded and the release of DMS from PEI-CD/PBLA assemblies can be sustained for about 1 month. In addition, Chiavacci and coworkers have prepared a metal-organic framework structure with γ-CD as an organic linker (γ-CD-MOF) (Abucafy et al., 2018). γ-CD with symmetric arrangement ($C_8$) and good biocompatibility maintain the crystallization of MOF and improve its bioavailability. γ-CD-MOF was proven to effectively capsule and control the release of anti-inflammatory drugs, sodium diclofenac.

## Anticancer Drug Delivery

In recent years, chemotherapeutics and gene therapy have been widely developed for cancer therapy (da Silva-Diz et al., 2018; Liu et al., 2018a). Typically, the inclusion complexes of CDs carriers with some hydrophobic drugs such as doxorubicin, camptothecin, paclitaxel, and fluorouracil can increase their bioavailability and provide better therapeutic effects through membrane absorption enhancing properties and the stabilization ability with drugs (Tian et al., 2020). Besides the limited number of anticancer drug species, CD-grafted polymer transfection systems such as CD-linked PEI and CD inclusion complexes with guest moieties (e.g., adamantane, azobenzene, ferrocene, and cholesterol)-modified poly (ethylene glycol) (PEG) were also developed for antitumor gene therapy by improving gene transfection efficacy (Lai, 2014). Moreover, various responsive nanostructures (e.g., redox-, pH-, Photo-, voltage-, and thermosensitivity) can be built based on sensitive covalent/noncovalent interactions (e.g., disulfide bonds, the interactions between CD and N-methylbenzimidazole, azobenzene, ferrocene, etc.) or polymer properties (e.g., the reversible phase transition of PNIPAA polymers) to achieve controlled release under special tumor microenvironment (Zhang et al., 2020). As an example, β-CD functionalized with hyaluronic acid (HA) and adamantane modified with camptothecin (CPT) are self-assembled into nanocarriers through the specifically host-guest interaction, while a near-infrared absorbing dye IR825 was loaded in hydrophobic cavity (Zhang et al., 2018). In this way, the aqueous solubility of CPT had significantly increased. In tumor microenvironment, disulfide bond breakage leads to CPT release for the chemotherapy. Nevertheless, the dye IR825 could efficiently absorb light energy into heat for the photothermal therapy. Chen et al. (Liu et al., 2018b) used the nucleobase guanine/cytosine (G/C)-terminated PEG and α-CD to prepare supramolecular hydrogels (SHGs), which enhanced DOX-loading efficiency and improved the storage moduli (G's) of the hydrogels. The SHGs exhibited good biocompatibility and thermal response and were expected to apply in local chemotherapy of cancers. Moreover, as shown in **Figure 3C**, Qiu and coworkers (Hu et al., 2016) performed pioneering work with developing a DOX·HCl-loaded polymersome (Ps-DOX·HCl) with high drug loading capability to improve oral bioavailability of DOX·HCl, which self-assembled by amphiphilic β-CD-centered triarm star polymer ($mPEG^{2k}$ -$PLA^{3k}$)$_3$-CD. In this system, β-CD modification on mPEG-*b*-PLA copolymers can improve the loading of DOX·HCl and change the transmembrane pathway of DOX·HCl. Pharmacokinetic studies in mice showed that the oral bioavailability and extended half-life of the Ps-DOX·HCl were significantly higher than that of free DOX·HCl.

# MOLECULAR PROBES FOR BIOMEDICAL DIAGNOSIS

Molecular imaging is an early noninvasive diagnostic method to visualize the physiological or pathological processes at the cellular and tissue level (Herschman, 2003). In general, a typical probe for molecular imaging is composed of imaging element with magnetic, echogenic, radioactive, luminescent, or multimode signals and targeting moiety for specific recognition of the disease-related biomarkers. CDs are considered ideal scaffolds for the design of molecular probes, which have the competitive advantages of (Lai et al., 2017): 1) easy functionalization with targeting ligands and imaging elements to obtain high imaging specificity and multimodal imaging; 2) tunable cavity sizes to optimize their load capacity, imaging time, and excretion behavior; and 3) optical transparency in a broad wavelength range without any signal interferences.

## Probes for Magnetic Resonance Molecular Imaging

Magnetic resonance imaging (MRI) is a rapid and precise diagnostic technique that uses strong magnetic fields and radio waves for high quality imaging of soft tissues. Currently, this method is still confronted with the problems of low magnetic signal and sensitivity, which requires a contrast agent to enhance signal contrast. The construction of paramagnetic contrast agent by modifying CDs with the chelators (e.g diethylenetriaminepentaacetic acid (DTPA) and 1,4,7,10-tetraazacyclododecane-1,4,7,10-tetraacetic acid (DOTA)) is a feasible strategy to improve the relaxation properties and signal intensities by slowing down the rotation of their ion complexes (e.g., Gd3+ complexes). Similarly, the relaxivity value can be modulated by inclusion complexation of CDs or their derivatives with the chelators to restrict the rotational freedom. The targeting capacity is also easily introduced by incorporating specific ligands into CDs for selective recognition of biomarkers. Lu et al. fabricated a CD-based carrier by conjugating β-CD molecules to

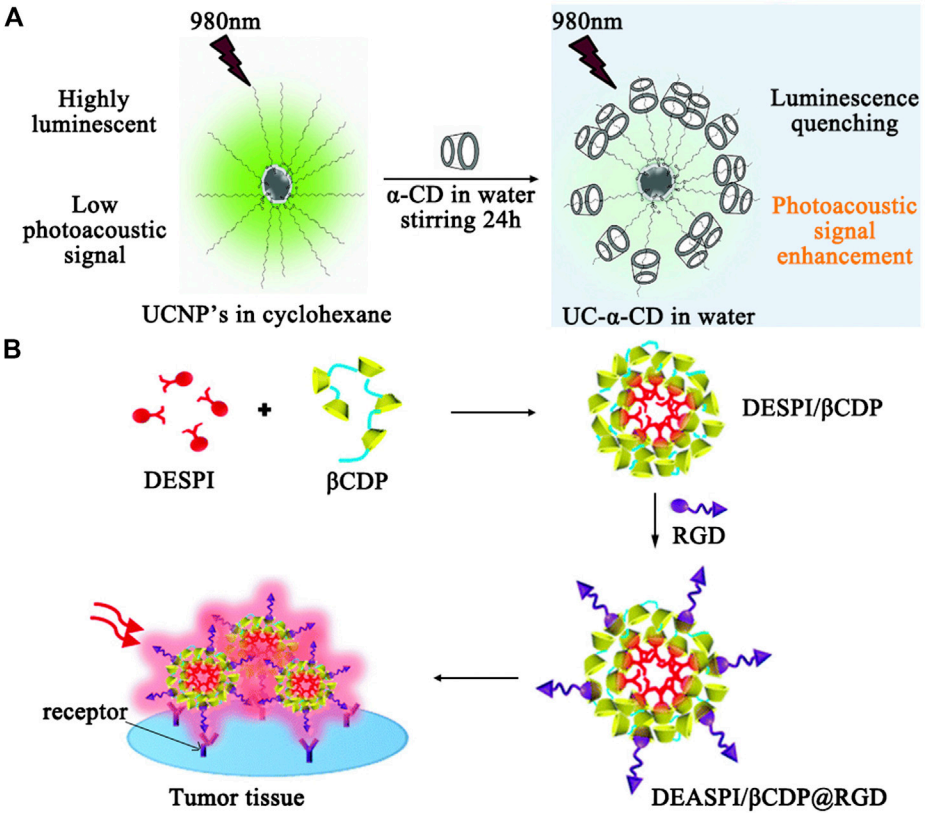


**FIGURE 4 | (A)** Illustration of luminescence quenching effect and subsequent photoacoustic signal enhancement from UC-α-CD in water. **(B)** Illustration of fabrication of the DEASPI/βCDP nanomicelles and application in TPE tumor tissue imaging.

polyhedral silsesquioxane (POSS) (Zhou et al., 2016b). The adamantane modified cyclic RGDfK peptide and the macrocyclic $Gd^{3+}$ chelate were incorporated into the carrier via host–guest chemistry to generate a targeted contrast agent for cancer. The complex of $Gd^{3+}$ chelate and CD cavity can increase the relaxivity value. The contrast agent leads to strong and prolonged contrast enhancement in tumor tissues, as compared to the nontargeting counterpart in mice bearing 4T1-GFP-Luc2 flank tumors.

## Probes for Ultrasound-Based Molecular Imaging

Compared to MRI, ultrasound (US) imaging is a more safe and affordable technique, which evaluates the reflected echoes based on the variations such as sound attenuation effects, backscattering coefficients, and sound speeds. CD-coated microbubbles are new US contrast agents that not only create strong ultrasound reflections by reducing gas dissolution, but also can improve the signal-to-noise ratio of imaging when targeting moieties are incorporated into CDs via host-guest interactions to obtain the enhanced target specificity. As an extension to 2D imaging, ultrasound-based 3D imaging provides more information such as morphological, functional, and molecular data for lesion analysis. Photoacoustic (PAI) imaging is a recently developed hybrid technique that combines the high selectivity of optical imaging and the deep penetration of US imaging using endogenous contrast for real-time molecular imaging. Zhao and coworkers reported an upconversion nanoparticles (UCNP)/α-cyclodextrin (α-CD) inclusion complex (UC-α-CD) for *in vivo* PAI (Maji et al., 2014) (see **Figure 4A**). UCNP and $NaYF_4$ co-doped with ytterbium ($Yb^{3+}$) and erbium ($Er^{3+}$), cannot be dispersed in aqueous solution due to the presence of oleic acid (OA). By forming the inclusion complexes with α-cyclodextrin (α-CD), water-dispersible UCNPs (UC-α-CD) were prepared. Under 980 nm excitation, the luminescence of UC-αCD was quenched to generate enhanced PA signal in aqueous conditions for *in vivo* PAI in live mice. The obtained images of the mouse kidney before and after the injection of UC-α-CD demonstrated the excellent PAI generation capability of UC-α-CD. The surface of UC-α-CD can be further integrated with various functional groups for specific cancer imaging.

## Probes for Radiation-Based Molecular Imaging

Radionuclide imaging is another form of noninvasive imaging technique that uses biologically active compound labelled with a small amount of radioactive substance to detect the disease-associated molecular phenotype of tissues. This technique has significant advantages of high sensitivity low dose, quantitative and qualitative localization, unlimited tissue penetration, and observation of dynamic metabolism, but shows lower spatial resolutioThe selection of different

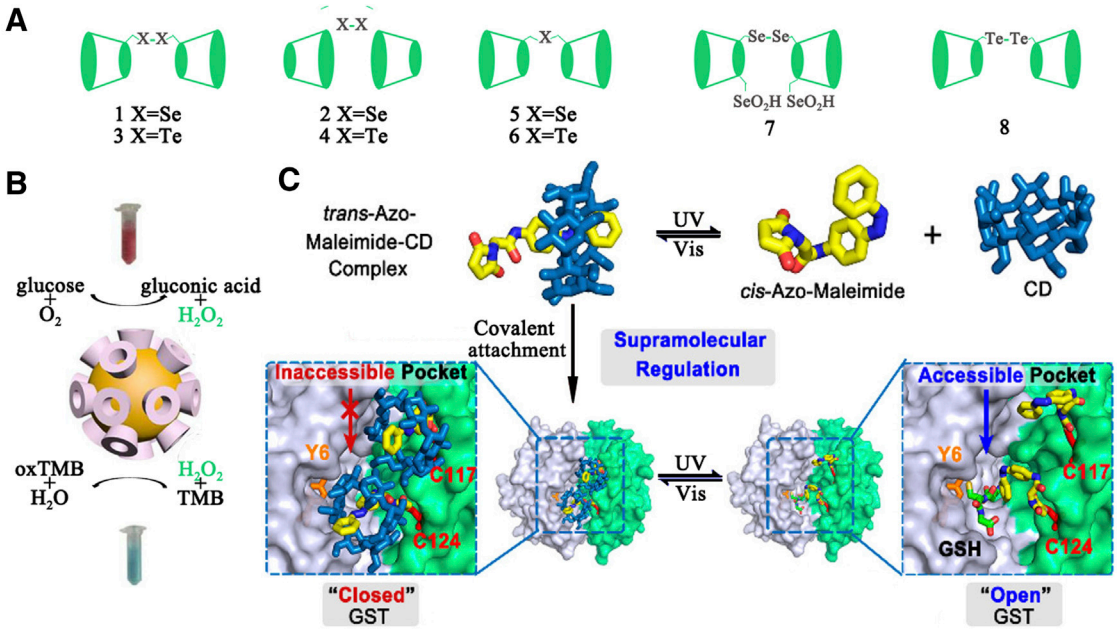


**FIGURE 5 | (A)** CD-based artificial enzymes. **(B)** Illustration of the cascade catalysis system using the -CD@AuNPs as the only catalyst. **(C)** Illustration of the optically controlled supramolecular switch for Glutathione S-Transferase (GST).

radionuclides, especiallyradioactiveisotopes such as $^{99m}$Tc, $^{111}$In and $^{131}$I that produce $\gamma$-rays is crucial for label tracers to produce tomographic images. Based on the early reports, CD are favorable to improve the bioadhesion of radiolabelled probes via hydrogen-bonding interaction. For instance, Peñuelas and coworkers labeled CD-poly (anhydride) nanoparticles (CD-NP) with technetium-99 m ($^{99m}$Tc) for biodistribution studies after oral administration (Areses et al., 2011). Single photon emission computed tomography (SPECT) fused computed tomography (CT) images revealed that CD-NP moved remarkably more slowly inside the gut than conventional NP, derived from stronger interactions between the gut mucosa and CD. Actually, there is still great potential for further optimization of CD-based probes, whose biological half-life is ideally shorter than the half-life of the radionuclide. This allows the non-specific signals to be eliminated within the imaging timeframe, leading to a cleaner signal of interest.

## Probes for Luminescence-Based Molecular Imaging

Luminescence-based imaging is still considered as the most reliable tool to obtainchemical images using fluorescent probe technology. To date, a wide range of fluorochromes/bio-luminescence materials can be used to monitor the real-time behavior of biologically active species (e.g. ROS) by studying their localization or bio-distribution for pathologicalexaminations. The conjugation of CDs to these systems are able to generate selective optical signals for molecular imaging through improving their recognition ability, which has been confirmed by the earlier study using coumarin-methyl–CD to track hydroxyl radicals. Based on the recognition specificity of CDs, various CD-based fluorescent probes (e.g. the bridged bis-CDs-dye complex, metallocyclodextrins, and CD nanomicelles) have been developed for multiplex detection through one-photon or two-photon excitation. Tan and coworkers performed pioneering work with a two-photon absorption (TPA) nanomicelle based on $\beta$-CD polymer ($\beta$-CDP) through the inclusion interaction between $\beta$-CD and *trans*-4-[p-(N,N-diethylamino)styryl]-N-methylpyridinium iodide (DEASPI); then, a cyclic RGD peptide, which selectively recognizes $\alpha_v\beta_3$ and $\alpha_v\beta_5$ integrin receptors, conjugated adamantine was anchored on the surface of the $\beta$-CDP-based nanomicelle to form a TPA bionanoprobe (DEASPI/$\beta$-CDP@RGD) by the $\beta$-CD/adamantine host-guest inclusion strategy (Yan et al., 2014) (see **Figure 4B**). The probe has been successfully applied to the targeted imaging of tumor cells and tissues with bright TPE fluorescence emission penetration depth up to 300 m$\mu$.

## SUPRAMOLECULAR SCAFFOLD FOR ENZYMATIC CATALYSIS

Enzymes are highly efficient and selective catalysts that can accelerate reactions by more than $10^{17}$ folds.(Richard, 2013) The active site is a key structure of the enzyme to bind a particular substrate for suppressing undesired competing reactions. CDs are ideal candidates for the development of enzyme mimics due to their remarkable guest-inclusion capabilities with small hydrophobic compounds. In most cases, the desired functional groups (e.g. the catalytic groups and substrate-binding groups) can be introduced into the core cyclic structure or at the periphery of CDs to create the structural features of natural enzymes for specific substrate binding or activation (Kataky and Morgan, 2003; Dong et al.,

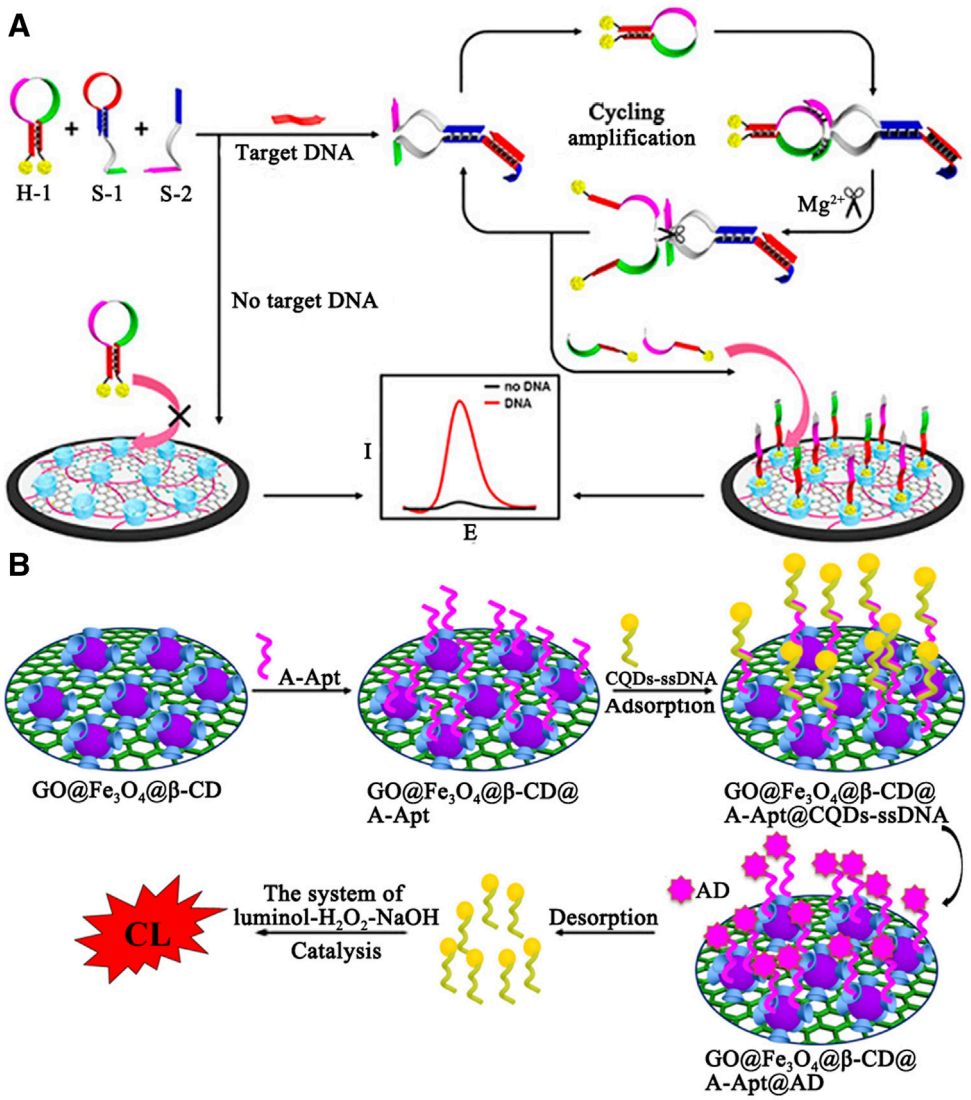


**FIGURE 6 | (A)** Illustration of the electrochemical DNA biosensor based on the host–guest interaction and $Mg^{2+}$ -assistant DNA recycling. **(B)** The schematic diagram construction of GO@Fe3O4@β-CD@A-Apt/CQDs-ssDNA-CL biosensor.

2012). Another strategy is to develop CD-based nanomaterials with enzyme-like activity by stabilizing metal clusters/nanoparticles or inducing the formation of larger aggregates, in which the catalytic core possesses multi-metal catalytic sites and thus exhibits strong rate enhancement.(Li et al., 2008) Furthermore, CDs can be also explored as a modulator to control the activity of artificial enzymes based on the reversibility of host-guest interactions. CD-based supramolecular chemistry creates a great diversity in the design of different enzyme models for effective simulation of various catalytic functions..

## Artificial Enzyme

As early as 1970s, numerous successful examples have been reported by using natural or modified CDs as supramolecular scaffolds to construct artificial enzymes. In these enzyme designs, site-selective modification at the primary or the secondary hydroxyl groups of CDs was performed to introduce the coenzyme factors, including thiazolium salt, isoalloxazine, phosphate esters, pyridoxamine/pyridoxal, imidazole, oxime anion, metalloporphyrins, and etc. Furthermore, some modifications were also applied to provide additional noncovalent interactions (e.g. electrostatic, hydrogen-bonding, charge transfer, and metal-coordination interactions) or to change the CDs' cavity sizes, shapes, and properties for more favorable geometrical accommodation of the substrates. To date, three different types of CD-based supramolecular enzyme mimics that contain metal free CD-based artificial enzymes, CD-based artificial metalloenzymes, and CD-based artificial enzymes have been created. A variety of enzymatic functions, including oxidase (e.g. CD aldehydes or CD diacids with copper, zinc and iron), reductase (e.g. CD-sandwiched porphyrinatoiron), dehydrogenase (nicotinamide-linked -CD), esterase (tripodal tris(2-aminoethyl)amine (tren)-

linked CDhomodimer), aminotransferase (e.g. pyridoxamine-modified -CD), glycosidase (e.g.CD derivatives with cyanohydrin and carboxylate groups), protease (e.g. imidazolyl CD), and nuclease (e.g.copper(II) complex with -CD ) were obtained to rival the activity and specificity of natural ones. In addition, CDs can form a complex supramolecular structure through the complex of host and guest to obtain more excellent enzymatic properties or multiple enzymatic activities. Glutathione peroxidase is a kind of important mammalian selenoenzyme. Liu et al. reported the first cyclodextrin-based artificial enzyme model 1 (**Figure 5A**) by attaching a diselenide group to the primary face of -CD. Strong substrate binding ability made its GPx activity 4.3 times higher than ebselen. Similarly, enzyme model **2** with a diselenide group bound to the secondary face of -CD was also reported. Due to the stronger binding capacity between **2** and the substrate GSH, **2** exhibited higher catalytic activity. On the basis of **1** and **2**, the same group explored a array of artificial selenoenzymes **3**-**7** based on CDs and investigated their catalytic mechanism. Recently, 6,6'-ditellurobis bridged-CD **(8)** was reported as the best inhibitor which significantly suppressed ferrous sulfate/ascorbateinduced cytotoxicity.

## Nanoenzymes

Some nanomaterials, such as noble metal nanoparticles, ferromagnetic nanoparticles, metal–organic framework, and graphene oxides, have been confirmed to have enzymatic activity. Nanozymes are used to mimic the activity of four types of redox enzymes, including peroxidase, oxidase, catalase, and superoxide dismutase (Wei and Wang, 2013). The unique topology of CDs was often employed to regulate the activity of nanoenzymes (Wang et al., 2018b). For example, Xia and coworkers chose CD molecules as both reducing agents and stabilizers to synthesize gold nanoparticles (CD@AuNPs) for cascade catalysis (Zhao et al., 2016) (see **Figure 5A**). In the cascade reaction, CD@AuNPs exhibited mimicking properties of both glucose oxidase (GOx) and horseradish peroxidase (HRP) simultaneously and could play a role in the sole catalyst. According to density functional theory (DFT), the authors proposed that the specific topological structures of CD molecules and their unique electron transfer effects with the appended Au surface lead to unpredictable catalytic properties. Furthermore, due to possessing macrocyclic structures on the particle surface, CD@AuNPs can be employed for fluorescent sensing and self-assembly. CDs also could be managed to modify on the surface of nanoenzymes for improving catalytic functions (Vazquez-Gonzalez et al., 2017; Lu et al., 2020).

## Enzyme Switches

The catalytic function of enzymes is usually strictly controlled by various triggering factors during life activities. Typically the "on/off" effect of the variable domain on the catalytic site of an enzyme has a great influence on the enzyme-substrate recognition, and thereby control its catalytic performance reversibly. Inspired by Nature, a large number of artificial intelligence catalysts that contain azobenzene, spiropyran, diarylethylene, and other stimulus response groups have been developed to simulate the strict regulation behavior of natural enzyme (Blanco et al., 2014). CDs with different cavity sizes can be complexed with a variety of stimulus-responsive guest molecules. Luo and coworkers constructed an optically controlled supramolecular switch for Glutathione S-Transferase (GST) (Liu et al., 2017b) (see **Figure 5B**).The host-guest system of azobenzene/CD was introduced into the catalytic pocket of GST. The photoisomerization of *cis*-azobenzene and *trans*-azobenzene lead to the dissociation and recombination of CD, and the later hinders the binding of the substrate GSH to the active site. The optical-controlled switch is still active after several cycles. Similarly, the same light-controlled switch was also used in palladium-catalyzed bioorthogonal reactions (Wang et al., 2018b).

# MOLECULAR RECEPTORS FOR BIOCHEMICAL SENSING

Biosensors for diabetes and pregnancy tests have been commercialized and used in large numbers (Wu et al., 2019b). Moreover, the application of sensors for other biomolecules has also made incredible progress (Luong et al., 2008). However, there are still some challenges in the design of biosensors that can meet actual application requirements, such as designing biosensors with higher specificity, repeatability, sensitivity, and immobilization of biosensors (Jensen, 2006; Pinalli et al., 2018). With the development of supramolecular chemistry, CDs as molecular receptors have been introduced into biosensors (Smith et al., 2015). According to the different properties of analytes, a variety of cavity sizes and functionalized CD derivatives can be employed (Fragoso et al., 2002; Shi et al., 2014).

## Electrochemical Sensors

Electrochemical sensors have received increasing interests, which can be designed simply, ensured reversibly and reproducibly, and analyzed accurately. Diao and coworkers demonstrated an electrochemical sensor based on nanocomposites and $Mg^{2+}$-dependent DNAzyme for sensitive detection of DNA and miRNA (Jiang et al., 2017) (see **Figure 6**). β-Cyclodextrin polymer (β-CDP) with high water solubility and recognition capability was adsorbed on the nitrogen-doped reduced graphene oxide (NRGO) with superior electrocatalytic activity and placed on the electrode surface to form a sensing platform. In the presence of a target, the hairpin structure of subunit DNA (S-1) was opened to generate activity of catalytic the cleavage of hairpin probe (H-1). Then H-1 binding to S-1 was divided into two single-stranded oligonucleotides with the assistance of cofactor $Mg^{2+}$. Single-stranded oligonucleotides was recognized by β-CDP according to the principle of dimension matching, resulting in an obvious increase in peak current. In contrast, the formation of $Mg^{2+}$-dependent DNAzyme was inhibited, leading to a weak current response. In the sensitive determination of DNA, the calculated detection limit was 3.2 fM, at a signal-to-noise ratio of 3 (S/N = 3). Furthermore, the authors applied this method to the detection of target miRNA. The detection limit was estimated to be 18 fM (S/N = 3).

## Optical Chemical Sensors

Optical chemical sensors based on fluorescence or chemiluminescence (CL) were also employed for biomolecule detection. In **Figure 6B**, Luo and coworkers designed a highly selective and sensitive CL biosensor for adenosine (AD) detection (Sun et al., 2018). The author first synthesized GO@$Fe_3O_4$@$\beta$-CD as a sensing platform. Among them, $\beta$-CD provides a binding site for adenosine polymers (A-Apt), which is a kind of synthetic single-stranded oligonucleotides. Then, CQDs that could be catalyzing the CL system of luminal-$H_2O_2$-NaOH was modified by ssDNA (a single stranded DNA partially complementary to A-Apt). When AD existed, CQDs-ssDNA was released from the surface of GO@$Fe_3O_4$@β-CD@A-Apt and catalyzed CL. The detection limit was $2.1 \times 10^{-13}$ M. Finally, the sensor has been successfully applied to detection of AD in urine samples and recoveries ranged from 98.6 to 101.0%.

## CONCLUSION

This review summarized the recent development of CD-related systems including CD derivatives and their supramolecular assemblies, which provide versatile platforms and useful properties in the construction of supramolecular materials by forming the inclusion complexes. Some representative examples clearly demonstrate the functional diversity and excellent performances of CDs when having covalently/noncovalently linked bioactive moieties, which endow them with desirable abilities for biomedical applications in bioseparation, enzymatic catalysis, biochemical sensing, biomedical diagnosis, and therapy. Despite the remarkable advances in these fields, the structure-activity relationship is still complicated and remains to be further explored for the improved efficiency. Moreover, new concepts and theories should be conceived to guide the performance-targeted design and construction of more advanced CD-based functional systems.

## AUTHOR CONTRIBUTIONS

QL and JL designed the review; WX and XL wrote the article; and LW, SL, SC, JW, YL, and JH helped to evaluate and edit the manuscript.

## FUNDING

This work was supported by the National Key R&D Program of China (grant nos. 2020YFA0907003, 2018YFA0901600, and YS2020YFA090023), the Natural Science Foundation of China (no. 21871109), the Science Development Program of Jilin Province (nos. 20180201062SF and 20200403063SF), and the Shenzhen Science and Technology Innovation Commission for Basic Research (free exploration) project (JCYJ20170306171048350) and the China Postdoctoral Science Foundation (2017N622921) and Key Laboratory of Emergency and Trauma (Hainan Medical University), Ministry of Education (Grant. KLET-202012).

## REFERENCES

Abucafy, M. P., Caetano, B. L., Chiari-Andreo, B. G., Fonseca-Santos, B., Do Santos, A. M., Chorilli, M., et al. (2018). Supramolecular cyclodextrin-based metal-organic frameworks as efficient carrier for anti-inflammatory drugs. *Eur. J. Pharm. Biopharm.* 127, 112–119. doi:10.1016/j.ejpb.2018.02.009

Andrade, P. F., De Faria, A. F., Da Silva, D. S., Bonacin, J. A., and Goncalves Mdo, C. (2014). Structural and morphological investigations of β-cyclodextrin-coated silver nanoparticles. *Coll. Surf. B. Biоint.* 118, 289–297. doi:10.1016/j.colsurfb.2014.03.032

Areses, P., Agueros, M. T., Quincoces, G., Collantes, M., Richter, J. A., Lopez-Sanchez, L. M., et al. (2011). Molecular imaging techniques to study the biodistribution of orally administered (99m)Tc-labelled naive and ligand-tagged nanoparticles. *Mol. Imag. Biol.* 13, 1215–1223. doi:10.1007/s11307-010-0456-0

Arslan, M., Sanyal, R., and Sanyal, A. (2020). Cyclodextrin embedded covalently crosslinked networks: synthesis and applications of hydrogels with nano-containers. *Polym. Chem.* 11, 615–629. doi:10.1039/c9py01679a

Bellia, F., La Mendola, D., Pedone, C., Rizzarelli, E., Saviano, M., and Vecchio, G. (2009). Selectively functionalized cyclodextrins and their metal complexes. *Chem. Soc. Rev.* 38, 2756–2781. doi:10.1039/b718436k

Berthod, A. (2010). *Chiral recognition in separation methods*. Berlin, Germany: Springer.

Blanco, V., Leigh, D. A., Marcos, V., Morales-Serna, J. A., and Nussbaumer, A. L. (2014). A switchable [2]rotaxane asymmetric organocatalyst that utilizes an acyclic chiral secondary amine. *J. Am. Chem. Soc.* 136, 4905–4908. doi:10.1021/ja501561c

Brewster, M. E., and Loftsson, T. (2007). Cyclodextrins as pharmaceutical solubilizers. *Adv. Drug Deliv. Rev.* 59, 645–666. doi:10.1016/j.addr.2007.05.012

Calcaterra, A., and D'acquarica, I. (2018). The market of chiral drugs: chiral switches versus de novo enantiomerically pure compounds. *J. Pharmaceut. Biomed. Anal.* 147, 323–340. doi:10.1016/j.jpba.2017.07.008

Carrier, R. L., Miller, L. A., and Ahmed, I. (2007). The utility of cyclodextrins for enhancing oral bioavailability. *J. Contr. Release* 123, 78–99. doi:10.1016/j.jconrel.2007.07.018

Chen, G., and Jiang, M. (2011). Cyclodextrin-based inclusion complexation bridging supramolecular chemistry and macromolecular self-assembly. *Chem. Soc. Rev.* 40, 2254–2266. doi:10.1039/c0cs00153h

Chiu, T.-C. (2013). Recent advances in on-line concentration and separation of amino acids using capillary electrophoresis. *Anal. Bioanal. Chem.* 405, 7919–7930. doi:10.1007/s00216-013-6906-1

Chumakov, I., Blumenfeld, M., Guerassimenko, O., Cavarec, L., Palicio, M., Abderrahim, H., et al. (2002). Genetic and physiological data implicating the new human gene G72 and the gene for D-amino acid oxidase in schizophrenia. *Proc. Natl. Acad. Sci. U.S.A.* 99, 13675–13680. doi:10.1073/pnas.182412499

Coleman, A. W., Nicolis, I., Keller, N., and Dalbiez, J. P. (1992). Aggregation of cyclodextrins: an explanation of the abnormal solubility of β-cyclodextrin. *J. Inclusion Phenom. Macrocycl. Chem.* 13, 139–143. doi:10.1007/bf01053637

Cutrone, G., Casas-Solvas, J. M., and Vargas-Berenguel, A. (2017). Cyclodextrin-Modified inorganic materials for the construction of nanocarriers. *Int. J. Pharm.* 531, 621–639. doi:10.1016/j.ijpharm.2017.06.080

Da Silva-Diz, V., Lorenzo-Sanz, L., Bernat-Peguera, A., Lopez-Cerda, M., and Munoz, P. (2018). Cancer cell plasticity: impact on tumor progression and therapy response. *Semin. Canc. Biol.* 53, 48–58. doi:10.1016/j.semcancer.2018.08.009

Davis, M. E., and Brewster, M. E. (2004). Cyclodextrin-based pharmaceutics: past, present and future. *Nat. Rev. Drug Discov.* 3, 1023–1035. doi:10.1038/nrd1576

Dong, X., Liang, W., Meziani, M. J., Sun, Y.-P., and Yang, L. (2020). Carbon dots as potent antimicrobial agents. *Theranostics* 10, 671. doi:10.7150/thno.39863

Dong, Z., Luo, Q., and Liu, J. (2012). Artificial enzymes based on supramolecular scaffolds. *Chem. Soc. Rev.* 41, 7890–7908. doi:10.1039/c2cs35207a

FDA (1992). FDA's policy statement for the development of new stereoisomeric drugs. *Chirality* 4, 338–340. doi:10.1002/chir.530040513

Fillet, M., Hubert, P., and Crommen, J. (2000). Enantiomeric separations of drugs using mixtures of charged and neutral cyclodextrins. *J. Chromatogr. A.* 875, 123–134. doi:10.1016/s0021-9673(00)00084-4

Fragoso, A., Caballero, J., Almirall, E., Villalonga, R., and Cao, R. (2002). Immobilization of adamantane-modified cytochromecat electrode surfaces through supramolecular interactions. *Langmuir* 18, 5051–5054. doi:10.1021/la0256679

Frijlink, H. W., Eissens, A. C., Hefting, N. R., Poelstra, K., Lerk, C. F., and Meijer, D. K. (1991). The effect of parenterally administered cyclodextrins on cholesterol levels in the rat. *Pharm. Res. (N. Y.)* 8, 9–16. doi:10.1023/a:1015861719134

Gübitz, G., and Schmid, M. G. (2008). Chiral separation by capillary electromigration techniques. *J. Chromatogr. A.* 1204, 140–156. doi:10.1016/j.chroma.2008.07.071

Guo, X., Wei, X., Chen, Z., Zhang, X., Yang, G., and Zhou, S. (2020). Multifunctional nanoplatforms for subcellular delivery of drugs in cancer therapy. *Prog. Mater. Sci.* 107, 100599. doi:10.1016/j.pmatsci.2019.100599

Hägele, J. S., Hubner, E. M., and Schmid, M. G. (2019). Chiral separation of cathinone derivatives using β-cyclodextrin-assisted capillary electrophoresis-comparison of four different β-cyclodextrin derivatives used as chiral selectors. *Electrophoresis* 40, 1787–1794. doi:10.1002/elps.201900085

He, Y., Hou, X., Liu, Y., and Feng, N. (2019). Recent progress in the synthesis, structural diversity and emerging applications of cyclodextrin-based metal-organic frameworks. *J. Mater. Chem. B.* 7, 5602–5619. doi:10.1039/c9tb01548e

Herschman, H. R. (2003). Molecular imaging: looking at problems, seeing solutions. *Science* 302, 605–608. doi:10.1126/science.1090585

Hu, Q. D., Tang, G. P., and Chu, P. K. (2014). Cyclodextrin-based host-guest supramolecular nanoparticles for delivery: from design to applications. *Acc. Chem. Res.* 47, 2017–2025. doi:10.1021/ar500055s

Hu, M., Shen, Y., Zhang, L., and Qiu, L. (2016). Polymersomes via self-assembly of amphiphilic β-cyclodextrin-centered triarm star polymers for enhanced oral bioavailability of water-soluble chemotherapeutics. *Biomacromolecules* 17, 1026–1039. doi:10.1021/acs.biomac.5b01676

Huang, X., Liu, X., Luo, Q., Liu, J., and Shen, J. (2011). Artificial selenoenzymes: designed and redesigned. *Chem. Soc. Rev.* 40, 1171–1184. doi:10.1039/c0cs00046a

Jensen, O. N. (2006). Interpreting the protein language using proteomics. *Nat. Rev. Mol. Cell Biol.* 7, 391–403. doi:10.1038/nrm1939

Jiang, D., Ni, D., Rosenkrans, Z. T., Huang, P., Yan, X., and Cai, W. (2019). Nanozyme: new horizons for responsive biomedical applications. *Chem. Soc. Rev.* 48, 3683–3704. doi:10.1039/c8cs00718g

Jiang, J., Lin, X., and Diao, G. (2017). Smart combination of cyclodextrin polymer host-guest recognition and Mg. *ACS Appl. Mater. Interfaces* 9, 36688–36694. doi:10.1021/acsami.7b13132

Kataky, R., and Morgan, E. (2003). Potential of enzyme mimics in biomimetic sensors: a modified-cyclodextrin as a dehydrogenase enzyme mimic. *Biosens. Bioelectron.* 18, 1407–1417. doi:10.1016/s0956-5663(03)00077-0

Kirkorian, K., Ellis, A., and Twyman, L. J. (2012). Catalytic hyperbranched polymers as enzyme mimics; exploiting the principles of encapsulation and supramolecular chemistry. *Chem. Soc. Rev.* 41, 6138–6159. doi:10.1039/c2cs35238a

Kurkov, S. V., and Loftsson, T. (2013). Cyclodextrins. *Int. J. Pharm.* 453, 167–180. doi:10.1016/j.ijpharm.2012.06.055

Lai, W. F. (2014). Cyclodextrins in non-viral gene delivery. *Biomaterials* 35, 401–411. doi:10.1016/j.biomaterials.2013.09.061

Lai, W. F., Rogach, A. L., and Wong, W. T. (2017). Chemistry and engineering of cyclodextrins for molecular imaging. *Chem. Soc. Rev.* 46, 6379–6419. doi:10.1039/c7cs00040e

Liu, J.-N., Bu, W., and Shi, J. (2017a). Chemical design and synthesis of functionalized probes for imaging and treating tumor hypoxia. *Chem. Rev.* 117, 6160–6224. doi:10.1021/acs.chemrev.6b00525

Liu, J., Song, L., Liu, S., Jiang, Q., Liu, Q., Li, N., et al. (2018a). A DNA-based nanocarrier for efficient gene delivery and combined cancer therapy. *Nano Letters* 18, 3328–3334. doi:10.1021/acs.nanolett.7b04812

Liu, L., and Breslow, R. (2003). Dendrimeric pyridoxamine enzyme mimics. *J. Am. Chem. Soc.* 125, 12110–12111. doi:10.1021/ja0374473

Liu, L., Feng, X., Pei, Y., Wang, J., Ding, J., and Chen, L. (2018b). Alpha-Cyclodextrin concentration-controlled thermo-sensitive supramolecular hydrogels. *Mater. Sci. Eng. C. Mater. Biol. Appl.* 82, 25–28. doi:10.1016/j.msec.2017.08.045

Liu, L., and Guo, Q.-X. (2002). The driving forces in the inclusion complexation of cyclodextrins. *J. Inclusion Phenom. Macrocycl. Chem.* 42, 1–14. doi:10.1023/a:1014520830813

Liu, Y., and Chen, Y. (2006). Cooperative binding and multiple recognition by bridged bis (β-cyclodextrin)s with functional linkers. *Acc. Chem. Res.* 39, 681–691. doi:10.1021/ar0502275

Liu, Y., Pan, T., Fang, Y., Ma, N., Qiao, S., Zhao, L., et al. (2017b). Construction of smart glutathione S-transferase via remote optically controlled supramolecular switches. *ACS Catal.* 7, 6979–6983. doi:10.1021/acscatal.7b02821

Liu, Y., Shi, L., Su, L., Van Der Mei, H. C., Jutte, P. C., Ren, Y., et al. (2019). Nanotechnology-based antimicrobials and delivery systems for biofilm-infection control. *Chem. Soc. Rev.* 48, 428–446. doi:10.1039/c7cs00807d

Lu, W., Zhang, J., Li, N., You, Z., Feng, Z., Natarajan, V., et al. (2020). $Co_3O_4$@β-cyclodextrin with synergistic peroxidase-mimicking performance as a signal magnification approach for colorimetric determination of ascorbic acid. *Sensor. Actuator. B. Chem.* 303, 127106. doi:10.1016/j.snb.2019.127106

Luong, J. H., Male, K. B., and Glennon, J. D. (2008). Biosensor technology: technology push versus market pull. *Biotechnol. Adv.* 26, 492–500. doi:10.1016/j.biotechadv.2008.05.007

Maji, S. K., Sreejith, S., Joseph, J., Lin, M., He, T., Tong, Y., et al. (2014). Upconversion nanoparticles as a contrast agent for photoacoustic imaging in live mice. *Adv. Mater.* 26, 5633–5638. doi:10.1002/adma.201400831

Moellering, R. C., Jr (2011). Discovering new antimicrobial agents. *Int. J. Antimicrob. Agents* 37, 2–9. doi:10.1016/j.ijantimicag.2010.08.018

Nagula, R. L., and Wairkar, S. (2019). Recent advances in topical delivery of flavonoids: a review. *J. Contr. Release* 296, 190–201. doi:10.1016/j.jconrel.2019.01.029

Nagy, G., Chouinard, C. D., Attah, I. K., Webb, I. K., Garimella, S. V., Ibrahim, Y. M., et al. (2018). Distinguishing enantiomeric amino acids with chiral cyclodextrin adducts and structures for lossless ion manipulations. *Electrophoresis* 39, 3148–3155. doi:10.1002/elps.201800294

Nakahata, M., Takashima, Y., and Harada, A. (2017). Supramolecular polymeric materials containing cyclodextrins. *Chem. Pharm. Bull.* 65, 330–335. doi:10.1248/cpb.c16-00778

Paul, P., and De Belleroche, J. (2012). The role of D-amino acids in amyotrophic lateral sclerosis pathogenesis: a review. *Amino Acids* 43, 1823–1831. doi:10.1007/s00726-012-1385-9

Peng, Y., Bariwal, J., Kumar, V., Tan, C., and Mahato, R. I. (2020). Organic nanocarriers for delivery and targeting of therapeutic agents for cancer treatment. *Advanced Therapeutics* 3, 1900136. doi:10.1002/adtp.201900136

Pinalli, R., Pedrini, A., and Dalcanale, E. (2018). Biochemical sensing with macrocyclic receptors. *Chem. Soc. Rev.* 47, 7006–7026. doi:10.1039/c8cs00271a

Pinho, E., Grootveld, M., Soares, G., and Henriques, M. (2014). Cyclodextrins as encapsulation agents for plant bioactive compounds. *Carbohydr. Polym.* 101, 121–135. doi:10.1016/j.carbpol.2013.08.078

Rainsford, K. (2007). "Anti-inflammatory drugs in the 21st century," in *Inflammation in the pathogenesis of chronic diseases*. Berlin, Germany: Springer, 3–27.

Rajkumar, T., Kukkar, D., Kim, K.-H., Sohn, J. R., and Deep, A. (2019). Cyclodextrin-metal–organic framework (CD-MOF): from synthesis to applications. *J. Ind. Eng. Chem.* 72, 50–66. doi:10.1016/j.jiec.2018.12.048

Rezanka, P., Navratilova, K., Rezanka, M., Kral, V., and Sykora, D. (2014). Application of cyclodextrins in chiral capillary electrophoresis. *Electrophoresis* 35, 2701–2721. doi:10.1002/elps.201400145

Řezanka, M. (2019). Synthesis of substituted cyclodextrins. *Environ. Chem. Lett.* 17, 49–63. doi:10.1007/s10311-018-0779-7

Saenger, W. (1980). Cyclodextrin inclusion compounds in research and industry. *Angew Chem. Int. Ed. Engl.* 19, 344–362. doi:10.1002/anie.198003441

Sánchez-López, E., Castro-Puyana, M., Marina, M., and Crego, A. (2015). Chiral separations by capillary electrophoresis. *Anal. Sep. Sci.* 2, 731–775. doi:10.1002/9783527678129

Schmid, M. G., and Hagele, J. S. (2020). Separation of enantiomers and positional isomers of novel psychoactive substances in solid samples by chromatographic and electrophoretic techniques—a selective review. *J. Chromatogr. A*. 1624, 461256. doi:10.1016/j.chroma.2020.461256

Sharma, P., Brown, S., Walter, G., Santra, S., and Moudgil, B. (2006). Nanoparticles for bioimaging. *Adv. Colloid Interface Sci.* 123, 471–485. doi:10.1016/j.cis.2006.05.026

Shi, X., Chen, G., Yuan, L., Tang, Z., Liu, W., Zhang, Q., et al. (2014). Integrating a thermoresponsive copolymer with host–guest interactions for fabricating molecular recognition surfaces. *Materials Horizons* 1, 540–545. doi:10.1039/c4mh00081a

Sies, H. (1986). Biochemistry of oxidative stress. *Angew Chem. Int. Ed. Engl.* 25, 1058–1071. doi:10.1002/anie.198610581

Sievers, S. A., Karanicolas, J., Chang, H. W., Zhao, A., Jiang, L., Zirafi, O., et al. (2011). Structure-based design of non-natural amino-acid inhibitors of amyloid fibril formation. *Nature* 475, 96–100. doi:10.1038/nature10154

Smith, B. D., Anslyn, E., Gokel, G., Kubik, S., Wang, B., Hong, J.-I., et al. (2015). *Synthetic receptors for biomolecules: design principles and applications*. London, United Kingdom: Royal Society of Chemistry.

Sun, J., Ma, S., Liu, B., Yu, J., and Guo, X. (2019). A fully derivatized 4-chlorophenylcarbamate-β-cyclodextrin bonded chiral stationary phase for enhanced enantioseparation in HPLC. *Talanta* 204, 817–825. doi:10.1016/j.talanta.2019.06.071

Sun, Y., Ding, C., Lin, Y., Sun, W., Liu, H., Zhu, X., et al. (2018). Highly selective and sensitive chemiluminescence biosensor for adenosine detection based on carbon quantum dots catalyzing luminescence released from aptamers functionalized graphene@magnetic beta-cyclodextrin polymers. *Talanta* 186, 238–247. doi:10.1016/j.talanta.2018.04.068

Syukri, Y., Fernenda, L., Utami, F. R., Qiftayati, I., Kusuma, A. P., and Istikaharah, R. (2015). Preperation and characterization of B-cyclodextrin inclusion complexes oral tablets containing poorly water soluble glimipiride using freeze drying method. *Indones. J. Pharm.* 26, 71. doi:10.14499/indonesianjpharm26iss2pp71

Szejtli, J. (1998). Introduction and general overview of cyclodextrin chemistry. *Chem. Rev.* 98, 1743–1754. doi:10.1021/cr970022c

Szökő, É., Vincze, I., and Tábi, T. (2016). Chiral separations for d-amino acid analysis in biological samples. *J. Pharmaceut. Biomed. Anal.* 130, 100–109. doi:10.1016/j.jpba.2016.06.054

Tian, B., Hua, S., and Liu, J. (2020). Cyclodextrin-based delivery systems for chemotherapeutic anticancer drugs: a review. *Carbohydr. Polym.* 232, 115805. doi:10.1016/j.carbpol.2019.115805

Uekama, K., Hirayama, F., and Irie, T. (1998). Cyclodextrin drug carrier systems. *Chem. Rev.* 98, 2045–2076. doi:10.1021/cr970025p

Vazquez-Gonzalez, M., Liao, W. C., Cazelles, R., Wang, S., Yu, X., Gutkin, V., et al. (2017). Mimicking horseradish peroxidase functions using Cu(2+)-modified carbon nitride nanoparticles or Cu(2+)-modified carbon dots as heterogeneous catalysts. *ACS Nano* 11, 3247–3253. doi:10.1021/acsnano.7b00352

Wang, B., and Bols, M. (2017). Artificial metallooxidases from cyclodextrin diacids. *Chemistry* 23, 13766–13775. doi:10.1002/chem.201702530

Wang, C., Wang, Z., Zhao, T., Li, Y., Huang, G., Sumer, B. D., et al. (2018a). Optical molecular imaging for tumor detection and image-guided surgery. *Biomaterials* 157, 62–75. doi:10.1016/j.biomaterials.2017.12.002

Wang, F., Zhang, Y., Du, Z., Ren, J., and Qu, X. (2018b). Designed heterogeneous palladium catalysts for reversible light-controlled bioorthogonal catalysis in living cells. *Nat. Commun.* 9, 1209. doi:10.1038/s41467-018-03617-x

Wang, X., Guo, W., Hu, Y., Wu, J., and Wei, H. (2016). *Nanozymes: next wave of artificial enzymes*. Berlin, Germany: Springer.

Wang, Y., Zhuo, S., Hou, J., Li, W., and Ji, Y. (2019). Construction of beta-cyclodextrin covalent organic framework-modified chiral stationary phase for chiral separation. *ACS Appl. Mater. Interfaces* 11, 48363–48369. doi:10.1021/acsami.9b16720

Wei, H., and Wang, E. (2013). Nanomaterials with enzyme-like characteristics (nanozymes): next-generation artificial enzymes. *Chem. Soc. Rev.* 42, 6060–6093. doi:10.1039/c3cs35486e

Wei, Y., Zhang, J., Memon, A. H., and Liang, H. (2017). Molecular model and *in vitro* antioxidant activity of a water-soluble and stable phloretin/hydroxypropyl-β-cyclodextrin inclusion complex. *J. Mol. Liq.* 236, 68–75. doi:10.1016/j.molliq.2017.03.098

Wirth, T. (2015). Small organoselenium compounds: more than just glutathione peroxidase mimics. *Angew. Chem. Int. Ed.* 54, 10074–10076. doi:10.1002/anie.201505056

Wu, J., Wang, X., Wang, Q., Lou, Z., Li, S., Zhu, Y., et al. (2019a). Nanomaterials with enzyme-like characteristics (nanozymes): next-generation artificial enzymes (II). *Chem. Soc. Rev.* 48, 1004–1076. doi:10.1039/c8cs00457a

Wu, Y., Tilley, R. D., and Gooding, J. J. (2019b). Challenges and solutions in developing ultrasensitive biosensors. *J. Am. Chem. Soc.* 141, 1162–1170. doi:10.1021/jacs.8b09397

Xu, D., Hu, M. J., Wang, Y. Q., and Cui, Y. L. (2019). Antioxidant activities of quercetin and its complexes for medicinal application. *Molecules* 24. doi:10.3390/molecules24061123

Yan, H., He, L., Ma, C., Li, J., Yang, J., Yang, R., et al. (2014). Poly beta-cyclodextrin inclusion-induced formation of two-photon fluorescent nanomicelles for biomedical imaging. *Chem. Commun.* 50, 8398–8401. doi:10.1039/c4cc02412e

Yi, Y., Zhang, D., Ma, Y., Wu, X., and Zhu, G. (2019). Dual-signal electrochemical enantiospecific recognition system via competitive supramolecular host-guest interactions: the case of phenylalanine. *Anal. Chem.* 91, 2908–2915. doi:10.1021/acs.analchem.8b05047

Zhang, J., Sun, H., and Ma, P. X. (2010). Host– guest interaction mediated polymeric assemblies: multifunctional nanoparticles for drug and gene delivery. *ACS Nano* 4, 1049–1059. doi:10.1021/nn901213a

Zhang, Y., Yang, D., Chen, H., Lim, W. Q., Phua, F. S. Z., An, G., et al. (2018). Reduction-sensitive fluorescence enhanced polymeric prodrug nanoparticles for combinational photothermal-chemotherapy. *Biomaterials* 163, 14–24. doi:10.1016/j.biomaterials.2018.02.023

Zhang, Y. M., Liu, Y. H., and Liu, Y. (2020). Cyclodextrin-based multistimuli-responsive supramolecular assemblies and their biological functions. *Adv. Mater.* 32, e1806158. doi:10.1002/adma.201806158

Zhao, Y., Huang, Y., Zhu, H., Zhu, Q., and Xia, Y. (2016). Three-in-One: sensing, self-assembly, and cascade catalysis of cyclodextrin modified gold nanoparticles. *J. Am. Chem. Soc.* 138, 16645–16654. doi:10.1021/jacs.6b07590

Zhou, C., Wang, D., Cao, M., Chen, Y., Liu, Z., Wu, C., et al. (2016a). Self-aggregation, antibacterial activity, and mildness of cyclodextrin/cationic trimeric surfactant complexes. *ACS Appl. Mater. Interfaces* 8, 30811–30823. doi:10.1021/acsami.6b11667

Zhou, J., Tang, J., and Tang, W. (2015). Recent development of cationic cyclodextrins for chiral separation. *Trac. Trends Anal. Chem.* 65, 22–29. doi:10.1016/j.trac.2014.10.009

Zhou, Z., Han, Z., and Lu, Z.-R. (2016b). A targeted nanoglobular contrast agent from host-guest self-assembly for MR cancer molecular imaging. *Biomaterials* 85, 168–179. doi:10.1016/j.biomaterials.2016.02.002

**Conflict of Interest:** The authors declare that the research was conducted in the absence of any commercial or financial relationships that could be construed as a potential conflict of interest.

frontiers in Chemistry

REVIEW
published: 26 March 2021
doi: 10.3389/fchem.2021.635315

# Macrocycles in Bioinspired Catalysis: From Molecules to Materials

*Jie Shang*[1], *Yao Liu*[2] *and Tiezheng Pan*[1]*

[1]School of Life Sciences, Northwestern Polytechnical University, Xi'an, China, [2]State Key Laboratory of Analytical Chemistry for Life Sciences, School of Chemistry and Chemical Engineering, Nanjing University, Nanjing, China

Macrocyclic compounds have been studied extensively as the host molecules in supramolecular chemistry. Their structural characteristics make macrocycles desirable in the field of molecular recognition, which is the key to high catalytic efficiencies of natural enzymes. Therefore, macrocycles are ideal building blocks for the design of bioinspired catalysts. This mini review highlights recent advances ranging from single-molecule to metal-organic framework materials, exhibiting multilevel macrocycle catalysts with unique catalytic centers and substrate-binding affinities.

**Keywords: macrocycle, catalysis, cyclodextrin, cucurbituril, rotaxane, porphyrin**

OPEN ACCESS

***Edited by:***
*Pavel Padnya,*
*Kazan Federal University, Russia*

***Reviewed by:***
*Dong-Sheng Guo,*
*Nankai University, China*
*Xiao-Yu Hu,*
*Nanjing University of Aeronautics and Astronautics, China*
*Tangxin Xiao,*
*Changzhou University, China*

***Correspondence:**
*Tiezheng Pan*
*pantiezheng@outlook.com*

***Specialty section:***
*This article was submitted to Supramolecular Chemistry, a section of the journal Frontiers in Chemistry*

***Received:*** *30 November 2020*
***Accepted:*** *16 February 2021*
***Published:*** *26 March 2021*

***Citation:***
*Shang J, Liu Y and Pan T (2021) Macrocycles in Bioinspired Catalysis: From Molecules to Materials. Front. Chem. 9:635315. doi: 10.3389/fchem.2021.635315*

## INTRODUCTION

Natural enzymes are innately endowed with substrate-binding sites, which are essential for the formation of enzyme-substrate complex and crossing the activation energy barrier of catalytic reactions. These binding sites are generated by the elaborated folding of peptides into cavity-like conformations that are spatially complementary to the substrates. From the perspective of supramolecular chemistry, many synthetic macrocycles provide the structural feature of substate-binding sites, which leads to a broad application of macrocyclic compounds in the areas of ion recognition (Ding et al., 2017), gas storage (Zhou et al., 2020), stimuli-responsive materials (Lei et al., 2020), drug delivery (Webber and Langer, 2017), and catalysis (Pairault et al., 2020). Most of all, the nanosized confined spaces in the macrocycles are excellent platforms for highly efficient and selective catalytic reactions. With the development of host-guest chemistry, cyclodextrins (Breslow, 1982), calixarenes (Li et al., 2020a; Li et al., 2020b), pillararenes (Xiao et al., 2018; Xiao et al., 2019), cucurbiturils (Wagner et al., 2020), and many other macrocyclic compounds with enzyme-like substrate affinity and selectivity, have been studied for specific molecular recognition, binding, and bioinspired catalysis. The rising hotspot of porphyrins-based polymers and crystalline organic materials has produced tremendous achievements with high guest uptake performance and structural stability (Farha et al., 2011). Inspired by the natural enzymes, macrocycle-based systems, including single molecules (Dong et al., 2012), supramolecular macrocycle systems (Lewandowski et al., 2013), covalently linked porphyrins (Cheung et al., 2019), and metal-organic framework materials (Shultz et al., 2009), become an indispensable role as bioinspired catalysts.

Except for the cavity-like structure, the convenient modification of macrocycles provides unlimited possibilities to mimic the active sites of natural enzymes. The functionalization of supramolecular macrocyclic structures brought dynamic control of the activity and enantioselectivity into organic catalysis. For instance, the selenium-incorporated cyclodextrins (CDs) were used as a glutathione peroxidase mimic for their antioxidant activity (Huang et al., 2011). Moreover, macrocycles functionalized with transition metals showed specific activity for asymmetric catalytic reactions (Li et al., 2015a; Li et al., 2015b). Various catalytic groups have

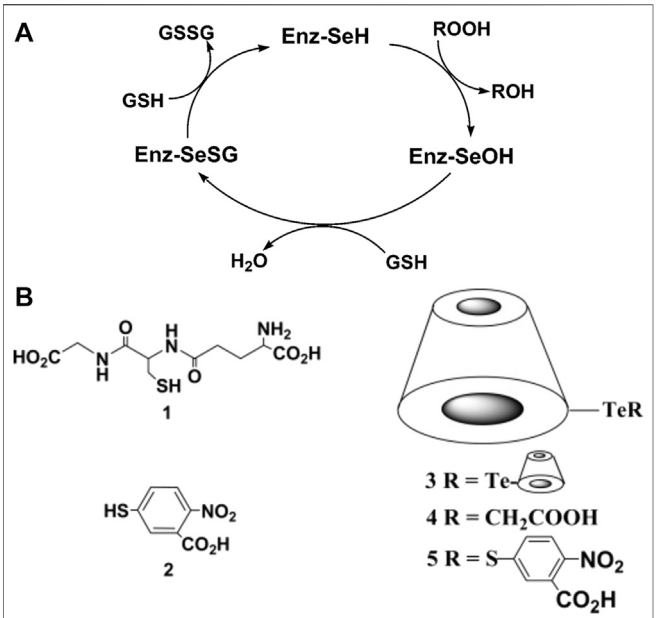


**FIGURE 1 | (A)** The catalytic mechanism of GPx. GPxs catalyze the reduction of peroxides at the expense of glutathione molecules, involving the formation and breaking of Se-S covalent bond. **(B)** Chemical structures of the substrates of GPx (left) and the tellurium-containing CD (right). A and B Reproduced from Dong et al. (2004) with permission. Copyright 2004 American Chemical Society.

expanded the application scope of macrocycles in both enzyme catalysis and organocatalysis. Also, the supramolecular assembly and covalent crosslinking of macrocycles further take advantage of the cluster effect to enhance their structural stability, material performance, and catalytic activity. This review covers the recent work of macrocycle-based catalysts ranging from the synthetic macrocycles, self-assembled supramolecular scaffolds, to nanoscale materials. These works have facilitated both the academic study and industrial applications of macrocyclic catalysts.

## SINGLE-MOLECULE MACROCYCLES AS BIOINSPIRED CATALYSTS

Supramolecular chemistry has brought a great opportunity to the development of macrocycle catalysis. To mimic the cavity of natural enzymes, many single-molecule macrocycles, including CDs, cyclophanes, cavitands, calixarenes have been developed (Ikeda and Shinkai, 1997; Diederich et al., 2008; Brotin and Dutasta, 2009; Hooley and Rebek, 2009; Klöck et al., 2009; Schühle et al., 2011). These macrocycles could promote the reactions in a confined hydrophobic space and carry the reactions in a specific path in a bioinspired manner with specificity and selectivity. Following the pioneering work contributed by Breslow (Breslow, 1982), Tabushi (Tabushi, 1982), Saenger (Saenger, 1980), and D'Souza and Bender (D'Souza and Bender, 1987), many CD-based artificial enzymes have been extensively developed. In addition, CD derivatives are widely used as scaffolds for the construction of artificial glutathione peroxidase (GPx), an efficient antioxidant enzyme with the selenium catalytic center (**Figure 1A**). Numerous CD-based GPx models have been designed via incorporating selenium/tellurium functional groups on macrocyclic building blocks (Huang et al., 2011). By modification of CD and with ditelluride moiety, 2,2′-ditellurobis (2-deoxy-β-CD) showed excellent GPx-like activity in the presence of substrate thiols (**Figure 1B**) (Liu et al., 1998; Liu et al., 2000; Liu et al., 2002; Dong et al., 2004; McNaughton et al., 2004; Dong et al., 2006a; Dong et al., 2006b; Dong et al., 2007). When an aromatic substrate was used instead of natural substrate glutathione, the activity could be 200,000-fold more efficiently than the common GPx mimic PhSeSePh (Dong et al., 2004). The kinetic constant was similar to that of natural GPx ($10^7\ M^{-1}min^{-1}$). These single-molecule macrocyclic catalysts broke the traditional design strategy focusing on organocatalytic mechanisms, paying more attention to the molecular binding affinity to the substrate.

Besides CDs, more kinds of macrocyclic compounds have been developed to push the boundary of macrocycle catalysis to heterogeneous catalysis and asymmetric catalysis. Reisner, Scherman, and coworkers presented the surface-adsorbed host-guest interactions (Wagner et al., 2020). In this work, the reduction of $CO_2$ to CO was highly corelated to the complexation behaviors of cucurbit (6)uril [CB (6)]. It was proved that the reaction site located inside the cavity of CB (6) just like the binding between enzymes and their substrates. The experiment results indicated that differences between this CB (6)-based electrocatalytic reaction and traditional $CO_2$ reduction existed, but not reflected in the $H_2$ production of the reaction process. Therefore the unique $CO_2$-hosting ability of CB (6) played the critical role in the catalysis. Also, an efficient enantioselective reaction was reported by Wang's group, showing that chiral macrocyclic compounds with delicate hydrogen-bonding network could conduct an artificial dimerization (Guo et al., 2020). The catalytic cavity based on the macrocyclic compounds was achieved by dimerization for the catalytic reaction (**Figure 2**). Inside the catalytic cavity, the Mannich reaction of cyclic aldimine substrates was promoted by this assembly system. The imine substrate was activated by the H-bond network that generated through the dimerization. Besides, Wang's group developed a counteranion trapping strategy with macrocyclic compounds for enantioselective catalysis. The macrocycles contained cooperative moieties to construct a chiral catalytic cavity (Ning et al., 2020). Their catalytic microenvironment was further optimized with functionalization for the regulation of substrate-binding. These catalytic macrocycles exhibited high yield and stereoselectivity in the Friedel-Crafts reaction using ethanedisulfonic acid as substrates. The high activity was attributed to the catalytic cavity of macrocycles that enhanced the acidity and ion-pairing. These works above showed that the different properties of macrocyclic compounds, such as hosting ability, cavity size, structural symmetry, and electrostatic distribution, could largely enrich the variety of potential catalytic reactions for macrocyclic catalysts.

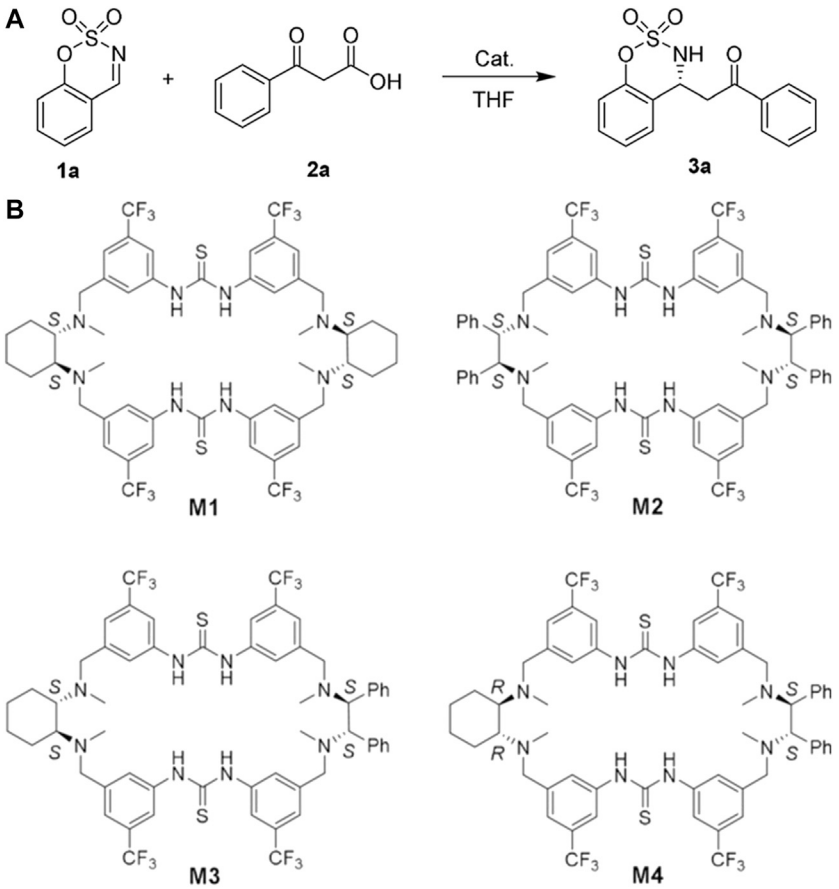


**FIGURE 2 | (A)** The decarboxylative Mannich reaction 'promoted by chiral macrocycle catalysts for asymmetric catalysis. **(B)** The effects of different macrocyclic conformations and chiral microenvironments on catalytic efficiency and enantioselectivity were studied by evaluating the catalytic behaviors of macrocycle M1-M4. M4 achieved a 99% yield and 94:6 enantiomeric ratio (er) under optimal conditions, while M1-M3 gave a relatively lower. A and B Reproduced from Guo et al. (2020) with permission. Copyright 2020 Wiley-VCH Verlag GmbH & Co. KGaA, Weinheim.

## SUPRAMOLECULAR MACROCYCLE SYSTEMS AS BIOINSPIRED CATALYSTS

Compare to single-molecule macrocycles, supramolecular macrocycle systems consist of not only one macrocycle, but also other components that non-covalently bound to the host molecule (e.g., the axle and guest molecules), allowing multiple catalytic behaviors and functionalization possibilities. Leigh's group developed a rotaxane structure that showed ribosome-like activity to synthesize peptides in a successive manner. (Lewandowski et al., 2013). The substrate amino acids were linked sequentially to a strand, and a tethered thiol-functionalized macrocycle transported the amino acids on to another end of the strand to form a new peptide oligomer. The catalytic system represents a significant step to mimic the function of ribosomes chemically. The dynamic feature of supramolecular structures provides "smart control" over the catalytic reaction. Inspired by the rotaxane catalysis and the trigger-induced effects that regulate enzymatic syntheses, a pH-responsive pseudorotaxane switch was constructed with a CB (6) macrocycle and an organoselenium molecular strand (Li et al., 2015). The organoselenium strand contains an antioxidant selenium center for catalysis and two regulation imino groups to position the CB (6) macrocycle along the strand. When pH < 6,

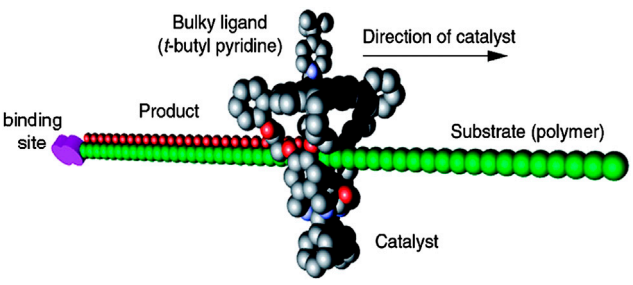


**FIGURE 3 |** The processive catalytic system containing a linear polymer and a macrocycle. The macrocycle is modified with catalytic center and restrained to the polymer, which acts as axle molecule in the rotaxane system. As the macrocycle moves from one end to the other, the axle is functionalized (e.g., oxidation) sequentially by the catalyst. Reproduced from Deutman et al. (2014) with permission. Copyright 2014 American Chemical Society.

no enzyme activity was observed as the active site was concealed by CB (6). When pH > 7, the active site was exposed as CB (6) bound to the imino groups. Therefore, the enzyme activity of the complex was turned on. Although these supramolecular macrocycle systems do not focus on the substrate binding ability, they could mimic the activity-regulation mechanism of natural enzymes to control the catalytic reaction process.

The supramolecular macrocycle systems were also applied in the study of processive catalysis (**Figure 3**). Inspired by the DNA polymerase that operates by allowing multiple catalysis rounds to occur, artificial catalytic supramolecular structures acting in this processive manner were constructed. A porphyrin-containing rotaxane system with a manganese macrocycle was developed for polybutadiene epoxidation (Thordarson et al., 2003; Coumans et al., 2006; Monnereau et al., 2010; Deutman et al., 2014). The macrocycle could act as a catalytic site and catalyze polybutadiene into 80% *trans*- and 20% *cis*-epoxide polybutadieneepoxide. This stereoselectivity difference indicated the steric mechanism of the reaction. Takata's group synthesized a macrocyclic rotaxane containing Pd moiety for hydroamination (Miyagawa et al., 2010). The processive catalysis took place inside the cavity of the macrocycle, like enzyme catalysis. Also, Harada's group introduced a molecular clamp that polymerized δ-valerolactone (δ-VL) (Takashima et al., 2011). It consists of *a*- and *ß*-CD dimer connected with terephthalamide. The system afforded poly (δ-VL) with a number-average molecular Weight (Mn) = 11,000 and that a mixture of *a*- and *ß*-CDs without dimerization afforded Mn = 2,300. The processive catalysis was hardly achieved by traditional catalysts, and it also requires plenty of protein components and complicated mechanism in nature. However, this special catalytic behavior based on supramolecular macrocycle systems could play a critical role in the modification of polymers, peptides, and other macromolecules in future.

## COVALENTLY LINKED PORPHYRINS AS BIOINSPIRED CATALYSTS

Porphyrin is a heteroatom-containing macrocyclic compound constructed by four pyrrole units which are connected by four methines as the bridge and are in a planar conformation to form 18π electrons conjugation system, and porphyrin can coordinate with many metals to form metallated porphyrins with extensive applications in many scientific fields, such as catalytic reaction and chemosensors (Ding et al., 2017; To and Chan, 2017; Zhang et al., 2017). Covalent organic frameworks (COFs) are crystalline porous organic polymers linked by covalent bonds with porous and ordered structures, attracting considerable attention due to their porosity, stability, and versatility. The chemical and structural tunability makes them have great potential applications in catalysis, separation, gas storage (Geng et al., 2020; Lee et al., 2020; Li et al., 2020). Moreover, many examples of COFs-based metalloporphyrin building blocks have been fabricated to apply in different catalytic fields (Singh et al., 2018; Cheung et al., 2019; Hao et al., 2019; Gong et al., 2020).

One important reaction for the fabrication of COFs is Shiff-base condensation between aldehyde and amine. It is an important strategy to introduce different amino groups and aldehyde groups to porphyrin building blocks, design linkers of porphyrin building blocks, and change metallic ions to construct COFs based on metalloporphyrin. Some examples have achieved recyclability with high catalytic activity. Banerjee group reported a COF (2,3-DhaTph) incorporating bifunctional (acid/base) catalytic sites based on porphyrin (Shinde et al., 2015). By reversible Schiff-base reaction using 2,3-dihydroxyterephthalaldehyde (2,3-Dha, **Figure 4A**) and a 5,10,15,20-tetrakis (4-amino phenyl)-21H, 23H-porphine unit (Tph, **Figure 4B**), The COF 2,3-DhaTph (**Figure 4C**) was synthesized. This COF has high thermal stability up to 300°C and could keep well aqueous stability for more than 7 days. The COF with weak acidic and basic sites could most significantly catalyze the cascade reaction with high product yield (~90%) and possess recyclability over five cycles. According to similar strategies, Dai's group successfully introduced $Fe^{2+}$ to COF-366 and detected the oxidation using the Fe-COF as peroxidase Mimics (Wang et al., 2018). The Fe-COF can catalyze the $H_2O_2$ oxidation to show that Fe-COF has an inner peroxidase-like catalytic activity. Additionally, the kinetic studies demonstrated that the Fe-COF structure has a higher affinity toward the substrates than the natural enzyme, horseradish peroxidase. Furthermore, the Fe-COF could be applied in a colorimetric sensor for the sensitive detection of $H_2O_2$ and measure glucose. As a peroxidase mimic, the Fe-COF exhibits the advantages of easy preparation and ultrahigh catalytic efficiency. In addition, the covalent bonds linking macrocycle monomers largely enhanced the stability of catalysts, allowing more practical applications in industry than those of macrocycle systems constructed by weak interactions.

## METAL–ORGANIC FRAMEWORK MATERIALS AS BIOINSPIRED CATALYSTS

Metal-organic frameworks (MOFs) are a class of porous crystalline materials based on the coordination of metal ions/clusters and organic linkers. Unlike other materials, a significant MOF feature is that their structure can be facilely designed, functionalized, and offer a high surface area. They have attracted considerable attention in these years and have many potential applications in storage, catalysis, and separation (Cui et al., 2016; Yang et al., 2017; Wei et al., 2020). In recent years, multilevel MOFs using porphyrin as building blocks have been developed to mimic catalyst. As a pioneering example of using metalloporphyrin as a building block to design MOF, in 2009 Nguyen's group reported a mixed-ligand strategy that combines 1,2,4,5-tetrakis-(4-carboxyphenyl)benzene 1) (5,15-dipyridyl-10,20-bis[pentafluorophenyl])porphyrin 2) and $Zn(NO_3)_2{\cdot}6H_2O$ under solvothermal conditions (**Figure 5**) obtained purple block crystals of Zn-MOF with large pores (surface area of ~500 $m^2/g$), and further studies demonstrated that the Zn-MOF is available for a catalytic acyl-transfer reaction between a N-acetylimidazole and 3-pyridinemethanol with huge rate enhancement (Shultz et al., 2009). For the catalytic reaction, Zn serves as a catalytic site, and the size of the cavity plays an

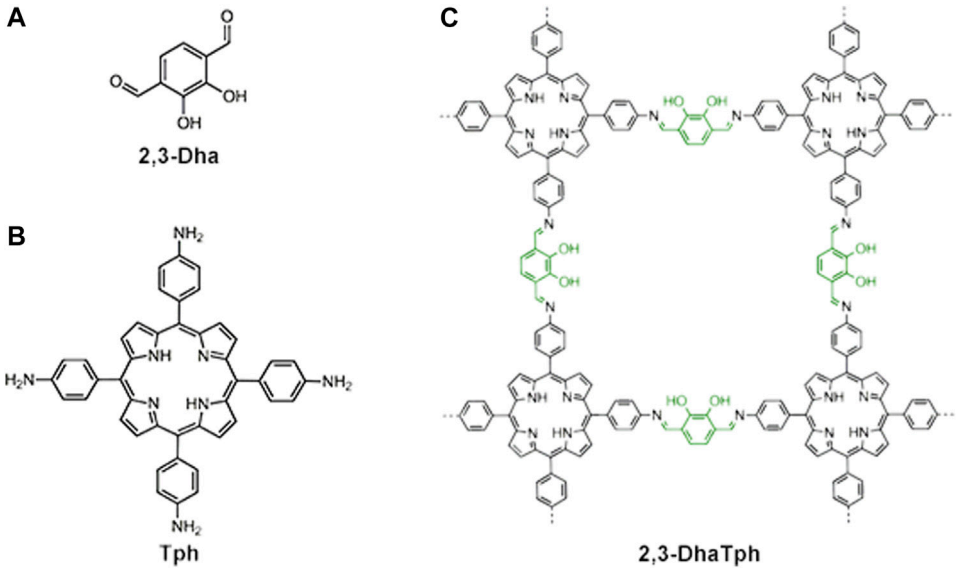


**FIGURE 4 |** The chemical structures of 2,3-Dha **(A)**, Tph **(B)**, and 2,3-DhaTph **(C)**. The hydroxy groups (green) act as acidic sites, whereas porphyrin and imine bonds (black) act as basic sites for an acid-base catalyzed cascade reaction. Adapted from Shinde et al. (2015) with permission. Copyright 2015 the Royal Society of Chemistry.

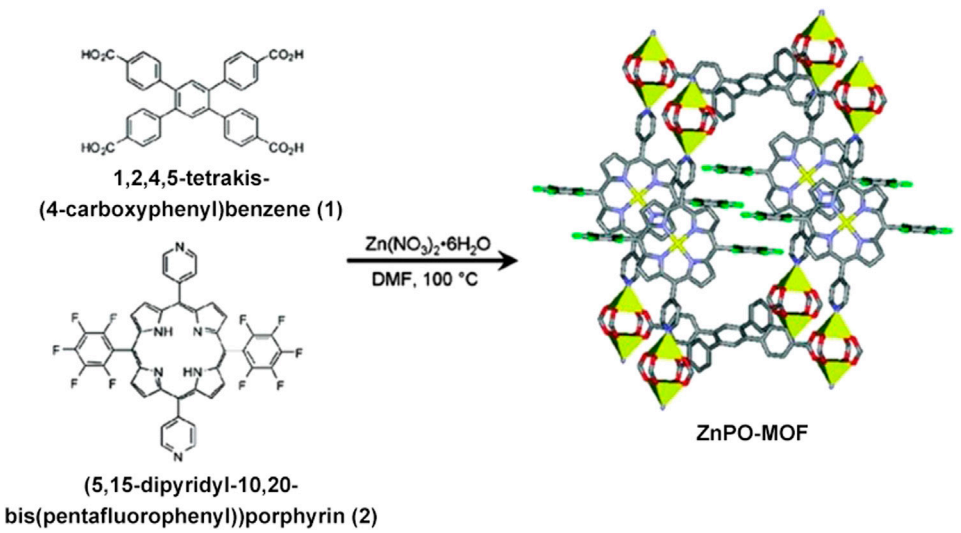


**FIGURE 5 |** The synthesis of ZnPO-MOF. The MOF (right) has multiple features for catalysis, such as large pores, permanent microporosity, and fully reactant-accessible active sites. Reproduced from Shultz et al. (2009) with permission. Copyright 2009 American Chemical Society.

essential role in enhancing the reaction rate. Based on this work, Nguyen group introduced different metallic ion ($Al^{3+}$, $Zn^{2+}$, $Pd^{2+}$, $Fe^{3+}$, and $Mn^{3+}$) to coordinate with porphyrin in this system to obtain different COFs materials, which can serve as effective catalysts for the oxidation of alkenes and alkanes (Farha et al., 2011). The work offered a strategy to incorporate macrocyclic metalloporphyrin with catalytic property into nanomaterials to develop heterogeneous catalysts. So, many MOFs based on metalloporphyrin with catalytic activity have been developed, which were designed by changing substitutes in porphyrin, metallic ion coordinating with porphyrin, metal nodes or organic linkers (Feng et al., 2013; Beyzavi et al., 2015; Liu et al., 2015; Lin et al., 2016; Jiang et al., 2017; Liang et al., 2018; Pereira et al., 2019). For instance, Zhou's group prepared a series of isostructural zirconium-based MOFs, which differ in porphyrin unit functionalized by ethyl, bromo, chloro, and fluoro groups to study the electron effect of substitutes on the catalytic activity of MOFs. These structures

showed excellent structural tunability and outstanding chemical stability. The oxidation of 3-methylpentane to corresponding alcohols and ketones was utilized as a model reaction to study the catalytic activity and selectivity. Study results demonstrated that the Br-containing MOF catalyst showed higher catalytic efficiency and a remarkable 99% selectivity of the tertiary alcohol over the five other possible byproducts (Huang et al., 2017).

The disadvantages of the traditional homogeneous catalysts, including difficult recyclability and easy deactivation, limit industry application. Some examples of porphyrin-MOFs have realized high activity and recyclability of the heterogeneous catalyst compared to the homogeneous analog catalysts (Feng et al., 2013). Zhou group designed and prepared a perfluorophenylene functionalized metalloporphyrins MOF (PCN-624) which was constructed by 12-connected $[Ni_8(OH)_4(H_2O)_2Pz_{12}]$ (Pz = pyrazolide) nodes and porphyrin derivative linker. This MOF exhibits excellent stability under different conditions, such as organic solvents, strong acid, and aqueous-based solutions. Attractively, the MOF can be used as an efficient heterogeneous catalyst for the selective synthesis of fullerene–anthracene bisadduct and recycled over five times without significant loss of its catalytic efficiency (Huang et al., 2018). Additionally, many metalloporphyrin-MOFs have also been developed to use as an electrochemical catalyst and photochemical catalyst, which were designed through similar strategies (Kornienko et al., 2015; Jin et al., 2020). These porous crystalline materials could not only provide well-defined molecular recognition sites (Tashiro and Shionoya, 2020), but also metal ions with catalytic activities, combining the keys to making natural enzymes highly efficient.

## OUTLOOK

From the single-molecular level to materials, macrocycles have been developed for various functional building blocks. The unique cavity-like structures of the macrocyclic compounds could promote the catalytic reactions in a bioinspired way. Not only novel macrocycles modified with catalytic functional groups expanded the application scope of macrocycle catalysis, but the supramolecular assembly of macrocycles brought dynamic control and processive catalysis into this research area. In addition, the covalent crosslinking further endowed catalytic porphyrin macrocycles with stability and clustering effects. The combination of macrocycles and catalysis is going to prove its economic value and its academic potential.

However, there are still many challenges ahead in this field. For instance, macrocycle catalysts' substrate-recognition ability is generally weak compared to natural enzymes, which is the main reason for the relatively low catalytic activity. Also, the catalytic selectivity of macrocycle catalysts is limited by the simplicity of the substrate-binding cavity. Nevertheless, these macrocycles provide novel scaffolds to construct advanced catalysts for synthetic routes. We believe that elaborate structures and practical activities are going to emerge.

## AUTHOR CONTRIBUTIONS

JS investigated the current development of porphyrins-based macrocycle catalysts and rafted *Covalently Linked Porphyrins as Bioinspired Catalysts* and *Metal–Organic Framework Materials as Bioinspired Catalysts* sections. YL drafted the introduction and abstract. TP drafted, *Single-Molecule Macrocycles as Bioinspired Catalysts*, *Supramolecular Macrocycle Systems as Bioinspired Catalysts* and *Outlook* sections and organized the manuscript.

## FUNDING

This work was supported by the Natural Science Foundation of China (Nos. 21901209 and 201901210) and Natural Science Foundation of Shaanxi Province (No. 2019JQ-626).

## REFERENCES

Beyzavi, M. H., Vermeulen, N. A., Howarth, A. J., Tussupbayev, S., League, A. B., Schweitzer, N. M., et al. (2015). A hafnium-based metal-organic framework as a nature-inspired tandem reaction catalyst. *J. Am. Chem. Soc.* 137, 13624–13631. doi:10.1021/jacs.5b08440

Breslow, R. (1982). Artificial enzymes. *Science* 218, 532–537. doi:10.1126/science.7123255

Brotin, T., and Dutasta, J.-P. (2009). Cryptophanes and their complexes-present and future. *Chem. Rev.* 109, 88–130. doi:10.1021/cr0680437

Cheung, P. L., Lee, S. K., and Kubiak, C. P. (2019). Facile solvent-free synthesis of thin iron porphyrin COFs on carbon cloth electrodes for $CO_2$ reduction. *Chem. Mater.* 31, 1908–1919. doi:10.1021/acs.chemmater.8b04370

Coumans, R. G. E., Elemans, J. A. A. W., Nolte, R. J. M., and Rowan, A. E. (2006). Processive enzyme mimic: kinetics and thermodynamics of the threading and sliding process. *Proc. Natl. Acad. Sci. U. S. A.* 103, 19647–19651. doi:10.1073/pnas.0603036103

Cui, Y., Li, B., He, H., Zhou, W., Chen, B., and Qian, G. (2016). Metal-organic frameworks as platforms for functional materials. *Acc. Chem. Res.* 49, 483–493. doi:10.1021/acs.accounts.5b00530

D'Souza, V. T., and Bender, M. L. (1987). Miniature organic models of enzymes. *Acc. Chem. Res.* 20, 146–152. doi:10.1021/ar00136a004

Deutman, A. B. C., Cantekin, S., Elemans, J. A. A. W., Rowan, A. E., and Nolte, R. J. M. (2014). Designing processive catalytic systems. threading polymers through a flexible macrocycle ring. *J. Am. Chem. Soc.* 136, 9165–9172. doi:10.1021/ja5032997

Diederich, F., Stang, P. J., and Tykwinski, R. R. (2008). *Modern supramolecular chemistry: strategies for macrocycle synthesis*. Weinheim, Germany: Wiley VCH.

Ding, Y., Zhu, W. H., and Xie, Y. (2017). Development of ion chemosensors based on porphyrin analogues. *Chem. Rev.* 117, 2203–2256. doi:10.1021/acs.chemrev.6b00021

Dong, Z. Y., Huang, X., Mao, S. Z., Liang, K., Liu, J. Q., Luo, G. M., et al. (2006a). Cyclodextrin-derived mimic of glutathione peroxidase exhibiting enzymatic specificity and high catalytic efficiency. *Chem. Eur. J.* 12, 3575–3579. doi:10.1002/chem.200501098

Dong, Z., Liu, J., Mao, S., Huang, X., Luo, G., and Shen, J. (2006b). A glutathione peroxidase mimic 6,6′-ditellurobis (6-deoxy-β-cyclodextrin) with high substrate specificity. *J. Incl. Phenom. Macrocycl. Chem.* 56, 179–182. doi:10.1007/s10847-006-9080-7

Dong, Z., Liang, K., Wang, C., Huang, X., Mao, S., Li, X., et al. (2007). A study of biomimetic system: exploration of factors modulating the catalytic capacity of

glutathione peroxidase mimics. *J. Mol. Catal. A. Chem.* 277, 193–201. doi:10.1016/j.molcata.2007.08.003

Dong, Z., Liu, J., Mao, S., Huang, X., Yang, B., Ren, X., et al. (2004). Aryl thiol substrate 3-carboxy-4-nitrobenzenethiol strongly stimulating thiol peroxidase activity of glutathione peroxidase mimic 2, 2'-ditellurobis(2-deoxy-β-cyclodextrin). *J. Am. Chem. Soc.* 126, 16395–16404. doi:10.1021/ja045964v

Dong, Z., Luo, Q., and Liu, J. (2012). Artificial enzymes based on supramolecular scaffolds. *Chem. Soc. Rev.* 41, 7890–7908. doi:10.1039/c2cs35207a

Farha, O. K., Shultz, A. M., Sarjeant, A. A., Nguyen, S. T., and Hupp, J. T. (2011). Active-site-accessible, porphyrinic metal–organic framework materials. *J. Am. Chem. Soc.* 133, 5652–5655. doi:10.1021/ja111042f

Feng, D., Chung, W. C., Wei, Z., Gu, Z. Y., Jiang, H. L., Chen, Y. P., et al. (2013). Construction of ultrastable porphyrin Zr metal-organic frameworks through linker elimination. *J. Am. Chem. Soc.* 135, 17105–17110. doi:10.1021/ja408084j

Geng, K., He, T., Liu, R., Dalapati, S., Tan, K. T., Li, Z., et al. (2020). Covalent organic frameworks: design, synthesis, and functions. *Chem. Rev.* 120, 8814–8933. doi:10.1021/acs.chemrev.9b00550

Gong, Y. N., Zhong, W., Li, Y., Qiu, Y., Zheng, L., Jiang, J., et al. (2020). Regulating photocatalysis by spin-state manipulation of cobalt in covalent organic frameworks. *J. Am. Chem. Soc.* 142, 16723–16731. doi:10.1021/jacs.0c07206

Guo, H., Zhang, L. W., Zhou, H., Meng, W., Ao, Y. F., Wang, D. X., et al. (2020). Substrate-induced dimerization assembly of chiral macrocycle catalysts toward cooperative asymmetric catalysis. *Angew. Chem. Int. Ed.* 59, 2623–2627. doi:10.1002/anie.201910399

Hao, W., Chen, D., Li, Y., Yang, Z., Xing, G., Li, J., et al. (2019). Facile synthesis of porphyrin based covalent organic frameworks via an $A_2B_2$ monomer for highly efficient heterogeneous catalysis. *Chem. Mater.* 31, 8100–8105. doi:10.1021/acs.chemmater.9b02718

Hiroto, S., Miyake, Y., and Shinokubo, H. (2017). Synthesis and functionalization of porphyrins through organometallic methodologies. *Chem. Rev.* 117, 2910–3043. doi:10.1021/acs.chemrev.6b00427

Hooley, R. J., and Rebek, J. (2009). Chemistry and catalysis in functional cavitands. *Chem. Biol.* 16, 255–264. doi:10.1016/j.chembiol.2008.09.015

Huang, N., Wang, K., Drake, H., Cai, P., Pang, J., Li, J., et al. (2018). Tailor-made pyrazolide-based metal-organic frameworks for selective catalysis. *J. Am. Chem. Soc.* 140, 6383–6390. doi:10.1021/jacs.8b02710

Huang, N., Yuan, S., Drake, H., Yang, X., Pang, J., Qin, J., et al. (2017). Systematic engineering of single substitution in zirconium metal-organic frameworks toward high-performance catalysis. *J. Am. Chem. Soc.* 139, 18590–18597. doi:10.1021/jacs.7b09553

Huang, X., Liu, X., Luo, Q., Liu, J., and Shen, J. (2011). Artificial selenoenzymes: designed and redesigned. *Chem. Soc. Rev.* 40, 1171–1184. doi:10.1039/C0CS00046A

Ikeda, A., and Shinkai, S. (1997). Novel cavity design using calix[n]arene skeletons: toward molecular recognition and metal binding. *Chem. Rev.* 97, 1713–1734. doi:10.1021/cr960385x

Jiang, W., Yang, J., Liu, Y.-Y., Song, S.-Y., and Ma, J.-F. (2017). A stable porphyrin-based porous mog metal-organic framework as an efficient solvent-free catalyst for C-C bond formation. *Inorg. Chem.* 56, 3036–3043. doi:10.1021/acs.inorgchem.6b03174

Jin, L., Lv, S., Miao, Y., Liu, D., and Song, F. (2020). Recent development of porous porphyrin-based nanomaterials for photocatalysis. *ChemCatChem* 13, 140–152. doi:10.1002/cctc.202001179

Klöck, C., Dsouza, R. N., and Nau, W. M. (2009). Cucurbituril-mediated supramolecular acid catalysis. *Org. Lett.* 11, 2595–2598. doi:10.1021/ol900920p

Kornienko, N., Zhao, Y., Kley, C. S., Zhu, C., Kim, D., Lin, S., et al. (2015). Metal–organic frameworks for electrocatalytic reduction of carbon dioxide. *J. Am. Chem. Soc.* 11, 14129–14135. doi:10.1021/jacs.5b08212

Lee, J.-S. M., and Cooper, A. I. (2020). Advances in conjugated microporous polymers. *Chem. Rev.* 120, 2171–2214. doi:10.1021/acs.chemrev.9b00399

Lei, S.-N., Xiao, H., Zeng, Y., Tung, C.-H., Wu, L.-Z., and Cong, H. (2020). BowtieArene: a dual macrocycle exhibiting stimuli-responsive fluorescence. *Angew. Chem. Int. Ed.* 59, 10059–10065. doi:10.1002/anie.201913340

Lewandowski, B., De Bo, G., Ward, J. W., Papmeyer, M., Kuschel, S., Aldegunde, M. J., et al. (2013). Sequence-specific peptide synthesis by an artificial small-molecule machine. *Science* 339, 189–193. doi:10.1126/science.1229753

Li, J., Jing, X., Li, Q., Li, S., Gao, X., Feng, X., et al. (2020a). Bulk COFs and COF nanosheets for electrochemical energy storage and conversion. *Chem. Soc. Rev.* 49, 3565–3604. doi:10.1039/D0CS00017E

Li, Z., Xiao, T., Yang, K., Chen, Y., and Wang, L. (2020b). "Systems based on calixarenes for the creation of catalysts," in *Supramolecular catalysts*. Editors L. Wang (Singapore: World Scientific), Vol. 7, 117–148.

Li, J., Si, C., Sun, H., Zhu, J., Pan, T., Liu, S., et al. (2015a). Reversible pH-controlled switching of an artificial antioxidant selenoenzyme based on pseudorotaxane formation and dissociation. *Chem. Commun.* 51, 9987–9990. doi:10.1039/C5CC02038G

Li, Y.-Y., Yu, S.-L., Shen, W.-Y., and Gao, J.-X. (2015b). Iron-, cobalt-, and nickel-catalyzed asymmetric transfer hydrogenation and asymmetric hydrogenation of ketones. *Acc. Chem. Res.* 48, 2587–2598. doi:10.1021/acs.accounts.5b00043

Liang, J., Xie, Y.Q., Wu, Q., Wang, X. Y., Liu, T. T., Li, H. F., et al. (2018). Zinc porphyrin/imidazolium integrated multivariate zirconium metal–organic frameworks for transformation of $CO_2$ into cyclic carbonates. *Inorg. Chem.* 57, 2584–2593. doi:10.1021/acs.inorgchem.7b02983

Lin, Z., Zhang, Z.-M., Chen, Y.-S., and Lin, W. (2016). Highly efficient cooperative catalysis by $Co^{III}$ (porphyrin) pairs in interpenetrating metal-organic frameworks. *Angew. Chem. Int. Ed.* 55, 13739–13743. doi:10.1002/anie.201605802

Liu, J.-Q., Gao, S.-J., Luo, G.-M., Yan, G.-L., and Shen, J.-C. (1998). Artificial imitation of glutathione peroxidase with 6-selenium-bridged β-cyclodextrin. *Biochem. Biophys. Res. Commun.* 247, 397–400. doi:10.1006/bbrc.1998.8545

Liu, J.-Q., Luo, G.-M., Ren, X.-J., Mu, Y., Bai, Y., and Shen, J.-C. (2000). A bis-cyclodextrin diselenide with glutathione peroxidase-like activity. *Biochim. Biophys. Acta.* 1481, 222–228. doi:10.1016/s0167-4838(00)00130-8

Liu, Y., Li, B., Li, L., and Zhang, H.-Y. (2002). Synthesis of organoselenium-modified β-cyclodextrins possessing a 1,2-benzisoselenazol-3(*2H*)-one moiety and their enzyme-mimic study. *Helv. Chim. Acta.* 85, 9–18. doi:10.1002/1522-2675(200201)85:1<9::AID-HLCA9>3.0.CO;2-H

Liu, Y., Moon, S.-Y., Hupp, J. T., and Farha, O. K. (2015). Dual-function metal-organic framework as a versatile catalyst for detoxifying chemical warfare agent simulants. *ACS Nano.* 9 (12), 12358–12364. doi:10.1021/acsnano.5b05660

McNaughton, M., Engman, L., Birmingham, A., Powis, G., and Cotgreave, I. A. (2004). Cyclodextrin-derived diorganyl tellurides as glutathione peroxidase mimics and inhibitors of thioredoxin reductase and cancer cell growth. *J. Med. Chem.* 47, 233–239. doi:10.1021/jm030916r

Miyagawa, N., Watanabe, M., Matsuyama, T., Koyama, Y., Moriuchi, T., Hirao, T., et al. (2010). Successive catalytic reactions specific to Pd-based rotaxane complexes as a result of wheel translation along the axle. *Chem. Commun.* 46, 1920–1922. doi:10.1039/B917053G

Monnereau, C., Ramos, P. H., Deutman, A. B. C., Elemans, J. A. A. W., Nolte, R. J. M., and Rowan, A. E. (2010). Porphyrin macrocyclic catalysts for the processive oxidation of polymer substrates. *J. Am. Chem. Soc.* 132, 1529–1531. doi:10.1021/ja908524x

Ning, R., Zhou, H., Nie, S.-X., Ao, Y.-F., Wang, D.-X., and Wang, Q.-Q. (2020). Chiral macrocycle-enabled counteranion trapping for boosting highly efficient and enantioselective catalysis. *Angew. Chem. Int. Ed.* 59, 10894–10898. doi:10.1002/anie.202003673

Pairault, N., Zhu, H., Jansen, D., Huber, A., Daniliuc, C. G., Grimme, S., et al. (2020). Heterobifunctional rotaxanes for asymmetric catalysis. *Angew. Chem. Int. Ed.* 59, 5102–5107. doi:10.1002/anie.201913781

Pereira, C. F., Liu, Y., Howarth, A., Figueira, F., Rocha, J., Hupp, J. T., et al. (2019). Detoxification of a mustard-gas simulant by nanosized porphyrin-based metal-organic frameworks. *ACS Appl. Nano Mater.* 2, 465–469. doi:10.1021/acsanm.8b02014

Saenger, W. (1980). Cyclodextrin inclusion compounds in research and industry. *Angew. Chem. Int. Ed. Engl.* 19, 344–362. doi:10.1002/anie.198003441

Schühle, D. T., Peters, J. A., and Schatz, J. (2011). Metal binding calixarenes with potential biomimetic and biomedical applications. *Coord. Chem. Rev.* 255, 2727–2745. doi:10.1016/j.ccr.2011.04.005

Shinde, D. B., Kandambeth, S., Pachfule, P., Kumar, R. R., and Banerjee, R. (2015). Bifunctional covalent organic frameworks with two dimensional organocatalytic micropores. *Chem. Commun.* 51, 310–313. doi:10.1039/c4cc07104b

Shultz, A. M., Farha, O. K., Hupp, J. T., and Nguyen, S. T. (2009). A catalytically active, permanently microporous MOF with metalloporphyrin struts. *J. Am. Chem. Soc.* 131, 4204–4205. doi:10.1021/ja900203f

Singh, A., Roy, S., Das, C., Samanta, D., and Maji, T. K. (2018). Metallophthalocyanine-based redox active metal-organic conjugated microporous polymers for OER catalysis. *Chem. Commun.* 54, 4465–4468. doi:10.1039/c8cc01291a

Tabushi, I. (1982). Cyclodextrin catalysis as a model for enzyme action. *Acc. Chem. Res.* 15, 66–72. doi:10.1021/ar00075a001

Takashima, Y., Osaki, M., Ishimaru, Y., Yamaguchi, H., and Harada, A. (2011). Artificial molecular clamp: a novel device for synthetic polymerases. *Angew. Chem. Int. Ed.* 50, 7524–7528. doi:10.1002/anie.201102834

Tashiro, S., and Shionoya, M. (2020). Novel porous crystals with macrocycle-based well-defined molecular recognition sites. *Acc. Chem. Res.* 53, 632–643. doi:10.1021/acs.accounts.9b00566

Thordarson, P., Bijsterveld, E. J. A., Rowan, A. E., and Nolte, R. J. M. (2003). Epoxidation of polybutadiene by a topologically linked catalyst. *Nature* 424, 915–918. doi:10.1038/nature01925

To, C. T., and Chan, K. S. (2017). Selective aliphatic carbon-carbon bond activation by rhodium porphyrin complexes. *Acc. Chem. Res.* 50, 1702–1711. doi:10.1021/acs.accounts.7b00150

Wagner, A., Ly, K. H., Heidary, N., Szabó, I., Földes, T., Assaf, K. I., et al. (2020). Host-guest chemistry meets electrocatalysis: cucurbit[6]uril on a Au surface as a hybrid system in $CO_2$ reduction. *ACS Catal.* 10, 751–761. doi:10.1021/acscatal.9b04221

Wang, J., Yang, X., Wei, T., Bao, J., Zhu, Q., and Dai, Z. (2018). Fe-Porphyrin-based covalent organic framework as a novel peroxidase mimic for a one-pot glucose colorimetric assay, *ACS Appl. Bio Mater.* 1, 382–388. doi:10.1021/acsabm.8b00104

Webber, M. J., and Langer, R. (2017). Drug delivery by supramolecular design. *Chem. Soc. Rev.* 46, 6600–6620. doi:10.1039/C7CS00391A

Wei, Y.-S., Zhang, M., Zou, R., and Xu, Q. (2020). Metal-organic framework-based catalysts with single metal sites. *Chem. Rev.* 120, 12089–12174. doi:10.1021/acs.chemrev.9b00757

Xiao, T., Xu, L., Zhong, W., Zhou, L., Sun, X.-Q., Hu, X.-Y., et al. (2018). Advanced functional materials constructed from pillar[n]arenes. *Isr. J. Chem.* 58, 1219–1229. doi:10.1002/ijch.201800026

Xiao, T., Zhou, L., Xu, L., Zhong, W., Zhao, W., Sun, X.-Q., et al. (2019). Dynamic materials fabricated from water soluble pillar[n]arenes bearing triethylene oxide groups. *Chin. Chem. Lett.* 30, 271–276. doi:10.1016/j.cclet.2018.05.039

Yang, Q., Xu, Q., and Jiang, H.-L. (2017). Metal-organic frameworks meet metal nanoparticles: synergistic effect for enhanced catalysis. *Chem. Soc. Rev.* 46, 4774–4808. doi:10.1039/C6CS00724D

Zhang, W., Lai, W., and Cao, R. (2017). Energy-related small molecule activation reactions: oxygen reduction and hydrogen and oxygen evolution reactions catalyzed by porphyrin- and corrole-based systems. *Chem. Rev.* 117, 3717–3797. doi:10.1021/acs.chemrev.6b00299

Zhou, Y., Jie, K., Zhao, R., and Huang, F. (2020). Supramolecular-macrocycle-based crystalline organic materials. *Adv. Mater.* 32, 1904824. doi:10.1002/adma.201904824

**Conflict of Interest:** The authors declare that the research was conducted in the absence of any commercial or financial relationships that could be construed as a potential conflict of interest.

frontiers in Chemistry

MINI REVIEW
published: 06 April 2021
doi: 10.3389/fchem.2021.658548

# Applications of Macrocyclic Host Molecules in Immune Modulation and Therapeutic Delivery

*Shreya S. Soni, Abdulrahman Alsasa and Christopher B. Rodell**

*School of Biomedical Engineering, Science and Health Systems, Drexel University, Philadelphia, PA, United States*

The immune system plays a central role in the development and progression of human disease. Modulation of the immune response is therefore a critical therapeutic target that enables us to approach some of the most vexing problems in medicine today such as obesity, cancer, viral infection, and autoimmunity. Methods of manipulating the immune system through therapeutic delivery centralize around two common themes: the local delivery of biomaterials to affect the surrounding tissue or the systemic delivery of soluble material systems, often aided by context-specific cell or tissue targeting strategies. In either case, supramolecular interactions enable control of biomaterial composition, structure, and behavior at the molecular-scale; through rational biomaterial design, the realization of next-generation immunotherapeutics and immunotheranostics is therefore made possible. This brief review highlights methods of harnessing macromolecular interaction for immunotherapeutic applications, with an emphasis on modes of drug delivery.

**Keywords: macrocycle, polymer, hydrogel, nanoparticle, drug delivery, immunotherapy, immunology**

OPEN ACCESS

***Edited by:***
*Susana Santos Braga,*
*University of Aveiro, Portugal*

***Reviewed by:***
*Tangxin Xiao,*
*Changzhou University, China*
*Ruibing Wang,*
*University of Macau, China*

****Correspondence:***
*Christopher B. Rodell*
*cbr58@drexel.edu*

***Specialty section:***
*This article was submitted to Supramolecular Chemistry, a section of the journal Frontiers in Chemistry*

***Received:*** *26 January 2021*
***Accepted:*** *12 March 2021*
***Published:*** *06 April 2021*

***Citation:***
*Soni SS, Alsasa A and Rodell CB (2021) Applications of Macrocyclic Host Molecules in Immune Modulation and Therapeutic Delivery. Front. Chem. 9:658548. doi: 10.3389/fchem.2021.658548*

## INTRODUCTION

Drug delivery strategies seek to improve therapeutic efficacy by increasing the proportion of drug that reaches its target site (drug targeting), increasing the duration of drug presentation (controlled release), or presenting the drug in response to appropriate triggers (responsive delivery) (Farokhzad and Langer, 2009; Tibbitt et al., 2016; Webber and Langer, 2017). Supramolecular chemistries can advance these goals through the provision of specific, tunable, and thermodynamically reversible bonds. These properties lend themselves to the development of drug delivery systems (Rodell et al., 2015a; Webber and Langer, 2017), especially those that can sequester drugs for subsequent release at the target site, can be tuned to improve pharmacological properties, and can release therapeutic cargo passively or via responsive chemistries.

Immune system dysfunction is a driver of human disease, for which the delivery of biologic and small molecule drugs to specific tissues and cells is critically needed. Prevalent immune-related diseases include those rooted in non-resolving inflammation, such as cardiovascular disease, arthritis, and tissue injury (Nathan and Ding, 2010). In many such cases, non-specific inflammation manifests in the development of maladaptive autoimmune responses, wherein the body mounts an immune attack against its tissues (Epelman et al., 2015; Jain and Pasare, 2017). Conversely, conditions such as cancer can co-opt the innate immune system to suppress inflammation, thereby thwarting adaptive immunity necessary to combat tumor growth (Engblom et al., 2016). Therapeutic modulation of the immune system is therefore essential and may be used to home in the body's response to various diseases, including mitigation of tissue-damaging inflammation or

provocation of an immune response against cancer or infection. To achieve these goals, macrocyclic supramolecules are foundational building blocks that enable drug formulation, cell- and tissue-targeted drug carriers, and local delivery depots to instruct immune cell and systems behavior (**Figure 1**).

## MACROCYCLES FOR DRUG SOLUBILIZATION AND DELIVERY

The development of stable drug formulations and the targeted delivery of therapeutics remain major challenges in pharmacology (Rosenblum et al., 2018; Pasut, 2019; Sanku et al., 2019), and many drugs and drug classes are directly relevant to immune modulation. These include biopharmaceuticals (antibodies, cytokines, chemokines, or peptides) that exhibit biological specificity with well-characterized functions. Many biopharmaceuticals, however, face challenges in formulation stability or rapid blood clearance (Shire et al., 2004; Veronese and Pasut, 2005), and exhibit limited interaction with host macrocycles due to large size and aqueous solubility. Alternatively, small molecule pharmaceuticals are more amenable to guest-host interaction and benefit directly from improved solubility, shielding from degradation, and altered bioavailability. These same supramolecular interactions may also be used to reduce the toxicity of poisonous compounds, either through sequestration or improved clearance (Yin et al., 2021). Macrocycles aid in these processes by acting as hosts to small molecules, imparting aqueous solubility and altered pharmacokinetics by properties inherent to the host molecule structure, through selective chemical functionalization, or by accessing higher-order material structures.

Guest-host interactions are a subset of supramolecular associations characterized by the transient complexation of a macrocyclic cavitand (host) with a small molecule (guest) through hydrophobic interaction, often aided by van der Waal's or electrostatic forces. These macrocycles include cyclodextrins (α-, β-, and γ-CD), cucurbit[n]urils (CB[n]), calix[n]arenes, and pillar[n]arenes (Szejtli, 1998; Lagona et al., 2005; Song and Yang, 2014); all of which potentially enhance drug solubility

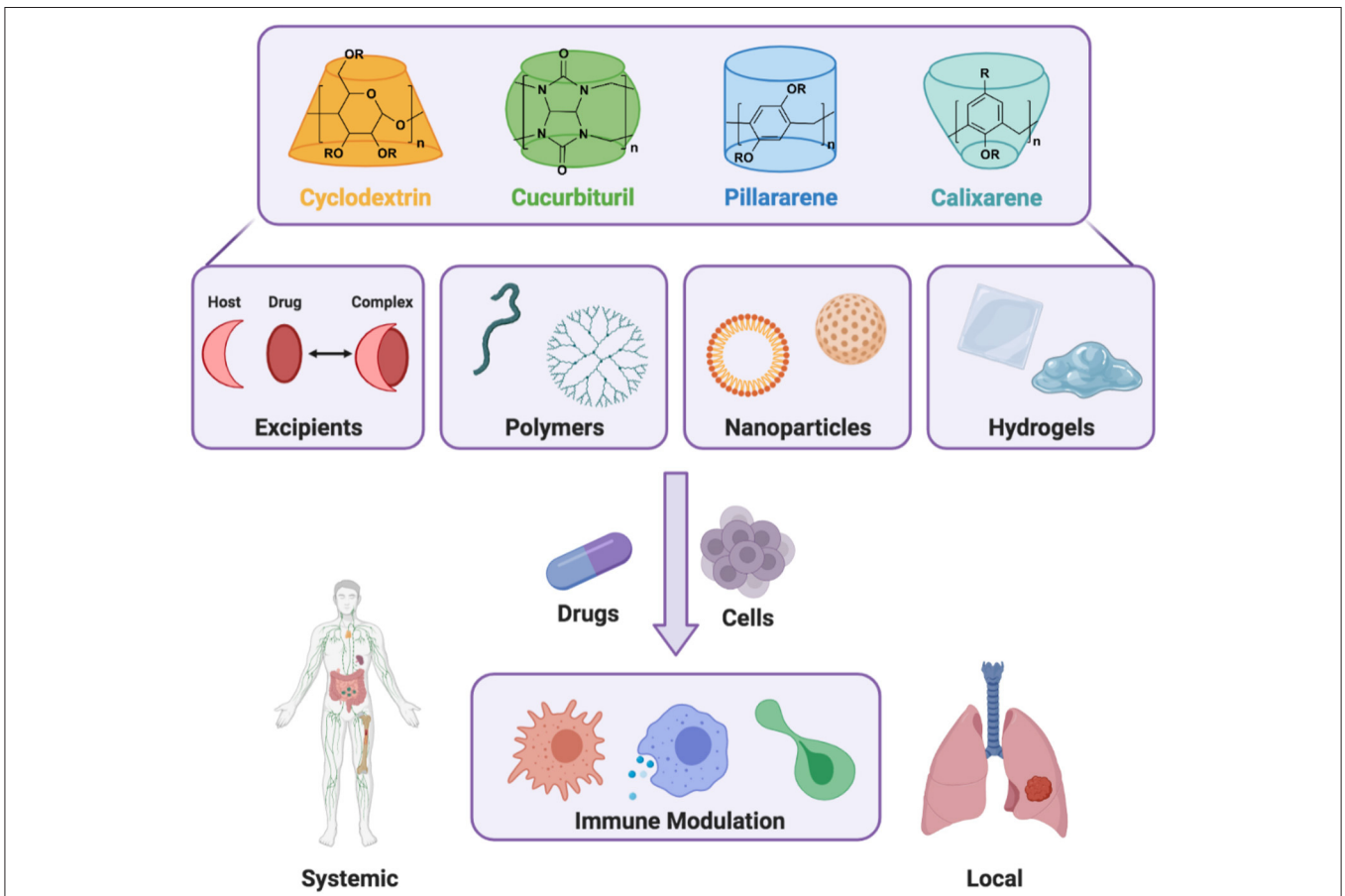


**FIGURE 1 |** Host macrocycles include the families of cyclodextrins, cucurbiturils, pillararenes, and calixarenes. These molecules contribute to the development of dynamic supramolecular materials, including as formulation excipients and functional building blocks for polymers, nanoparticles, and hydrogels. Through the inclusion of therapeutic cargo (drugs, cells), a range of immunomodulatory outcomes are possible that may span activity throughout the body (systemic effects) or activity at a specific location (local effects), achieved through either targeted systemic delivery or local biomaterial implantation.

and bioavailability (Brewster and Loftsson, 2007; Carrier et al., 2007; Loftsson and Brewster, 2011; Walker et al., 2011; Zhou et al., 2015). In many cases, chemical modifications are beneficial toward these goals. For example, sulfobutylether-β-cyclodextrin (SBE-β-CD, Captisol®) is a sulfonic acid derivative of β-CD, currently in 13 FDA approved formulations including antibiotics, antifungals, and antivirals (remdesivir; emergency use approval for COVID-19) (Stella and Rajewski, 2020). Studies by Rajewski demonstrated the derivative's ability to improve drug solubility, formulation stability, and toxicity (Rajewski et al., 1995). Another common CD derivative, 2-hydroxypropyl-β-cyclodextrin (HP-β-CD), possesses excellent water solubility and an improved affinity toward guests such as anti-inflammatory flavonoids, polyphenols, and other compounds (Gould and Scott, 2005; D'Aria et al., 2017; dos Santos Lima et al., 2019). In comparison to CDs, CBs can confer higher affinity interactions that contribute to their utility as potential pharmaceutical excipients, but use may currently be limited by cost and sparing water solubility (Walker et al., 2011; Kuok et al., 2017). Calix[n]arenes and pillar[n]arenes are emergent, synthetically flexible platforms from which a toolbox of drug delivery vehicles is emerging (Zhou et al., 2015; Xiao et al., 2019a,c; Xue et al., 2020).

Macrocyclic delivery vehicles can improve drug pharmacokinetics, including through improved drug solubility (Brewster and Loftsson, 2007; Loftsson and Brewster, 2011) or via receptor-mediated targeted delivery. At the most rudimentary level, macrocycles themselves can serve as targeting agents. CD or its mannose conjugated derivatives are internalized by macrophages and dendritic cells via recognition by cell surface receptors, scavenger receptor A1 (SR-A1) and mannose receptor (MRC1) (Chao et al., 2012; Pustylnikov et al., 2014). For example, mannose-modified β-CD served as a vehicle for the delivery of molecular chaperones to the cytoplasm of macrophages to correct protein misfolding (Rodríguez-Lavado et al., 2014). Similarly, CD-based nanoparticles (NPs) exhibit macrophage uptake, used to achieve trafficking of NPs into glioma (Alizadeh et al., 2010) and the delivery of encapsulated immune agonists to tumor-associated macrophages (TAMs) for cancer immunotherapy (Rodell et al., 2018). Mannose and folate are well-recognized targeting agents for anti-inflammatory (M2-like) and pro-inflammatory (M1-like) macrophages (Ngambenjawong et al., 2017; Rodell et al., 2019a), respectively, and the modification of macrocycles by these moieties enables both macrophage- and tumor-targeted therapies (Okamatsu et al., 2013; Ye et al., 2016; Elamin et al., 2018; Li et al., 2019).

Interestingly, some macrocycles have been investigated for their ability to directly modulate immune response. HP-β-CD may serve as a functional vaccine adjuvant, reportedly altering human dendritic cell maturation, as indicated by an upregulation of inflammatory cytokines (IL-6, TNF-α), production of costimulatory molecules (MHC, PD-L1/2), and activation of co-cultured T lymphocytes (Kim et al., 2016). CB[7] exhibited similar immunostimulatory properties. When complexed with tuftsin, an immunostimulatory tetrapeptide, the complex induced inflammatory cytokine production (TNF-α, IL-2, and IFN-γ) exceeding that of tuftsin alone in mononuclear cells (Kovalenko et al., 2017). While both of these macrocycles exert adjuvant effects, the exact mechanisms of action remain ambiguous. In contrast to these immunostimulatory effects, Zimmer et al. rationalized that the ability of HP-β-CD to bind cholesterol would reduce cholesterol crystal formations known to stimulate macrophage activation. In atherosclerotic plaques, HP-β-CD increased cholesterol efflux, reducing crystal load, inflammation, and disease progression (Zimmer et al., 2016). Similar effects have been observed in monocytes derived from HIV-positive donors (Matassoli et al., 2018), and the compound has been explored clinically for treatment of Niemann-Pick disease type C1, a neurodegenerative disease characterized by excessive cholesterol and lipid accumulation (Liu, 2012; Ottinger et al., 2014).

## POLYMER-BOUND MACROCYCLES

Conventionally, polymer-drug conjugates are formed through the covalent tethering of drugs to a polymer. Owing to their relatively large size, polymers dominate the resultant physiochemical properties, and can therefore improve drug solubility, reduce drug clearance rate, and offer sites for attachment of targeting moieties. A distinguishing property of these systems is the structural diversity, which includes end-modified linear polymers, dendrimeric architectures, or pendant modified polymer systems (Elvira et al., 2005; Larson and Ghandehari, 2012). While supramolecular polymer-drug conjugates parallel this structural diversity, they possess advantageous qualities in terms of biocompatibility, ease of modular assembly, and capacity for dynamic behavior (Das et al., 2019).

Conjugation to PEG (i.e., PEGylation) is common in biopharmaceutical modification (Roberts et al., 2002; Alconcel et al., 2011), used to overcome aggregation and denaturation during storage or rapid blood clearance *in vivo* (JevsìŒEvar et al., 2010; Aggarwal, 2014). The interaction between end-modified CB[7]-PEG and the aromatic amino acid residues of proteins enabled PEGylation without chemical modification, including for anti-CD20 antibodies similar to clinical Rituximab (Webber et al., 2016). For small-molecule delivery applications, end-modification of dendrimeric structures has also been explored, including poly(amidoamine) dendrimers modified by α-, β-, or γ-CD that exhibited selective interaction of CD units with small molecule drugs (Wang et al., 2012). Interchain modifications of PEG may also be useful, as for self-assembly of polymeric NPs. CRLX101 (i.e., IT-101) was formed through covalent conjugation of camptothecin to a linear β-CD-PEG copolymer (Davis, 2009). Due to interaction of camptothecin and β-CD, the polymer chains condensed into NPs that modulated the immune response in tumor-bearing mice, including activation of natural killer cells and T cell proliferation (Chen Y. F. et al., 2019).

The modification of linear polymers by pendant groups has been accomplished through several means. Polyrotaxanes are one such dynamic macromolecular structure, composed of macrocycles threaded along a polymer chain. When modified by targeting ligands, such as maltose or mannose, macrocycles slide along the polymer chain to form multivalent interactions

with target receptors, improving molecular recognition and macrophage uptake (Ooya et al., 2003; Shibaguchi et al., 2019). These methods emphasize how the design of dynamic supramolecular structures can improve targeted delivery. In an excellent example of modular conjugation, Jung et al. covalently modified hyaluronic acid with pendent CB[6] groups (Jung et al., 2011). The resulting CB[6]-HA was decorated with FITC for bioimaging and/or a formyl peptide receptor like 1 (FPRL1) peptide ligand with application in leukocyte recruitment, both using spermidine (CB[6] guest) as a supramolecular tether. The multi-functional approach provides a means of modular on-demand assembly that can achieve targeting, bioimaging, and drug delivery in a single supramolecular vehicle; such supramolecular theranostics have been recently reviewed (Yu and Chen, 2019).

## NANOPARTICULATE SYSTEMS

Particulate platforms are among the most explored systemic drug delivery systems, exhibiting similar effects as polymeric drug conjugates: enhanced drug solubility, prolonged blood clearance, and targeted delivery (Mudshinge et al., 2011). Numerous methods have been developed to leverage guest-host interactions in nanotherapeutic design, including the self-assembly of subunits, surface modifications of pre-formed particles, and nanogels for affinity-based delivery.

An excellent application of supramolecular assembly is in gene delivery systems, wherein cationic polymers complex with nucleic acids through electrostatic interactions to form polyplexes, protecting the cargo from enzymatic degradation and facilitating cytoplasmic delivery (Lächelt and Wagner, 2015). While branched polyethyleneimine (PEI) is regarded as the "gold standard" polymeric vehicle, it is limited by cytotoxicity (Godbey et al., 1999; Lungwitz et al., 2005). CD-PEI conjugated systems have therefore been established that decrease the molecular weight of PEI necessary for effective transfection, hence improving cell viability (Wong et al., 2018). Similar methods have been applied to other cationic polymers with comparable limitations, like poly(2-dimethylaminoethyl methacrylate) (PDMAEMA) and dioleoyl-3-trimethylammonium propane (DOTAP) (Cherng et al., 1996; Loh and Wu, 2015; Fan et al., 2018; Zhou et al., 2018). Arima et al. prepared a sugar-appended CD-dendrimer conjugate as a macrophage-targeted carrier for systemic delivery of gene therapies (Arima et al., 2013), while local delivery has been enabled by CD-PEI conjugates for siRNA delivery from injectable hydrogels (Wang et al., 2017). In addition, Chang and colleagues investigated the co-delivery of an anticancer drug and small interfering RNA (siRNA) in a self-assembled redox-responsive pillar[5]arene nanocarrier, designed to overcome chemotherapeutic drug resistance (Chang et al., 2014). In sum, macrocycles are effective in enhancing gene delivery, due to their ability to reduce the cytotoxicity of cationic polymeric vectors, increase membrane permeability, and contribute to targeted or responsive delivery systems. Further developments in these areas have been recently reviewed (Xiao et al., 2019a; Haley et al., 2020).

Particulate materials are likewise of utility in vaccine delivery, aided by modular supramolecular assembly. In anti-tumor applications, the self-assembly of a MUC1 vaccine nanoparticle was achieved through CB[8] linkage of an amphiphilic TLR2 agonist ($Pam_3CSK_4$) with the desired antigen. Resulting nanostructures triggered a more robust immune response in mice than soluble controls (Gao et al., 2014). Interestingly, macrocycles may also serve to open new avenues for orally administered vaccines. He et al. encapsulated an ovalbumin β-CD complex in chitosan NPs. Oral administration to mice increased antibody levels in the digestive tract mucosa and serum, demonstrating the nanostructure's ability to induce an adaptive immune response (He et al., 2019). Anti-inflammatory regulation of the digestive tract has also been achieved, including by the intravenous administration of rosiglitazone-loaded redox-responsive nanoparticles that modulated macrophage response in ulcerative colitis (Sun et al., 2020).

Hydrogel NPs, or nanogels, are composed of cross-linked polymeric networks that provide a large surface area for multivalent supramolecular conjugation, making them excellent materials for drug loading, targeting, and release (Oh et al., 2008; Suhail et al., 2019). Park and colleagues formulated liposomal polymeric gels, composed of β-CD (for conjugation of a TGF-inhibitor) and a polymeric network (for IL-2 encapsulation) that significantly delayed tumor growth by synergistically activating the innate and adaptive immune response, increasing survival of tumor-bearing mice (Park J. et al., 2012). More recently, cyclodextrin nanoparticles were prepared by crosslinking succinylated β-CD with *L*-lysine. Resulting NPs exhibited uptake by myeloid cells (macrophages, dendritic cells) for the targeted delivery of immunostimulatory drugs, including TLR7/8 agonists (Kim et al., 2018; Rodell et al., 2018, 2019b), non-canonical NF-κB activators (Koch et al., 2020), and other drugs (Ahmed et al., 2019). These applications have demonstrated improved targeting of drugs to macrophage-rich tissues and a concurrent reduction in off-target drug effects, particularly for drugs with high-affinity interactions.

## BULK MATERIALS FOR LOCALIZED ACTION

Complementary to systemic drug delivery by soluble polymeric and nanomaterial systems, macroscale biomaterials provide an opportunity for highly localized therapeutic delivery. Local therapy poses potential advantages (Weiser and Saltzman, 2014), including a reduction in off-target side effects such as adverse immune suppression or activation, which place patients at risk for infection or hyperinflammatory conditions (cytokine release syndrome), respectively. Related applications encompass device coatings, implantable delivery depots, and injectable hydrogels that leverage supramolecular guest-host interactions either for therapeutic drug sequestration or hydrogel crosslinking.

Medical device implantation is commonplace in modern medicine, such as for diagnostic or reconstructive procedures.

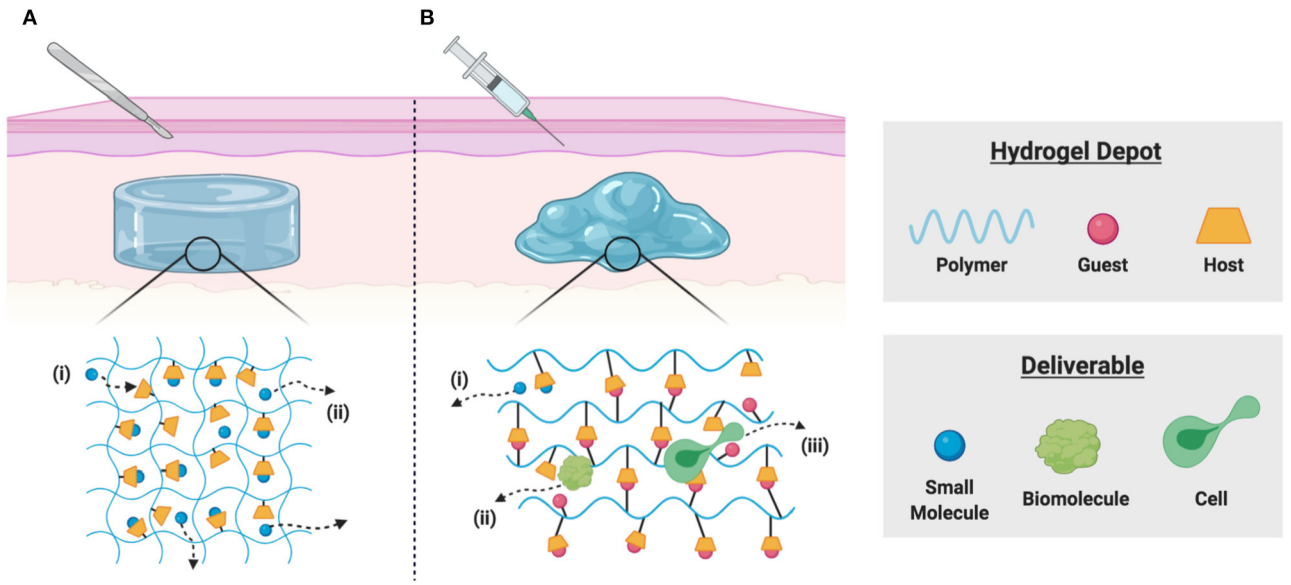


**FIGURE 2 |** Schematic representation of local delivery from implantable and injectable hydrogels. **(A)** Polymer-bound macrocycles form inclusion complexes with desired deliverables in implantable hydrogels, allowing for (i) sequestration of drugs through guest-host complexation and (ii) affinity-based release by diffusion of unbound drug molecules. **(B)** Polymer-bound host macrocycles can form reversible physical bonds with hydrophobic guest molecules, allowing for the formulation of dynamic supramolecular crosslinks. These shear-thinning and injectable materials enable (i) drug sequestration through guest-host affinity, (ii) diffusive release of soluble biomolecules, and (iii) dynamic bond rearrangement necessary for cell migration into or out of the scaffold.

Yet, these devices are hampered by biofilm formation: the colonization of the implant surface by bacteria or fungi (Arciola et al., 2018). To impede biofilm formation, antifouling and/or drug-eluting surfaces are of great interest. Covalent tethering of CD to implant surfaces (El Ghoul et al., 2008; Nava-Ortiz et al., 2010), as well as polymerized CD coatings have been investigated (Learn et al., 2020). These methods generally reduced protein adsorption and cell adhesion. Moreover, they provided affinity-based release of antibiotic and antifungal drugs, thereby inhibiting biofilm formation (El Ghoul et al., 2008; Nava-Ortiz et al., 2010; Thatiparti and Von Recum, 2010; Learn et al., 2020). In sum, surface modification by macrocycles is a promising method for the provision of antifouling surfaces that allows for biofilm inhibition by local prophylactic drug delivery.

To achieve local delivery within tissues, the formation of hydrogel depots is widely used for various applications. These water-swollen polymer networks enable controlled release via diffusive, degradation-mediated, or externally triggered mechanisms (Li and Mooney, 2016). Small molecule drugs, however, exhibit rapid diffusive release due to the relatively large mesh size (Bertz et al., 2013), motivating the development of hydrogels which include macrocyclic supramolecules for affinity-based delivery (**Figure 2A**). Partially crosslinked CDs and CD-modified gellan gum have been used to develop injectable polymers useful as viscosupplements with concurrent intraarticular release of anti-inflammatory glucocorticoids with applications in osteoarthritis treatment (Rivera-Delgado et al., 2018; Choi et al., 2020). Researchers have used these hydrogel formulations to deliver cyclosporin A (CsA), an immunosuppressant used to prevent organ transplant rejection and whose systemic administration is limited by off-target effects (Liddicoat and Lavelle, 2019; Park et al., 2020). Hydrogels prepared from poly(HEMA-co-HP-β-CD) provided controlled release of CsA over 2 months *in vitro,* with potential applications in subjunctival delivery following corneal graft procedures (Başbag et al., 2014). For the promotion of burn wound healing, dual delivery strategies have been described, including *in situ* polymerizable hydrogels for affinity-based release of resveratrol (an anti-inflammatory) and a plasmid encoding vascular endothelial growth factor (to promote vascularization) (Wang et al., 2019). Co-delivery of resveratrol and histatin-1 has been similarly demonstrated, using co-polymerization of acrylated β-CD and methacrylated gelatin for controlled release (Zheng et al., 2020).

Injectable hydrogel formulations are a convenient means of delivery, requiring less invasive procedures for implantation than solid hydrogels formed *ex vivo* (Yu and Ding, 2008). Injectable hydrogels may be delivered in a liquid state, later solidifying as a result of thermo-responsive condensation or external triggers (Nguyen and Lee, 2010). In contrast, supramolecular assembly enables the formation of shear-thinning, injectable hydrogels (Guvendiren et al., 2012; Rodell et al., 2015a). The hydrogels can be pre-formed in a syringe with encapsulated therapeutics, injected into the tissue, and re-form as a depot for subsequent therapeutic release. One avenue for hydrogel formation is through pseudo-polyrotaxane formation between α-CD and PEG (Li et al., 1994). These hydrogels have found recent use in cancer immunotherapies, where the constraint

of immune activation to the tumor environment is desirable to prevent systemic toxicity. Wang and colleagues used a hydrogel composed of α-CD and 4-arm PEG for local delivery of an adenoviral vector encoding Flagrp170, a flagellin-derived NF-κB stimulating sequence shown to enhance tumor immunogenicity (Wang et al., 2020). In a murine melanoma model, the hydrogel improved vector retention at the tumor site, facilitating local immune activation and suppression of tumor growth. CDs have also been recently used to create a hydrogel-particle composite for synergistic photothermal immunotherapy. In this work, IR820-α-CD was used in hydrogel formation, and localized heating by IR light induced tumor cell death; embedded CpG nanoparticles supported the immunotherapeutic effect of tumor-derived antigens (Dong et al., 2019).

The modification of polymers by pendant guest and host groups is an alternative means of constructing supramolecular hydrogels (Rodell et al., 2015a; Xiao et al., 2019b). Hydrogels crosslinked by β-CD and adamantane interaction have been widely investigated as injectable therapeutics (Loebel et al., 2017), including for the delivery of small-molecule drugs (Mealy et al., 2015; Zheng et al., 2020), biomolecules (Rodell et al., 2013, 2015b; Soranno et al., 2016), extracellular vesicles (Chen et al., 2018; Chung et al., 2020), and cells (Gaffey et al., 2015, 2019; Sisso et al., 2020) (**Figure 2B**). The delivery of IL-10 has been demonstrated, both from these guest-host hydrogels in the injured kidney (Rodell et al., 2015b; Soranno et al., 2016), and from related supramolecular hydrogel/microgel composites in the infarcted heart (Chen M. H. et al., 2019) as a means of promoting tissue healing. Similar guest-host hydrogels may be formed through the association of CB[n] hosts with polymer-bound guests (Appel et al., 2010), which has been used to improve local cell retention and in the development of numerous responsive drug delivery systems (Park K. et al., 2012; Ding et al., 2019). In an interesting application, guest-host hydrogels were prepared from the interaction of gelatin with photocrosslinkable acrylated β-CD as a 3D co-culture platform for TAM repolarization. IFN-γ reverted macrophages to a pro-inflammatory phenotype *in vitro* and decreased tumor cell migration and proliferation. Hydrogels were readily disassembled by competitive binding of free adamantane, allowing co-cultured cells to be transplanted into tumor growth models *in vivo*, where TAM repolarization inhibited tumor growth (Huang et al., 2020). Such platforms are a valuable drug discovery tool, and such accessible platforms for 3D cell culture are highly desirable (Caliari and Burdick, 2016; Rodell et al., 2019a). These self-assembling systems may furthermore be useful for immune modulation *in vivo*. For example, Widener et al. recently reported the preparation of granular hydrogel assemblies, wherein microgels were separately modified by β-CD or adamantane groups to yield self-assembling and injectable granular assemblies (Widener et al., 2020). The highly interconnected pores between the microgels allowed rapid immune cell migration and may provide an excellent platform for cellular reprogramming. Indeed, related polymer-nanoparticle composites enable recruitment and differentiation of discrete cell subsets (Fenton et al., 2019), and microgel architecture itself can promote distinct changes in the secretory profile of cells upon their arrival (Caldwell et al., 2020).

## CONCLUSION

Supramolecular chemistry has emerged as a new frontier for biomedicine, providing a synthetically tractable route to the design of dynamic supramolecular, macromolecular, and multiscale material systems. By appropriate use of the custom design of macrocyclic building blocks, influence over material properties and biological outcomes is made possible. In immune engineering, these tools uniquely enable access to the same thermodynamic principles that underly biological structures, which has rapidly led to the development of methods to overcome previously insurmountable pharmacological obstacles, including drug solubility and instability or roadblocks to physiological transport. Moreover, the expanding toolbox of macrocyclic biomaterials now accessing multifunctional materials, such as immunotheranostics that perpetuate the combined study of vehicle and drug pharmacokinetics alongside pharmacodynamic outcomes. Such platforms will allow the unification of cell and tissue level response with vehicle and drug biodistributions, which previously have been difficult to access (Rodell et al., 2020). Moreover, the modularity of macrocyclic interactions perpetuates the development of delivery systems with tunable drug compositions. Importantly, cargo sequestration typically requires no chemical modification and therefore forgoes the formation of new chemical entities. In contrast, the addition of well-understood guest anchors to existing drugs also allows for tunable drug affinities for applications in controlled release, responsive delivery, and *in situ* refillable drug reservoirs (Rodell et al., 2019b; Zou et al., 2019; Dogan and von Recum, 2020; Dogan et al., 2020). Looking forward, these tools may be leveraged to directly address shortcomings in therapeutic efficacy, off-target drug effects, and dosing frequency that hamper the success of immunotherapeutic drugs in practice.

## AUTHOR CONTRIBUTIONS

SS and AA conducted the initial primary literature review, and all authors contributed to the writing and editing of the final manuscript.

## FUNDING

This work was supported by Startup Funds provided by the School of Biomedical Engineering, Science and Health Systems at Drexel University.

## ACKNOWLEDGMENTS

Figures were prepared using BioRender.

## REFERENCES


Aggarwal, R. S. (2014). What's fueling the biotech engine-2012 to 2013. *Nat. Biotechnol.* 32, 32–39. doi: 10.1038/nbt.2794

Ahmed, M. S., Rodell, C. B., Hulsmans, M., Kohler, R. H., Aguirre, A. D., Nahrendorf, M., et al. (2019). A supramolecular nanocarrier for delivery of amiodarone anti-arrhythmic therapy to the heart. *Bioconjug. Chem.* 30, 733–740. doi: 10.1021/acs.bioconjchem.8b00882

Alconcel, S. N. S., Baas, A. S., and Maynard, H. D. (2011). FDA-approved poly(ethylene glycol)–protein conjugate drugs. *Polym. Chem.* 2:1442. doi: 10.1039/c1py00034a

Alizadeh, D., Zhang, L., Schluep, T., and Badie, B. (2010). Tumor-associated macrophages are predominant carriers of cyclodextrin-based nanoparticles into gliomas. *Nanomed. Nanotechnol. Biol. Med.* 6, 382–390. doi: 10.1016/j.nano.2009.10.001

Appel, E. A., Biedermann, F., Rauwald, U., Jones, S. T., Zayed, J. M., and Scherman, O. A. (2010). Supramolecular cross-linked networks via host– guest complexation with cucurbit [8] uril. *J. Am. Chem. Soc.* 132, 14251–14260. doi: 10.1021/ja106362w

Arciola, C. R., Campoccia, D., and Montanaro, L. (2018). Implant infections: adhesion, biofilm formation and immune evasion. *Nat. Rev. Microbiol.* 16, 397–409. doi: 10.1038/s41579-018-0019-y

Arima, H., Motoyama, K., and Higashi, T. (2013). Sugar-appended polyamidoamine dendrimer conjugates with cyclodextrins as cell-specific non-viral vectors. *Adv. Drug Deliv. Rev.* 65, 1204–1214. doi: 10.1016/j.addr.2013.04.001

Başbag, A. B., Gümüşderelioglu, M., Simşek, M., and Güner, A. (2014). Poly(HEMA)/cyclodextrin-based hydrogels for subconjunctival delivery of cyclosporin A. *J. Appl. Polymer Sci.* 131, 1–9. doi: 10.1002/app.40397

Bertz, A., Wöhl-Bruhn, S., Miethe, S., Tiersch, B., Koetz, J., Hust, M., et al. (2013). Encapsulation of proteins in hydrogel carrier systems for controlled drug delivery: influence of network structure and drug size on release rate. *J. Biotechnol.* 163, 243–249. doi: 10.1016/j.jbiotec.2012.06.036

Brewster, M. E., and Loftsson, T. (2007). Cyclodextrins as pharmaceutical solubilizers. *Adv. Drug Deliv. Rev.* 59, 645–666. doi: 10.1016/j.addr.2007.05.012

Caldwell, A. S., Rao, V. V., Golden, A. C., and Anseth, K. S. (2020). Porous bio-click microgel scaffolds control hMSC interactions and promote their secretory properties. *Biomaterials* 232:119725. doi: 10.1016/j.biomaterials.2019.119725

Caliari, S. R., and Burdick, J. A. (2016). A practical guide to hydrogels for cell culture. *Nat. Methods* 13, 405–414. doi: 10.1038/nmeth.3839

Carrier, R. L., Miller, L. A., and Ahmed, I. (2007). The utility of cyclodextrins for enhancing oral bioavailability. *J. Control. Release* 123, 78–99. doi: 10.1016/j.jconrel.2007.07.018

Chang, Y., Yang, K., Wei, P., Huang, S., Pei, Y., Zhao, W., et al. (2014). Cationic vesicles based on amphiphilic pillar[5]arene capped with ferrocenium: a redox-responsive system for drug/siRNA co-delivery. *Angew. Chem. Int. Ed.* 53, 13126–13130. doi: 10.1002/anie.201407272

Chao, Y., Karmali, P. P., and Simberg, D. (2012). Role of carbohydrate receptors in the macrophage uptake of dextran-coated iron oxide nanoparticles. *Adv. Exp. Med. Biol.* 733, 115–123. doi: 10.1007/978-94-007-2555-3_11

Chen, C. W., Wang, L. L., Zaman, S., Gordon, J., Arisi, M. F., Venkataraman, C. M., et al. (2018). Sustained release of endothelial progenitor cell-derived extracellular vesicles from shear-thinning hydrogels improves angiogenesis and promotes function after myocardial infarction. *Cardiovasc. Res.* 114, 1029–1040. doi: 10.1093/cvr/cvy067

Chen, M. H., Chung, J. J., Mealy, J. E., Zaman, S., Li, E. C., Arisi, M. F., et al. (2019). Injectable supramolecular hydrogel/microgel composites for therapeutic delivery. *Macromol. Biosci.* 19:1800248. doi: 10.1002/mabi.201800248

Chen, Y.-F., Wang, Y.-H., Lei, C.-S., Changou, C. A., Davis, M. E., and Yen, Y. (2019). Host immune response to anti-cancer camptothecin conjugated cyclodextrin-based polymers. *J. Biomed. Sci.* 26:85. doi: 10.1186/s12929-019-0583-0

Cherng, J. Y., van de Wetering, P., Talsma, H., Crommelin, D. J., and Hennink, W. E. (1996). Effect of size and serum proteins on transfection efficiency of poly ((2-dimethylamino)ethyl methacrylate)-plasmid nanoparticles. *Pharm. Res.* 13, 1038–1042. doi: 10.1023/A:1016054623543

Choi, J. H., Park, A., Lee, W., Youn, J., Rim, M. A., Kim, W., et al. (2020). Preparation and characterization of an injectable dexamethasone-cyclodextrin complexes-loaded gellan gum hydrogel for cartilage tissue engineering. *J. Control. Release* 327, 747–765. doi: 10.1016/j.jconrel.2020.08.049

Chung, J. J., Han, J., Wang, L. L., Arisi, M. F., Zaman, S., Gordon, J., et al. (2020). Delayed delivery of endothelial progenitor cell-derived extracellular vesicles via shear thinning gel improves postinfarct hemodynamics. *J. Thorac. Cardiovasc. Surg.* 159, 1825–1835.e2. doi: 10.1016/j.jtcvs.2019.06.017

D'Aria, F., Serri, C., Niccoli, M., Mayol, L., Quagliariello, V., Iaffaioli, R. V., et al. (2017). Host–guest inclusion complex of quercetin and hydroxypropyl-β-cyclodextrin. *J. Therm. Anal. Calorim.* 130, 451–456. doi: 10.1007/s10973-017-6135-5

Das, D., Assaf, K. I., and Nau, W. M. (2019). Applications of cucurbiturils in medicinal chemistry and chemical biology. *Front. Chem.* 7:619. doi: 10.3389/fchem.2019.00619

Davis, M. E. (2009). Design and development of IT-101, a cyclodextrin-containing polymer conjugate of camptothecin. *Adv. Drug Deliv. Rev.* 61, 1189–1192. doi: 10.1016/j.addr.2009.05.005

Ding, Y.-F., Sun, T., Li, S., Huang, Q., Yue, L., Zhu, L., et al. (2019). Oral colon-targeted konjac glucomannan hydrogel constructed through noncovalent cross-linking by cucurbit [8] uril for ulcerative colitis therapy. *ACS Appl. Bio Mater.* 3, 10–19. doi: 10.1021/acsabm.9b00676

Dogan, A., and von Recum, H. (2020). Engineering selective molecular tethers to enhance suboptimal drug properties. *Acta Biomater.* 115, 383–392. doi: 10.1016/j.actbio.2020.07.045

Dogan, A. B., Dabkowski, K., and von Recum, H. (2020). Leveraging affinity interactions to prolong drug delivery of protein therapeutics. *bioRxiv [preprint]*. doi: 10.1101/2020.12.03.410621

Dong, X., Liang, J., Yang, A., Qian, Z., Kong, D., and Lv, F. (2019). Fluorescence imaging guided CpG nanoparticles-loaded IR820-hydrogel for synergistic photothermal immunotherapy. *Biomaterials* 209, 111–125. doi: 10.1016/j.biomaterials.2019.04.024

dos Santos Lima, B., de Alcântara Campos, C., da Silva Santos, A. C. R., Santos, V. C. N., Trindade Gd, G. G., Shanmugam, S., et al. (2019). Development of morin/hydroxypropyl-β-cyclodextrin inclusion complex: enhancement of bioavailability, antihyperalgesic and anti-inflammatory effects. *Food Chem. Toxicol.* 126, 15–24. doi: 10.1016/j.fct.2019.01.038

El Ghoul, Y., Blanchemain, N., Laurent, T., Campagne, C., El Achari, A., Roudesli, S., et al. (2008). Chemical, biological and microbiological evaluation of cyclodextrin finished polyamide inguinal meshes. *Acta Biomater.* 4, 1392–1400. doi: 10.1016/j.actbio.2008.02.019

Elamin, K. M., Motoyama, K., Higashi, T., Yamashita, Y., Tokuda, A., and Arima, H. (2018). Dual targeting system by supramolecular complex of folate-conjugated methyl-β-cyclodextrin with adamantane-grafted hyaluronic acid for the treatment of colorectal cancer. *Int. J. Biol. Macromol.* 113, 386–394. doi: 10.1016/j.ijbiomac.2018.02.149

Elvira, C., Gallardo, A., Roman, J., and Cifuentes, A. (2005). Covalent polymer-drug conjugates. *Molecules* 10, 114–125. doi: 10.3390/10010114

Engblom, C., Pfirschke, C., and Pittet, M. J. (2016). The role of myeloid cells in cancer therapies. *Nat. Rev. Cancer* 16:447. doi: 10.1038/nrc.2016.54

Epelman, S., Liu, P. P., and Mann, D. L. (2015). Role of innate and adaptive immune mechanisms in cardiac injury and repair. *Nat. Rev. Immunol.* 15, 117–129. doi: 10.1038/nri3800

Fan, X., Cheng, H., Wu, Y., Loh, X. J., Wu, Y.-L., and Li, Z. (2018). Incorporation of polycaprolactone to cyclodextrin-based nanocarrier for potent gene delivery. *Macromol. Mater. Eng.* 303:1800255. doi: 10.1002/mame.201800255

Farokhzad, O. C., and Langer, R. (2009). Impact of nanotechnology on drug delivery. *ACS Nano* 3, 16–20. doi: 10.1021/nn900002m

Fenton, O. S., Tibbitt, M. W., Appel, E. A., Jhunjhunwala, S., Webber, M. J., and Langer, R. (2019). Injectable polymer–nanoparticle hydrogels for local immune cell recruitment. *Biomacromolecules* 20, 4430–4436. doi: 10.1021/acs.biomac.9b01129

Gaffey, A. C., Chen, M. H., Trubelja, A., Venkataraman, C. M., Chen, C. W., Chung, J. J., et al. (2019). Delivery of progenitor cells with injectable shear-thinning hydrogel maintains geometry and normalizes strain to stabilize cardiac function after ischemia. *J. Thorac. Cardiovasc. Surg.* 157, 1479–1490. doi: 10.1016/j.jtcvs.2018.07.117

Gaffey, A. C., Chen, M. H., Venkataraman, C. M., Trubelja, A., Rodell, C. B., Dinh, P. V., et al. (2015). Injectable shear-thinning hydrogels used to deliver endothelial progenitor cells, enhance cell engraftment, and

improve ischemic myocardium. *J. Thorac. Cardiovasc. Surg.* 150, 1268–1277. doi: 10.1016/j.jtcvs.2015.07.035

Gao, Y., Sun, Z. Y., Huang, Z. H., Chen, P. G., Chen, Y. X., Zhao, Y. F., et al. (2014). Covalent bond or noncovalent bond: a supramolecular strategy for the construction of chemically synthesized vaccines. *Chem. Eur. J.* 20, 13541–13546. doi: 10.1002/chem.201404013

Godbey, W. T., Wu, K. K., and Mikos, A. G. (1999). Tracking the intracellular path of poly(ethylenimine)/DNA complexes for gene delivery. *Proc. Natl. Acad. Sci. U.S.A.* 96, 5177–5181. doi: 10.1073/pnas.96.9.5177

Gould, S., and Scott, R. C. (2005). 2-Hydroxypropyl-β-cyclodextrin (HP-β-CD): a toxicology review. *Food Chem. Toxicol.* 43, 1451–1459. doi: 10.1016/j.fct.2005.03.007

Guvendiren, M., Lu, H. D., and Burdick, J. A. (2012). Shear-thinning hydrogels for biomedical applications. *Soft Matter*. 8, 260–272. doi: 10.1039/C1SM06513K

Haley, R. M., Gottardi, R., Langer, R., and Mitchell, M. J. (2020). Cyclodextrins in drug delivery: applications in gene and combination therapy. *Drug Deliv. Transl. Res.* 10, 661–677. doi: 10.1007/s13346-020-00724-5

He, M., Zhong, C., Hu, H., Jin, Y., Chen, Y., Lou, K., et al. (2019). Cyclodextrin/chitosan nanoparticles for oral ovalbumin delivery: preparation, characterization and intestinal mucosal immunity in mice. *Asian J. Pharm. Sci.* 14, 193–203. doi: 10.1016/j.ajps.2018.04.001

Huang, Y., Feng, Q., Jiang, H., Zhou, W., Chen, J., Gao, J., et al. (2020). Mimicking the endometrial cancer tumor microenvironment to reprogram tumor-associated macrophages in disintegrable supramolecular gelatin hydrogel. *Int. J. Nanomed.* 15, 4625–4637. doi: 10.2147/IJN.S252074

Jain, A., and Pasare, C. (2017). Innate control of adaptive immunity: beyond the three-signal paradigm. *J. Immunol.* 198, 3791–3800. doi: 10.4049/jimmunol.1602000

JevsìŒEvar, S., Kunstelj, M. I., and Porekar, V. G. (2010). PEGylation of therapeutic proteins. *Biotechnol. J.* 5, 113–128. doi: 10.1002/biot.200900218

Jung, H., Park, K. M., Yang, J. A., Oh, E. J., Lee, D. W., Park, K., et al. (2011). Theranostic systems assembled *in situ* on demand by host-guest chemistry. *Biomaterials* 32, 7687–7694. doi: 10.1016/j.biomaterials.2011.06.060

Kim, H.-Y., Li, R., Ng, T. S., Courties, G., Rodell, C. B., Prytyskach, M., et al. (2018). Quantitative imaging of tumor-associated macrophages and their response to therapy using 64Cu-labeled macrin. *ACS Nano* 12, 12015–12029. doi: 10.1021/acsnano.8b04338

Kim, S. K., Yun, C.-H., and Han, S. H. (2016). Induction of dendritic cell maturation and activation by a potential adjuvant, 2-hydroxypropyl-β-cyclodextrin. *Front. Immunol.* 7:435. doi: 10.3389/fimmu.2016.00435

Koch, P. D., Rodell, C. B., Kohler, R. H., Pittet, M. J., and Weissleder, R. (2020). Myeloid cell-targeted nanocarriers efficiently inhibit cellular inhibitor of apoptosis for cancer immunotherapy. *Cell Chem. Biol.* 27, 94–104.e5. doi: 10.1016/j.chembiol.2019.12.007

Kovalenko, E. A., Pashkina, E. A., Kanazhevskaya, L. Y., Masliy, A. N., and Kozlov, V. A. (2017). Chemical and biological properties of a supramolecular complex of tuftsin and cucurbit[7]uril. *Int. Immunopharmacol.* 47, 199–205. doi: 10.1016/j.intimp.2017.03.032

Kuok, K. I., Li, S., Wyman, I. W., and Wang, R. (2017). Cucurbit [7] uril: an emerging candidate for pharmaceutical excipients. *Ann. N. Y. Acad. Sci.* 1398, 108–119. doi: 10.1111/nyas.13376

Lächelt, U., and Wagner, E. (2015). Nucleic acid therapeutics using polyplexes: a journey of 50 years (and beyond). *Chem. Rev.* 115, 11043–11078. doi: 10.1021/cr5006793

Lagona, J., Mukhopadhyay, P., Chakrabarti, S., and Isaacs, L. (2005). The cucurbit [n] uril family. *Angew. Chem. Int. Ed.* 44, 4844–4870. doi: 10.1002/anie.200460675

Larson, N., and Ghandehari, H. (2012). Polymeric conjugates for drug delivery. *Chem. Mater.* 24, 840–853. doi: 10.1021/cm2031569

Learn, G. D., Lai, E. J., and von Recum, H. A. (2020). Cyclodextrin polymer coatings resist protein fouling, mammalian cell adhesion, and bacterial attachment. *bioRxiv [preprint]*. doi: 10.1101/2020.01.16.909564

Li, J., Harada, A., and Kamachi, M. (1994). Sol–gel transition during inclusion complex formation between α-cyclodextrin and high molecular weight poly (ethylene glycol) s in aqueous solution. *Polym. J.* 26, 1019–1026. doi: 10.1295/polymj.26.1019

Li, J., and Mooney, D. J. (2016). Designing hydrogels for controlled drug delivery. *Nat. Rev. Mater.* 1:16071. doi: 10.1038/natrevmats.2016.71

Li, W., Xu, C., Li, S., Chen, X., Fan, X., Hu, Z., et al. (2019). Cyclodextrin based unimolecular micelles with targeting and biocleavable abilities as chemotherapeutic carrier to overcome drug resistance. *Mater. Sci. Eng. C.* 105:110047. doi: 10.1016/j.msec.2019.110047

Liddicoat, A. M., and Lavelle, E. C. (2019). Modulation of innate immunity by cyclosporine A. *Biochem. Pharmacol.* 163, 472–480. doi: 10.1016/j.bcp.2019.03.022

Liu, B. (2012). Therapeutic potential of cyclodextrins in the treatment of niemann–pick type C disease. *Clin. Lipidol.* 7, 289–301. doi: 10.2217/clp.12.31

Loebel, C., Rodell, C. B., Chen, M. H., and Burdick, J. A. (2017). Shear-thinning and self-healing hydrogels as injectable therapeutics and for 3D-printing. *Nat. Protoc.* 12:1521. doi: 10.1038/nprot.2017.053

Loftsson, T., and Brewster, M. E. (2011). Pharmaceutical applications of cyclodextrins: effects on drug permeation through biological membranes. *J. Pharm. Pharmacol.* 63, 1119–1135. doi: 10.1111/j.2042-7158.2011.01279.x

Loh, X. J., and Wu, Y.-L. (2015). Cationic star copolymers based on β-cyclodextrins for efficient gene delivery to mouse embryonic stem cell colonies. *Chem. Commun.* 51, 10815–10818. doi: 10.1039/C5CC03686K

Lungwitz, U., Breunig, M., Blunk, T., and Göpferich, A. (2005). Polyethylenimine-based non-viral gene delivery systems. *Eur. J. Pharm. Biopharm.* 60, 247–266. doi: 10.1016/j.ejpb.2004.11.011

Matassoli, F. L., Leão, I. C., Bezerra, B. B., Pollard, R. B., Lütjohann, D., Hildreth, J. E. K., et al. (2018). Hydroxypropyl-beta-cyclodextrin reduces inflammatory signaling from monocytes: possible implications for suppression of HIV chronic immune activation. *mSphere.* 3:e00497-18. doi: 10.1128/mSphere.00497-18

Mealy, J. E., Rodell, C. B., and Burdick, J. A. (2015). Sustained small molecule delivery from injectable hyaluronic acid hydrogels through host–guest mediated retention. *J. Mater. Chem. B.* 3, 8010–8019. doi: 10.1039/C5TB00981B

Mudshinge, S. R., Deore, A. B., Patil, S., and Bhalgat, C. M. (2011). Nanoparticles: emerging carriers for drug delivery. *Saudi Pharm. J.* 19, 129–141. doi: 10.1016/j.jsps.2011.04.001

Nathan, C., and Ding, A. (2010). Nonresolving inflammation. *Cell* 140, 871–882. doi: 10.1016/j.cell.2010.02.029

Nava-Ortiz, C. A. B., Burillo, G., Concheiro, A., Bucio, E., Matthijs, N., Nelis, H., et al. (2010). Cyclodextrin-functionalized biomaterials loaded with miconazole prevent Candida albicans biofilm formation *in vitro*. *Acta Biomater.* 6, 1398–1404. doi: 10.1016/j.actbio.2009.10.039

Ngambenjawong, C., Gustafson, H. H., and Pun, S. H. (2017). Progress in tumor-associated macrophage (TAM)-targeted therapeutics. *Adv. Drug Deliv. Rev.* 114, 206–221. doi: 10.1016/j.addr.2017.04.010

Nguyen, M. K., and Lee, D. S. (2010). Injectable biodegradable hydrogels. *Macromol. Biosci.* 10, 563–579. doi: 10.1002/mabi.200900402

Oh, J. K., Drumright, R., Siegwart, D. J., and Matyjaszewski, K. (2008). The development of microgels/nanogels for drug delivery applications. *Prog. Polym. Sci.* 33, 448–477. doi: 10.1016/j.progpolymsci.2008.01.002

Okamatsu, A., Motoyama, K., Onodera, R., Higashi, T., Koshigoe, T., Shimada, Y., et al. (2013). Folate-appended β-cyclodextrin as a promising tumor targeting carrier for antitumor drugs *in vitro* and *in vivo*. *Bioconjug. Chem.* 24, 724–733. doi: 10.1021/bc400015r

Ooya, T., Eguchi, M., and Yui, N. (2003). Supramolecular design for multivalent interaction: maltose mobility along polyrotaxane enhanced binding with concanavalin A. *J. Am. Chem. Soc.* 125, 13016–13017. doi: 10.1021/ja034583z

Ottinger, E., Kao, M., Carrillo-Carrasco, N., Yanjanin, N., Shankar, R., Janssen, M., et al. (2014). Collaborative development of 2-hydroxypropyl-β-cyclodextrin for the treatment of niemann-pick type C1 disease. *Curr. Top. Med. Chem.* 14, 330–339. doi: 10.2174/1568026613666131127160118

Park, J., Wrzesinski, S. H., Stern, E., Look, M., Criscione, J., Ragheb, R., et al. (2012). Combination delivery of TGF-β inhibitor and IL-2 by nanoscale liposomal polymeric gels enhances tumour immunotherapy. *Nat. Mater.* 11, 895–905. doi: 10.1038/nmat3355

Park, K. M., Yang, J.-A., Jung, H., Yeom, J., Park, J. S., Park, K.-H., et al. (2012). *In situ* supramolecular assembly and modular modification of hyaluronic acid hydrogels for 3D cellular engineering. *ACS Nano.* 6, 2960–2968. doi: 10.1021/nn204123p

Park, Y. J., Yoo, S. A., Kim, M., and Kim, W. U. (2020). The role of calcium-calcineurin-NFAT signaling pathway in health and autoimmune diseases. *Front. Immunol.* 11:195. doi: 10.3389/fimmu.2020.00195

Pasut, G. (2019). Grand challenges in nano-based drug delivery. *Front. Med. Technol.* 1:1. doi: 10.3389/fmedt.2019.00001

Pustylnikov, S., Sagar, D., Jain, P., and Khan, Z. K. (2014). Targeting the C-type lectins-mediated host-pathogen interactions with dextran. *J. Pharm. Pharm. Sci.* 17, 371–392. doi: 10.18433/J3N590

Rajewski, R. A., Traiger, G., Bresnahan, J., Jaberaboansar, P., Stella, V. J., and Thompson, D. O. (1995). Preliminary safety evaluation of parenterally administered sulfoalkyl ether β-cyclodextrin derivatives. *J. Pharm. Sci.* 84, 927–932. doi: 10.1002/jps.2600840805

Rivera-Delgado, E., Djuhadi, A., Danda, C., Kenyon, J., Maia, J., Caplan, A. I., et al. (2018). Injectable liquid polymers extend the delivery of corticosteroids for the treatment of osteoarthritis. *J. Control. Release* 284, 112–121. doi: 10.1016/j.jconrel.2018.05.037

Roberts, M. J., Bentley, M. D., and Harris, J. M. (2002). Chemistry for peptide and protein PEGylation. *Adv. Drug Deliv. Rev.* 54, 459–476. doi: 10.1016/S0169-409X(02)00022-4

Rodell, C. B., Ahmed, M. S., Garris, C. S., Pittet, M. J., and Weissleder, R. (2019b). Development of adamantane-conjugated TLR7/8 agonists for supramolecular delivery and cancer immunotherapy. *Theranostics* 9, 8426–8436. doi: 10.7150/thno.35434

Rodell, C. B., Arlauckas, S. P., Cuccarese, M. F., Garris, C. S., Li, R., Ahmed, M. S., et al. (2018). TLR7/8-agonist-loaded nanoparticles promote the polarization of tumour-associated macrophages to enhance cancer immunotherapy. *Nat. Biomed. Eng.* 2, 578–588. doi: 10.1038/s41551-018-0236-8

Rodell, C. B., Baldwin, P., Fernandez, B., Weissleder, R., Sridhar, S., Dubach, J. M. (2020). Quantification of cellular drug biodistribution addresses challenges in evaluating *in vitro* and *in vivo* encapsulated drug delivery. *Adv. Ther.* doi: 10.1002/adtp.202000125. [Epub ahead of print].

Rodell, C. B., Kaminski, A. L., and Burdick, J. A. (2013). Rational design of network properties in guest–host assembled and shear-thinning hyaluronic acid hydrogels. *Biomacromolecules* 14, 4125–4134. doi: 10.1021/bm401280z

Rodell, C. B., Koch, P. D., and Weissleder, R. (2019a). Screening for new macrophage therapeutics. *Theranostics* 9:7714. doi: 10.7150/thno.34421

Rodell, C. B., Mealy, J. E., and Burdick, J. A. (2015a). Supramolecular guest–host interactions for the preparation of biomedical materials. *Bioconjug. Chem.* 26, 2279–2289. doi: 10.1021/acs.bioconjchem.5b00483

Rodell, C. B., Rai, R., Faubel, S., Burdick, J. A., and Soranno, D. E. (2015b). Local immunotherapy via delivery of interleukin-10 and transforming growth factor β antagonist for treatment of chronic kidney disease. *J. Control. Release* 206, 131–139. doi: 10.1016/j.jconrel.2015.03.025

Rodríguez-Lavado, J., de la Mata, M., Jiménez-Blanco, J. L., García-Moreno, M. I., Benito, J. M., Díaz-Quintana, A., et al. (2014). Targeted delivery of pharmacological chaperones for gaucher disease to macrophages by a mannosylated cyclodextrin carrier. *Organ. Biomol. Chem.* 12, 2289–2301. doi: 10.1039/C3OB42530D

Rosenblum, D., Joshi, N., Tao, W., Karp, J. M., and Peer, D. (2018). Progress and challenges towards targeted delivery of cancer therapeutics. *Nat. Commun.* 9:1410. doi: 10.1038/s41467-018-03705-y

Sanku, R. K. K., Karakus, O. O., Ilies, M., and Ilies, M. A. (2019). "Inclusion complexes in drug delivery and drug targeting: formation, characterization, and biological applications," in *Targeted Nanosystems for Therapeutic Applications: New Concepts, Dynamic Properties, Efficiency, and Toxicity, ACS Symposium Series. 1309*, eds K. Sakurai, and M. A. Ilies (Washington, DC: American Chemical Society), 187–221. doi: 10.1021/bk-2019-1309.ch009

Shibaguchi, K., Tamura, A., Terauchi, M., Matsumura, M., Miura, H., and Yui, N. (2019). Mannosylated polyrotaxanes for increasing cellular uptake efficiency in macrophages through receptor-mediated endocytosis. *Molecules* 24:439. doi: 10.3390/molecules24030439

Shire, S. J., Shahrokh, Z., and Liu, J. (2004). Challenges in the development of high protein concentration formulations. *J. Pharm. Sci.* 93, 1390–1402. doi: 10.1002/jps.20079

Sisso, A. M., Boit, M. O., and DeForest, C. A. (2020). Self-healing injectable gelatin hydrogels for localized therapeutic cell delivery. *J. Biomed. Mater. Res. A* 108, 1112–1121. doi: 10.1002/jbm.a.36886

Song, N., and Yang, Y.-W. (2014). Applications of pillarenes, an emerging class of synthetic macrocycles. *Sci. China Chem.* 57, 1185–1198. doi: 10.1007/s11426-014-5190-z

Soranno, D. E., Rodell, C. B., Altmann, C., Duplantis, J., Andres-Hernando, A., Burdick, J. A., et al. (2016). Delivery of interleukin-10 via injectable hydrogels improves renal outcomes and reduces systemic inflammation following ischemic acute kidney injury in mice. *Am. J. Physiol. Renal Physiol.* 311, F362–F72. doi: 10.1152/ajprenal.00579.2015

Stella, V. J., and Rajewski, R. A. (2020). Sulfobutylether-β-cyclodextrin. *Int. J. Pharm.* 583:119396. doi: 10.1016/j.ijpharm.2020.119396

Suhail, M., Rosenholm, J. M., Minhas, M. U., Badshah, S. F., Naeem, A., Khan, K. U., et al. (2019). Nanogels as drug-delivery systems: a comprehensive overview. *Ther. Deliv.* 10, 697–717. doi: 10.4155/tde-2019-0010

Sun, T., Kwong, C. H., Gao, C., Wei, J., Yue, L., Zhang, J., et al. (2020). Amelioration of ulcerative colitis via inflammatory regulation by macrophage-biomimetic nanomedicine. *Theranostics* 10:10106. doi: 10.7150/thno.48448

Szejtli, J. (1998). Introduction and general overview of cyclodextrin chemistry. *Chem. Rev.* 98, 1743–1754. doi: 10.1021/cr970022c

Thatiparti, T. R., and Von Recum, H. A. (2010). Cyclodextrin complexation for affinity-based antibiotic delivery. *Macromol. Biosci.* 10, 82–90. doi: 10.1002/mabi.200900204

Tibbitt, M. W., Dahlman, J. E., and Langer, R. (2016). Emerging frontiers in drug delivery. *J. Am. Chem. Soc.* 138, 704–717. doi: 10.1021/jacs.5b09974

Veronese, F. M., and Pasut, G. (2005). PEGylation, successful approach to drug delivery. *Drug Discov. Today.* 10, 1451–1458. doi: 10.1016/S1359-6446(05)03575-0

Walker, S., Oun, R., McInnes, F. J., and Wheate, N. J. (2011). The potential of cucurbit [n] urils in drug delivery. *Isr. J. Chem.* 51, 616–624. doi: 10.1002/ijch.201100033

Wang, H., Shao, N., Qiao, S., and Cheng, Y. (2012). Host–guest chemistry of dendrimer–cyclodextrin conjugates: selective encapsulations of guests within dendrimer or cyclodextrin cavities revealed by NOE NMR techniques. *J. Phys. Chem. B* 116, 11217–11224. doi: 10.1021/jp3062916

Wang, J., Guo, C., Wang, X. Y., and Yang, H. (2020). "Double-punch" strategy for delivery of viral immunotherapy with prolonged tumor retention and enhanced transfection efficacy. *J. Control. Release.* 329, 328–336. doi: 10.1016/j.jconrel.2020.11.043

Wang, L. L., Sloand, J. N., Gaffey, A. C., Venkataraman, C. M., Wang, Z., Trubelja, A., et al. (2017). Injectable, guest–host assembled polyethylenimine hydrogel for siRNA delivery. *Biomacromolecules* 18, 77–86. doi: 10.1021/acs.biomac.6b01378

Wang, P., Huang, S., Hu, Z., Yang, W., Lan, Y., Zhu, J., et al. (2019). *In situ* formed anti-inflammatory hydrogel loading plasmid DNA encoding VEGF for burn wound healing. *Acta Biomater.* 100, 191–201. doi: 10.1016/j.actbio.2019.10.004

Webber, M. J., Appel, E. A., Vinciguerra, B., Cortinas, A. B., Thapa, L. S., Jhunjhunwala, S., et al. (2016). Supramolecular PEGylation of biopharmaceuticals. *Proc. Natl. Acad. Sci. U. S. A.* 113, 14189–14194. doi: 10.1073/pnas.1616639113

Webber, M. J., and Langer, R. (2017). Drug delivery by supramolecular design. *Chem. Soc. Rev.* 46, 6600–6620. doi: 10.1039/C7CS00391A

Weiser, J. R., and Saltzman, W. M. (2014). Controlled release for local delivery of drugs: barriers and models. *J. Control. Release* 190, 664–673. doi: 10.1016/j.jconrel.2014.04.048

Widener, A. E., Bhatta, M. S., Angelini, T. E., and Phelps, E. A. (2020). Guest-host interlinked PEG-MAL granular hydrogels as an engineered cellular microenvironment. *Biomater. Sci.* doi: 10.1039/D0BM01499K. [Epub ahead of print].

Wong, L.-Y., Xia, B., Wolvetang, E., and Cooper-White, J. (2018). Targeted, stimuli-responsive delivery of plasmid DNA and miRNAs using a facile self-assembled supramolecular nanoparticle system. *Biomacromolecules* 19, 353–363. doi: 10.1021/acs.biomac.7b01462

Xiao, T., Qi, L., Zhong, W., Lin, C., Wang, R., and Wang, L. (2019a). Stimuli-responsive nanocarriers constructed from pillar[n]arene-based supra-amphiphiles. *Mater. Chem. Front.* 3, 1973–1993. doi: 10.1039/C9QM00428A

Xiao, T., Xu, L., Zhou, L., Sun, X.-Q., Lin, C., and Wang, L. (2019b). Dynamic hydrogels mediated by macrocyclic host–guest interactions. *J. Mate. Chem. B.* 7, 1526–1540. doi: 10.1039/C8TB02339E

Xiao, T., Zhong, W., Xu, L., Sun, X.-Q., Hu, X.-Y., and Wang, L. (2019c). Supramolecular vesicles based on pillar[n]arenes: design, construction, and applications. *Organ. Biomol. Chem*. 17, 1336–1350. doi: 10.1039/C8OB03095B

Xue, W., Zavalij, P. Y., and Isaacs, L. (2020). Pillar [n] MaxQ: a new high affinity host family for sequestration in water. *Angew. Chem. Int. Ed*. 59, 13313–13319. doi: 10.1002/anie.202005902

Ye, Z., Zhang, Q., Wang, S., Bharate, P., Varela-Aramburu, S., Lu, M., et al. (2016). Tumour-targeted drug delivery with mannose-functionalized nanoparticles self-assembled from amphiphilic β-cyclodextrins. *Chemistry* 22, 15216–15221. doi: 10.1002/chem.201603294

Yin, H., Zhang, X., Wei, J., Lu, S., Bardelang, D., and Wang, R. (2021). Recent advances in supramolecular antidotes. *Theranostics* 11:1513. doi: 10.7150/thno.53459

Yu, G., and Chen, X. (2019). Host-guest chemistry in supramolecular theranostics. *Theranostics* 9:3041. doi: 10.7150/thno.31653

Yu, L., and Ding, J. (2008). Injectable hydrogels as unique biomedical materials. *Chem. Soc. Rev*. 37:1473. doi: 10.1039/b713009k

Zheng, Y., Yuan, W., Liu, H., Huang, S., Bian, L., and Guo, R. (2020). Injectable supramolecular gelatin hydrogel loading of resveratrol and histatin-1 for burn wound therapy. *Biomater. Sci*. 8, 4810–4820. doi: 10.1039/D0BM00391C

Zhou, Y., Li, H., and Yang, Y.-W. (2015). Controlled drug delivery systems based on calixarenes. *Chinese Chem. Lett*. 26, 825–828. doi: 10.1016/j.cclet.2015.01.038

Zhou, Z., Guo, F., Wang, N., Meng, M., and Li, G. (2018). Dual pH-sensitive supramolecular micelles from star-shaped PDMAEMA based on β-cyclodextrin for drug release. *Int. J. Biol. Macromol*. 116, 911–919. doi: 10.1016/j.ijbiomac.2018.05.092

Zimmer, S., Grebe, A., Bakke, S. S., Bode, N., Halvorsen, B., Ulas, T., et al. (2016). Cyclodextrin promotes atherosclerosis regression via macrophage reprogramming. *Sci. Transl. Med*. 8:333ra50-ra50. doi: 10.1126/scitranslmed.aad6100

Zou, L., Braegelman, A. S., and Webber, M. J. (2019). Spatially defined drug targeting by *in situ* host–guest chemistry in a living animal. *ACS Central Sci*. 5, 1035–1043. doi: 10.1021/acscentsci.9b00195

**Conflict of Interest:** The authors declare that the research was conducted in the absence of any commercial or financial relationships that could be construed as a potential conflict of interest.

frontiers in Chemistry

ORIGINAL RESEARCH
published: 14 April 2021
doi: 10.3389/fchem.2021.660927

# Cucurbituril Ameliorates Liver Damage Induced by Microcystis aeruginosa in a Mouse Model

*Na'il Saleh*[1]*, *Saad Al-Jassabi*[2], *Ali H. Eid*[3,4] and *Werner M. Nau*[5]

[1] Department of Chemistry, College of Science, United Arab Emirates (UAE) University, Al Ain, United Arab Emirates, [2] Faculty of Medicine, Unishams University, Kuala Ketil, Malaysia, [3] Department of Basic Medical Sciences, College of Medicine, QU Health, Qatar University, Doha, Qatar, [4] Biomedical and Pharmaceutical Research Unit, QU Health, Qatar University, Doha, Qatar, [5] School of Engineering and Science, Jacobs University Bremen, Bremen, Germany

*Microcystis aeruginosa* is a cyanobacterium that produces a variety of cyclic heptapeptide toxins in freshwater. The protective effects of the macromolecular container cucurbit[7]uril (CB7) were evaluated using mouse models of cyanotoxin-induced liver damage. Biochemical analysis of liver function was performed to gauge the extent of liver damage after exposure to cyanobacterial crude extract [CCE; $LD_{50}$ = 35 mg/kg body weight; intraperitoneal (i.p.)] in the absence or presence of CB7 (35 mg/kg body weight, i.p.). CCE injection resulted in liver enlargement, potentiated the activities of alanine aminotransferase (ALT) and glutathione S-transferase (GST), increased lipid peroxidation (LPO), and reduced protein phosphatase 1 (PP1) activity. CCE-induced liver enlargement, ALT and GST activities, and LPO were significantly reduced when CB7 was coadministered. Moreover, the CCE-induced decline of PP1 activity was also ameliorated in the presence of CB7. Treatment with CB7 alone did not affect liver function, which exhibited a dose tolerance of 100 mg/kg body wt. Overall, our results illustrated that the addition of CB7 significantly reduced CCE-induced hepatotoxicity ($P < 0.05$).

**Keywords: cyanobacterial crude extract, chemoprotectant, cucurbituril, *Microcystis aeruginosa*, liver damage**

OPEN ACCESS

***Edited by:***
*Pavel Padnya,*
*Kazan Federal University, Russia*

***Reviewed by:***
*Narayanan Selvapalam,*
*Kalasalingam University, India*
*Ziyi Yu,*
*Nanjing Tech University, China*
*Ruibing Wang,*
*University of Macau, China*
*Nial Wheate,*
*The University of Sydney, Australia*

***Correspondence:**
*Na'il Saleh*
*n.saleh@uaeu.ac.ae*

***Specialty section:***
*This article was submitted to Supramolecular Chemistry, a section of the journal Frontiers in Chemistry*

***Received:*** *29 January 2021*
***Accepted:*** *16 March 2021*
***Published:*** *14 April 2021*

***Citation:***
*Saleh N, Al-Jassabi S, Eid AH and Nau WM (2021) Cucurbituril Ameliorates Liver Damage Induced by Microcystis aeruginosa in a Mouse Model. Front. Chem. 9:660927. doi: 10.3389/fchem.2021.660927*

## INTRODUCTION

The use of synthetic macromolecules for biological and medicinal applications has always been a popular approach (Yin et al., 2021). Accordingly, several studies have demonstrated the non-toxic and biocompatible nature of synthetic cucurbiturils (CBs) (Uzunova et al., 2010; Zhang et al., 2018). CBs are molecular containers comprising two hydrophilic carbonyl-lined portals with a central hydrophobic cavity. They have been synthesized in different sizes (**Figure 1** for cucurbit[7]uril [CB7]) (Lee et al., 2003). Because of these properties, the bioactivity of the CB7 host–guest complexes (Cheng et al., 2018) and their clinical applications *in vitro* and *in vivo* have been confirmed by several studies. For example, a previous study revealed that CB significantly decreased the hepatotoxicity caused by nitidine chloride (Li W. et al., 2017) as well as trazodone and its metabolite *m*-chlorophenylpiperazine (Huang et al., 2018a). Further, the antidotal activity of CB7 against paraquat, a toxic pesticide, was observed both *in vitro* and *in vivo* (Zhang et al., 2019a,b). Another study reported that a high affinity between CB7 and sorafenib, an anticancer drug (Yang et al., 2017), and bedaquiline (Kuok et al., 2018) and clofazimine (Li et al., 2016), antituberculosis drugs, enabled the host to decrease the cardiotoxicity of these drugs without

affecting their activity *in vitro* and *in vivo* in zebrafish models (Yang et al., 2017). In the same year, it was reported that CB reduced the neurotoxicity of pentylenetetrazol in zebrafish and mouse models (Huang et al., 2018b). Additionally, acyclic CB derivatives were shown to have antidotal activity against methamphetamine in rats (Ganapati et al., 2017).

Although several macrocyclic hosts have been used to reverse the effects of poisonous substances (Yin et al., 2021), CB7 as an antidote to the toxicity of cyanobacterial crude extract (CCE) has been validated in in *vivo* studies. Cyanobacteria produce a wide range of cyclic peptide hepatotoxins, such as microcystins and nodularin. These secondary metabolites of cyanobacteria can be detected both in freshwater and marine environments. **Figure 1** presents the chemical structure of microcystin-LR (MC-LR), a predominant toxin in CCE, as an example (Dittmann and Wiegand, 2006). Cyanobacteria are responsible for wildlife fatalities and adverse health effects in humans in countries where drinking water supplies are contaminated with these microorganisms (Al-Jassabi, 2005). Alarmingly, some of these cyanobacterial toxins are powerful promoters of liver tumor and potent inhibitors of protein phosphatase 1 (PP1) and PP2A catalytic subunits (PP1c/PP2Ac) that are critical for cytoskeletal integrity (Goldberg et al., 1995). During cyanobacterial bloom lysis in aquatic ecosystems, a mixture of toxins and other cyanobacterial and bacterial components are released in the water, which affects various aquatic organisms.

In this study, we analyzed the effects of CCE on liver function in mice with and without CB7 co-administration. Previous studies reported that the maximum tolerated dosage of CB7 is 250 mg/kg in mice, which is at least three-fold less than its $LD_{50}$ (Uzunova et al., 2010). The $LD_{50}$ of CCE in this study was 35 mg/kg body weight intraperitoneally (i.p.). International guidelines permit the analysis of doses at least 20-fold less than the $LD_{50}$ of CB7 to evaluate its protective activity, which justifies the use of CB7 as an antidote agent at a dose of 35 mg/kg body weight.

## MATERIALS AND METHODS

### Chemicals

All chemicals were purchased from Sigma-Aldrich. To calculate the CB7 concentrations, the water content in the bottle was assumed to be 20%, as stated by the supplier.

### Microcystis Cells

Different sites of the King Talal reservoir, Jordan, were targeted as sources of *Microcystis aeruginosa* during summer (May to October). We followed previously reported methods for isolating

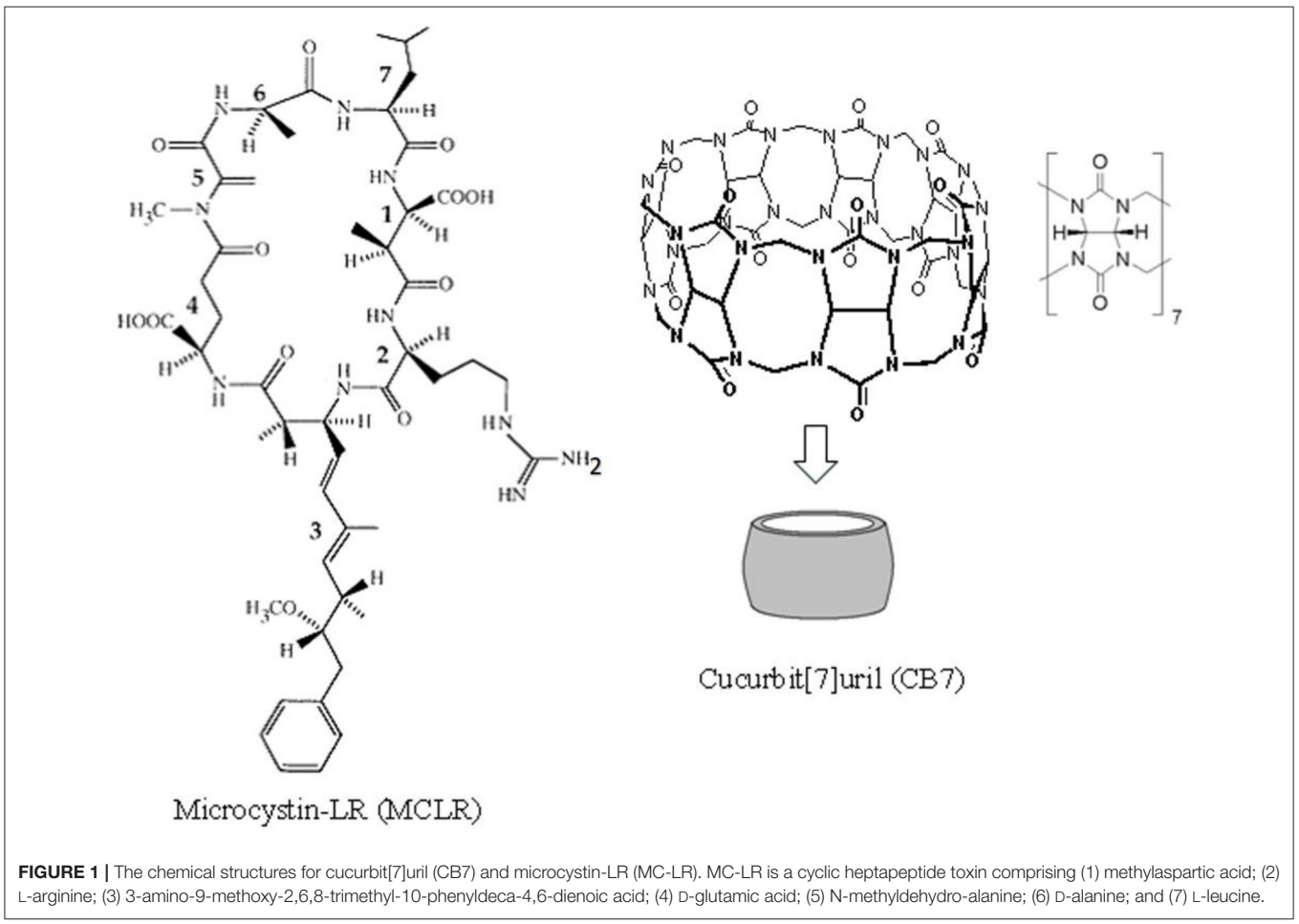


**FIGURE 1 |** The chemical structures for cucurbit[7]uril (CB7) and microcystin-LR (MC-LR). MC-LR is a cyclic heptapeptide toxin comprising (1) methylaspartic acid; (2) L-arginine; (3) 3-amino-9-methoxy-2,6,8-trimethyl-10-phenyldeca-4,6-dienoic acid; (4) D-glutamic acid; (5) N-methyldehydro-alanine; (6) D-alanine; and (7) L-leucine.

the cells and culturing them in medium (Dittmann and Wiegand, 2006). During cultivation, freeze-dried cells were used to extract cyanobacterial toxins using the method introduced by Mazur and Plinski (2003). To determine the $LD_{50}$ of the extracted toxin, we followed the method reported by (Fawell et al., 1999).

## Animal Treatment and Blood Sample Collection

We used 5–7-week-old male BALB/c mice (average weight, 30 g). Mice were obtained from the animal house unit of the Yarmouk University and were housed in stainless metal cages, with *ad libitum* access to food and tap water for the duration of the study. The animals were maintained on a 12/12-h light–dark cycle at a temperature of 23–26°C. The Animal Care and Use Committee at Yarmouk University approved the study procedure.

The mice were divided into four groups of 10 animals each. Group 1 (control) received only a single 0.5-mL i.p. dose of physiologic saline (neutral pH); group 2 received CB7 injection (35 mg/kg); group 3 received free toxin CCE (35 mg/kg), and group 4 received both the toxin and CB7 (35 mg/kg each). Mice were sacrificed after 24 h. A second set of experiments (groups 5–8) was performed in which the mice received i.p. injections of CB7 aqueous solutions (2–100 mg/kg) at physiological pH (10 mice for each concentration).

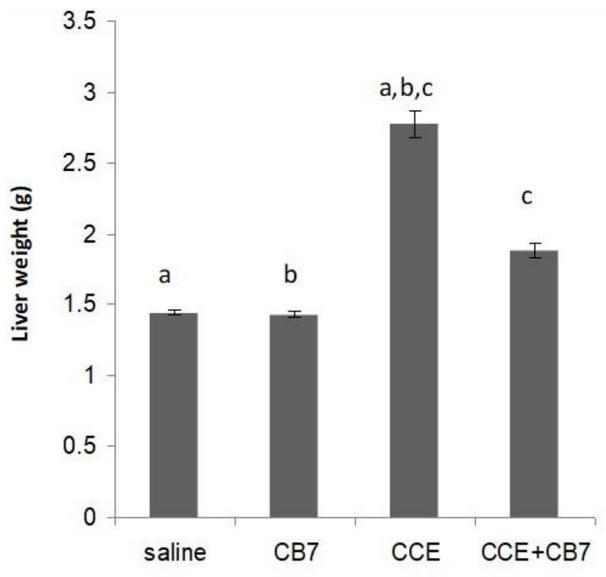


**FIGURE 2 |** Effects of cucurbit[7]uril (CB7) on cyanobacterial crude extract (CCE)-induced liver damage. Mice were divided into groups 1–4 and the livers from mice in each group were weighed. Data are presented as mean ± SEM. Bars with similar letters represent statistically significant differences. Ten mice per group ($n = 10$).

To assess the activities of alanine aminotransferase (ALT) and glutathione S-transferase (GST), blood was collected from the animals and the serum was stored at −70°C. The excess blood was then removed by perfusing the liver with Hanks' balanced salt solution. The IKA Ultra-Turax homogenizer was used to homogenize liver tissues in phosphate-buffered saline (pH 7.2). The supernatant in the centrifuged homogenate was stored at −70°C to measure PP1 activity and lipid peroxidation (LPO).

## ALT Assay

To measure ALT activity in the serum samples, we followed the method outlined previously by Gehringer et al. (2003).

## GST Assay

GST (EC 2.5.1.18) activity was measured in the liver homogenate using 1-chloro-2,4-dinitrobenzene as a substrate according to the method outlined by Habig et al. (1974).

## LPO Assay

The thiobarbituric acid (TBA) method recommended by Hosseinzadeh et al. (2007) was used to assess LPO.

## PP1 Activity Assay

To determine the activity of PP1, the kinetics of the generation of a yellow product from the dephosphorylation of *para*-nitrophenyl phosphate was estimated using a spectrophotometer, as described by Yuan et al. (2006).

## Statistical Analysis

All results were expressed as mean ± standard error of the mean (SEM) for 10 mice per group. One-way analysis of variance followed by Tukey's *post-hoc* test was used to determine the significance of differences between the groups. Statistical significance was indicated by a $P$ of $\leq 0.05$. All statistical analyses were performed using SigmaStat statistical software (version 3.5).

# RESULTS

Twenty-four hours after the i.p. injection, a significant increase in the liver mass was observed in group 3 (**Figure 2** and

**TABLE 1 |** Effects of microcystin-LR on the liver function of BALB/c mice in the presence and absence of cucurbit[7]uril (CB7); 10 mice per group ($n = 10$).

| Groups | Liver weight (g) | ALT (U/L) | GST (U/L) | LPO (μM) | PP1 (U/mg) |
|---|---|---|---|---|---|
| Group 1 (Normal) | 1.44 ± 0.02 | 550 ± 5 | 2.57 ± 0.07 | 0.067 ± 0.01 | 0.880 ± 0.01 |
| Group 2 (CB7) | 1.43 ± 0.02 | 620 ± 5 | 2.59 ± 0.06 | 0.072 ± 0.01 | 0.566 ± 0.01 |
| Group 3 (Toxin) | 2.77 ± 0.09 | 1950 ± 51 | 12.22 ± 0.33 | 2.152 ± 0.04 | 0.165 ± 0.002 |
| Group 4 (Toxin + CB7) | 1.88 ± 0.05 | 1485 ± 39 | 10.34 ± 0.34 | 1.877 ± 0.04 | 0.311 ± 0.007 |

*ALT, alanine aminotransferase; GST, glutathione S-transferase; LPO, lipid peroxidation; PP1, protein phosphatase-1.*

**TABLE 2 |** Effects of various concentrations of cucurbit[7]uril (CB7) on liver function in BALB/c mice; 10 mice per group ($n = 10$).

| Groups | Liver weight (g) | ALT (U/L) | GST (U/L) | LPO (μM) | PP1 (U/mg) |
|---|---|---|---|---|---|
| Group 5 (2 mg/kg) | 1.41 ± 0.02 | 575 ± 5 | 2.55 ± 0.06 | 0.071 ± 0.01 | 0.583 ± 0.01 |
| Group 6 (10 mg/kg) | 1.47 ± 0.03 | 545 ± 5 | 2.55 ± 0.06 | 0.069 ± 0.01 | 0.660 ± 0.01 |
| Group 7 (40 mg/kg) | 1.42 ± 0.02 | 562 ± 6 | 2.59 ± 0.07 | 0.078 ± 0.01 | 0.638 ± 0.02 |
| Group 8 (100 mg/kg) | 1.44 ± 0.03 | 628 ± 7 | 2.57 ± 0.06 | 0.097 ± 0.02 | 0.648 ± 0.02 |

*ALT, alanine aminotransferase; GST, glutathione S-transferase; LPO, lipid peroxidation; PP1, protein phosphatase-1.*

**Table 1**) compared with group 1 (1.44 vs. 2.77 g; $P < 0.05$). This increase was attributable to massive intrahepatic hemorrhage and the pooling of blood in the liver (data not shown). CB7 alone (**Table 2**) did not significantly affect the liver mass ($P > 0.05$). However, co-administration of CB7 and CCE significantly nullified the increase in liver mass that was seen in group 3 (1.88 vs. 2.77 g; $P < 0.05$), which implies a protective effect of CB7 on CCE-induced liver enlargement.

The effects of CCE on various biochemical markers of hepatic function were also determined in the presence and absence of CB7 (**Figure 3A** and **Table 1**). Group 2 did not exhibit a significant increase in ALT activity; however, group 3 exhibited a robust increase in ALT activity compared with that in the control group 1 (1950 vs. 550 U/L; $P < 0.05$; **Figure 3A** and **Table 1**). This activity was significantly diminished by co-treatment with CB7 (1485 U/L; $P < 0.05$) (**Figure 3A** and **Table 1**). Similarly, GST activity in the livers was significantly lower in group 4 than in group 3 (10.34 vs. 12.22 U/L; $p < 0.05$) (**Figure 3B** and **Table 1**). CB7 alone did not significantly affect GST activity (**Figure 3B** and **Table 2**).

We then assessed LPO by measuring the number of TBA-reactive substances. Compared with the control group 1, a marked increase in LPO was observed in group 3 (0.067 vs. 2.152 μM; $P < 0.001$; **Figure 4**). However, group 4 showed reduced LPO compared with group 3 (1.877 vs. 2.152 μM; $P < 0.05$). Furthermore, LPO was not significantly affected in group 2 compared with the control (0.072 μM; $P > 0.05$).

**Figure 5** and **Table 1** present the spectrophotometric determination of PP1 activity for the four groups. The injection of CCE alone (group 3) significantly diminished PP1 activity. This decrease was partially but significantly reversed in group 4. Surprisingly, CB7 alone (group 2) also decreased PP1 activity, though not as markedly as CCE.

The safety and toxicity of CB7 in mice were further tested and validated. The results revealed the absence of any significant changes in various biochemical markers of hepatic function (**Table 2**).

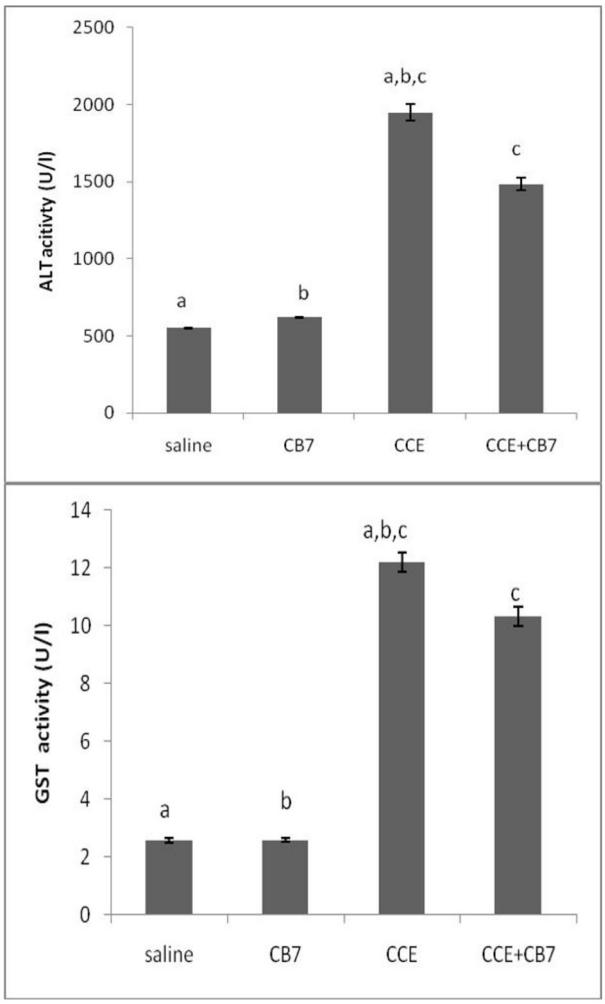


**FIGURE 3 | (A)** The activity of alanine aminotransferase (ALT) and **(B)** glutathione S-transferase (GST) in the livers of mice in each group. Data are presented as mean ± SEM. Bars with similar letters represent statistically significant differences. Ten mice per group ($n = 10$).

## DISCUSSION

The present study illustrated that CB7 can serve as a chemoprotectant and can effectively diminish CCE-induced liver damage in mice. This is the first report that demonstrated the protective role of CB7 against CCE-induced liver damage. Our results show that CCE induced liver enlargement resulting from massive intrahepatic hemorrhage, which is consistent with previous findings that MC-LR inhibits PP1, a serine/threonine phosphatase (Honkanen et al., 1990). Inhibition of PP1 is known to increase cytoskeletal protein phosphorylation (Ohta et al., 1992), thereby disrupting the liver cytoskeleton

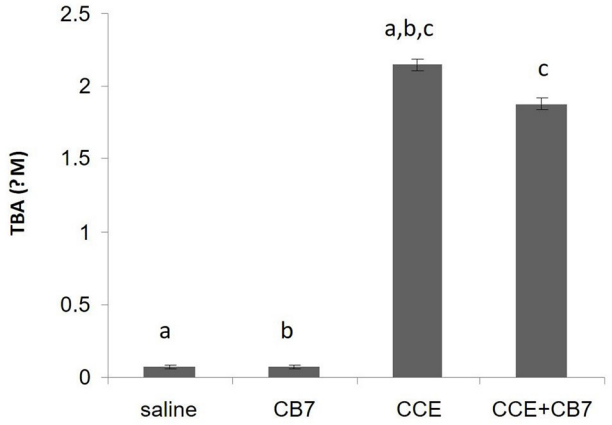


**FIGURE 4 |** Levels of thiobarbituric acid (TBA), which is indicative of lipid peroxidation, calculated from the livers of mice in each group. Data are presented as mean ± SEM. Bars with similar letters represent statistically significant differences. Ten mice per group ($n = 10$).

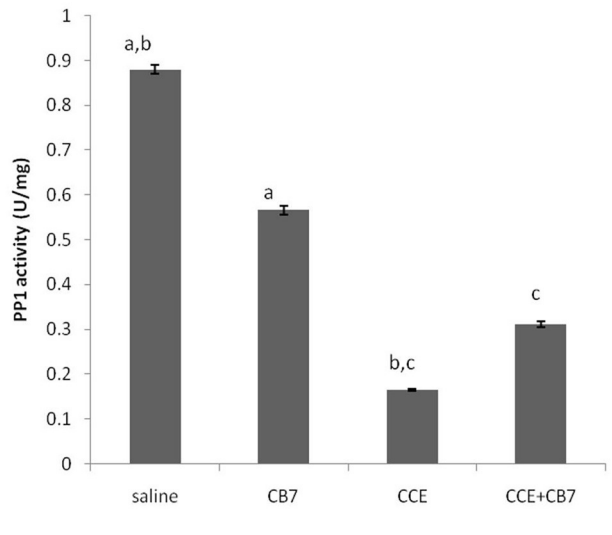


**FIGURE 5 |** Protein phosphatase-1 (PP1) activity in the livers of mice in each group. Data are presented as mean ± SEM. Bars with similar letters represent statistically significant differences. Ten mice per group ($n = 10$).

(Hooser et al., 1989, 1991). Our observation that CB7 alone reduced PP1 activity without affecting liver size suggests that the hyperphosphorylation of cytoskeletal proteins was not sufficiently robust to significantly disrupt the integrity of hepatic cells. However, the detailed mechanism of such interactions remains to be investigated, especially considering that the crude extract contains several other components. In fact, the low water solubility of the crude sample precludes a nuclear magnetic resonance measurement that is necessary to determine the site or mode of interactions. It is also notable that CB7 is not entirely soluble in organic solvents (Uzunova et al., 2010). Therefore, regardless of the chemical tool used, the binding patterns can only be studied by monitoring the interaction of CB7 containers with standard MC-LR (Harada et al., 1990).

ALT is a routinely used clinical indicator of hepatocellular injury. The present study illustrated that CB7 protects mice against CCE-induced liver damage by reducing ALT activity upon the coadministration of CB7 and CCE. Similar results were observed for GST, a phase II detoxification enzyme, which was also revealed to detoxify MC-LR (Pflugmacher et al., 1998). Taken together, these observations clearly indicate the protective role of CB7 against CCE-induced liver damage.

The pharmacokinetic profile of CB7 has already been studied both in Balb/c mice and in Sprague Dawley rats after i.p. or i.v. administration, respectively. The i.p. plasma clearance in mice fits a 2-compartment model with exponential decay profile, where clearances of $t_{1/2}\alpha = 17.0$ min and $t_{1/2}\beta = 270.7$ min are noted. Likewise, in Sprague Dawley rats, i.v. administration appeared to follow a multiphasic clearance model. Bio-distribution of CB7 in mice following i.p. administration show detection in the spleen, liver and brain 10 min post-administration, while activity in the kidneys occurred in two phases, at around 20 and 180 min. Due to this significantly higher activity in the kidneys (compared to that in liver), it was suggested that CB7 is excreted from the kidneys unchanged. It is worth mentioning that low levels of CB7 accumulate in the spleen and liver compared with the plasma and kidneys, while the brain accumulates the least activity, likely indicating that CB7 in unlikely to be able to cross the blood brain barrier (Li F. et al., 2017).

## Conclusion

Based on the biochemical examination of the extracted livers of mice following CCE treatment with or without CB7, CB7 reduced the toxicity of CCE *in vivo*. The use of chemoprotectants against *M. aeruginosa* cyanobacterial toxicity has been the subject of several studies. However, the novelty of the present study lies on the use of a synthetic organic receptor instead of free radical scavengers, $Ca^{2+}$ channel blockers, or enzyme inducers (Hermansky et al., 1991; Atencio et al., 2009). We demonstrated the potential application of CB7 as an adjuvant in toxicological pharmacology.

## DATA AVAILABILITY STATEMENT

The raw data supporting the conclusions of this article will be made available by the authors, without undue reservation.

## ETHICS STATEMENT

The animal study was reviewed and approved by Animal house unit of Yarmouk University.

## AUTHOR CONTRIBUTIONS

NS created the idea and wrote the final draft. NS and SA-J conducted all experimental work. AE and WN evaluated the final draft and added more references. All authors contributed to the article and approved the submitted version.

## FUNDING

The financial support from the Deutsche Forschingsgesellschaft (DFG, NA 686/4-1), Yarmouk University (2008/4), and UAE University (grant number 12R025) are gratefully acknowledged.

## REFERENCES

Al-Jassabi, S. (2005). Biochemical studies on the role of lycopene in the protection of mice against microcystin toxicity. *Chem. Ecol.* 21, 143–148. doi: 10.1080/02757540500093089

Atencio, L., Moreno, I., Jos, A., Prieto, A. I., Moyano, R., Blanco, A., et al. (2009). Effects of dietary selenium on the oxidative stress and pathological changes in tilapia (*Oreochromis niloticus*) exposed to a microcystin-producing cyanobacterial water bloom. *Toxicon* 53, 269–282. doi: 10.1016/j.toxicon.2008.11.011

Cheng, Q., Yin, H., Rosas, R., Gigmes, D., Ouari, O., Wang, R., et al. (2018). A pH-driven ring translocation switch against cancer cells. *Chem. Commun.* 54, 13825–13828. doi: 10.1039/C8CC08681H

Dittmann, E., and Wiegand, C. (2006). Cyanobacterial toxins–occurrence, biosynthesis, and impact on human affairs. *Mol. Nutr. Food Res.* 50, 7–17. doi: 10.1002/mnfr.200500162

Fawell, J. K., Mitchell, R. E., Everett, D. J., and Hill, R. E. (1999). The toxicity of cyanobacterial toxins in the mouse: I microcystin-LR. *Hum. Exp. Toxicol.* 18, 162–167. doi: 10.1177/096032719901800305

Ganapati, S., Grabitz, S. D., Murkli, S., Scheffenbichler, F., Rudolph, M. I., Zavalij, P. Y., et al. (2017). Molecular containers bind drugs of abuse *in vitro* and reverse the hyperlocomotive effect of methamphetamine in rats. *ChemBioChem* 18, 1583–1588. doi: 10.1002/cbic.201700289

Gehringer, M. M., Downs, K. S., Downing, T. G., Naudé, R. J., and Shephard, E. G. (2003). An investigation into the effect of selenium supplementation on microcystin hepatotoxicity. *Toxicon* 41, 451–458. doi: 10.1016/S0041-0101(02)00362-8

Goldberg, J., Huang, H. B., Kwon, Y. G., Greengard, P., Nairn, A. C., and Kuriyan, J. (1995). Three-dimensional structure of the catalytic subunit of protein serine/threonine phosphatase-1. *Nature* 376, 745–753. doi: 10.1038/376745a0

Habig, W. H., Pabst, M. J., and Jakoby, W. B. (1974). Glutathione S-transferases. The first enzymatic step in mercapturic acid formation. *J. Biol. Chem.* 249, 7130–7139. doi: 10.1016/S0021-9258(19)42083-8

Harada, K., Matsuura, K., Suzuki, M., Watanabe, M. F., Oishi, S., Dahlem, A. M., et al. (1990). Isolation and characterization of the minor components associated with microcystins LR and RR in the cyanobacterium (blue-green algae). *Toxicon* 28, 55–64. doi: 10.1016/0041-0101(90)90006-S

Hermansky, S. J., Stohs, S. J., Eldeen, Z. M., Roche, V. F., and Mereish, K. A. (1991). Evaluation of potential chemoprotectants against microcystin-LR hepatotoxicity in mice. *J. Appl. Toxicol.* 11, 65–73. doi: 10.1002/jat.2550110112

Honkanen, R. E., Zwiller, J., Moore, R. E., Daily, S. L., Khatra, B. S., Dukelow, M., et al. (1990). Characterization of microcystin- LR, a potent inhibitor of type 1 and type 2A protein phosphatases. *J. Biol. Chem.* 265, 19401–19404. doi: 10.1016/S0021-9258(17)45384-1

Hooser, S. B., Beasley, V. R., Lovell, R. A., Carmichael, W. W., and Haschek, W. M. (1989). Toxicity of microcystin LR, a cyclic heptapeptide hepatotoxin from *Microcystis aeruginosa* to rats and mice. *Vet. Pathol.* 26, 246–252. doi: 10.1177/030098588902600309

Hooser, S. B., Beasley, V. R., Waite, L. L., Kuhlenschmidt, M. S., Carmichael, W. W., and Haschek, W. M. (1991). Actin filament alterations in rat hepatocytes induced *in vivo* and *in vitro* by microcystin-LR, a hepatotoxin from the blue-green alga, *Microcystis aeruginosa*. *Vet. Pathol.* 28, 259–266. doi: 10.1177/030098589102800401

Hosseinzadeh, H., Parvardeh, S., Asl, M. N., Sadeghnia, H. R., and Ziaee, T. (2007). Effect of thymoquinone and nigella sativa seeds oil on lipid peroxidation level during global cerebral ischemia-reperfusion injury in rat hippocampus. *Phytomedicine* 14, 621–627. doi: 10.1016/j.phymed.2006.12.005

Huang, Q., Kuok, K. I., Zhang, X., Yue, L., Lee, S. M. Y., Zhang, J., et al. (2018b). Inhibition of drug-induced seizure development in both zebrafish and mouse models by a synthetic nanoreceptor. *Nanoscale* 10, 10333–10336. doi: 10.1039/C8NR02041H

Huang, Q., Li, S., Yin, H., Wang, C., Lee, S. M. Y., and Wang, R. (2018a). Alleviating the hepatotoxicity of trazodone via supramolecular encapsulation. *Food Chem. Toxicol.* 112, 421–426. doi: 10.1016/j.fct.2017.12.016

Kuok, K. I., In Ng, P. C., Ji, X., Wang, C., Yew, W. W., Chan, D. P. C., et al. (2018). Supramolecular strategy for reducing the cardiotoxicity of bedaquiline without compromising its antimycobacterial efficacy. *Food Chem. Toxicol.* 119, 425–429. doi: 10.1016/j.fct.2017.12.022

Lee, J. W., Samal, S., Selvapalam, N., Kim, H. J., and Kim, K. (2003). Cucurbituril homologues and derivatives: new opportunities in supramolecular chemistry. *Acc. Chem. Res.* 36, 621–630. doi: 10.1021/ar020254k

Li, F., Gorle, A. K., Ranson, M., Vine, K. L., Kinobe, R., Feterl, M., et al. (2017). Probing the pharmacokinetics of cucurbit[7, 8, and 10]uril: and a dinuclear ruthenium antimicrobial complex encapsulated in cucurbit[10]uril. *Org. Biomol. Chem.*15, 4172–4179. doi: 10.1039/C7OB00724H

Li, S., Chan, J. Y.-W., Li, Y., Bardelang, D., Zheng, J., Yew, W. W., et al. (2016). Complexation of clofazimine by macrocyclic cucurbit[7]uril reduced its cardiotoxicity without affecting the antimycobacterial efficacy. *Org. Biomol. Chem.* 14, 7563–7569. doi: 10.1039/C6OB01060A

Li, W., Yin, H., Bardelang, D., Xiao, J., Zheng, Y., and Wang, R. (2017). Supramolecular formulation of nitidine chloride can alleviate its hepatotoxicity and improve its anticancer activity. *Food Chem. Toxicol.* 109, 923–929. doi: 10.1016/j.fct.2017.02.022

Mazur, H., and Plinski, M. (2003). Nodularia spumigena blooms and the occurrence of hepatotoxin in the Gulf of Gdansk. *Oceanologia* 45, 305–316.

Ohta, T., Nishiwaki, R., Yatsunami, J., Komori, A., Suganuma, M., and Fujiki, H. (1992). Hyperphosphorylation of cytokeratins 8 and 18 by microcystin-LR, a new liver tumor promoter, in primary cultured rat hepatocytes. *Carcinogenesis* 13, 2443–2447. doi: 10.1093/carcin/13.12.2443

Pflugmacher, S., Wiegand, C., Oberemm, A., Beattie, K. A., Krause, E., Codd, G. A., et al. (1998). Identification of an enzymatically formed glutathione conjugate of the cyanobacterial hepatotoxin microcystin-LR: the first step in detoxification. *Biochim. Biophys. Acta* 1425, 527–533. doi: 10.1016/S0304-4165(98)00107-X

Uzunova, V. D., Cullinane, C., Brix, K., Nau, W. M., and Day, A. I. (2010). Toxicity of cucurbit[7]uril and cucurbit[8]uril: an exploratory *in vitro* and *in vivo* study. *Org. Biomol. Chem.* 8, 2037–2042. doi: 10.1039/b925555a

Yang, X., Huang, Q., Bardelang, D., Wang, C., Lee, S. M. Y., and Wang, R. (2017). Supramolecular alleviation of cardiotoxicity of a small-molecule kinase inhibitor. *Org. Biomol. Chem.* 15, 8046–8053. doi: 10.1039/C7OB01505D

Yin, H., Bardelang, D., and Wang, R. (2021). Macrocycles and related hosts as supramolecular antidotes. *Trends Chem.* 3, 1–4. doi: 10.1016/j.trechm.2020.08.008

Yuan, M., Carmichael, W. W., and Hilborn, E. D. (2006). Microcystin analysis in human sera and liver from human fatalities in Caruaru, Brazil 1996. *Toxicon* 48, 627–640. doi: 10.1016/j.toxicon.2006.07.031

Zhang, X., Huang, Q., Zhao, Z. Z., Xu, X., Li, S., Yin, H., et al. (2019a). An eco- and user-friendly herbicide. *J. Agric. Food Chem.* 67, 7783–7792. doi: 10.1021/acs.jafc.9b00764

Zhang, X., Xu, X., Li, S., Li, L., Zhang, J., and Wang, R. (2019b). A synthetic receptor as a specific antidote for paraquat poisoning. *Theranostics* 9, 633–645. doi: 10.7150/thno.31485

Zhang, X., Xu, X., Li, S., Wang, L. H., Zhang, J., and Wang, R. (2018). A systematic evaluation of the biocompatibility of cucurbit[7]uril in mice. *Sci. Rep.* 8:8819. doi: 10.1038/s41598-018-27206-6

**Conflict of Interest:** The authors declare that the research was conducted in the absence of any commercial or financial relationships that could be construed as a potential conflict of interest.

frontiers in Chemistry

REVIEW
published: 30 April 2021
doi: 10.3389/fchem.2021.659845

# Macrocycle-Antibiotic Hybrids: A Path to Clinical Candidates

*Abdrrahman Shemsu Surur and Dianqing Sun**

*Department of Pharmaceutical Sciences, The Daniel K. Inouye College of Pharmacy, University of Hawai'i at Hilo, Hilo, HI, United States*

The tale of abate in antibiotics continued defense mechanisms that chaperone the rise of drug-defying superbugs—on the other hand, the astray in antibacterial drug discovery and development. Our salvation lies in circumventing the genesis of resistance. Considering the competitive advantages of antibacterial chemotherapeutic agents equipped with multiple warheads against resistance, the development of hybrids has rejuvenated. The adoption of antibiotic hybrid paradigm to macrocycles has advanced novel chemical entities to clinical trials. The multi-targeted TD-1792, for instance, retained potent antibacterial activities against multiple strains that are resistant to its constituent, vancomycin. Moreover, the antibiotic conjugation of rifamycins has provided hybrid clinical candidates with desirable efficacy and safety profiles. In 2020, the U.S. FDA has granted an orphan drug designation to TNP-2092, a conjugate of rifamycin and fluoroquinolone, for the treatment of prosthetic joint infections. DSTA4637S is a pioneer antibacterial agent under clinical development and represents a novel class of bacterial therapy, that is, antibody–antibiotic conjugates. DSTA4637S is effective against the notorious persistent *S. aureus* bacteremia, a revelation of the abracadabra potential of antibiotic hybrid approaches.

**Keywords: antibiotic hybrid, macrocycle, macrocycle hybrid, TD-1792, TD-1607, TNP-2092, TNP-2198, DSTA4637S**

OPEN ACCESS

***Edited by:***
*Pavel Padnya,*
*Kazan Federal University, Russia*

***Reviewed by:***
*Frank Schweizer,*
*University of Manitoba, Canada*
*Lihua Yuan,*
*Sichuan University, China*

****Correspondence:***
*Dianqing Sun*
*dianqing@hawaii.edu*

***Specialty section:***
*This article was submitted to Supramolecular Chemistry, a section of the journal Frontiers in Chemistry*

***Received:*** *28 January 2021*
***Accepted:*** *15 April 2021*
***Published:*** *30 April 2021*

***Citation:***
*Surur AS and Sun D (2021) Macrocycle-Antibiotic Hybrids: A Path to Clinical Candidates. Front. Chem. 9:659845. doi: 10.3389/fchem.2021.659845*

## INTRODUCTION

Relentlessness in developing resistance is imperiling the competence of the antibacterial arsenal. A global health crisis is heightened by the emergence and prevalence of multidrug-resistant bacteria pathogens, which are untreatable with commonly used antibiotics (Aslam et al., 2018). According to the landmark 2019 Centers for Disease Control and Prevention (CDC) estimate, there are over 2.8 million antibiotic-resistant infections every year in the United States, which account for a death every 15 min (CDC, 2019). The once though magic bullets are no longer producing magical chemotherapeutic effects. The rising and compounding antimicrobial resistances continue to mandate novel strategies in the antibacterial drug discovery and development process (Silver, 2011; Brown and Wright, 2016; Shang et al., 2020). The 2019 analysis of antibacterial agents in clinical development by the World Health Organization (WHO) indicates the current clinical pipeline is insufficient to alleviate the threats posed by antimicrobial resistance (WHO, 2019a).

## ANTIBIOTIC COMBINATIONS VERSUS ANTIBIOTIC HYBRIDS

Single-target agents have dominated the current antibacterial collection, and bacteria seem capable of rendering all ineffective (East and Silver, 2013). Simultaneous use of drug molecules having different

molecular targets, or polypharmacology, was then considered more reliable to eliminate or at least slow the onset of resistance (Gray and Wenzel, 2020). Accordingly, concomitant use of antibiotics is often practiced by clinicians to prevent the development of resistance, broaden the spectrum of activity, and/or optimize the dose of drugs. In combination therapy, an adjuvant which may be inactive on its own is used with an antibiotic—a strategy called antibiotic–adjuvant approach (Liu et al., 2019). The adjuvant may enable entrance of the bona fide antibiotic by improving the membrane permeability, inhibit enzymes responsible for inactivation, or prevent the active efflux of the antibiotic (Liu et al., 2019; Tyers and Wright, 2019). Antibiotic–antibiotic combination approach, on the other hand, entails the use of dynamic dual antibiotics to achieve drug synergism or suppress the development of resistance, hypothesizing that bacteria will not survive the one-two punch of the antibiotics (Tyers and Wright, 2019). This antibiotic cocktail approach has prolonged the clinical utilities of some antibiotics, albeit potential problems due to unfavorable pharmacokinetic (PK) interactions, and for several reasons, the boosted *in vitro* activity often does not translate well into *in vivo* efficacy in animal models or clinical settings (Klahn and Bronstrup, 2017; Domalaon et al., 2018). In a scenario where the combined drugs lack PK complementarities, such as dissimilar half-lives where a short-acting drug is excreted rapidly, or different tissue distributions where one component is barely distributed, the other component will become vulnerable from the aspect of development of resistance (Domalaon et al., 2018). For example, multiple resistance mechanisms have gradually limited the clinical use of co-trimoxazole involving the dihydrofolate reductase (DHFR) inhibitor trimethoprim and the dihydropteroate synthase (DHPS) inhibitor sulfamethoxazole, the esteemed example of the antibiotic combination approach (Eliopoulos and Huovinen, 2001). Pharmacokinetic disparities, such as dissimilar volume of distributions by the virtue of differences in hydrophobic properties between trimethoprim and sulfamethoxazole, might have contributed to the development of resistance (Brown, 2014). In addition, drug combination or co-formulation is also vulnerable to additive toxicities (Tamma et al., 2012). The need for taking multiple drugs, especially if different routes of administrations are involved, may also deflate patients' convenience (Fisher et al., 2020).

An attractive alternative to the mix and match antibiotic combinations is to bridge two pharmacophores by a metabolically stable covalent bond to generate a heteromeric synthetic construct, which behaves as a single chemical entity pertaining to PK parameters, a strategy otherwise known as an antibiotic hybrid (Pokrovskaya and Baasov, 2010; Klahn and Bronstrup, 2017). Diverse subjective definitions are forged for antibiotic hybrids. Generally, the antibiotic hybrid umbrella covers dual-acting antibiotic hybrids, divalent or multivalent antibiotics, antibiotic conjugates, chimeric antibiotics, and antibiotic hybrid prodrugs (Wang et al., 2016; Domalaon et al., 2018). The latter involves a cleavable linker between synthons, which can be metabolized only by a specific strain, a very useful strategy for the development of narrow-spectrum antibacterial agents (Domalaon et al., 2018; Jubeh et al., 2020). In the belligerence of drug resistance, molecules composed of two or more active structure motifs that are capable of acting at their respective targets have been extensively explored (Shavit et al., 2017). Selection of a matching partner in the antibiotic hybrid strategy is crucial so that the resulting dual-acting hybrid will unlikely suffer from cross-resistance. An organism may develop resistance to a dual-acting hybrid if it is not susceptible to the action of either drug (Parkes and Yule, 2016).

Over the past few decades, significant advances have been made in medicinal chemistry and chemical biology of macrocyclic compounds (Yu and Sun, 2013; Yudin, 2015). In contrast to large macromolecules and small synthetic molecules, macrocycles possess unique structural advantages and benefits from featuring both large molecules such as high potency and impeccable selectivity, and small molecules such as reasonable manufacturing costs, favorable PK, and the lack of immunogenicity (Peterson, 2017). The up-to-date comprehensive review of antibacterial agents in clinical pipeline (Butler and Paterson, 2020) along with reviews regarding the 14- to 15-membered macrolide hybrids (Janas and Przybylski, 2019) and their potential as anti-infective and anti-inflammatory agents (Paljetak et al., 2017) indicates the antibiotic hybrid approach is trending in the development of macrocyclic compounds. In this review, using terms such as "drugs" and "bacterial infections," clinical trials listed in clinicaltrials.gov were searched meticulously. More than 2,000 clinical trials matched our search criteria, and the search results were cross-checked with the 2019 global observatory of the WHO for antibacterial products in clinical development (WHO, 2019b). Five novel macrocycle-based antibiotic hybrids under clinical developments, that is, TD-1792, TD-1607, TNP-2092, TNP-2198, and DSTA3647S, are highlighted and discussed.

## HYBRIDS OF VANCOMYCIN

Although about 6 decades have passed since vancomycin (VAN, **1**, **Figure 1**) was initially approved by the U.S. Food and Drug Administration (FDA) in 1958 and introduced into clinical practice, it is still commonly used for the treatment of many Gram-positive bacterial infections and often the last resort in modern treatment of drug-resistant infections (Okano et al., 2017). However, a dark cloud lids over the use of **1**, as evidenced by widespread VAN-resistant *Enterococci* (VRE) and VAN-resistant *Staphylococcus aureus* (VRSA) and the loss of clinical efficacy against severe methicillin-resistant *S. aureus* (MRSA) infections (Faron et al., 2016). Vancomycin has continued to be captured in the spotlight in antibacterial drug development; its unique clinical successes, absence of cross-resistance with other antibacterial classes, a significant time span (30 years) between discovery and appearance of the first resistant strains in VRE, and advances in structural determinations

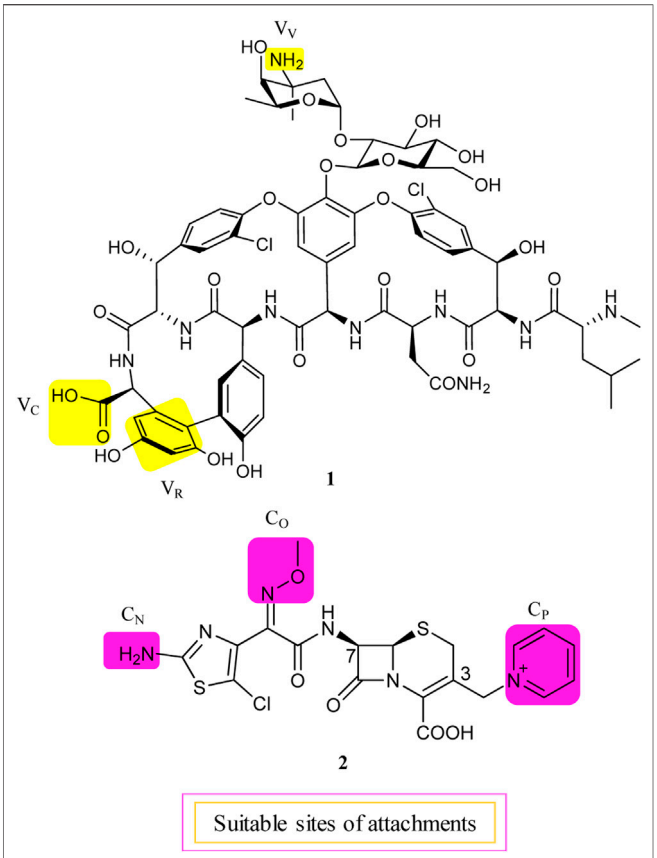


**FIGURE 1 |** Suitable attachment positions in vancomycin (**1**) and THRX-169797 (**2**).

or synthetic methods are among the reasons accounted (Blaskovich et al., 2018). Notably, three new structural analogs, that is, telavancin (Vibativ®), dalbavancin (Dalvance®), and oritavancin (Orbactiv®), were approved by the U.S. FDA in September 2009, May 2014, and August 2014, respectively, for the treatments of complicated skin and skin structure infections (cSSSIs) and acute bacterial skin and skin structure infections (ABSSSIs) (Lexicomp, 2021). Besides its historical clinical success and impact, **1** has also been targeted in the antibiotic hybrid paradigm for two main reasons. First, the glycopeptide scaffold in **1** provides several substituents suitable for binding a partner—in particular, the free C-terminal carboxylic acid ($V_C$), the primary amine in vancosamine sugar ($V_V$), and the aryl group of the seventh amino acid ($V_R$) (**Figure 1**, Long et al., 2008a; Long et al., 2008b; Blaskovich et al., 2018). Second, **1** increases the affinity to the target *via* cooperative back-to-back dimerization. This opens a characteristic possibility to design potent conjugates where two vancomycin residues are dimerized or **1** is covalently linked to another partner such as **2** (Blaskovich et al., 2018). Although **1** has been dimerized or conjugated with siderophores or fluorophores, only its antibiotic hybrids have provided advanced candidates under clinical development, that is, cefilavancin (**3**, also known as TD-1792) and TD-1607 (**4**) in **Figure 2** (Negash et al., 2019; Theuretzbacher, 2020).

The lipid intermediate II (a membrane-anchored cell wall precursor) and transpeptidase (the penicillin-binding protein), the cellular targets of **1** and cephalosporins, respectively, are in close proximity and catalyze sequential roles in the bacterial cell wall biosynthesis. Consequently, their hybrid molecule might be able to inhibit both targets simultaneously and therefore have superior bactericidal properties (Long et al., 2008a). As mentioned above, **1** is equipped with at least three potential attachment sites ($V_V$, $V_C$, and $V_R$) (Long et al., 2008a; Blaskovich et al., 2018). Similarly, the C-3 pyridinium ($C_P$) moiety, the *Z*-oriented oxime ($C_O$), and thiazolylamino ($C_N$) groups of the C-7 side chain of 2 are suitable attachment sites in a cephalosporin nucleus (**Figure 1**, Long et al., 2008a). All possible nine hybrid heteromers between the above-mentioned attachment sites were synthesized *via* an amide linker and exhibited excellent activity against a select panel of Gram-positive bacteria pathogens, including MRSA and vancomycin intermediate-resistant *S. aureus* (VISA) (Long et al., 2008a). Cefilavancin was among the two most promising heteromers, with an $MIC_{90}$ value of 0.03 μg/ml against MRSA isolates (Long et al., 2008a; Blais et al., 2012). Furthermore, *in vitro* studies revealed that THRX-169797 (**2**), the cephalosporin constituent of **3**, was much less active than **3** against all *S. aureus* isolates tested (Blais et al., 2012). The murine neutropenic thigh infection model of MRSA was extended to **3**. The $ED_{50}$ of 0.19 mg/kg for **3** was 40 times more effective than the $ED_{50}$ of that for **1**, with an $ED_{50}$ of 8.1 mg/kg in their assay (Long et al., 2008a). Consequently, **3** was selected and advanced as a clinical candidate for further development.

Cefilavancin also showed very potent activity against the heterogeneous VISA (hVISA), with minimum inhibitory concentration ($MIC_{90}$) values of 0.03 μg/ml against 39 isolated strains of hVISA, relative to 2 μg/ml for **1** (Blais et al., 2012). In addition, **3** was the most active ($MIC_{90}$ = 0.125 μg/ml) against various clinical isolates of VAN-intermediate staphylococcal species (VISS), heterogeneous VISS (hVISS), and VRSA, compared to daptomycin, quinupristin–dalfopristin, and linezolid (Leuthner et al., 2010). A similar study identified the effect of plasma proteins on the potency of **3** as low, and the $MIC_{90}$ value remained the lowest compared to all comparators (Leuthner et al., 2010). Moreover, the positive results from clinical trials have supported the continued development of **3**. In phase 1 studies, plasma concentrations after intravenous (IV) administration of 2 mg/kg body weight were continuously above the MIC value at which 100% MRSA isolates were inhibited (Blais et al., 2012). In phase 2 studies, the efficacy of **3** was compared with that of **1** in the treatment of cSSSIs. The cure rate at the end of the treatments with **1** and **3** was 90.7% and 91.7%, respectively (Stryjewski et al., 2012). The incidence of the most common adverse effects was similar in both groups, except for itching, which was more common in volunteers in the VAN arm (NCT00442832, 2006; Stryjewski et al., 2012). Currently, Theravance Biopharma and R-Pharm are conducting a phase 3 clinical development of **3** in Russia (WHO, 2019a; Adis Insight, 2020).

The hybridization of the nuclei in **3**, but with a longer amide linker and different attachment positions, led to TD-1607 (**4**) (**Figure 2**, Fatheree et al., 2005). In **4**, the aryl group closest to the C-terminus of **1** ($V_R$) is aminomethylated and linked to the pyridinyl substituent ($C_P$) from the bicyclic lactam of cephalosporin

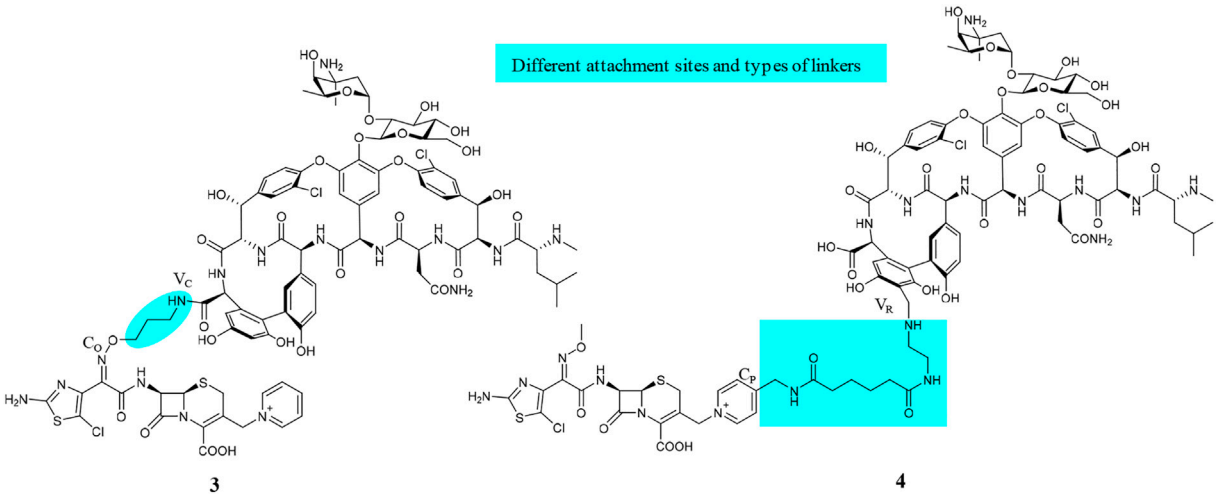


**FIGURE 2 |** Chemical structures of VAN hybrids, cefilavancin (**3**, TD-1792), and TD-1607 (**4**).

(Fatheree et al., 2005; Blaskovich et al., 2018). TD-1607 exerts its antibacterial activity by inhibiting cell wall biosynthesis; *in vitro* microbiological profiling showed a rapid and potent bactericidal effect against Gram-positive organisms (Sader et al., 2014). Compound **4** proved to be the most effective against all comparators, including **1**, with MIC values between 0.008 and 0.06 μg/ml against 1,026 MRSA isolates procured worldwide (Sader et al., 2014; Liapikou et al., 2017). Single and multiple ascending dose phase 1 studies on the safety, tolerability, and PK of **4** were conducted in healthy volunteers (NCT01791049, 2013; NCT01949103, 2013). However, Theravance BioPharma has discontinued further clinical developments of **4** (Butler and Paterson, 2020).

## Synthesis of Vancomycin Hybrids

Chemical syntheses of VAN conjugates **3** and **4** involved a series of steps to construct the cephalosporin synthon attached to a linker and an eventual coupling with vancomycin (Scheme 1). The synthesis of a cephalosporin and an amide anchor motif in **3** started by coupling *N*-Boc–protected bromopropylamine **5** with the hydroxylimino moiety of a trityl-protected aminothiazolyl residue **6** (Long et al., 2008a). Following ester hydrolysis of **7** and subsequent chlorination of the thiazolyl ring in **7** or **8** using *N*-chlorosuccinimide (NCS) yielded **9** or **10**, respectively. Intermediates **9** and **10** were next coupled with 7-amino-3-chloromethyl-3-cephem-4-carboxylic acid *p*-methoxybenzyl ester hydrochloride salt (ACLE). The 3-chloro good leaving group in the ACLE moiety was replaced with pyridine or 4-(*N*-*tert*-butoxycarbonyl)aminomethyl pyridine to give **11** or **12**, respectively (Fatheree et al., 2005; Long et al., 2008a). The key cephalosporin intermediates **13** and **14** were synthesized by global deprotection of their corresponding precursors in TFA. Finally, VAN **1** was attached directly to **13** through amide bond formation to afford target compound **3** (Fatheree et al., 2005; Long et al., 2008a). Unlike the direct coupling in **3**, target compound **4** was synthesized *via* sequential bifunctional amide coupling of the cephalosporin $C_P$ synthon **14** and the VAN $V_R$ synthon *via* the di-HOAt ester of adipic acid (Fatheree et al., 2005; Long et al., 2008a).

## HYBRIDS OF RIFAMYCINS

Various clinical guidelines for the treatment of staphylococcal prosthetic joint infection (PJI), including the Infectious Diseases Society of America (IDSA) guideline, recommend rifampin with a fluoroquinolone companion (Osmon et al., 2013; Berbari et al., 2020). First, rifamycins are the drug of choice for persistent bacterial infections such as PJI (Robertson et al., 2008). Rifampin intervenes critical gene transcription process and prevents spread to deep-seated infection sites, crafting a clinical success against slow-growing and nonreplicating metabolic stages of bacteria (Robertson et al., 2008; Ma and Lynch, 2016). Second, the formation of bacterial biofilms, a polysaccharide glycocalyx that provides a mechanical shield from antibiotics and immune system of the host, over the prosthesis is a central mechanism in the pathogenesis of PJI (Taha et al., 2018). According to various *in vitro* and/or *in vivo* animal model studies, rifampin diffuses well into biofilm and produces effective killing against biofilm-associated bacteria (Sanchez et al., 2015). Third, a point mutation in the *rpoB* gene that encodes the β-subunit of RNA polymerase confers a high resistance to rifampin (Aubry-Damon et al., 1998; Silver, 2011), and a companion drug may be needed to slow down the development of resistance. In this context, *in vivo* and clinical data indicated fluoroquinolones as the best concomitant drugs with rifampin (Wells et al., 2018). However, the *in vitro* antagonism observed between rifampin and the fluoroquinolone class (Murillo et al., 2008) and the need to take rifampin orally and fluoroquinolones intravenously during the initial phase of the treatment regimen are major limitations for clinical use of this combination (Ma and Lynch, 2016). Rifampin inhibits bacterial RNA synthesis which may weaken the bactericidal effect of fluoroquinolones by impeding the supercoiling of DNA (Zimmerli and Sendi, 2019). To address these, a resolution by introducing a covalently linked hybrid of rifampin and a fluoroquinolone pharmacophore was proposed. Furthermore, fluoroquinolones

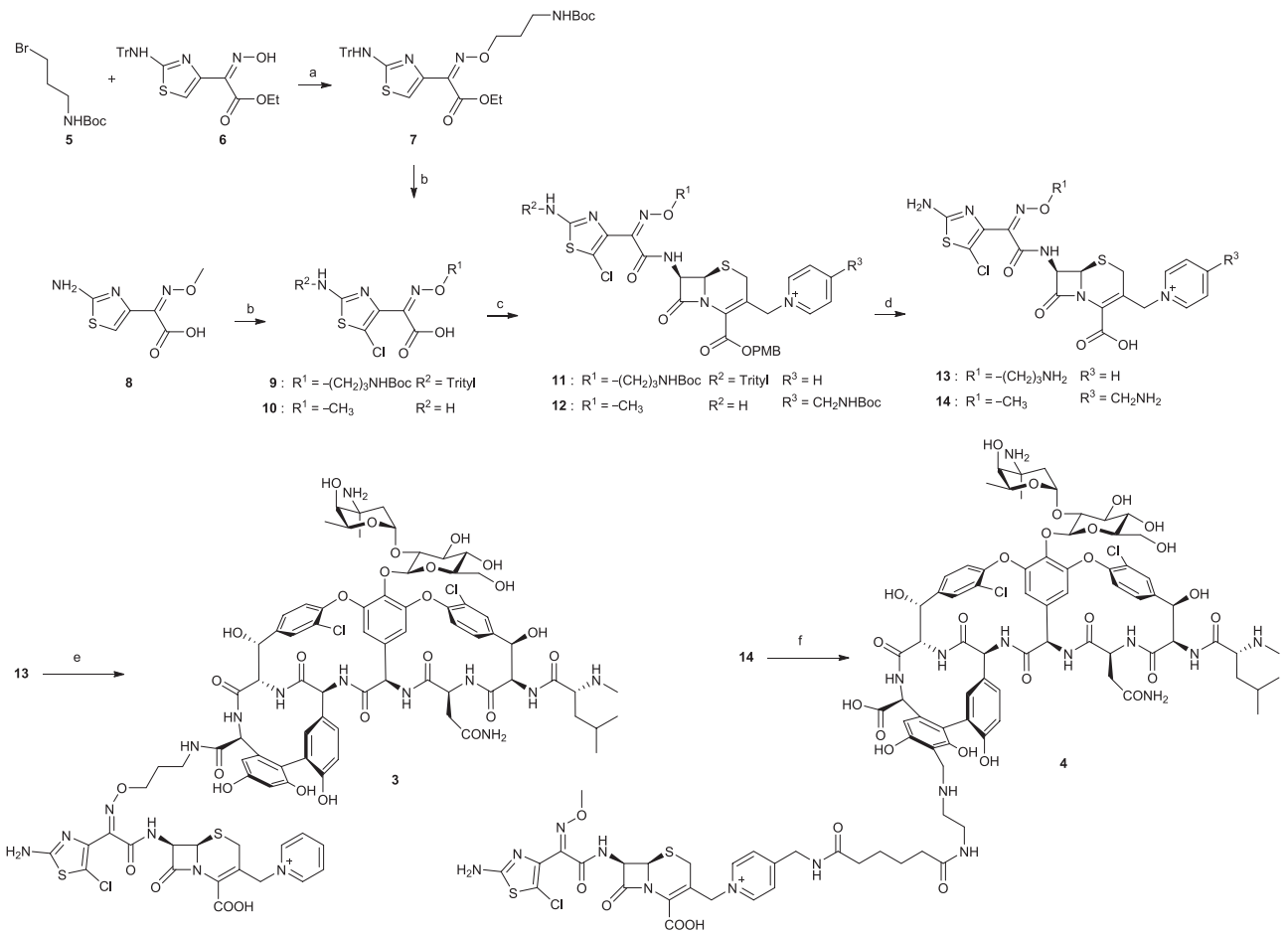

**SCHEME 1 |** Synthesis of VAN hybrids **3** and **4** (Long et al., 2008a). **(a)** $Cs_2CO_3$, tetrabutylammonium iodide, DMF, rt, 2 h. **(b)** for **9**: i. KOH, ethanol, 80°C, 30 min; ii. NCS, $CHCl_3$, rt, overnight; for **10**: NCS, DMF, rt, overnight. **(c)** for **11**: i. ACLE, THF, –45°C, 2,4,6-collidine, $POCl_3$, 10 min; ii. NaI, acetone, $N_2$, rt, 80 min, then pyridine, 150 min; for **12**: i. ACLE, *N*-[3-dimethylaminopropyl]-*N′*-ethylcarbodiimide hydrochloride (EDCI), 2,4,6-collidine, DMF, rt, 2 h; ii. Acetone, NaI, $N_2$, 4-(*N-tert*-butoxycarbonyl)aminomethyl pyridine, rt, 2 h. **(d)** TFA, dichloromethane, anisole, rt, 2–3 h. **(e) 1**, benzotriazol-1-yl-oxytripyrrolidinophosphonium hexafluorophosphate (PyBOP), HOAt, DIPEA, DMSO, DMF, rt, 30 min, then 2,4,6-collidine, 4 h. **(f)** di-HOAt adipic ester, DMF, ice bath, 2,4,6-collidine, 15 min, then the $V_R$ synthon of **1**, DMF, ice bath, 2,4,6-collidine, 20 min.

are one of the most widely used classes in the antibiotic hybrid paradigm (Pham et al., 2019). A dual mechanism against topoisomerase IV and DNA gyrase, which may compensate for any interference shadowed by steric hindrance from a linker (Pokrovskaya and Baasov, 2010) or a second component with suitable attachment sites for bulky partners and stability under different synthetic conditions, are the arguments put forward for the fluoroquinolones (Fedorowicz and Sączewski, 2018).

As previously reported (Ma and Lynch, 2016), open spaces and hence convenient positions for attachments to the C-3 and C-25 positions of rifampin were identified from a co-crystallized structure of rifampin and RNA polymerase. This is further illustrated in **Figure 3** using a recently reported co-crystal structure (Molodtsov et al., 2017). Structure–activity relationships (SARs) from a series of spirorifamycins disclosed that a heterocycle fused with both C-3 and adjacent C-4 of rifamycin can serve as an attachment site for the second partner (Kim et al., 2007). The carbonyl group at C-11 can be used as a conjugation site. Functionalization of the C-11 carbonyl to oxime led to a series of novel 11-deoxy-11-hydroxyiminorifamycin derivatives, with better or equivalent activity against the RNA polymerase of *S. aureus* (Li et al., 2007). Similarly, the C-25 position can be used for attachment of a companion after replacement of the acetyl group with a carbamate. A series of C-25 carbamate rifamycins showed improved antimycobacterial activity and absence of inactivation through ribosylation of C-23 alcohol by ADP-ribosyl transferase of *Mycobacterium smegmatis* (Combrink et al., 2007).

Various matching partners of rifamycins have been explored, with rifamycin–quinolones being the most studied (Ma and Lynch, 2016). SARs from approximately 300 rifamycin–quinolone hybrids revealed that the linker significantly influenced biological activity (Robertson et al., 2008; Klahn and Bronstrup, 2017). Partnering a rifamycin nucleus with a quinazolinone, a bioisostere of quinolone, provided the activity-leading conjugate, called CBR-2092 or TNP-2092 (**15**) (**Figure 4**, Ma and Lynch, 2016). Furthermore, the

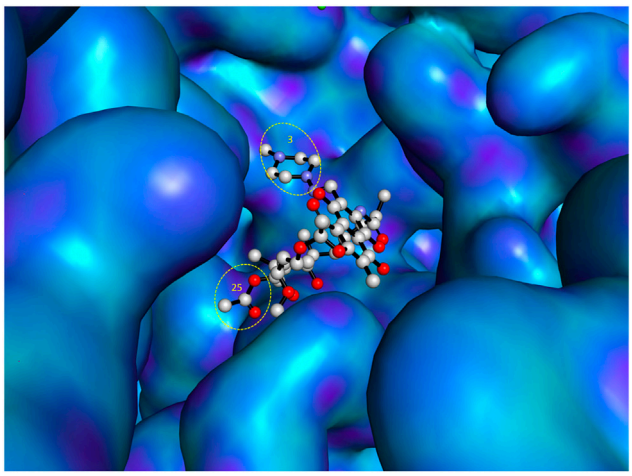

**FIGURE 3 |** Most accessible positions for conjugation in the chemical structure of rifampin. The figure was generated from the crystal structure (Pdb 5UAL) (Molodtsov et al., 2017) using PyMOL (Delano, 2002).

quinazolinone core possesses activity against the ParCS80F variant of topoisomerase IV, the activity that is not retained by ciprofloxacin. This provides an explanation for the activity of **15** against bacterial isolates that are resistant to ciprofloxacin alone or in combination with rifampin (Fisher et al., 2020). In **15**, the C-3 of rifamycin and the C-8 of quinazolinone pharmacophores are bound by a linker that resembles a covalently bound side chain of rifampin and ABT-719 (Ma and Lynch, 2016). The optimal linker in **15** also clamps the binding of rifamycin and quinazolinone motifs to their respective binding sites (Ma and Lynch, 2016).

TNP-2092 was superior to rifampin plus ciprofloxacin in several facets, a credence to hybrid pharmaceuticals in the antibacterial pipeline. 1) In *S. aureus* and coagulase-negative *Staphylococci* (coNS), the main causative agents and major elements of treatment failure in PJI, **15** has multi-targeted activities against RNA polymerase, DNA gyrase, and topoisomerase IV (Robertson et al., 2008; Ma and Lynch, 2016). 2) TNP-2092 is not a substrate for efflux pumps such as NorA or MepA and therefore retains activity against resistance mediated by mutations of the efflux

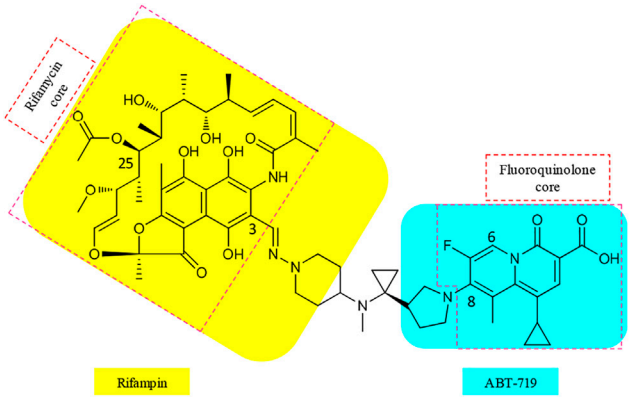


**FIGURE 4 |** Cores and linker in the structure of TNP-2092 (**15**).

system. In addition, the lack of efflux effectively traps **15** within bacteria (Ma and Lynch, 2016). Almost half of fluoroquinolone-resistant strains have enhanced expression of *norA* or *mepA* gene (Robertson et al., 2008). 3) TNP-2092 appears to overcome the antagonism between rifampin and ciprofloxacin (Murillo et al., 2008); in a minimum biofilm bactericidal concentration (MBBC) evaluation, ciprofloxacin plus rifampin exhibited MBBC levels higher than the MBBC values of ciprofloxacin alone in 11 of 40 *S. aureus* and in zero of 40 *S. epidermidis* isolates (Fisher et al., 2020). 4) TNP-2092 showed strong activity against pathogens resistant to its constituents. The difference in MIC values of **15** between the wild-type (CB190) and rifamycin-resistant *S. aureus* (CB370, $rpoB^{H481Y}$) was smaller, unlike 31,250 folds for rifampin. Compound **15** exhibited no activity difference between CB190 and fluoroquinolone-resistant *S. aureus* (CB814, $gyrA^{S84L}$ $ParC^{S80F}$), while nearly 67-fold difference was observed for ciprofloxacin (Robertson et al., 2008). Against rifampin-resistant *S. epidermidis* strains, IDRL-10005 ($rpoB^{D471E}$ $rpoB^{I527Y}$) and IDRL-10692 ($rpoB^{S486F}$), on the other hand, **15** had MIC values of 0.06 and 0.125 μg/ml, respectively; in contrast, rifampin had high MIC values of ≥4 μg/ml, and ciprofloxacin had MIC values of 8 and 1 μg/ml, respectively (Fisher et al., 2020). 5) Safety concerns related to constituent elements such as hERG inhibition and induction of CYP3A4 isoenzyme were not observed in **15** (Ma and Lynch, 2016).

Rifaximin, a member of the rifamycin family and a nonsystemic antibiotic, has been approved for the treatments of travelers' diarrhea, hepatic encephalopathy, and irritable bowel syndrome without constipation (Lexicomp, 2021). Its clinical benefits were thought to be mediated through altered gastrointestinal (GI) microbiota or dysbiosis (Chey et al., 2020). Antibacterial evaluations of **15** against a representative panel of GI bacteria revealed similarities with rifaximin (Yuan et al., 2020). Interestingly, **15** was more active against Gram-negative bacteria such as *E. coli* and *A. baumannii*, which were resistant to rifampin (Ma and Lynch, 2016). The low oral bioavailability of **15**, 1.81% in rats and 0.315% in dogs, can offer additional benefits for local treatment of intestinal diseases (Yuan et al., 2020). The main strategy for the treatment of hepatic encephalopathy, which is closely related to hyperammonemia, is to regulate urease-producing bacteria located in the gut (Liu et al., 2018). Against a panel of urease-producing strains, **15** was more active than rifampin against Gram-negative bacteria such as *Helicobacter pylori* (*H. pylori*) and *Salmonella* strains but lower activity against beneficial commensals such as *B. infantis* and *B. bifidum* (Yuan et al., 2020). TNP-2092 appears to be an attractive candidate for the treatment of the urease-producing *C. difficile*. Compared to the standard treatments of *C. difficile* infections (CDIs), vancomycin and metronidazole, **15** showed superior activity against various isolates of *C. difficile* (Yuan et al., 2020). In addition, following 7 days' treatment with **15**, the changes in the percentage of intestinal microbiota were temporary and generally returned to pretreatment levels. This explains the nonrecurrence of CDIs after treatment with **15** (Yuan et al., 2020). The standard treatments interfere with the intestinal microbiota and are the leading factors for the recurrence of CDIs (Tsutsumi et al., 2014).

The phase 1 study of **15** on tissue distribution, PK, safety, and tolerability in participants undergoing primary total hip replacement or knee arthroplasty is being planned, but

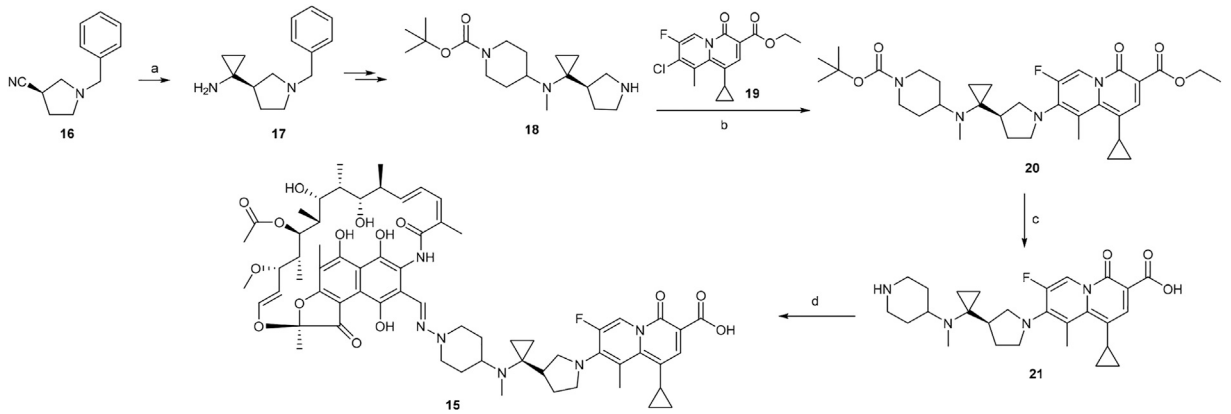


**SCHEME 2 |** Synthesis of rifamycin hybrid **15** (Ma and Lynch, 2016). **(a)** Ti(O-*i*Pr)$_4$, EtMgBr, Et$_2$O/THF, −78°C, 20 min, then Et$_2$O/BF$_3$, rt, 2 h. **(b)** NaHCO$_3$, acetonitrile, reflux, 5 h. **(c)** i. LiOH, ethanol, 60°C, 1 h; ii. TFA, dichloromethane, 0°C to rt, 1 h. **(d)** i. NaOH, H$_2$N–OSO$_3$H, 0°C, 1 h; ii. 3-formyl rifamycin, MeOH/THF, rt, 30 min.

participants have not been recruited yet (NCT04294862, 2021). Nevertheless, the phase 2 study of **15** for the treatment of ABSSSIs was completed in September 2020 (NCT03964493, 2019). TenNor Therapeutics presented "topline" phase 2 results of **15** for the treatment of ABSSSIs at the 2020 China Biomed Innovation and Investment Conference (CBIIC) (TenNor, 2020b). In 2020, the FDA has granted an orphan drug status for the IV use of **15** for the treatment of PJI (PR Newswire, 2020).

## Synthesis of TNP-2092

A scheme suitable for kilogram quantity synthesis of **15** was reported (Ma and Lynch, 2016). The scheme involved an initial five-step synthesis of the linker intermediate **18**, which was subsequently coupled with the fluoroquinolone core **19** under reflux in acetonitrile, to give **20**. The fluoroquinolone-linker motif **20** was further processed *via* hydrolysis of ethyl ester and Boc deprotection to afford **21** using LiOH and TFA, respectively. Eventually, following the conversion of the piperidine moiety in **21** to a hydrazine, **15** was produced by coupling the hydrazine variant of **21** with 3-formyl rifamycin (Ma and Lynch, 2016; Scheme 2).

Besides **15**, TenNor Therapeutics is also developing a conjugate of rifamycin and metronidazole (**Figure 5**), also known as TNP-2198 (**22**). Metronidazole is used to treat infections caused by anaerobic bacteria and is the first-line treatment for bacterial vaginosis (BV) (Jones, 2019). However, the effectiveness of metronidazole against *Gardnerella vaginalis* (GV), the leading cause of BV, is associated with 58% recurrence (Bradshaw et al., 2012). The underlying factor for treatment failure is resistance by biofilms that form a protective shield to reduce the penetration of metronidazole (Ma et al., 2020). Leaving the essential nitroimidazole moiety intact, conjugates of metronidazole (Patel et al., 2021), *via* $N^1$-alkyl or 2-methyl linker or both, with different structural nuclei such as thiomorpholine-1,1-dioxide, have resulted in hybrids with superior activity against metronidazole sensitive as well as resistant *H. pylori* strains (Rossi and Ciofalo, 2020). Accordingly, the pharmacophore of metronidazole, a 5-nitroimidazole motif, was conjugated with rifamycin, an established agent against biofilm-forming pathogens. The resulting **22** showed strong synergistic property against GV (Ma et al., 2020). The MIC value of 0.004 μg/ml of **22** against GV was significantly lower than those of its constituents, with MICs of 4 and 0.5 μg/ml for metronidazole and rifampicin, respectively (Ma et al., 2020). In addition, the spectrum activity of **22** was not limited to GV but also active against other pathogens that can cause BV and other anaerobic bacteria. Apart from a few BV-causing bacteria where equivalent activity was displayed, the MIC values of **22** were 100 to 1,000 folds lower than those of metronidazole (Ma et al., 2020). Very recently, TenNor Therapeutics initiated a phase 1b/2a clinical development of **22** for the treatment of *H. pylori* infection (TenNor, 2020a). Additional clinical development status of **22** is listed in **Table 1**.

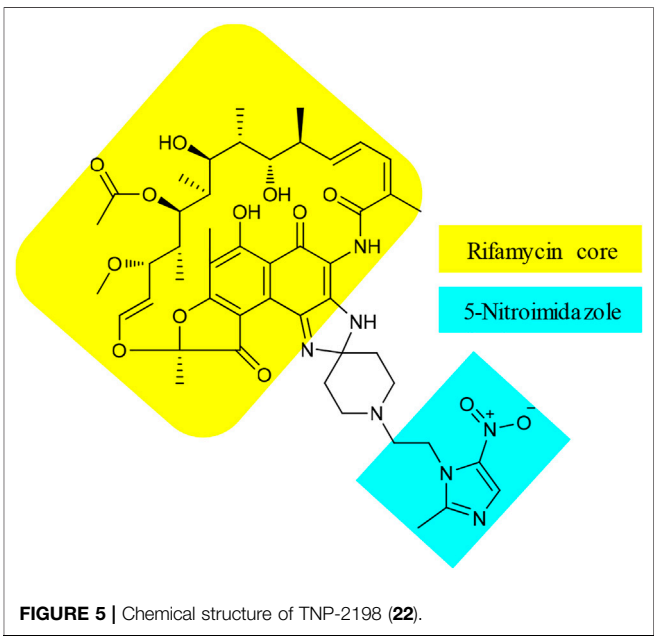


**FIGURE 5 |** Chemical structure of TNP-2198 (**22**).

**TABLE 1 |** Overview and key parameters of clinical macrocycle–antibiotic hybrids.

| Macrocycle hybrid | Molecular weight (Dalton) | miLogP | tPSA | Select $MIC_{90}$ (μg/ml) | Microorganism | *In vivo* $ED_{50}$ (mg/kg) | Half-life (h) | Company | RoA | Clinical development status |
|---|---|---|---|---|---|---|---|---|---|---|
| TD-1792[a] | 1,984.28 | −4.68 | 673.39 | 0.03 | MRSA, hVISA | 0.19 | 1.7 | Theravance biopharma/ R-pharm | IV | Phase 2 completed in 2007 NCT00442832, (2006); phase 3 registered in Russia WHO (2019a) |
| TD-1607[b] | 2,170.49 | −4.98 | 751.81 | 0.008–0.06 | MRSA | 0.11 | N/A | Theravance biopharma/ R-pharm | IV | Phase 1 completed in 2014 NCT01949103, (2013); phase 1b completed in 2013 NCT01791049, (2013) |
| TNP-2092[c] | 1,205.39 | 5.85 | 282.18 | 0.015 | MSSA, MRSA | 1.4–3.8 | 0.4–4.1 | TenNor therapeutics | IV | Phase 1 for PJI (not yet recruiting) NCT04294862, (2021); phase 2 for ABSSSIs completed NCT03964493, (2019) |
| | | | | | | | | | PO | Phase 2 ongoing in China |
| | | | | | | | | | Topical | Preclinical development |
| TNP-2198[d] | 944.05 | 2.70 | 269.21 | 0.004 | GV | N/A | N/A | TenNor therapeutics | PO | Phase 1b/2a ongoing in China |
| DSTA4637S[e] | 149 kDa (DSTA4637A TAb); 927.06 (dmDNA31) | 4.30 (dmDNA31) | 230.67 (dmDNA31) | 0.004 μM (dmDNA31) | MRSA (USA300) | N/A | 16.5–21.5 days | Genentech, Inc./ Roche | IV | Phase 1 completed in 2016 NCT02596399, (2015) Phase 1b completed in 2020 NCT03162250, (2017) |

*MiLogP: the logP prediction developed at Molinspiration. tPSA: topological polar surface area. Both miLogP and tPSA values were calculated using Molinspiration cheminformatics (https://www.molinspiration.com/). RoA: route of administration; N/A: not available.*

[a]*MIC value (Blais et al., 2012); in vivo $ED_{50}$ value (Long et al., 2008a); terminal half-life in mice (Hegde et al., 2012).*

[b]*MIC value (Sader et al., 2014); in vivo $ED_{50}$ value (Long et al., 2008a).*

[c]*MIC value, in vivo $ED_{50}$, and plasma half-life (Ma and Lynch, 2016); IV for medical device associated bacterial biofilm infections, PO for hepatic encephalopathy and irritable bowel symptom diarrhea, topical for superbugs and diabetic foot infection (TenNor Therapeutics, 2021).*

[d]*MIC value (Ma et al., 2020); PO for H. pylori and other anaerobic bacterial infections (TenNor Therapeutics, 2021).*

[e]*MIC value (Lehar et al., 2015); mean half-life of DSTA4637S TAb from phase 1 clinical trial (Peck et al., 2019).*

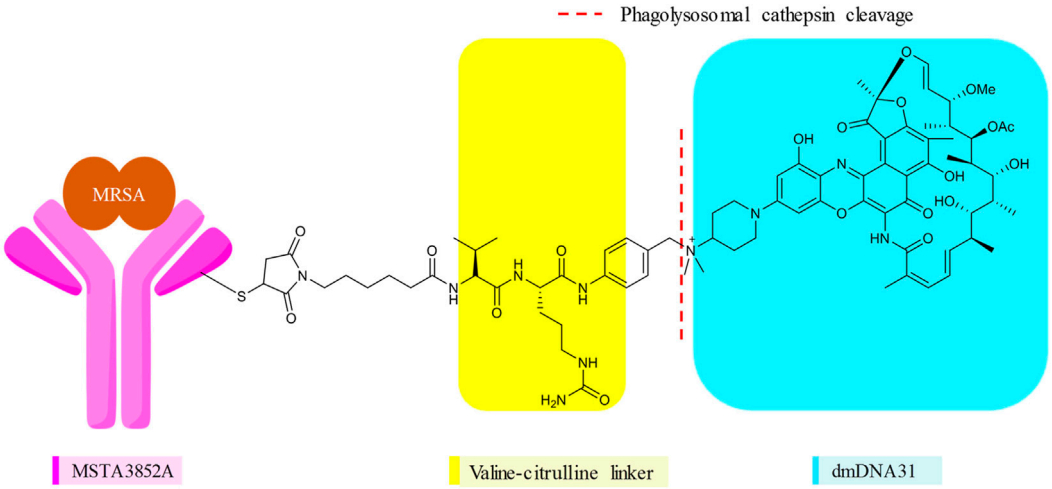


**FIGURE 6 |** Monoclonal antibody, linker, and the antibiotic of DSTA4637S (**23**).

Antibody–antibiotic conjugation (AAC), in addition to the antibiotic-antibiotic hybrids mentioned above, is practiced for the conjugation of rifamycins. The antibody–drug conjugate (ADC) is mainly used in cancer immunotherapy, to selectively deliver a cytotoxic warhead using a labeling antibody bound *via* a linker (Beck et al., 2017). In 2015, the extension of ADC to the treatment of bacterial infections caused by *S. aureus* was first coined by Lehar et al. (2015). The infamous *S. aureus* is able to survive the wrath of antibiotics by internalizing into phagocytes (Fraunholz and Sinha, 2012). This intracellular reservoir has enabled long-term colonization of a host and promoted development of resistance, which explains the recurrences associated with invasive *S. aureus* infections (Lehar et al., 2015; Peyrusson et al., 2020). Despite available appropriate treatments, *S. aureus* remains a leading cause of death related to bacterial infections, with mortality rates of around 20–30% (Yilmaz et al., 2016). A new strategy capable of effectively eliminating the responsible intracellular foci of *S. aureus* was needed. As such, a novel AAC platform, THIOMAB™ antibody–antibiotic conjugate (TAC), was utilized to target the intracellular *S. aureus*. DSTA4637S (**23**) (**Figure 6**) is a novel conjugate of an antibiotic with an anti–*S. aureus* antibody, which represents the first AAC in this class under clinical development (Lehar et al., 2015; Mariathasan and Tan, 2017; Poreba, 2020). Mechanistically, the large-sized **23** cannot diffuse into mammalian cells. In systemic circulation and tissues, the antibody directs the binding of the conjugate to *S. aureus*, enabling the uptake of appended bacteria into phagocytes *via* opsonization (Cai et al., 2020). The linker is cleaved by cathepsins inside the phagolysosome to release the active antibiotic that can eliminate the conjugate bound and other existing bacteria (Lehar et al., 2015; Cai et al., 2020).

In DSTA4637S, an artificially engineered monoclonal antibody MSTA3852A against *S. aureus* from human immunoglobulin (IgG1) and 4-dimethylaminopiperidino-hydroxybenzoxazino rifamycin, dmDNA31 (rifalogue), are linked by a protease cleavable valine–citrulline (vc) linker (Lehar et al., 2015; Poreba, 2020). MSTA3852A was selected from >40 anti–*S. aureus* antibodies that originated from the blood of patients recovering from different *S. aureus* infections. The highest level of binding by those antibodies was directed against a major component in the cell wall of *S. aureus*, the wall-teichoic acids (WTAs) (Lehar et al., 2015; Deng et al., 2019).

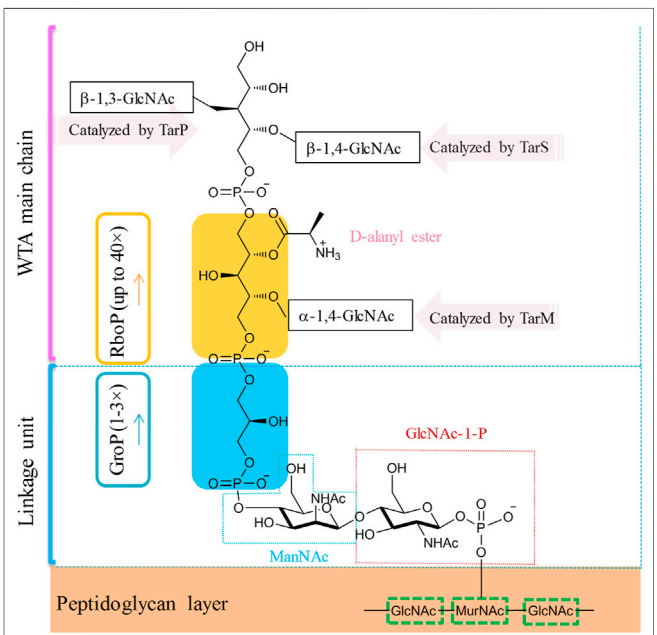


**FIGURE 7 |** Simplified molecular structure of the WTA of common *S. aureus*.

In the majority of *S. aureus* lineages, WTA is composed of up to 40 repeating units of ribitol phosphate (RboP) that are

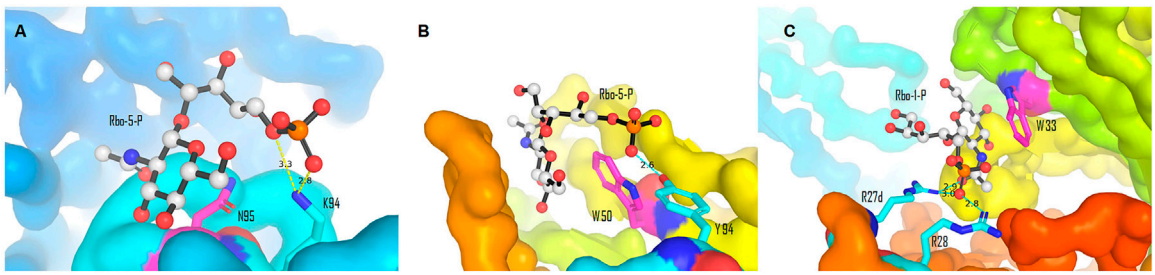


**FIGURE 8 |** Binding interactions between the β-WTA mimic and anti–*S. aureus* antibodies. **(A)** Stacking and ionic interactions between antibody 4462 and Rbo-5-P (Pdb 6DWI). **(B)** Interactions between antibody 6078 and Rbo-5-P (Pdb 6DW2). **(C)** Arginine "tweezers" motif (Pdb 5D6C). Pictures **(A)**–**(C)** were generated from reported Pdb files (Lehar et al., 2015; Fong et al., 2018) using PyMOL (Delano, 2002).

covalently linked to the *N*-acetylmuramic acid (MurNAc) residue of the peptidoglycan layer by a short polysaccharide anchor unit (**Figure 7**, Weidenmaier and Peschel, 2008; Fong et al., 2018). The anchor unit is composed of glycerol-phosphate (GroP) units (1–3×), *N*-acetyl-D-mannosamine (ManNAc), and *N*-acetyl-D-glucosamine-1-phosphate (GlcNAc-1-P) (Winstel et al., 2014). RboP can be modified with α- or β-*O*-linked *N*-acetyl-D-glucosamine (α/β-*O*-GlcNAc) residues and D-alanine. Those modifications were reported to be essential for developing resistance to methicillin and cationic antimicrobial peptides (Brown et al., 2012). In MRSA strains, modifications with β-1,4-GlcNAc and α-1,3-GlcNAc are catalyzed by glycotransferases TarS and TarM, respectively (Brown et al., 2012; van Dalen et al., 2019). Recently, Gerlach et al. have identified an alternative glycotransferase for MRSA, TarP, which catalyzes the glycosylation of β-1,3-GlcNAc on WTA (Gerlach et al., 2018). This alternative glycan modification was poorly immunogenic and sabotaged the recognition by host antibodies (Gerlach et al., 2018). WTAs are promising antigens being pursued for the development of novel vaccines against MRSA (van Dalen et al., 2019).

The majority of the host anti–*S. aureus* antibodies target β-1,4-GlcNAc, followed by β-1,3-GlcNAc, and few antibodies are reactive to α-1,4-GlcNAc, albeit the underlying reason is not fully understood (van Dalen et al., 2020). The binding pattern between antibodies and β-WTA was then characterized by co-crystallizing the Fab fragment of anti–β-WTA antibodies with a minimal synthetic repeat of β-WTA, a β-glycosidic bonded unit between ribitol-1-phosphate (Rbo-1-P) or ribitol-5-phosphate (Rbo-5-P) and GlcNAc (Lehar et al., 2015; Fong et al., 2018). Antibodies displayed a conserved mechanism to specifically recognize the β-anomer mimic, albeit different residues were involved in different antibodies (Fong et al., 2018). In the co-crystal structures of antibody 4462 or 6078, for example, the pyranose ring of GlcNAc of the mimic was stacked against the amide chain of N95 or the indole side chain of W50, respectively (**Figure 8**, Fong et al., 2018). In antibody 4462, the C-5 phosphate of the WTA mimic formed ionic interactions with K94 (**Figure 8A**). Similarly, the interaction between the 5-phosphate and Y94 in antibody 6078 was indicated for selectivity to β-linked GlcNAc (**Figure 8B**, Fong et al., 2018). Lehar et al., using a co-crystal structure of antibody 4497 with 1-phosphoribitol β-WTA, also revealed an arginine "tweezers" motif by Arg27d and 28 that dictated the β-anomer–specific recognition *via* triangulation of the ribitol phosphodiester backbone in relation to the GlcNAc moiety (**Figure 8C**, Lehar et al., 2015).

Various features of rifalogue (dmDNA31) were considered in the selection of the payload for anti–*S. aureus* antibody 4497. dmDNA31 had an MIC value of $4 \times 10^{-9}$ M against MRSA (USA300), with effective killing property against these well-recognized persister cells (Lehar et al., 2015). Persister cells are dormant, nonreplicating bacteria with a high level of tolerance to antibiotics. Nondividing MRSA isolates inside macrophages were effectively eliminated by dmDNA31 (Lehar et al., 2015). Moreover, dmDNA31 conjugate was inactive against extracellular bacteria, indicating the safety of the conjugate (Shopsin et al., 2016).

V112C mutagenesis of the antibody MSTA3852A, in which a valine in the light chain IgG1 is precisely replaced by a reactive cysteine residue, enables site-specific conjugation with a drug–antibody ratio (DAR) of two vc-dmDNA31 per antibody (Deng et al., 2019). Site-specific conjugation in ADC enables a direct and homogeneous conjugation of a drug (Zhou, 2017). Stochastic or random conjugation, on the other hand, often leads to heterogeneous products, with each subtype having different PK properties, efficacy, and safety profiles. In stochastic conjugates, there are also concerns about higher DAR, which are relatively more active *in vitro*, less tolerated, and exhibit rapid elimination than conjugates with lower DAR (Gauzy-Lazo et al., 2020). THIOMAB™ is one such site-specific conjugation technology that led to **23** (Lehar et al., 2015; Wang-Lin and Balthasar, 2018; Gauzy-Lazo et al., 2020). The linker in **23** will be cleaved within minutes following the entry of the opsonized *S. aureus*, and when tested inside human macrophages, epithelial and endothelial cells, AAC-opsonized MRSA isolates were killed in all cases (Lehar et al., 2015). In an intravenous mice infection model, the efficacy of **23** was superior than that of **1**. The efficacy of **1** declined when administered after 7–24 h of infections, suggesting the failure of **1** due to the internalization of MRSA into host cells (Lehar et al., 2015). After 24 h of infection, a single dose of TAC was effective and superior to the twice-daily dose of **1** (Lehar et al., 2015).

The preclinical PK properties of TAC **23** were profiled in mice, rats, and cynomolgus monkey (Zhou et al., 2016; Deng et al., 2019). The PK profiling of TAC involved the analysis of three analytes: TAC total antibody (TAb) which includes fully conjugated (DAR 2), partially conjugated (DAR 1), and unconjugated antibodies (Zhou et al., 2016). The PK properties of typical monoclonal antibody-based therapeutics, that is, short distribution, slow clearance, and long half-life, were demonstrated by DSTA4637A (the preclinical liquid formulation of **23**) in various *in vivo* animal studies (Zhou et al., 2016; Deng et al., 2019). In mice, the conjugation extended the half-life (~3–4 h) of unconjugated dmDNA31 to 4 days in ac-dmDNA31. A similar clearance between **23** and the unconjugated antibody in mice indicated the conjugation of dmDNA31 had relatively little effect on the clearance of the TAb (Zhou et al., 2016). Comparable PK properties of DSTA4637A TAb and MSTA3852A were also found in rats and monkey (Deng et al., 2019). Three main reasons can explain the similar PK profiles between DSTA4637A and MSTA3852A. First, conjugates with a DAR of 2–4 generally have slower clearance rates and longer half-lives than conjugates with a higher DAR (Deng et al., 2019). Second, THIOMAB™ technology allows uniform conjugation on the engineered cysteine without disrupting the inter-disulfide bonds in the antibody (Sussman et al., 2018), and therefore minimal PK changes after conjugation. Third, drug loading and hydrophobicity are factors that cause significant changes in PK properties (Kamath and Iyer, 2016). The hydrophilic property of dmDNA31 is expected to slow down clearance and extend the half-life of **23** (Deng et al., 2019). A minimal physiologically based PK model in mice indicated a low level of drug interactions between DSTA4637A and cytochrome P450 substrates. This model of PK disposition also indicated the liver and spleen, where phagocytes are usually accumulated, may contain high concentrations of dmDNA31 (Wang-Lin et al., 2018).

Preclinical safety evaluations with high doses of **23**, up to 250 and 500 mg/kg in monkeys and rats, respectively, were well tolerated (Deng et al., 2019). In 2019, the results of the phase 1 investigations on the safety, PK, and immunogenicity in healthy volunteers were published, which showcased the favorable profiles of **23** for human use (NCT02596399, 2015; Peck et al., 2019). No serious adverse effects were observed in the dose range between 5 and 150 mg/kg; no clinically significant changes in laboratory or vital signs or antibody responses induced by **23** were observed (Peck et al., 2019). Therefore, further clinical development of **23** for *S. aureus* infections is expected following these favorable safety and PK profiles in human volunteers (Peck et al., 2019).

## LIMITATIONS AND WAYS FORWARD IN MACROCYCLE-ANTIBIOTIC HYBRID APPROACH

The increase in molecular weight is a major limitation of the antibiotic hybrid approach. The resulting low oral bioavailability of such conjugates may impede oral dosage formulations for systemic applications (Gupta and Datta, 2019). However, this opens the door to selectivity and efficacy for local treatments of gut and liver diseases (Ma and Lynch, 2016). In addition, given that the structure of the outer membrane (OM) in the cell wall of Gram-negative bacteria is well designed for intrinsic resistance to various antibacterial agents, the high molecular weight of antibiotic hybrids is also detrimental to their activity against Gram-negative microorganisms. Moreover, the hydration sphere, created by hydrophilic carbohydrates, and the reduced fluidity caused by efficient packing of the lipid component restrict the passage of hydrophobic molecules across the OM (Domalaon et al., 2018). What remains is a passage through unspecific, barrel-shaped protein channels called porins. Nevertheless, only small molecules with a molecular weight of ≤600 g/mol are more favorable to pass the molecular sieve imposed by the porins (Vergalli et al., 2020). Fortunately, some antibiotics with a molecular weight of >600 g/mol, such as polymyxins, are able to pass through OM *via* various uptake mechanisms (e.g., self-promoted entry) (Moubareck, 2020). Agents of this nature are capable of disturbing the electrostatic interactions between the divalent cations such as $Mg^{2+}$ or $Ca^{2+}$ and phosphate groups in the lipid, thereby creating a passage through (Deris et al., 2014). Further clarifications of the structural or physicochemical criteria for self-promoted mechanism can extend the antibacterial spectrum of macrocycle-antibiotic hybrids against Gram-negative organisms (Domalaon et al., 2018).

Pioneered by cefiderocol, a cephalosporin siderophore antibiotic approved by the U.S. FDA in November 2019 (Lexicomp, 2021), antibiotic–siderophore conjugates represent an attractive antibiotic hybrid class by conjugating iron-chelating microbial siderophores with an antibiotic to facilitate uptake and antibacterial efficacy (Schalk, 2018; Negash et al., 2019). Specifically, a macrocycle siderophore hybrid, involving the conjugation of a macrocyclic antibiotic with a microbial siderophore or a siderophore mimetic, may overcome the penetration issue to pass through the OM of Gram-negative bacteria. Siderophores benefit bacteria by dissolving and importing iron (Ji et al., 2012). Conjugating with a siderophore can facilitate the entry of the corresponding hybrid through a ferri-siderophore uptake pathway that internalizes iron by an active transport mechanism, that is, a Trojan horse mechanism (Schalk, 2018). Similarly, a self-promoted passage through means of polymyxins can be exploited to force the entry of macrocycle polymyxin conjugates (Negash et al., 2019). Conjugation with polymyxins can not only extend activity against Gram-negative bacteria but also retain activity against resistance mechanism involving overexpression of efflux pumps as well (Negash et al., 2019). Various other hybrid chemical entities have also been reported, including polymyxin B3-tobramycin hybrids with *Pseudomonas eruginosa*–selective antibacterial activity and strong potentiation of rifampicin, minocycline, and vancomycin (Domalaon et al., 2017), azithromycin–benzoxaborole hybrid derivatives (Tevyashova et al., 2019), as well as antitubercular rifampicin and clofazimine hybrid (Saravanan et al., 2021). Very recently, design and synthesis of vitamin B12–antibiotic conjugates led to advanced candidates with >500-fold improved activity against Gram-negative bacteria including *E. coli*, relative to ampicillin, demonstrating that the vitamin B12 conjugate strategy is effective for enabling cellular uptake and antibiotic delivery, thus

improving antibacterial efficacy (Zhao et al., 2020). Furthermore, among numerous elegant examples by the Schweizer group (Gorityala et al., 2016a; Gorityala et al., 2016b; Yang et al., 2017; Domalaon et al., 2019), the use of antibiotic hybrids as adjuvants such as nebramine-based hybrids (Yang et al., 2019) and lysine-tobramycin conjugates (Lyu et al., 2019) has potentiated the activities of current existing antibiotics including rifampicin and erythromycin, respectively. Similarly, rifamycin–tobramycin conjugate adjuvants were able to break intrinsic resistance of *Pseudomonas aeruginosa* to tetracyclines and chloramphenicol (Idowu et al., 2019).

Some key questions remain to be answered despite the progress and new advances of antibiotic hybrids to clinical development (Domalaon et al., 2018), highlighting the potential to burgeon the antibacterial pipeline. Structure-based drug design, exemplified by X-ray co-crystal studies and molecular modeling, is among techniques capable of ameliorating the way forward of antibiotic hybrids. For example, the co-crystal structure of rifampin with RNA polymerase has highlighted steric-free sites of attachments for conjugates, *vide supra* (Ma and Lynch, 2016; Molodtsov et al., 2017). In addition, TenNor Therapeutics very recently presented the outcome of their phase 2 clinical trial of TNP-2092 and disclosed the co-crystal structure of TNP-2092 bound with bacterial RNA polymerase, along with its interaction with DNA, at the 2020 CBIIC, which was held in Suzhou, China, in September 2020 (TenNor, 2020b). Computational strategies were also applied in the design of promising hybrids which are in the early stage of development. For example, in the design of macrocyclic peptide–peptoid hybrids, the crystal structure of the chemokine receptor CXCR4 was used as a template for the homology model of CXCR7 (Boehm et al., 2017). Besides identifying residues important for activity, binding poses from an induced fit docking also spotted spaces in the CXCR7 model that are not occupied by the macrocycle peptide (Boehm et al., 2017). Virtual tools also facilitated the design of VAN–nicin conjugates, by predicting the optimal length of the linker and suitable attachment sites (Arnusch et al., 2008). Nicin is an antimicrobial peptide that binds to lipid II and inhibits the transglycosylation step in the cell wall biosynthesis (Le et al., 2017). Although each has different modes of action, lipid II is targeted by both VAN and nicin. Predicting the optimal spacer and sites of connection was essential to place the constituting elements to their respective binding sites in lipid II (Olsufyeva and Tevyashova, 2017). Computationally guided design of VAN–nicin hybrids led to promising derivatives, with the most active hybrid displaying a 40-fold higher activity than VAN or nicin (Arnusch et al., 2008).

Besides activity profiling, virtual tools depending on prior knowledge or machine learning may enable prediction of specificity, solubility, permeability, and general toxicity of hybrids (Mulligan, 2020; Zin et al., 2020). Prediction of physical properties using molecular dynamics, a computer simulation of the movement of a molecule surrounded by water, may provide a more unbiased model than tools dependent on a database of a large number of compounds with known properties (Mulligan, 2020). Efficient and reliable computational tools for predicting physicochemical properties such as permeability can be essential in the design of macrocyclic hybrids. Macrocycles and their antibiotic hybrids/conjugates are generally considered poor drug-like compounds and often violate desirable parameters for orally bioavailable drug molecules (Lipinski et al., 1997; Zin et al., 2020). Diverse functionalization strategies of macrocycles can modulate physicochemical properties by changing the rigidity, conformation, and basicity of the macrocycle core and/or its side chain (Mallinson and Collins, 2012). In addition, the decrease in degree of freedom by macrocyclization may improve cell permeability of macrocycles (Dougherty et al., 2019). A recent study demonstrated modulation of scaffold rigidity to engineer favorable ADME properties in macrocyclic peptides (Furukawa et al., 2020). Finally, drug design strategies, such as *N*-methylation or replacing NH with sulfur (or vice versa), were found to improve pharmacological activity, solubility, and/or permeability of macrocycles (Mallinson and Collins, 2012; Liras and McClure, 2019; Stadelmann et al., 2020; Buckton et al., 2021). Extending studies of this nature to macrocyclic hybrids is expected to improve their oral bioavailability for systemic uses.

## AUTHOR CONTRIBUTIONS

ASS and DS designed and prepared the manuscript, and critically reviewed and approved the submission of the final version of the manuscript.

## FUNDING

This work was supported in part by Leahi Fund to Treat and Prevent Pulmonary Diseases of the Hawai'i Community Foundation (19ADVC-95335).

## REFERENCES

Adis Insight (2020). *Cefilavancin - Theravance Biopharma*. Springer Nature. Available: https://adisinsight.springer.com/drugs/800020586 (Accessed January 11, 2021).

Arnusch, C. J., Bonvin, A. M. J. J., Verel, A. M., Jansen, W. T. M., Liskamp, R. M. J., de Kruijff, B., et al. (2008). The Vancomycin–Nisin(1–12) Hybrid Restores Activity against Vancomycin Resistant Enterococci. *Biochemistry* 47, 12661–12663. doi:10.1021/bi801597b

Aslam, B., Wang, W., Arshad, M. I., Khurshid, M., Muzammil, S., Rasool, M. H., et al. (2018). Antibiotic Resistance: a Rundown of a Global Crisis. *Infect. Drug Resist.* 11, 1645–1658. doi:10.2147/IDR.S173867

Aubry-Damon, H., Soussy, C.-J., and Courvalin, P. (1998). Characterization of Mutations in the *rpoB* Gene that Confer Rifampin Resistance in *Staphylococcus aureus*. *Antimicrob. Agents Chemother.* 42, 2590–2594. doi:10.1128/AAC.42.10.2590

Beck, A., Goetsch, L., Dumontet, C., and Corvaïa, N. (2017). Strategies and Challenges for the Next Generation of Antibody-Drug Conjugates. *Nat. Rev. Drug Discov.* 16, 315–337. doi:10.1038/nrd.2016.268

Berbari, E. F., Baddour, L. M., and Chen, A. F. (2020). "Prosthetic Joint Infection: Treatment," in *UpToDate*. Editors D. Spelman and E. L. Baron (Waltham, MA: Wolters Kluwer). https://www.uptodate.com/contents/prosthetic-joint-infection-treatment (Accessed December 21, 2021).

Blais, J., Lewis, S. R., Krause, K. M., and Benton, B. M. (2012). Antistaphylococcal Activity of TD-1792, a Multivalent Glycopeptide-Cephalosporin Antibiotic. *Antimicrob. Agents Chemother.* 56, 1584–1587. doi:10.1128/AAC.05532-11

Blaskovich, M. A. T., Hansford, K. A., Butler, M. S., Jia, Z., Mark, A. E., and Cooper, M. A. (2018). Developments in Glycopeptide Antibiotics. *ACS Infect. Dis.* 4, 715–735. doi:10.1021/acsinfecdis.7b00258

Boehm, M., Beaumont, K., Jones, R., Kalgutkar, A. S., Zhang, L., Atkinson, K., et al. (2017). Discovery of Potent and Orally Bioavailable Macrocyclic Peptide-Peptoid Hybrid CXCR7 Modulators. *J. Med. Chem.* 60, 9653–9663. doi:10.1021/acs.jmedchem.7b01028

Bradshaw, C. S., Vodstrcil, L. A., Hocking, J. S., Law, M., Pirotta, M., Garland, S. M., et al. (2012). Recurrence of Bacterial Vaginosis Is Significantly Associated with Posttreatment Sexual Activities and Hormonal Contraceptive Use. *Clin. Infect. Dis.* 56, 777–786. doi:10.1093/cid/cis1030

Brown, E. D., and Wright, G. D. (2016). Antibacterial Drug Discovery in the Resistance Era. *Nature* 529, 336–343. doi:10.1038/nature17042

Brown, G. R. (2014). Cotrimoxazole - Optimal Dosing in the Critically Ill. *Ann. Intensive Care* 4, 13. doi:10.1186/2110-5820-4-13

Brown, S., Xia, G., Luhachack, L. G., Campbell, J., Meredith, T. C., Chen, C., et al. (2012). Methicillin Resistance in *Staphylococcus aureus* Requires Glycosylated Wall Teichoic Acids. *Proc. Natl. Acad. Sci. U S A.* 109, 18909–18914. doi:10.1073/pnas.1209126109

Buckton, L. K., Rahimi, M. N., and McAlpine, S. R. (2021). Cyclic Peptides as Drugs for Intracellular Targets: The Next Frontier in Peptide Therapeutic Development. *Chem. Eur. J.* 27, 1487–1513. doi:10.1002/chem.201905385

Butler, M. S., and Paterson, D. L. (2020). Antibiotics in the Clinical Pipeline in October 2019. *J. Antibiot.* 73, 329–364. doi:10.1038/s41429-020-0291-8

Cai, H., Yip, V., Lee, M. V., Wong, S., Saad, O., Ma, S., et al. (2020). Characterization of Tissue Distribution, Catabolism, and Elimination of an Anti-*Staphylococcus aureus* THIOMAB Antibody-Antibiotic Conjugate in Rats. *Drug Metab. Dispos.* 48, 1161–1168. doi:10.1124/dmd.120.000092

CDC (2019). *Antibiotic Resistance Threats in the United States, 2019*. Atlanta, GA: U.S. Department of Health and Human Services, Centers for Disease Control and Prevention. Available: https://www.cdc.gov/drugresistance/pdf/threats-report/2019-ar-threats-report-508.pdf (Accessed January 27, 2021).

Chey, W. D., Shah, E. D., and DuPont, H. L. (2020). Mechanism of Action and Therapeutic Benefit of Rifaximin in Patients with Irritable Bowel Syndrome: a Narrative Review. *Ther. Adv. Gastroenterol.* 13, 175628481989753–16. doi:10.1177/1756284819897531

Combrink, K. D., Denton, D. A., Harran, S., Ma, Z., Chapo, K., Yan, D., et al. (2007). New C25 Carbamate Rifamycin Derivatives Are Resistant to Inactivation by ADP-Ribosyl Transferases. *Bioorg. Med. Chem. Lett.* 17, 522–526. doi:10.1016/j.bmcl.2006.10.016

Delano, W. L. (2002). *The PyMOL Molecular Graphics System*. San Carlos, CA, USA: Delano Scientific.

Deng, R., Zhou, C., Li, D., Cai, H., Sukumaran, S., Carrasco-Triguero, M., et al. (2019). Preclinical and Translational Pharmacokinetics of a Novel THIOMAB Antibody-Antibiotic Conjugate against *Staphylococcus aureus*. *mAbs* 11, 1162–1174. doi:10.1080/19420862.2019.1627152

Deris, Z. Z., Swarbrick, J. D., Roberts, K. D., Azad, M. A. K., Akter, J., Horne, A. S., et al. (2014). Probing the Penetration of Antimicrobial Polymyxin Lipopeptides into Gram-Negative Bacteria. *Bioconjug. Chem.* 25, 750–760. doi:10.1021/bc500094d

Domalaon, R., Ammeter, D., Brizuela, M., Gorityala, B. K., Zhanel, G. G., and Schweizer, F. (2019). Repurposed Antimicrobial Combination Therapy: Tobramycin-Ciprofloxacin Hybrid Augments Activity of the Anticancer Drug Mitomycin C against Multidrug-Resistant Gram-Negative Bacteria. *Front. Microbiol.* 10, 1556. doi:10.3389/fmicb.2019.01556

Domalaon, R., Idowu, T., Zhanel, G. G., and Schweizer, F. (2018). Antibiotic Hybrids: the Next Generation of Agents and Adjuvants against Gram-Negative Pathogens?. *Clin. Microbiol. Rev.* 31, e00077-17. doi:10.1128/CMR.00077-17

Domalaon, R., Yang, X., Lyu, Y., Zhanel, G. G., and Schweizer, F. (2017). Polymyxin B3-Tobramycin Hybrids with *Pseudomonas Aeruginosa*-Selective Antibacterial Activity and Strong Potentiation of Rifampicin, Minocycline, and Vancomycin. *ACS Infect. Dis.* 3, 941–954. doi:10.1021/acsinfecdis.7b00145

Dougherty, P. G., Sahni, A., and Pei, D. (2019). Understanding Cell Penetration of Cyclic Peptides. *Chem. Rev.* 119, 10241–10287. doi:10.1021/acs.chemrev.9b00008

East, S. P., and Silver, L. L. (2013). Multitarget Ligands in Antibacterial Research: Progress and Opportunities. *Expert Opin. Drug Discov.* 8, 143–156. doi:10.1517/17460441.2013.743991

Eliopoulos, G. M., and Huovinen, P. (2001). Resistance to Trimethoprim-Sulfamethoxazole. *Clin. Infect. Dis.* 32, 1608–1614. doi:10.1086/320532

Faron, M. L., Ledeboer, N. A., and Buchan, B. W. (2016). Resistance Mechanisms, Epidemiology, and Approaches to Screening for Vancomycin-Resistant *Enterococcus* in the Health Care Setting. *J. Clin. Microbiol.* 54, 2436–2447. doi:10.1128/jcm.00211-16

Fatheree, P. R., Linsell, M. S., Marquess, D. G., Trapp, S. G., Moran, E. J., and Aggen, J. B. (2005). *Cross-linked Glycopeptide-Cephalosporin Antibiotics*. International Patent Application WO 2005/005436 A2. *January* 20, 2005.

Fedorowicz, J., and Sączewski, J. (2018). Modifications of Quinolones and Fluoroquinolones: Hybrid Compounds and Dual-Action Molecules. *Monatsh. Chem.* 149, 1199–1245. doi:10.1007/s00706-018-2215-x

Fisher, C. R., Schmidt-Malan, S. M., Ma, Z., Yuan, Y., He, S., and Patel, R. (2020). *In vitro* activity of TNP-2092 against Periprosthetic Joint Infection-Associated *Staphylococci*. *Diagn. Microbiol. Infect. Dis.* 97, 115040. doi:10.1016/j.diagmicrobio.2020.115040

Fong, R., Kajihara, K., Chen, M., Hotzel, I., Mariathasan, S., Hazenbos, W. L. W., et al. (2018). Structural Investigation of human *S. aureus*-Targeting Antibodies that Bind Wall Teichoic Acid. *MAbs* 10, 1–13. doi:10.1080/19420862.2018.1501252

Fraunholz, M., and Sinha, B. (2012). Intracellular *Staphylococcus aureus*: Live-in and let die. *Front. Cell Infect. Microbiol.* 2, 43. doi:10.3389/fcimb.2012.00043

Furukawa, A., Schwochert, J., Pye, C. R., Asano, D., Edmondson, Q. D., Turmon, A. C., et al. (2020). Drug-Like Properties in Macrocycles above MW 1000: Backbone Rigidity versus Side-Chain Lipophilicity. *Angew. Chem. Int. Ed. Engl.* 59, 21571–21577. doi:10.1002/anie.202004550

Gauzy-Lazo, L., Sassoon, I., and Brun, M.-P. (2020). Advances in Antibody-Drug Conjugate Design: Current Clinical Landscape and Future Innovations. *SLAS Discov.* 25, 843–868. doi:10.1177/2472555220912955

Gerlach, D., Guo, Y., De Castro, C., Kim, S.-H., Schlatterer, K., Xu, F.-F., et al. (2018). Methicillin-resistant *Staphylococcus aureus* Alters Cell Wall Glycosylation to Evade Immunity. *Nature* 563, 705–709. doi:10.1038/s41586-018-0730-x

Gorityala, B. K., Guchhait, G., Fernando, D. M., Deo, S., McKenna, S. A., Zhanel, G. G., et al. (2016a). Adjuvants Based on Hybrid Antibiotics Overcome Resistance in *Pseudomonas aeruginosa* and Enhance Fluoroquinolone Efficacy. *Angew. Chem. Int. Ed.* 55, 555–559. doi:10.1002/anie.201508330

Gorityala, B. K., Guchhait, G., Goswami, S., Fernando, D. M., Kumar, A., Zhanel, G. G., et al. (2016b). Hybrid Antibiotic Overcomes Resistance in *P. aeruginosa* by Enhancing Outer Membrane Penetration and Reducing Efflux. *J. Med. Chem.* 59, 8441–8455. doi:10.1021/acs.jmedchem.6b00867

Gray, D. A., and Wenzel, M. (2020). Multitarget Approaches against Multiresistant Superbugs. *ACS Infect. Dis.* 6, 1346–1365. doi:10.1021/acsinfecdis.0c00001

Gupta, V., and Datta, P. (2019). Next-generation Strategy for Treating Drug Resistant Bacteria: Antibiotic Hybrids. *Indian J. Med. Res.* 149, 97–106. doi:10.4103/ijmr.IJMR_755_18

Hegde, S. S., Okusanya, O. O., Skinner, R., Shaw, J.-P., Obedencio, G., Ambrose, P. G., et al. (2012). Pharmacodynamics of TD-1792, a Novel Glycopeptide-Cephalosporin Heterodimer Antibiotic Used against Gram-Positive Bacteria, in a Neutropenic Murine Thigh Model. *Antimicrob. Agents Chemother.* 56, 1578–1583. doi:10.1128/AAC.05382-11

Idowu, T., Arthur, G., Zhanel, G. G., and Schweizer, F. (2019). Heterodimeric Rifampicin-Tobramycin Conjugates Break Intrinsic Resistance of *Pseudomonas aeruginosa* to Doxycycline and Chloramphenicol In Vitro and in a Galleria Mellonella In Vivo Model. *Eur. J. Med. Chem.* 174, 16–32. doi:10.1016/j.ejmech.2019.04.034

Janas, A., and Przybylski, P. (2019). 14- and 15-Membered Lactone Macrolides and Their Analogues and Hybrids: Structure, Molecular Mechanism of Action and

Biological Activity. *Eur. J. Med. Chem.* 182, 111662. doi:10.1016/j.ejmech.2019.111662

Ji, C., Juárez-Hernández, R. E., and Miller, M. J. (2012). Exploiting Bacterial Iron Acquisition: Siderophore Conjugates. *Future Med. Chem.* 4, 297–313. doi:10.4155/fmc.11.191

Jones, A. (2019). Bacterial Vaginosis: A Review of Treatment, Recurrence, and Disparities. *J. Nurse Pract.* 15, 420–423. doi:10.1016/j.nurpra.2019.03.010

Jubeh, B., Breijyeh, Z., and Karaman, R. (2020). Antibacterial Prodrugs to Overcome Bacterial Resistance. *Molecules* 25, 1543. doi:10.3390/molecules25071543

Kamath, A. V., and Iyer, S. (2016). Challenges and Advances in the Assessment of the Disposition of Antibody-drug Conjugates. *Biopharm. Drug Dispos.* 37, 66–74. doi:10.1002/bdd.1957

Kim, I. H., Combrink, K. D., Ma, Z., Chapo, K., Yan, D., Renick, P., et al. (2007). Synthesis and Antibacterial Evaluation of a Novel Series of Rifabutin-like Spirorifamycins. *Bioorg. Med. Chem. Lett.* 17, 1181–1184. doi:10.1016/j.bmcl.2006.12.026

Klahn, P., and Brönstrup, M. (2017). Bifunctional Antimicrobial Conjugates and Hybrid Antimicrobials. *Nat. Prod. Rep.* 34, 832–885. doi:10.1039/c7np00006e

Le, C. F., Fang, C. M., and Sekaran, S. D. (2017). Intracellular Targeting Mechanisms by Antimicrobial Peptides. *Antimicrob. Agents Chemother.* 61, e02340–02316. doi:10.1128/aac.02340-16

Lehar, S. M., Pillow, T., Xu, M., Staben, L., Kajihara, K. K., Vandlen, R., et al. (2015). Novel Antibody-Antibiotic Conjugate Eliminates Intracellular *S. aureus*. *Nature* 527, 323–328. doi:10.1038/nature16057

Leuthner, K. D., Vidaillac, C., Cheung, C. M., and Rybak, M. J. (2010). *In vitro* activity of the New Multivalent Glycopeptide-Cephalosporin Antibiotic TD-1792 against Vancomycin-Nonsusceptible *Staphylococcus* Isolates. *Antimicrob. Agents Chemother.* 54, 3799–3803. doi:10.1128/aac.00452-10

Lexicomp (2021). *Lexicomp® Online, Lexi-Drugs Online, Hudson*. Ohio: UpToDate, Inc. (Accessed January 4, 2021).

Li, J., Ma, Z., Chapo, K., Yan, D., Lynch, A. S., and Ding, C. Z. (2007). Preparation and In Vitro Anti-staphylococcal Activity of Novel 11-Deoxy-11-Hydroxyiminorifamycins. *Bioorg. Med. Chem. Lett.* 17, 5510–5513. doi:10.1016/j.bmcl.2007.08.048

Liapikou, A., Cillóniz, C., and Torres, A. (2017). Investigational Drugs in Phase I and Phase II Clinical Trials for the Treatment of Community-Acquired Pneumonia. *Expert Opin. Investig. Drugs* 26, 1239–1248. doi:10.1080/13543784.2017.1385761

Lipinski, C. A., Lombardo, F., Dominy, B. W., and Feeney, P. J. (1997). Experimental and Computational Approaches to Estimate Solubility and Permeability in Drug Discovery and Development Settings. *Adv. Drug Deliv. Rev.* 23, 3–25. doi:10.1016/S0169-409X(96)00423-1

Liras, S., and McClure, K. F. (2019). Permeability of Cyclic Peptide Macrocycles and Cyclotides and Their Potential as Therapeutics. *ACS Med. Chem. Lett.* 10, 1026–1032. doi:10.1021/acsmedchemlett.9b00149

Liu, J., Lkhagva, E., Chung, H.-J., Kim, H.-J., and Hong, S.-T. (2018). The Pharmabiotic Approach to Treat Hyperammonemia. *Nutrients* 10, 140. doi:10.3390/nu10020140

Liu, Y., Li, R., Xiao, X., and Wang, Z. (2019). Antibiotic Adjuvants: an Alternative Approach to Overcome Multi-Drug Resistant Gram-Negative Bacteria. *Crit. Rev. Microbiol.* 45, 301–314. doi:10.1080/1040841X.2019.1599813

Long, D. D., Aggen, J. B., Chinn, J., Choi, S.-K., Christensen, B. G., Fatheree, P. R., et al. (2008a). Exploring the Positional Attachment of Glycopeptide/β-Lactam Heterodimers. *J. Antibiot.* 61, 603–614. doi:10.1038/ja.2008.80

Long, D. D., Aggen, J. B., Christensen, B. G., Judice, J. K., Hegde, S. S., Kaniga, K., et al. (2008b). A Multivalent Approach to Drug Discovery for Novel Antibiotics. *J. Antibiot.* 61, 595–602. doi:10.1038/ja.2008.79

Lyu, Y., Domalaon, R., Yang, X., and Schweizer, F. (2019). Amphiphilic Lysine Conjugated to Tobramycin Synergizes Legacy Antibiotics against Wild-type and Multidrug-Resistant *Pseudomonas aeruginosa*. *Pept. Sci.* 111, e23091. doi:10.1002/bip.23091

Ma, Z., and Lynch, A. S. (2016). Development of a Dual-Acting Antibacterial Agent (TNP-2092) for the Treatment of Persistent Bacterial Infections. *J. Med. Chem.* 59, 6645–6657. doi:10.1021/acs.jmedchem.6b00485

Ma, Z., Yuan, Y., Liu, Y., and Wang, X. (2020). *New Use of Rifamycin-Nitroimidazole Conjugate Molecules*. United States Patent Application US 2020/0093807 A1. *March* 26, 2020.

Mallinson, J., and Collins, I. (2012). Macrocycles in New Drug Discovery. *Future Med. Chem.* 4, 1409–1438. doi:10.4155/fmc.12.93

Mariathasan, S., and Tan, M.-W. (2017). Antibody-antibiotic Conjugates: a Novel Therapeutic Platform against Bacterial Infections. *Trends Mol. Med.* 23, 135–149. doi:10.1016/j.molmed.2016.12.008

Molodtsov, V., Scharf, N. T., Stefan, M. A., Garcia, G. A., and Murakami, K. S. (2017). Structural Basis for Rifamycin Resistance of Bacterial RNA Polymerase by the Three Most Clinically Important RpoB Mutations Found in *Mycobacterium tuberculosis*. *Mol. Microbiol.* 103, 1034–1045. doi:10.1111/mmi.13606

Moubareck, C. A. (2020). Polymyxins and Bacterial Membranes: A Review of Antibacterial Activity and Mechanisms of Resistance. *Membranes* 10, 181. doi:10.3390/membranes10080181

Mulligan, V. K. (2020). The Emerging Role of Computational Design in Peptide Macrocycle Drug Discovery. *Expert Opin. Drug Discov.* 15, 833–852. doi:10.1080/17460441.2020.1751117

Murillo, O., Pachón, M. E., Euba, G., Verdaguer, R., Tubau, F., Cabellos, C., et al. (2008). Antagonistic Effect of Rifampin on the Efficacy of High-Dose Levofloxacin in *Staphylococcal* Experimental Foreign-Body Infection. *Antimicrob. Agents Chemother.* 52, 3681–3686. doi:10.1128/AAC.00458-08

NCT00442832 (2006). TD-1792 in Gram-Positive Complicated Skin and Skin Structure Infection. https://ClinicalTrials.gov/show/NCT00442832 (Accessed November 25, 2020).

NCT01791049 (2013). TD-1607 SAD Study in Healthy Subjects. https://clinicaltrials.gov/ct2/show/NCT01791049 (Accessed November 25, 2020).

NCT02596399 (2015). A Study to Investigate Safety, Tolerability and Pharmacokinetics of DSTA4637S in Healhy Volunteers. Available: https://clinicaltrials.gov/ct2/show/NCT02596399 (Accessed December 26, 2020).

NCT03162250 (2017). Study to Investigate the Safety, Tolerability, and Pharmacokinetics of DSTA4637S in Participants with *Staphylococcus aureus* Bacteremia Receiving Standard-Of-Care Antibiotics. Available: https://clinicaltrials.gov/ct2/show/NCT03162250 (Accessed December 28, 2020).

NCT03964493 (2019). TNP-2092 to Treat Acute Bacterial Skin and Skin Structure Infection. Available: https://clinicaltrials.gov/ct2/show/NCT03964493 (Accessed December 28, 2020).

NCT04294862 (2021). Tissue Distribution, Pharmacokinetics, Safety, and Tolerability after a Single Dose of TNP-2092 in Participants Undergoing Primary Total Hip or Knee Arthroplasty. Available: https://clinicaltrials.gov/ct2/show/NCT04294862 (Accessed January 11, 2021).

NCT01791049 (2013). *TD-1607 SAD Study in Healthy Subjects*. Available at: https://clinicaltrials.gov/ct2/show/NCT01791049 (Accessed November 25, 2020).

Negash, K. H., Norris, J. K. S., and Hodgkinson, J. T. (2019). Siderophore-antibiotic Conjugate Design: New Drugs for Bad Bugs?. *Molecules* 24, 3314. doi:10.3390/molecules24183314

Okano, A., Isley, N. A., and Boger, D. L. (2017). Total Syntheses of Vancomycin-Related Glycopeptide Antibiotics and Key Analogues. *Chem. Rev.* 117, 11952–11993. doi:10.1021/acs.chemrev.6b00820

Olsufyeva, E. N., and Tevyashova, A. N. (2017). Synthesis, Properties, and Mechanism of Action of New Generation of Polycyclic Glycopeptide Antibiotics. *Curr. Top. Med. Chem.* 17, 2166–2198. doi:10.2174/1568026617666170130115957

Osmon, D. R., Berbari, E. F., Berendt, A. R., Lew, D., Zimmerli, W., Steckelberg, J. M., et al. (2013). Diagnosis and Management of Prosthetic Joint Infection: Clinical Practice Guidelines by the Infectious Diseases Society of America. *Clin. Infect. Dis.* 56, e1–e25. doi:10.1093/cid/cis803

Paljetak, H., Tomaskovic, L., Matijasic, M., Bukvic, M., Fajdetic, A., Verbanac, D., et al. (2017). Macrolide Hybrid Compounds: Drug Discovery Opportunities in Anti-infective and Anti-inflammatory Area. *Curr. Top. Med. Chem.* 17, 919–940. doi:10.2174/1568026616666160927160036

Parkes, A. L., and Yule, I. A. (2016). Hybrid Antibiotics - Clinical Progress and Novel Designs. *Expert Opin. Drug Discov.* 11, 665–680. doi:10.1080/17460441.2016.1187597

Patel, O. P. S., Jesumoroti, O. J., Legoabe, L. J., and Beteck, R. M. (2021). Metronidazole-conjugates: A Comprehensive Review of Recent Developments towards Synthesis and Medicinal Perspective. *Eur. J. Med. Chem.* 210, 112994. doi:10.1016/j.ejmech.2020.112994

Peck, M., Rothenberg, M. E., Deng, R., Lewin-Koh, N., She, G., Kamath, A. V., et al. (2019). A Phase 1, Randomized, Single-Ascending-Dose Study to Investigate the Safety, Tolerability, and Pharmacokinetics of DSTA4637S, an Anti-*Staphylococcus aureus* THIOMAB Antibody-Antibiotic Conjugate, in Healthy Volunteers. *Antimicrob. Agents Chemother.* 63, e02588–02518. doi:10.1128/AAC.02588-18

Peterson, M. L. (2017). The Evolution of Macrocycles in Drug Discovery: from Technologies to Drugs. Available: https://www.americanpharmaceuticalreview.com/Featured-Articles/343609-The-Evolution-of-Macrocycles-in-Drug-Discovery-From-Technologies-to-Drugs/(Accessed January 27, 2021).

Peyrusson, F., Varet, H., Nguyen, T. K., Legendre, R., Sismeiro, O., Coppée, J.-Y., et al. (2020). Intracellular *Staphylococcus aureus* Persisters upon Antibiotic Exposure. *Nat. Commun.* 11, 2200. doi:10.1038/s41467-020-15966-7

Pham, T. D. M., Ziora, Z. M., and Blaskovich, M. A. T. (2019). Quinolone Antibiotics. *Med. Chem. Commun.* 10, 1719–1739. doi:10.1039/c9md00120d

Pokrovskaya, V., and Baasov, T. (2010). Dual-acting Hybrid Antibiotics: a Promising Strategy to Combat Bacterial Resistance. *Expert Opin. Drug Discov.* 5, 883–902. doi:10.1517/17460441.2010.508069

Poreba, M. (2020). Protease-activated Prodrugs: Strategies, Challenges, and Future Directions. *FEBS J.* 287, 1936–1969. doi:10.1111/febs.15227

PR Newswire (2020). TenNor Therapeutics Received FDA Orphan Drug Designation. Available: https://www.prnewswire.com/news-releases/tennor-therapeutics-received-fda-orphan-drug-designation-300989321.html (Accessed April 8, 2021).

Robertson, G. T., Bonventre, E. J., Doyle, T. B., Du, Q., Duncan, L., Morris, T. W., et al. (2008). *In vitro* evaluation of CBR-2092, a Novel Rifamycin-Quinolone Hybrid Antibiotic: Studies of the Mode of Action in *Staphylococcus aureus*. *Antimicrob. Agents Chemother.* 52, 2313–2323. doi:10.1128/AAC.01649-07

Rossi, R., and Ciofalo, M. (2020). An Updated Review on the Synthesis and Antibacterial Activity of Molecular Hybrids and Conjugates Bearing Imidazole Moiety. *Molecules* 25, 5133. doi:10.3390/molecules25215133

Sader, H. S., Rhomberg, P. R., Farrell, D. J., Flamm, R. K., and Jones, R. N. (2014). "Antimicrobial Activity of TD-1607 Tested against Contemporary (2010-2012) Methicillin-Resistant *Staphylococcus aureus* (MRSA) Strains," in 54th Interscience Conference on Antimicrobial Agents and Chemotherapy (Washington DC: Abstract No: F-970).

Sanchez, C. J., Shiels, S. M., Tennent, D. J., Hardy, S. K., Murray, C. K., and Wenke, J. C. (2015). Rifamycin Derivatives Are Effective against Staphylococcal Biofilms In Vitro and Elutable from PMMA. *Clin. Orthop. Relat. Res.* 473, 2874–2884. doi:10.1007/s11999-015-4300-3

Saravanan, P., Dusthackeer, V. N. A., Rajmani, R. S., Mahizhaveni, B., Nirmal, C. R., Rajadas, S. E., et al. (2021). Discovery of a Highly Potent Novel Rifampicin Analog by Preparing a Hybrid of the Precursors of the Antibiotic Drugs Rifampicin and Clofazimine. *Sci. Rep.* 11, 1029. doi:10.1038/s41598-020-80439-2

Schalk, I. J. (2018). Siderophore-antibiotic Conjugates: Exploiting Iron Uptake to Deliver Drugs into Bacteria. *Clin. Microbiol. Infect.* 24, 801–802. doi:10.1016/j.cmi.2018.03.037

Shang, Z., Chan, S. Y., Song, Q., Li, P., and Huang, W. (2020). The Strategies of Pathogen-Oriented Therapy on Circumventing Antimicrobial Resistance. *Research* 2020, 1–32. doi:10.34133/2020/2016201

Shavit, M., Pokrovskaya, V., Belakhov, V., and Baasov, T. (2017). Covalently Linked Kanamycin - Ciprofloxacin Hybrid Antibiotics as a Tool to Fight Bacterial Resistance. *Bioorg. Med. Chem.* 25, 2917–2925. doi:10.1016/j.bmc.2017.02.068

Shopsin, B., Kaveri, S. V., and Bayry, J. (2016). Tackling Difficult *Staphylococcus aureus* Infections: Antibodies Show the Way. *Cell Host Microbe* 20, 555–557. doi:10.1016/j.chom.2016.10.018

Silver, L. L. (2011). Challenges of Antibacterial Discovery. *Clin. Microbiol. Rev.* 24, 71–109. doi:10.1128/cmr.00030-10

Stadelmann, T., Subramanian, G., Menon, S., Townsend, C. E., Lokey, R. S., Ebert, M.-O., et al. (2020). Connecting the Conformational Behavior of Cyclic Octadepsipeptides with Their Ionophoric Property and Membrane Permeability. *Org. Biomol. Chem.* 18, 7110–7126. doi:10.1039/d0ob01447h

Stryjewski, M. E., Potgieter, P. D., Li, Y.-P., Barriere, S. L., Churukian, A., Kingsley, J., et al. (2012). TD-1792 versus Vancomycin for Treatment of Complicated Skin and Skin Structure Infections. *Antimicrob. Agents Chemother.* 56, 5476–5483. doi:10.1128/AAC.00712-12

Sussman, D., Westendorf, L., Meyer, D. W., Leiske, C. I., Anderson, M., Okeley, N. M., et al. (2018). Engineered Cysteine Antibodies: an Improved Antibody-Drug Conjugate Platform with a Novel Mechanism of Drug-Linker Stability. *Protein Eng. Des. Sel.* 31, 47–54. doi:10.1093/protein/gzx067

Taha, M., Abdelbary, H., Ross, F. P., and Carli, A. V. (2018). New Innovations in the Treatment of PJI and Biofilms-Clinical and Preclinical Topics. *Curr. Rev. Musculoskelet. Med.* 11, 380–388. doi:10.1007/s12178-018-9500-5

Tamma, P. D., Cosgrove, S. E., and Maragakis, L. L. (2012). Combination Therapy for Treatment of Infections with Gram-Negative Bacteria. *Clin. Microbiol. Rev.* 25, 450–470. doi:10.1128/cmr.05041-11

TenNor (2020a). TenNor Initiated TNP-2198 Phase 1b/IIa Clinical Trials. Available: http://www.tennorx.com/en/h-nd-63.html (Accessed December 25, 2020).

TenNor (2020b). TenNor Presented Phase II Results of TNP-2092 at 2020 CBIIC. Available: http://www.tennorx.com/en/h-nd-61.html#fai_2_top (Accessed December 25, 2020).

TenNor Therapeutics (2021). TenNor Therapeutics R&D Clinical Candidate Pipeline. Available: http://www.tennorx.com/en/ (Accessed January 27, 2021).

Tevyashova, A. N., Korolev, A. M., Mirchink, E. P., Isakova, E. B., and Osterman, I. A. (2019). Synthesis and Evaluation of Biological Activity of Benzoxaborole Derivatives of Azithromycin. *J. Antibiot.* 72, 22–33. doi:10.1038/s41429-018-0107-2

Theuretzbacher, U. (2020). Dual-mechanism Antibiotics. *Nat. Microbiol.* 5, 984–985. doi:10.1038/s41564-020-0767-0

Tsutsumi, L., Owusu, Y., Hurdle, J., and Sun, D. (2013). Progress in the Discovery of Treatments for *C. difficile* Infection: A Clinical and Medicinal Chemistry Review. *Curr. Top. Med. Chem.* 14, 152–175. doi:10.2174/1568026613666131113154753

Tyers, M., and Wright, G. D. (2019). Drug Combinations: a Strategy to Extend the Life of Antibiotics in the 21st Century. *Nat. Rev. Microbiol.* 17, 141–155. doi:10.1038/s41579-018-0141-x

van Dalen, R., Molendijk, M. M., Ali, S., van Kessel, K. P. M., Aerts, P., van Strijp, J. A. G., et al. (2019). Do Not Discard *Staphylococcus aureus* WTA as a Vaccine Antigen. *Nature* 572, E1–E2. doi:10.1038/s41586-019-1416-8

van Dalen, R., Peschel, A., and van Sorge, N. M. (2020). Wall Teichoic Acid in *Staphylococcus aureus* Host Interaction. *Trends Microbiol.* 28, 985–998. doi:10.1016/j.tim.2020.05.017

Vergalli, J., Bodrenko, I. V., Masi, M., Moynié, L., Acosta-Gutiérrez, S., Naismith, J. H., et al. (2020). Porins and Small-Molecule Translocation across the Outer Membrane of Gram-Negative Bacteria. *Nat. Rev. Microbiol.* 18, 164–176. doi:10.1038/s41579-019-0294-2

Wang, K. K., Stone, L. K., Lieberman, T. D., Shavit, M., Baasov, T., and Kishony, R. (2016). A Hybrid Drug Limits Resistance by Evading the Action of the Multiple Antibiotic Resistance Pathway. *Mol. Biol. Evol.* 33, 492–500. doi:10.1093/molbev/msv243

Wang-Lin, S., and Balthasar, J. (2018). Pharmacokinetic and Pharmacodynamic Considerations for the Use of Monoclonal Antibodies in the Treatment of Bacterial Infections. *Antibodies* 7, 5. doi:10.3390/antib7010005

Wang-Lin, S. X., Zhou, C., Kamath, A. V., Hong, K., Koppada, N., Saad, O. M., et al. (2018). Minimal Physiologically-Based Pharmacokinetic Modeling of DSTA4637A, A Novel THIOMAB Antibody Antibiotic Conjugate against *Staphylococcus aureus*, in a Mouse Model. *mAbs* 10, 1–13. doi:10.1080/19420862.2018.1494478

Weidenmaier, C., and Peschel, A. (2008). Teichoic Acids and Related Cell-Wall Glycopolymers in Gram-Positive Physiology and Host Interactions. *Nat. Rev. Microbiol.* 6, 276–287. doi:10.1038/nrmicro1861

Wells, C. M., Beenken, K. E., Smeltzer, M. S., Courtney, H. S., Jennings, J. A., and Haggard, W. O. (2018). Ciprofloxacin and Rifampin Dual Antibiotic-Loaded Biopolymer Chitosan Sponge for Bacterial Inhibition. *Mil. Med.* 183, 433–444. doi:10.1093/milmed/usx150

WHO (2019a). *2019 Antibacterial Agents in Clinical Development: An Analysis of the Antibacterial Clinical Development Pipeline*. Geneva, Switzerland: World Health Organization. Available: https://apps.who.int/iris/bitstream/handle/10665/330420/9789240000193-eng.pdf (Accessed January 27, 2021).

WHO (2019b). *Antibacterial Products in Clinical Development for Priority Pathogens*. Geneva, Switzerland: World Health Organization. Available:

https://www.who.int/research-observatory/monitoring/processes/antibacterial_products/en/ (Accessed January 11, 2021).

Winstel, V., Xia, G., and Peschel, A. (2014). Pathways and Roles of Wall Teichoic Acid Glycosylation in *Staphylococcus aureus*. *Int. J. Med. Microbiol.* 304, 215–221. doi:10.1016/j.ijmm.2013.10.009

Yang, X., Ammeter, D., Idowu, T., Domalaon, R., Brizuela, M., Okunnu, O., et al. (2019). Amphiphilic Nebramine-Based Hybrids Rescue Legacy Antibiotics from Intrinsic Resistance in Multidrug-Resistant *Gram-Negative Bacilli*. *Eur. J. Med. Chem.* 175, 187–200. doi:10.1016/j.ejmech.2019.05.003

Yang, X., Goswami, S., Gorityala, B. K., Domalaon, R., Lyu, Y., Kumar, A., et al. (2017). A Tobramycin Vector Enhances Synergy and Efficacy of Efflux Pump Inhibitors against Multidrug-Resistant Gram-Negative Bacteria. *J. Med. Chem.* 60, 3913–3932. doi:10.1021/acs.jmedchem.7b00156

Yilmaz, M., Elaldi, N., Balkan, İ. İ., Arslan, F., Batırel, A. A., Bakıcı, M. Z., et al. (2016). Mortality Predictors of *Staphylococcus aureus* Bacteremia: a Prospective Multicenter Study. *Ann. Clin. Microbiol. Antimicrob.* 15, 7. doi:10.1186/s12941-016-0122-8

Yu, X., and Sun, D. (2013). Macrocyclic Drugs and Synthetic Methodologies toward Macrocycles. *Molecules* 18, 6230–6268. doi:10.3390/molecules18066230

Yuan, Y., Wang, X., Xu, X., Liu, Y., Li, C., Yang, M., et al. (2020). Evaluation of a Dual-Acting Antibacterial Agent, TNP-2092, on Gut Microbiota and Potential Application in the Treatment of Gastrointestinal and Liver Disorders. *ACS Infect. Dis.* 6, 820–831. doi:10.1021/acsinfecdis.9b00374

Yudin, A. K. (2015). Macrocycles: Lessons from the Distant Past, Recent Developments, and Future Directions. *Chem. Sci.* 6, 30–49. doi:10.1039/c4sc03089c

Zhao, S., Wang, Z.-P., Wen, X., Li, S., Wei, G., Guo, J., et al. (2020). Synthesis of Vitamin B12-Antibiotic Conjugates with Greatly Improved Activity against Gram-Negative Bacteria. *Org. Lett.* 22, 6632–6636. doi:10.1021/acs.orglett.0c02403

Zhou, C., Lehar, S., Gutierrez, J., Rosenberger, C. M., Ljumanovic, N., Dinoso, J., et al. (2016). Pharmacokinetics and Pharmacodynamics of DSTA4637A: A Novel THIOMAB Antibody Antibiotic Conjugate against *Staphylococcus aureus* in Mice. *mAbs* 8, 1612–1619. doi:10.1080/19420862.2016.1229722

Zhou, Q. (2017). Site-specific Antibody Conjugation for ADC and beyond. *Biomedicines* 5, 64. doi:10.3390/biomedicines5040064

Zimmerli, W., and Sendi, P. (2019). Role of Rifampin against Staphylococcal Biofilm Infections *In Vitro*, in Animal Models, and in Orthopedic-Device-Related Infections. *Antimicrob. Agents Chemother.* 63, e01746–18. doi:10.1128/AAC.01746-18

Zin, P. P. K., Williams, G. J., and Ekins, S. (2020). Cheminformatics Analysis and Modeling with macrolactoneDB. *Sci. Rep.* 10, 6284. doi:10.1038/s41598-020-63192-4

**Conflict of Interest:** The authors declare that the research was conducted in the absence of any commercial or financial relationships that could be construed as a potential conflict of interest.

# Advantages of publishing in Frontiers

**OPEN ACCESS**
Articles are free to read for greatest visibility and readership

**FAST PUBLICATION**
Around 90 days from submission to decision

**HIGH QUALITY PEER-REVIEW**
Rigorous, collaborative, and constructive peer-review

**TRANSPARENT PEER-REVIEW**
Editors and reviewers acknowledged by name on published articles

**Frontiers**
Avenue du Tribunal-Fédéral 34
1005 Lausanne | Switzerland

**Visit us:** www.frontiersin.org
**Contact us:** frontiersin.org/about/contact

**REPRODUCIBILITY OF RESEARCH**
Support open data and methods to enhance research reproducibility

**DIGITAL PUBLISHING**
Articles designed for optimal readership across devices

**FOLLOW US**
@frontiersin

**IMPACT METRICS**
Advanced article metrics track visibility across digital media

**EXTENSIVE PROMOTION**
Marketing and promotion of impactful research

**LOOP RESEARCH NETWORK**
Our network increases your article's readership